THESIS FOR THE DEGREE OF DOCTOR OF PHILOSOPHY

Nonequilibrium Effects in Mesoscopic Josephson Junctions

PETER SAMUELSSON

Department of Microelectronics and Nanoscience
CHALMERS UNIVERSITY OF TECHNOLOGY
GÖTEBORG UNIVERSITY
Göteborg, Sweden 2001

Nonequilibrium Effects in Mesoscopic Josephson Junctions
PETER SAMUELSSON
ISBN 91-7291-008-9

Doktorsavhandlingar vid Chalmers tekniska högskola
Ny serie nr 1692
ISSN 0346-718x

Department of Microelectronics and Nanoscience
Chalmers University of Technology
SE-412 96 Göteborg Sweden
Telephone +46–(0)31–772 1000

Chalmersbibliotekets reproservice
Göteborg, Sweden 2001

Till Helena

Nonequilibrium Effects in Mesoscopic Josephson Junctions

PETER SAMUELSSON
Department of Microelectronics and Nanoscience
Chalmers University of Technology
Göteborg University

ABSTRACT

In this thesis we present theoretical investigations of current transport in mesoscopic Josephson junctions out of equilibrium. A nonequilibrium situation is created by either quasiparticle injection into the normal part of the junction, or by applying a dc-voltage between the two superconducting electrodes. The current is calculated from the scattering states, which are expressed in terms of the scattering matrix of the normal part of the junction and the Andreev reflection amplitudes at the normal conductor-superconductor (NS) interfaces.

The theory is first applied to a single-mode ballistic Josephson junction with an additional normal lead connected to the normal part of the junction, and the effect on the Josephson current due to current injection from the normal lead is investigated. It is found that there are two main effects of the nonequilibrium. First, there is a nonequilibrium population of the current carrying Andreev levels which, dependent on junction length and injection voltage, can result in a suppression, enhancement or even sign reversal of the Josephson current. Second, there is an anomalous nonequilibrium interference effect, which gives rise to a long range Josephson current, increasing with voltage eV up to the superconducting gap Δ. The study is then extended to a two-dimensional ballistic junction and the sign reversal effect of the critical Josephson current is studied in detail.

Subsequently, the theory is applied to a three-terminal Josephson junction where the normal part of the junction consists of a chaotic quantum dot. Using the statistical information of the scattering matrix of the dot, known from random matrix theory, the average nonequilibrium current and the sample-to-sample fluctuations of the current are studied. It is found that in junctions in the short dwell time regime, the average critical current is monotonically suppressed with increasing voltage, saturating at voltages $eV = \Delta$ at a value of order $\sqrt{N}(e\Delta/\hbar)$, where N is number of transverse modes in the contacts to the superconductor. At this voltage the critical current is entirely determined by the anomalous interference current. The sample-to-sample fluctuations at this voltage are of the same order, which is a magnitude $\sqrt{N}$ larger than the equilibrium current fluctuations.

Finally, a chaotic Josephson junction with a dc-voltage bias between the superconducting electrodes is studied, with the focus on the transition from a short to a long dwell time regime of the dot. It is found that a generic feature of the current voltage characteristics, besides the standard subharmonicic gap structures (SGS) at $eV = 2\Delta/n$, is current anomalies at voltages of order of the Thouless energy away from the SGS with even subgap positions, $n = 2, 4, 6...$ These anomalies are suppressed by a magnetic field in the dot large enough to break time reversal symmetry (TRS). For broken TRS, it is found that the current takes on a universal value, independent of Thouless energy or magnetic field, exactly coinciding with the current found from the well known OTBK-model.

Keywords: Josephson effect, nonequilibrium transport, mesoscopic superconductivity, ballistic transport, chaotic quantum dot, mesoscopic fluctuations, random matrix theory, multiple Andreev reflections

LIST OF PUBLICATIONS

This thesis consists of an introductory text and the following papers:

I **Long range Josephson effect in mesoscopic T-shaped superconductor-normal-superconductor junctions.**
P. Samuelsson, V.S. Shumeiko, and G. Wendin
Phys. Rev. B 56 R5763 (1997).

II **Nonequilibrium Josephson effect in mesoscopic ballistic SNS-junctions.**
P. Samuelsson, J.Lantz, V.S. Shumeiko, and G. Wendin
Phys. Rev. B 62 1319 (2000).

III **Nonequilibrium Josephson current in ballistic multiterminal SNS-junctions.**
P. Samuelsson, A. Ingerman, V.S. Shumeiko, and G. Wendin
cond-mat/0005141, to appear in Physica C.

IV **Large sample-to-sample fluctuations of the nonequilibrium critical current through mesoscopic Josephson junctions**
P. Samuelsson, and H. Schomerus
Phys. Rev. B 63 054512 (2001).

V **Current transport in voltage biased chaotic Josephson junctions.**
P. Samuelsson, G. Johansson, Å. Ingerman, V.S. Shumeiko, and G. Wendin,
to be submitted

Contents

CHAPTER 1

Introduction

This is a thesis about mesoscopic superconductivity. Mesoscopic physics is concerned with the study of physical phenomena in the regime between the microscopic world of the atoms, governed by the laws of quantum mechanics, and the macroscopic, governed by the laws of classical physics. This mesoscopic regime has become increasingly important from an applied point of view over the last decades, due to the ongoing miniaturization of electronic devices. There is a practical limit for how small electronic components can be, before new quantum mechanical effects become important, modifying the physical properties of the components. During the intense research in the eighties it became increasingly clear that the mesoscopic region constituted an interesting object of study also from a more fundamental point of view. What was originally suspected to be a rather dull physical transition region, turned out to contain a whole new world of physical phenomena.

At the end of the eighties and beginning of the nineties there was an increased interest in mesoscopic phenomena in small structures consisting of, or containing, superconductors. Superconductors are named after their property to conduct current without any resistance, when cooled down to low temperatures. The study of superconductors is an old field in physics, superconductivity was discovered at the beginning of the century and several discoveries in connection to superconductivity have been awarded the Nobel prize. The combination of the physics of superconductivity and mesoscopic physics turned out to be very fruitful, again both from applied and theoretical points of view. A large number of new interesting phenomena were discovered and many of the phenomena observed in normal mesoscopic conductors turned out to be modified in a nontrivial way. In this thesis we will discuss some of them.

1.1 Mesoscopic physics

From the point of view of applications, the natural quantity to study if one wants to construct a mesoscopic transistor, diode or any other electronic component, is the current transported through a mesoscopic conductor as a response on an applied voltage between two electrodes connected to the conductor. In mesoscopic conductors, the electrons, carrying the current, preserve their quantum mechanical phase throughout the conductor, i.e. the so called phase breaking length l_ϕ is larger than the lateral size L of the conductor. This means that we have to take into account the quantum mechanical wave nature of the electrons when studying the transport. It also means that we from the very beginning neglect all interactions between electrons or any other interaction mechanisms that cause the electrons to lose their memory of quantum mechanical phase.

One could imagine that this assumption of noninteracting electrons would make the issue of transport through mesoscopic conductors very simple. This is however not the case, as was shown in the early days of mesoscopic physics. The fact that electrons scatter on impurities or boundaries in the conductor without losing their phase memory, leads to a very complicated interference behavior. In most cases, the behavior is so complex that one has to give up all hope to exactly describe the motion of the individual electrons and instead turn to a statistical description. The second half of this thesis, is devoted to the study of current transport through one such type of mesoscopic conductors, called chaotic quantum dots, where the adjective chaotic signals that the classical motion of the electrons is chaotic. The first half of the thesis is devoted to the study of current transport in conductors that are in the complete opposite limit, ballistic conductors where the motion of electrons is highly regular. In ballistic conductors, the electrons propagate freely and they only very rarely scatter on impurities or boundaries. However, as is discussed in detail in these chapters, the transport properties of the structures where the normal mesoscopic conductors are connected to superconductors, are nevertheless nontrivial and interesting.

1.2 Superconductivity

In this thesis we will very briefly discuss the properties of superconductors themselves, and rather concentrate on the effect that superconductors have on normal conductors when they are coupled together. The superconductors are assumed to be large, macroscopic objects connected to the small, mesoscopic, normal conductors, and not affected by the connection to the normal conductors. The superconductors will thus merely serve as boundaries for the normal mesoscopic conductors. Superconductors are most commonly known for their properties to conduct current without any resistance and to expel magnetic field, the Meissner effect. Our focus is however on two other properties, which just can be seen as another side of the same coin. First, the property that superconductors act as macroscopic quantum objects with a quantum mechanical phase, and second that the superconductors have a gap in the spectrum around Fermi energy. Both properties can be seen as consequences of that superconductivity is a phenomena which on a microscopic level can be described by that electrons close to Fermi energy pair up into Cooper pairs. The Cooper pairs are correlated over a long range and form a large, quantum mechanical condensate characterized by a superconducting order parameter $\Delta e^{i\phi}$. The order parameter, which can be seen as the macroscopic wave function of the condensate, has a phase ϕ, the superconducting phase, and a magnitude Δ, which is just equal to half the size of the gap in the spectrum . Many of the properties of the superconductors were experimentally discovered during the first half of the century, but it was not until Bardeen, Cooper and Schriefer[32] presented their Nobel prize awarded theory of superconductivity, that all the properties of superconductors could be explained within a general and consistent framework.

1.3 Andreev reflection

The properties of an interface between a between a normal conductor and a superconductor (NS-interface) are nontrivial and interesting. Due to the gap in the spectrum, electrons in the normal conductor with energy close to Fermi energy, can not enter the superconductor. This suggests that an electron in the normal conductor incident on the superconductor, will be reflected back into the normal conductor. The gap is however not strong enough to normally reflect the incoming electrons. What happens instead is that an incident electron combines with another electron close to the interface and enters the superconductor as a Cooper pair, creating a hole which is retroreflected into the normal conductor. This phenomena was first discussed in 1964 by Andreev[14] and is therefore named Andreev reflection.

The importance of this discovery, was not fully appreciated before the beginning of the nineties, when it became clear that Andreev reflection is the microscopic mechanism for conversion of normal current to supercurrent at the NS-interface.

1.4 Josephson effect

In 1962, two year before Andreevs discovery, Josephson[129] predicted that when two bulk superconductors are put in contact with each other via an insulating layer, there will flow an equilibrium supercurrent between the superconductors proportional to the sinus of the difference between the phases of the superconductors. Moreover, he predicted that if a voltage is applied between the two superconductors, the phase difference will increase in time and thus produce a nonequilibrium current that oscillates in time. For the discovery of these effects, Josephson was later awarded the Nobel prize, and from the time of the discovery of the Josephson effect to the present day there has been a continuous interest, both experimentally and theoretically, in different aspects of the Josephson effects.

It soon became clear that an equilibrium Josephson current can flow between two superconductors weakly connected by any type of normal conductor and not only between superconductors connected by an insulating barrier. From a microscopic point of view, the Josephson current flowing between the two superconductors is an effect of repeated Andreev reflections at the two NS-interfaces, which effectively transports Cooper pair between the superconductors.[140] One aspect of the Josephson effect that came into focus some time after the discovery was the effect on the Josephson current of a nonequilibrium situation, in the superconductors or in the normal conductor. Of special interest for the work in this thesis is the studies in the end of the seventies and beginning of the eighties, both experimental[241] and theoretical,[25, 156, 250] where the effects on the dc-Josephson current of a nonequilibrium situation in the normal conductor due to weak electromagnetic irradiation or a small applied ac-voltage were investigated.

Almost simultaneously, there were a number of studies performed on the effect of nonequilibrium due to an applied constant voltage between the superconductors. It was shown that the mechanism responsible for the current transport between two superconductors at small applied bias, involves multiple Andreev reflections.[132] Electrons in the normal conductor propagating from one side of the normal conductor to the other are accelerated by the electric field present due to the applied voltage. They are Andreev reflected into holes at the NS-interfaces and travel back across the normal conductor, further accelerated by the field due to that the holes have opposite charge to electrons. In this way they electrons and holes successively increase their energy and eventually escape out into the superconductors at energies above the gap, effectively transporting current between the two superconductors.

The work presented in this thesis is focused on two types of non-equilibrium effects; the effect on the dc-Josephson current of nonequilibrium in the normal conductor due to current injection into the normal part of the junction, and the effect on the current through the junction due to an applied bias between the superconductors. The emphasis on how they are manifested in mesoscopic Josephson junctions, i.e junctions where two superconductors are connected via a normal conductor of mesoscopic size. Since the beginning of the eighties, there has been an large number of works presented on different aspects of these nonequilibrium effects. A number of these works are discussed in detail in the different chapters of the thesis.

1.5 Scattering approach to the Josephson effect

There has been a large number of theoretical methods employed in the calculation of the Josephson current. The calculations in this thesis are all based on a scattering approach, where the mesoscopic conductor is treated as a scatterer for electrons and holes injected from both normal and superconducting electrodes connected to the normal conductor. Underlying this approach is the idea pioneered by Landauer[151] and later formalized by Büttiker,[68] that conduction of current through a mesoscopic conductor can be described as a scattering process. The Landauer-Büttiker approach was originally formulated for normal conductors, but was later[54, 147] extended to junctions consisting of normal conductors and superconductors, via the inclusion of Andreev scattering at the NS-interfaces.

1.6 Experimental realizations of mesoscopic Josephson junctions

A typical mesoscopic Josepshon junction contains a normal conductor with a lateral size of order of a micrometer or smaller. If the size of the normal conductor is much larger, phase breaking effects become important and the model with noninteracting electrons has to be modified. Moreover, the phase breaking effects become stronger when the temperature is enhanced, therefore typical temperatures at which experiments are performed are a few Kelvins down to tenths of milli Kelvins. These are also the temperatures where the metal electrodes, typically of Niobium or Aluminum, have their transition to the superconducting state.

The normal conductor can be made from a large number of materials, from metals to semiconductors. The transport in metal conductors of mesoscopic size is diffusive, that is, the electrons scatter from a large number of impurities when propagating through the conductor. The average distance between collisions l, the mean free path, is thus much smaller than the size of the conductor. In semiconductors the number collisions with impurities can under certain circumstances be strongly reduced and the mean free path can be made longer than the size of the normal conductor. In this case the transport is ballistic.

One way to reduce the mean free path in semiconductors is to sandwich thin layers of different semiconducting materials, so called heterostructures, in a way that effectively creates a two dimensional conductor at the interface between two of the layers. The density of electrons in these two dimensional electron gases (2DEG) can be controlled by means of electrostatic metal gates on top of the semiconductors, which makes it possible to confine and control the conducting region in the electron gas, i.e to define a two dimensional normal conductor.

During the eighties, this technique was refined and developed to a high degree of accuracy, which enabled a number of detailed studies of mesoscopic phenomena.[40] The majority of these experiments were carried out in semiconductor heterostructures based on Gallium Arsenide, GaAs. In junctions containing superconducting metal electrodes, the GaAs heterstrostructures have the drawback that a strong potential barrier forms at the interface between the semiconductor and the superconductor, a Schottky barrier. Due to this drawback, the main focus has been on Josephson junctions with semiconductor heterostructures based on Indium Arsenide, InAs (see e.g. Refs. 74, 207, 228). Pure single crystal InAs has the property that a two dimensional spontaneously forms on the surface, which has made this material interesting for experiments as well.

In this thesis we study different properties of ballistic Josephson junctions where the electron motion in the normal conductor is regular or chaotic. In the latter case, the chaotic behavior can arise from irregular ballistic motion as well as diffusive motion. The results presented in the thesis are directly applicable to two dimensional normal heterostructure conductors connected to large superconducting metal electrodes; however in most cases the results can be generalized to junctions containing an arbitrary mesoscopic conductor.

1.7 Outline of the thesis

This thesis is built around a number of publications and projects about non-equilibrium effects in mesoscopic Josephson junctions. It is divide into eight chapters.

2. Scattering theory in normal conductor

A scattering theory to current transport in normal multi terminal mesoscopic conductors within the Landauer-Büttiker approach is presented. The concept of scattering and transmission matrices and their relation is discussed. A Hamiltonian approach, which expressed the scattering matrix in terms of the Hamiltonian of a mesoscopic conductor, is introduced. The concepts of scattering density of states and particle dwell times are presented.

3. Scattering theory based on time independent Bogoliubov- de Gennes equation.

The scattering theory in the preceding chapter is extended to mesoscopic superconducting junctions. The theory is based on the time independent Bogoliubov de Gennes equation. The concept of Andreev reflection is presented and general formulas for the conductance of a normal conductor-superconductor (NS) junction are presented. An expression for the equilibrium Josephson current is derived within the scattering approach and it is compared to the result from a free energy approach to Josephson current. Expressions for the equilibrium and nonequlibrium Josephson current and conductance in a superconductor-normal conductor-superconductor (SNS) junction connected to a third, normal, electrode are derived.

4. Nonequilibrium effects in multiterminal single mode SNS-junctions

The concept of current carrying Andreev bound states and the current carried by the continuum states in single mode ballistic SNS-junctions is discussed. Then, the theory derived in the previous chapter is applied to a single mode three terminal SNS-junction and the exact current expressions are presented and. The different parts of the nonequilibrium Josephson current are described in detail, focusing on the so called anomalous part of the Josephson current. Comparison to earlier theories and existing experiments are discussed.

5. Multiterminal two dimensional SNS-junctions, ballistic and sample specific regimes.

The analysis in the previous chapter is extended to two dimensional ballistic junctions. The main emphasis is on the nonequilibrium population of the current carrying Andreev levels and the corresponding modification of the critical nonequilibrium Josephson current. Normal reflection at the NS-interface is discussed in detail. The differences between the single mode junction and the two dimensional junction are discussed.

6. Random matrix theory of chaotic quantum dots.

To make the thesis more self consistent, a short review of some properties of a chaotic quantum dot, relevant for the subsequent chapters, is presented. A statistical theory for the scattering matrix of the dot is presented, allowing for the calculation of ensemble averaged properties as well as sample to sample fluctuations. The conductance of a chaotic dot-superconducting junction is presented as an example.

7. Nonequilibrium Josephson effect in chaotic Josephson junctions.

The nonequilibrium Josephson current in a three terminal chaotic Josephson junction, a SNS-junction with the normal conductor consisting of a chaotic dot, is studied. Combining the scattering theory in Chapter 3 with the statistical information for the scattering matrix of the dot, derived in Chapter 6, the average nonequilibrium Josephson current as well as the sample-to-sample fluctuations are calculated. It is predicted that the sample-to-sample fluctuations of the nonequilibrium current will be larger then the equilibrium current fluctuations with a factor proportional to the width of the contact between the superconductors and the dot.

8. Scattering theory based on time dependent Bogoliubov- de Gennes equation.

A scattering theory of a voltage biased mesoscopic Josephson junctions, based on the time dependent Bogoliuobov de Gennes equation, is presented. A general expression for the dc-current in terms of particle currents is derived. As an example, the theory is applied to a single mode junction. The so called OTBK-approach to calculating the current in voltage biased Josephson junctions is shortly reviewed and then extended to a general form which takes into account arbitrary normal scattering in the junction. The current from this general OTBK approach is then decomposed into particle currents.

9. Current transport in voltage biased chaotic Josephson junctions.

The scattering theory of the preceding chapter is applied to a voltage biased chaotic Josephson junction . The two limits, short and long dwell time regimes are discussed, as well as the single and multi mode limits. A number of features of the current, argued to be generic for mesoscopic junctions with sufficiently complex scattering, are discussed. The effect of magnetic field in the dot and tunnel barriers at the NS-interfaces are discussed. It is shown that for a magnetic field in the dot, large enough to break time reversal symmetry, the current coincides with the current obtained from the generalized OTBK-approach presented in the preceding chapter.

CHAPTER 2

Scattering theory for normal conductors

As was originally pointed out by Landauer,[151,152] the conductance of a mesoscopic sample, a conductor, can be studied within a scattering approach. Low probability for an electron to scatter throgh the conductor thus corresponds to high resistance. This intuitively reasonable idea was later formalized by Büttiker,[68] who presented a theory for conduction through arbitrary multiterminal mesoscopic conductors. This approach to transport in mesoscopic conductors is commonly known as the Landauer-Büttiker approach. Many others have also contributed to the development of the theory and it has been discussed in several books (see e.g. Ref.83). It has proved to be very successful in explaining a large range of mesoscopic experiments (see e.g. Ref. 40 for a review). One can note that the correct formulation of the approach was a long standing issue of discussion, finally resolved in the mid-eighties (see e.g Refs. 121, 220).

In this chapter we present a scattering theory for the transport properties of a normal conductor connected to two or more electron reservoirs in the normal state, based on the Landauer-Büttiker approach. Special attention is given the concept of the scattering matrix which characterizes the conductor and in which all transport quantities can be expressed. This theory will then serve as a basis for the discussion in the subsequent chapters, where we study junctions where one or several of the reservoirs are in the superconducting states. For simplicity, the theory is derived under certain simplifying assumptions relevant for the physical systems studied in this thesis, namely two dimensional conductors and weak applied magnetic fields; however, in principle these restrictions can be lifted and the theory can be generalized to mesoscopic conductors under very general conditions.

2.1 Calculation of the current from scattering states

The type of junction under consideration, shown schematically to the right in Fig. 2.1, consists of a two-dimensional mesoscopic conductor connected to large pads, acting as electron reservoirs. Constant voltages V_i are applied at the reservoirs. The conductor is mesoscopic in the sense that the lateral dimensions of the conductor, L, is smaller than the phase breaking length, l_ϕ. No assumption is made on the elastic mean free path l, i.e the conductor can be in the ballistic $l \gg L$, or the diffusive $l \ll L$ limit. The transport through the conductor is thus completely coherent. It is also assumed that the coupling to the reservoirs is so large that charging effects can be neglected. The reservoirs act as incoherent sources and sinks of electrons. In the figure, the conductor is connected to the reservoirs via perfect leads, which are introduced as a technical step to simplify the calculation. Under these conditions, the Landauer-Büttiker approach is appropriate for describing the current transport in the junction.

2.1.1 Two terminal junction

We start by studying the simplest junction, a conductor connected to two normal reservoirs, and then extend the discussion to multi terminal junctions below. A schematic picture of the two terminal suction is shown to the left in Fig. 2.1. The leads are, for simplicity, assumed to be identical, with width W. A local coordinate system (x_i, y_i) is introduced in each lead. The Schrödinger equation for the system is (assuming time independent potentials)

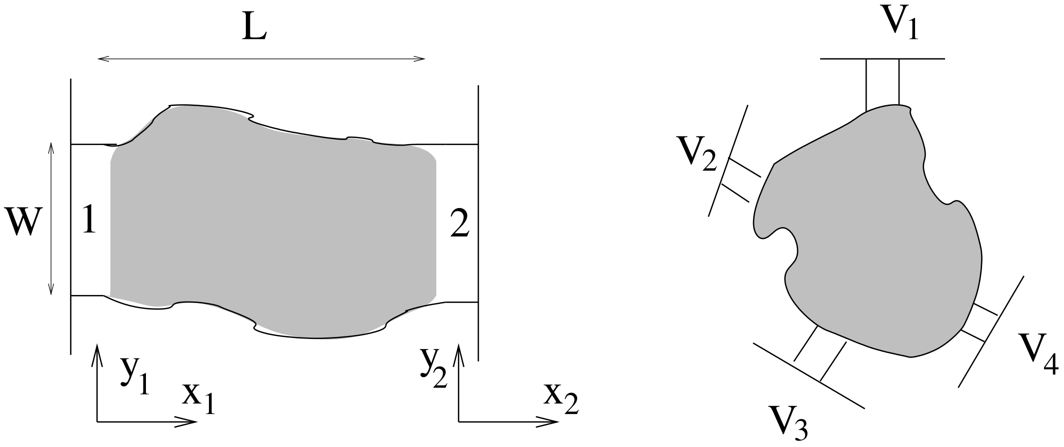

Figure 2.1: Left: Schematic picture of a mesoscopic conductor connected to two normal reservoirs via ideal leads. Right: Schematic picture of a general mesoscopic junction with voltages V_i applied at the reservoirs.

$$H\Psi = E\Psi,\ H = \frac{1}{2m}(i\hbar\nabla + eA)^2 + U - E_F, \tag{2.1}$$

where A is the vector potential, U is the electrostatic potential, m is the effective mass and the energy E is calculated from Fermi energy E_F. Spin independent transport is assumed and the spin degeneracy is taken into account by a factor of two in the current expressions below. To be able to work with the same wavefunctions in the leads throughout the thesis, we assume that the magnetic field, applied perpendicular to the conductor, is zero in the leads, $B = 0$. The vector potential in the leads is then just a constant, chosen to be zero in lead 1, $A_1 = 0$, and $A_2 = A\hat{y}$ i lead 2 (It should be pointed out that it is possible to work out a scattering approach to transport for arbitrary strong magnetic field in the leads, see e.g. Ref. 28).

Under these assumptions, the wavefunction in lead i is just a linear combination of plane wave solutions to the Schrödinger equation (expressed in the local coordinates)

$$\Psi_i = \sum_n \frac{1}{\sqrt{k_n}} \Theta_{in}(y_i) \left(a_{in} e^{ik_n x_i} + b_{in} e^{-ik_n x_i} \right), \tag{2.2}$$

where the transverse wavefunction in lead 1, $\Theta_{n1}(y_1)$, is given by the equation

$$\left(-\frac{\hbar^2}{2m}\frac{d^2}{dy_1^2} + \frac{\hbar^2 k_n^2}{2m} + U(y_1) - E_F \right) \Theta_{1n}(y_1) = E\Theta_{1n}(y_1) \tag{2.3}$$

and the transverse wavefunction in lead 2 is related to the wavefunction in lead 1 via a gauge transformation $\Theta_{2n}(y_2) = \exp(-ieAy_2/\hbar)\Theta_{1n}(y_2)$. The leads are thus acting as electronic waveguides with a well defined number of transport modes $N = \text{Int}[2W/\lambda_F]$ at Fermi energy, with Int the integer part and λ_F the Fermi wave length. [Evanescent modes are neglected]. It is assumed that the confining potential in the y_i-direction in the leads is a hard wall potential, i.e $U(x_i, y_i) = 0$ for $0 < y_i < W$ and infinity otherwise, which gives the transverse wavefunction in lead 1

$$\Theta_{1n}(y_1) = \sqrt{2/W}\sin(n\pi/Wy). \tag{2.4}$$

The transverse wavefunctions are thus normalized as $\int dy_i|\Theta_{in}(y_i)|^2 = 1$, which gives that the normalization of the wavefunctions is chosen such that each transverse mode carries the same amount of current. The wavenumber in mode n is given by

$$k_n = \sqrt{(2m/\hbar^2)(E_F - E_n + E)}, \tag{2.5}$$

where the $E_n = (\hbar n\pi)^2/(2mW^2)$ is the transverse mode energy. It should be pointed out that the choice of boundary conditions in the y-direction in the leads is not crucial for the discussion that follows; however our particular choice is reasonable for the type of junctions where the conductor is defined by etching or by other means cutting out a structure in a two dimensional electron gas. If the conductor would be defined by electrostatic gates, a parabolic potential or a flat-bottom potential with a parabolic edge potential in the y_i-direction would be more appropriate (see e.g Refs. 40, 83).

The scattering of the electrons in the junction can be described by a $2N \times 2N$ scattering matrix connecting the amplitudes of the outgoing and incoming electron waves

$$\begin{aligned} c^{out} &= [b_{11}, b_{12}, ..., b_{1N}, a_{21}, a_{22}, ..., a_{2N}], \\ c^{in} &= [a_{11}, a_{12}, ..., a_{1N}, b_{21}, b_{22}, ..., b_{2N}] \end{aligned} \tag{2.6}$$

as

$$c^{out} = Sc^{in},\ S = \begin{pmatrix} r & t' \\ t & r' \end{pmatrix}, \tag{2.7}$$

where r, t, r' and t' are $N \times N$ reflection and transmission amplitude matrices for a wave incident on the scatterer. Primed (unprimed) quantities denote incoming waves from right (left). The chosen normalization of the wavefunctions leads to that the scattering matrix S is unitary, due to that the current is conserved at the scattering,

$$I_{out} = c_{out}^{\dagger}c_{out} = c_{in}^{\dagger}S^{\dagger}Sc_{in} = c_{in}^{\dagger}c_{in} = I_{in} \Rightarrow S^{\dagger}S = 1,\ S^{-1} = S^{\dagger}, \tag{2.8}$$

where † is Hermitian conjugate. It follows from the Schrödiger equation in (2.1), that if $\Psi(B)$ is a solution, the complex conjugated wavefunction with reversed vector potential A (and thus reversed magnetic field $B = \nabla \times A$), $\Psi^*(-B)$ is also a solution. Since complex conjugation of the wavefunction turns an incoming wave into an outgoing, and vice versa, the scattering matrix $S^*(B) = S^{-1}(-B) = S^{\dagger}(-B)$ (the last step due to unitarity of S), i.e $S(B) = S^T(-B)$ where T denotes transpose. At zero magnetic field, the time reversal symmetry is conserved and the scattering matrix is symmetric $S = S^T$.

The conductor is connected to large electron reservoirs, bulk metallic pads, assumed to have the following important properties (see e.g Ref. 28 for a detailed discussion).

- The reservoirs are in thermal equilibrium with chemical potential $\mu_i = eV_i$, where V_i is the applied voltage at reservoir i.

- The reservoirs are so large compared to the conductor that the current flowing through the conductor and out in the reservoirs can be assumed not to affect the equilibrium of the reservoirs.
- All electrons entering the reservoirs suffer inelastic scattering and are thermalized and phase randomized before they return to the conductor, i.e the electrons are injected incoherently into the conductor, with a distribution given by the Fermi-Dirac distribution of the emitting reservoir.
- Electrons in the leads incident on the reservoirs enter the reservoirs without suffering any additional reflection, i.e the lead-reservoir contact is "reflectionless"[224] and each mode carries the maximal current $2e/h$ per unit energy (taking spin degeneracy into account).

Due to these properties of the reservoirs, the problem of calculating the current flowing between the two reservoirs under an applied voltage difference $V_1 - V_2$, can be approached in the following manner. The mesoscopic conductor is treated as a scatterer connected to semi-infinite leads. The scattering potential is thus nonzero only in the conductor, i.e the scattering problem is well defined. The scattering states for electrons incident from infinity are calculated by matching wavefunctions at the scatterer via the scattering matrix. From the scattering states, the current in the leads is calculated at infinity, thus neglecting the evanescent modes. The role of the reservoirs is then simply to populate the scattering states according to the Fermi-Dirac distribution of the reservoir from which the electron is incident.

Due to current conservation, the current can be calculated anywhere in the conductor, and we choose to calculate it in the leads where the wavefunction is known. The wavefunction in lead i resulting from an electron with energy E injected in mode q in lead j is labeled $\Psi_i^{jq}(E)$. The indices E, q and j, are the quantum numbers used to label the scattering state (It has been shown that the scattering states $\{jqE\}$, together with possible bound states of the conductor, form a complete set of states[28, 137] which implies that the Pauli exclusion principle is not violated, i.e that two electrons do not occupy the same state). The current of a scattering state $\{jqE\}$, flowing in lead i, is given by

$$I_i^{jq}(E) = \int_0^W dy\, j_i^{jq}(E) dy, \tag{2.9}$$

where the integral is performed at a constant position x_i somewhere in lead i. The current $j_i^{jq}(E)$ is given by the quantum mechanical expression

$$j_i^{jq}(E) = \frac{e\hbar}{m}\mathrm{Im}\left[\Psi_i^{jq}(E)^* \frac{d}{dx_i}\Psi_i^{jq}(E)\right]. \tag{2.10}$$

Performing the integration in (2.9), using the orthogonality of the transverse wavefunctions in Eq. (2.4) we arrive at

$$I_i^{jq}(E) = \frac{e\hbar}{n}\sum_n \left(|a_{in}^{jq}(E)|^2 - |b_{in}^{jq}(E)|^2\right), \tag{2.11}$$

where the subscript $\{ni\}$ denotes the lead i and mode n where the current is calculated. Note that the population of each scattering state is determined by the Fermi-Dirac distribution $f_j(E) = [1+\exp([E-V_j]/kT)]^{-1}$ of the injecting reservoir j. For an electron injected in mode q in lead $j = 1$ we get the amplitudes of the electrons in the leads

$$a_{in}^{1q} = f_1(E)\sqrt{k_q} \times \left\{ \begin{array}{ll} \delta_{qn} & i=1 \\ t_{qn} & i=2 \end{array} \right., \quad b_{in}^{1q} = f_1(E)\sqrt{k_q} \times \left\{ \begin{array}{ll} r_{qn} & i=1 \\ 0 & i=2 \end{array} \right. \tag{2.12}$$

where r_{qn} and t_{qn} are the reflection and transmission amplitudes from mode q to mode n in lead 1 and 2 respectively. For injection from reservoir 2 we instead get

$$a_{in}^{2q} = f_2(E)\sqrt{k_q} \times \left\{ \begin{array}{ll} t'_{qn} & i=1 \\ \delta_{qn} & i=2 \end{array} \right. , \; b_{in}^{2q} = f_2(E)\sqrt{k_q} \times \left\{ \begin{array}{ll} 0 & i=1 \\ r'_{qn} & i=2 \end{array} \right. \tag{2.13}$$

The current from individual scattering states can be calculated independently, since the electrons are injected independently, as pointed out above. Summing up the current over all scattering states, i.e injected wavenumbers, modes and contacts, we get the total current in lead i (proceeding from summation to integration over wave number and using that $dE/dk_q = \hbar^2 k_q/m$)

$$\begin{aligned} I_i &= \sum_{q,j}\sum_{k_q} I_i^{jq}(E) f_j(E) = \sum_{q,j}\int \frac{dk_q}{2\pi} I_i^{jq}(E) f_j(E) \\ &= \sum_{q,j}\int dE \frac{dk_q}{dE}\frac{1}{2\pi} I_i^{jq}(E) f_j(E) = \int dE \sum_j i_i^j(E) f_j(E), \end{aligned} \tag{2.14}$$

where the spectral current densities, found by inserting the relations in Eqs. (2.12) and (2.13), are

$$\begin{aligned} i_1^1(E) &= \frac{2e}{h}[N - \mathrm{tr}(rr^\dagger)],\; i_1^2(E) = \frac{2e}{h}\mathrm{tr}(t^{'}t^{'\dagger}), \\ i_2^1(E) &= \frac{2e}{h}\mathrm{tr}(tt^\dagger),\; i_2^2(E) = \frac{2e}{h}[N - \mathrm{tr}(r^{'}r^{'\dagger})]. \end{aligned} \tag{2.15}$$

We choose to calculate the current $I = I_1 = I_2$ in lead 1 (I_1=I_2 due to current conservation). Using the unitarity of the scattering matrix S, which gives $\mathrm{tr}(rr^\dagger) = \mathrm{tr}(r^{'}r^{'\dagger}) = N - \mathrm{tr}(tt^\dagger) = N - \mathrm{tr}(t't'^\dagger)$, the current in Eq. (2.14) becomes,

$$\begin{aligned} I &= \frac{2e}{h}\int_{-\infty}^{\infty} dE\; [\mathrm{tr}(1 - rr^\dagger) f_1(E) - \mathrm{tr}(t^{'}t^{'\dagger}) f_2(E)] \\ &= \frac{2e}{h}\int_{-\infty}^{\infty} dE\; \mathrm{tr}(tt^\dagger)[f_1(E) - f_2(E)], \end{aligned} \tag{2.16}$$

where the scattering amplitude t in general depend on energy and the applied potential. This form of the current clearly shows that only current flowing between the reservoirs at energies where the distribution functions are different, contribute to the net current.

Since we are free to choose our reference level for the potential, we can put $V_2 = 0$ and define $V_1 = V$. In the limit $eV = 0, kT = 0$, the differential conductance $G = dI/dV$ is given by

$$G = \frac{2e^2}{h}\mathrm{tr}(tt^\dagger) \tag{2.17}$$

with t evaluated at Fermi energy. This is the celebrated Landauer formula, first written down on this form in Ref. 90. The current formula in Eq. (2.16) is valid also outside the regime of small voltage and temperature, however, the scattering matrix is then dependent on applied voltage at the reservoirs. In the general case, one has to solve Poissons equation together with the Schrödinger equation to find the potential distribution in the scattering region and then calculate the scattering matrix (see e.g Ref. 83). This is in most cases very complicated and in this thesis only the simplified case where the potential drops at the interfaces between the leads and the reservoirs is considered. This is directly applicable when the contact resistance between the injecting reservoir and the conductor is the dominating in the junction.

2.1.2 Multiterminal junction

The approach above can be generalized to junctions with more than two reservoirs connected to the junction.[68] In this case the current flowing in lead i is given by

$$I_i \;=\; \frac{2e}{h}\int_{-\infty}^{\infty} dE\, \sum_j \bar{T}_{ij}(E)[f(V_i)-f(V_j)], \tag{2.18}$$

where $\bar{T}_{ij}=\sum_{n,q}|t_{ni}^{qj}|^2$ is the total transmission from lead j and i. In the linear response regime, the current formula reduces to

$$I_i \;=\; \sum_j G_{ij}(V_i-V_j),\; G_{ij}=\frac{2e^2}{h}\bar{T}_{ij}(0). \tag{2.19}$$

In a multiterminal measurement, usually a voltage is applied between two reservoirs and the current is measured, letting the other reservoirs “float”, i.e no current flows into the reservoirs. As an example, for a three terminal junction with a potential difference V applied between reservoir 1 and 2, and reservoir 3 floating, i.e $I_1=-I_2=I$ and $I_3=0$, the linear response conductance becomes

$$G=\frac{h}{2e^2}\frac{I}{V_1-V_2}=G_{12}+\frac{G_{13}G_{12}}{G_{31}+G_{32}}. \tag{2.20}$$

This means that the quantity G_{ij} can not be considered as the conductance between lead 1 and 2 (unless a two terminal junction is considered): one also has to take into account how the conductor is connected to all the reservoirs.

2.2 Scattering and transfer matrices

The incoming and outgoing wavefunction amplitudes are related via the scattering matrix S in Eq. (2.7). It is also possible to relate the wavefunction amplitudes on side 1 and 2,

$$c_i=[a_{i1},a_{i2},...,a_{iN},b_{i1},b_{i2},...,b_{iN}] \tag{2.21}$$

via a transmission matrix M, as

$$c_2=Mc_1,\; M=\begin{pmatrix} m_{11} & m_{12} \\ m_{21} & m_{22} \end{pmatrix}. \tag{2.22}$$

The elements in the transfer matrix can be related to the elements in the scattering matrix as

$$m_{11}=(t^{\dagger})^{-1},\; m_{12}=r'(t')^{-1},\; m_{21}=-(t')^{-1}r,\; (t')^{-1}, \tag{2.23}$$

or the other way around,

$$r=-m_{22}^{-1}m_{21},\; r'=m_{12}m_{22}^{-1},\; t=(m_{11}^{\dagger})^{-1},\; t'=m_{22}^{-1}. \tag{2.24}$$

The transfer matrix matrix is pseudo-unitary, $M^{-1}=\sigma_z M^{\dagger}\sigma_z$, following from the unitarity of the scattering matrix. If time reversal symmetry is conserved in the scattering the transfer matrix obeys $M^{*}=\sigma_x M\sigma_x$. The matrices σ_z and σ_x are the generalized Pauli matrices in left-right lead space.

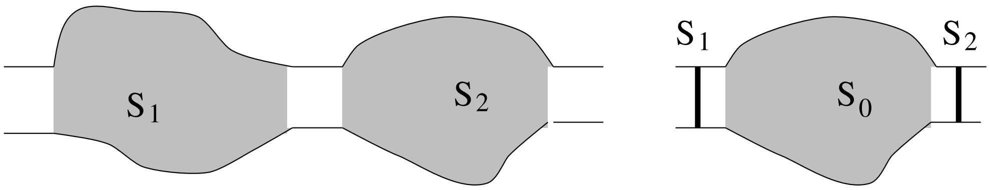

Figure 2.2: Schematic pictures of mesoscopic junctions Left: Two conductors, described by scattering matrices S_1 and S_2, connected via perfect leads. Right: A conductor, described by S_0, connected to nonideal leads containing tunnel barriers, described by S_1 and S_2

2.2.1 Combining matrices

The transfer matrix is very convenient when a system consisting of two or more scatterers in series is considered (see Fig. 2.2). The transfer matrix connecting the wave function amplitudes to the left and the rigth of the series of the scatters is then just given by the product of the transfer matrices; for the scatterers pictured in Fig. 2.2, $M = M_2M_1$ or $M = M_2M_0M_1$. The composition rule for the scattering matrices is more complicated,[60] giving for two scatterers in series

$$S = \tilde{r} + \tilde{t}'\sigma_x(1 - \tilde{r}'\sigma_x)^{-1}\tilde{t}, \tag{2.25}$$

where

$$\tilde{r} = \begin{pmatrix} r_1 & 0 \\ 0 & r_2' \end{pmatrix}, \tilde{r}' = \begin{pmatrix} r_1' & 0 \\ 0 & r_2 \end{pmatrix}, \tilde{t} = \begin{pmatrix} t_1 & 0 \\ 0 & t_2' \end{pmatrix}, \tilde{t}' = \begin{pmatrix} t_1' & 0 \\ 0 & t_2 \end{pmatrix}. \tag{2.26}$$

The reflection and transmission amplitude matrices of the total scattering matrix are then given by

$$\begin{aligned} r &= r_1 + t_1'r_2(1 - r_1'r_2)^{-1}t_1, \\ r' &= r_2' + t_2r_1(1 - r_2r_1')^{-1}t_2, \\ t &= t_2(1 - r_1'r_2)^{-1}t_1, \\ t' &= t_1'(1 - r_2r_1')^{-1}t_2. \end{aligned} \tag{2.27}$$

For three scatterers in a row, which e.g appears when a scatterer is placed between two tunnel barriers, shown in Fig. 2.2, the scattering matrix is given by

$$S = \tilde{r} + \tilde{t}'S_0(1 - \tilde{r}'S_0)^{-1}\tilde{t}, \tag{2.28}$$

i.e the Pauli matrix σ_x is just changed to the scattering matrix S_0 of the middle scatterer.

2.2.2 Nonideal leads

It is worth briefly to discuss the effect of nonideal leads, since tunnel barriers are often present at the lead-reservoir interfaces in the type of junctions studied. It should be pointed out that the term tunnel barrier is used in it's broadest sense, i.e any type of scattering potential, short on the scale of Fermi wavelength, with any transmission probability between zero and unity.

The most relevant example is when the conductor and the reservoirs are made of different materials, as is generically the case e.g in hybrid semiconductor-metal junctions, discussed further below in connection to transport in normal conductor-superconductor junctions. In this case there is an effective potential barrier present, due to the different Fermi velocities in the two materials, with transmission probability given by[55]

$$\Gamma = \frac{4(v_{F1}v_{F2})}{(v_{F1}+v_{F2})^2}, \tag{2.29}$$

where v_{Fi} is the Fermi velocity of the respective materials. Apart from this Fermi velocity mismatch, tunnel barriers may also be present due to bending of the conduction band in the semiconductor at the interface, a so called Schottky barrier, or simply due to imperfect, dirty interfaces from the junction processing.

2.3 Hamiltonian approach to the scattering matrix

As is clear from the discussion above, the current in any mesoscopic conductor can be expressed in terms of the scattering matrix of the conductor. In some idealized cases, e.g for a ballistic, regularly shaped conductor, discussed in the subsequent chapters, the scattering matrix can be found exactly. In most realistic cases it is however not possible to find the exact scattering matrix, and one has to turn to numerical schemes or make some statistical assumption about the distribution of the scattering matrix. The latter approach is taken in Chapter 6 in the thesis and discussed below, the former approach (presented in detail in e.g. Ref. 83) is not considered in this thesis, but constitutes a possible future object of study. In both these cases, however, the way to the scattering matrix goes via the Hamiltonian of the conductor disconnected from the leads.

Assuming we know the eigenstate representation of the Hamiltonian of the closed conductor, we can express the scattering matrix of the conductor coupled to the electron reservoirs via the leads, in terms of this Hamiltonian. This approach was originally developed in nuclear physics[162] and here we merely present the result. The Schrödinger equation in (2.1) can be written in an eigenstate representation

$$H_{tot}|\Psi\rangle = E|\Psi\rangle, \tag{2.30}$$

where the states $|\Psi\rangle$ are the eigenstates of the Hamiltonian, consisting of bound states of the conductor, not coupled to the leads and thus not contributing to the current, and the scattering states discussed above, carrying the current. It is convenient to decompose the Hamiltonian H_{tot} into the Hamiltonian of the closed conductor, the closed leads and the coupling between the conductor and the leads as[235]

$$\begin{aligned} H_{tot} &= \sum_n |n\rangle E\langle n| + \sum_{\mu,\nu} |\mu\rangle H_{\mu\nu}\langle\nu| \\ &+ \sum_{n,\mu} \left(|\mu\rangle W_{\mu n}\langle n| + (|n\rangle W^*_{\mu n}\langle\mu|\right), \end{aligned} \tag{2.31}$$

where the states $\{n\}$ are the propagating states in the leads such that $\langle y_i, x_i|n_i\rangle \propto \Theta_{ni}(y_i)e^{\pm ik_n x_i}$ and the states $\{\mu\}$ are the eigenstates of the Hamiltonian of the closed conductor, $\sum_{\mu,\nu}|\mu\rangle H_{\mu\nu}\langle\nu|$, where thus $H_{\mu\nu} = \langle\mu|H_{tot}|\nu\rangle$. The elements $W_{\mu n} = \langle\mu|H_{tot}|n\rangle$ describe the coupling between the propagating states in the leads and the bound states of the conductor. The scattering state $|\Psi_q\rangle$ from an incoming wave in mode q is found from the Lippman-Schwinger equation and can be expanded in the leads as $|\Psi_q\rangle = \sum_n S_{qn}|n\rangle$. Assuming that the coupling elements of W are independent of energy, the scattering matrix S_{qn} can be written on the form[162]

$$\begin{aligned} S &= 1-2i\pi W^{\dagger}(E-H+i\pi WW^{\dagger})^{-1}W \\ &= (1+i\pi W^{\dagger}(H-E)^{-1}W)(1-i\pi W^{\dagger}(H-E)^{-1}W)^{-1}, \end{aligned} \tag{2.32}$$

where we have defined that in the limit of no coupling, $W=0$, the scattering matrix just reduces to $S=1$, back reflection into the same mode of all electrons incident on the conductor (neglecting a so called background scattering). The scattering matrix in (2.32) is manifestly unitary since it is written on the form $S=(1+iK)(1-iK)^{-1}$ with $K=W^{\dagger}(H-E)^{-1}W$ a Hermitian matrix. An alternative derivation of this scattering matrix relation is given in e.g. Refs. 5, 99. We can note that the eigenvalues of $H+i\pi WW^{\dagger}$, given by $\varepsilon_{\mu}+i\varepsilon_{\mu}$, describes resonances of energies ε_{μ} and widths ε_{μ}, i.e the scattering matrix has poles in the lower complex plane at $\varepsilon_{\mu}+i\varepsilon_{\mu}$.

Thus, if the Hamiltonian of the closed conductor is known (and the coupling elements in W), the scattering matrix of the open conductor can be found. This form turns out to be very useful for the discussion of chaotic quantum dots in Chapter 6, where statistical information on the Hamiltonian is known and the elements of W can be expressed exactly in terms of the transparency Γ_n of the leads connecting the dot to the reservoirs.

2.4 Scattering density of states and dwell times

Above, an expression for the current flowing through the leads connecting the conductor to the electron reservoirs, was derived in terms of the scattering matrix. The scattering matrix can also be used to calculate the global density of states of the conductor, i.e the density of states from all scattering states integrated over the area of the conductor, defined as

$$\rho(E)=\int dA\sum_{qj}|\Psi^{qj}(x,y,E)|^{2}, \tag{2.33}$$

where the total probability density $\sum_{qj}|\Psi^{qj}(x,y,E)|^2$ of the injected electrons at energy E, is obtained by summing over injection leads j and modes q. This quantity is not directly related to transport, but is relevant for understanding the properties of mesoscopic conductors, as further discussed below. The scattering density of states can be expressed in terms of the scattering matrix, following Wigner[245] and Smith,[218] in a way briefly outlined below. First, the Schrödinger equation in (2.1) can be rewritten by taking the derivative with respect to energy and multiplying with the complex conjugated wave function, for a given scattering states $\{jqE\}$ as

$$|\Psi^{qj}|^{2}=-\frac{\hbar^{2}}{2m}\nabla\left([\Psi^{qj}]^{*}\nabla\frac{d}{dE}\Psi^{qj}-\frac{d}{dE}\Psi^{qj}\nabla[\Psi^{qj}]^{*}\right). \tag{2.34}$$

The integration over the conductor area in (2.33) can be converted to an integral along the boundaries of the conductor. Since the wavefunction vanishes everywhere at the boundary except in the leads, the surface integral over the right hand side of Eq. (2.34) reduces to

$$-\frac{\hbar^{2}}{2m}\left(\int_{0,x_1=0}^{W}dy_1-\int_{0,x_2=0}^{W}dy_2\right)\left([\Psi^{qj}]^{*}\frac{d^{2}}{dEdx}\Psi^{qj}-\frac{d}{dE}\Psi^{qj}\frac{d}{dx}[\Psi^{qj}]^{*}\right) \tag{2.35}$$

where positive probability flow is defined in the positive x-direction. Using the orthogonality of the transverse wavefunctions $\Theta_n(y)$ and the matching conditions in Eqs. (2.12) and (2.13) [assuming unity occupation probability], the integral in (2.35) in lead 2, for $x_2 = 0$, is given for an electron injected in mode q in lead 1, by

$$\begin{aligned}\sum_{n=1}^{N} & \left[\frac{1}{\sqrt{k_n}} t_{qn}^{\prime *} e^{-ik_n x} \frac{d^2}{dE dx}\left(\frac{1}{\sqrt{k_n}} t_{qn}^{\prime} e^{ik_n x}\right)\right. \\ - & \left.\frac{d}{dx}\left(\frac{1}{\sqrt{k_n}} t_{qn}^{\prime *} e^{-ik_n x}\right) \frac{d}{dE}\left(\frac{1}{\sqrt{k_n}} t_{qn}^{\prime} e^{ik_n x}\right)\right]_{x_2=0}, \end{aligned} \tag{2.36}$$

where the sum runs over modes n in lead 2. Performing the derivatives and summing over the injection modes q, the expression in Eq. (2.36) becomes

$$-\frac{i}{\pi} \sum_{q,n=1}^{N} t_{qn}^{\prime *} \frac{d}{dE} t_{qn}^{\prime} = -\frac{i}{\pi} \mathrm{tr}\left(t^{\prime \dagger} \frac{d}{dE} t^{\prime}\right). \tag{2.37}$$

Performing the same calculation for lead 1, and also for injection from lead 2, the total density of states becomes

$$\begin{aligned}\rho(E) &= -\frac{i}{\pi} \mathrm{tr}\left(t^{\dagger} \frac{d}{dE} t + r^{\dagger} \frac{d}{dE} r + t^{\prime \dagger} \frac{\partial}{\partial E} t^{\prime} + r^{\prime \dagger} \frac{d}{dE} r^{\prime}\right) \\ &= -\frac{i}{\pi} \mathrm{tr}\left(S^{\dagger} \frac{d}{dE} S\right), \end{aligned} \tag{2.38}$$

expressed directly in terms of the scattering matrix. The expression for the density of states in (2.38) can be rewritten in a convenient way, by noting that the unitary S matrix can be diagonalized as $S = U\lambda U^{\dagger}$, where U is the unitary matrix of the eigenvectors of S and $\lambda = \mathrm{diag}(\lambda_n)$ is a diagonal matrix with the elements, the eigenvalues of S, $\lambda_n = \exp(i\phi_n)$, being numbers with modulus unity, i.e phases. On has

$$\begin{aligned}\rho(E) &= -\frac{i}{\pi} \mathrm{tr}\left(S^{\dagger} \frac{d}{dE} S\right) = -\frac{i}{\pi} \mathrm{tr}\left(U\lambda U^{\dagger}\left[\frac{dU}{dE}\lambda U^{\dagger} + U\lambda \frac{dU^{\dagger}}{dE} + U\frac{d\lambda}{dE}U^{\dagger}\right]\right) \\ &= -\frac{i}{\pi} \mathrm{tr}\left(\frac{d}{dE}[UU^{\dagger}] + \lambda^{\dagger}\frac{d\lambda}{dE}\right) = \frac{1}{\pi}\sum_n \frac{d\phi_n}{dE} = -\frac{i}{\pi}\frac{d}{dE}\ln[\det(S)], \end{aligned} \tag{2.39}$$

where in the last step $\det(S) = \prod_n \lambda_n$ was used. This form of the density of states will be further used in the calculations below. Inserting the Hamiltonian form of the scattering matrix, in (2.32), into Eq. (2.39) we find[99]

$$\begin{aligned}\rho(E) &= -\frac{1}{\pi}\frac{d}{dE}\ln\left[\frac{\det(1 - i\pi W^{\dagger}(E-H)^{-1}W)}{\det(1 + i\pi W^{\dagger}(E-H)^{-1}W)}\right] \\ &= -\frac{1}{\pi}\frac{d}{dE}\ln\left[\frac{\det(1 - i\pi WW^{\dagger}(E-H)^{-1})}{\det(1 + i\pi WW^{\dagger}(E-H)^{-1})}\right] \\ &= -\frac{1}{\pi}\frac{d}{dE}\ln\left[\frac{\det(E-H - i\pi WW^{\dagger})}{\det(E-H + i\pi WW^{\dagger})}\right] = -\frac{1}{\pi}\mathrm{Im\ Tr}\ (E-H+i\pi WW^{\dagger})^{-1}, \end{aligned}$$

where we have used the general relation for any matrices (also rectangular) U and V that $\det(1 - UV) = \det(1 - VU)$ and that $\ln[\det(1-U)] = \mathrm{tr}[\ln(1-U)]$. Noting, as pointed out above, that since the matrix $H + iWW^{\dagger}$ can be diagonalized as $V\mathrm{diag}(\varepsilon_{\mu} + i\varepsilon_{\mu})V^{-1}$, the density of states is given as a number of resonances at energies ε_{μ} with width ε_{μ} due to the coupling to the leads. The scattering density of states thus describes the density of bound states (at E_μ) of the conductor, in the limit of vanishing coupling[85] to the leads, $\varepsilon_\mu \rightarrow 0^+$ (and $\varepsilon_\mu \rightarrow E_\mu$), as

$$\begin{aligned}\rho(E) &= -\frac{1}{\pi}\sum_\mu \mathrm{Im}\,(E - E_\mu + i0^+)^{-1} \\ &= \sum_\mu \delta(E - E_\mu),\end{aligned} \tag{2.40}$$

which is just the sum over δ-functions at the bound state energies.

Moreover, as was the main point of Wigner[245] and Smith,[218] the scattering density of states is directly related to the average time an electron spends in the scattering region, [the sum over all injection leads i and modes n, divided by the total number of modes $2N$ in both leads], such that

$$\tau_w = \frac{\hbar}{i2N}\mathrm{Tr}(S^\dagger \frac{\partial}{\partial E} S). \tag{2.41}$$

One can note that there are in principle two different types of processes contributing to this life time; electrons which are directly back scattered at the lead-conductor interface and electrons which enter the conductor, dwell a certain time in the conductor and then escapes from the conductor. It is the average dwell time τ_d of the latter type of processes that rigorously should be compared to the phase-breaking time τ_ϕ to decide whether the transport is coherent or not, i.e the time an electron spends in the conductor has to be smaller than the phase-breaking time.

CHAPTER 3

Scattering theory for normal conductor-superconductor junctions

An electron in a normal conductor connected to a superconductor cannot enter the superconductor if the energy of the electron is smaller than the excitation gap in the superconductor. Instead, the electron combines with another electron with almost opposite momentum, close to the interface, and forms a Cooper pair which propagates into the superconductor. As a result, a hole is retro reflected back into the normal conductor. This process is known as Andreev reflection[14] after A.F. Andreev who first discussed it in connection with heat transport through normal-superconductor(NS)-interfaces. Andreev reflection is thus the microscopic mechanism for current transport, i.e normal current-supercurrent conversion, through NS-interfaces and can be seen as the underlying mechanism for the so called proximity effect, the modification of the properties of a normal conductor connected to a superconductor.

A detailed, although transparent, approach to transport through NS-interfaces was presented by Blonder, Tinkham and Klapwijk (BTK).[54] It is based on the Bogoliubov-de Gennes (BdG) equation,[100] the equation corresponding to the Schrödinger equation for superconducting systems. The BTK-approach, formulated for one dimensional junctions, is straightforwardly generalized to mesoscopic NS-junctions, and allows one to formulate a generalized Landauer-Büttiker approach to normal conductor-superconductor junctions based on the BdG-equation. Extensions of the Landauer-Büttiker approach to normal conductor-superconducting (NS) systems, with one of the reservoirs in the superconducting state, were formulated in the early nineties, see e.g. Refs. 3, 44, 47, 147, 157, 163, 194, 227, 234.

There is a conceptual difference when two of the reservoirs are in the superconducting state: first the current flowing in the junction becomes dependent on the phase difference between the superconductors; secondly, a Josephson current can flow between the superconducting reservoirs. In a large number of works these SNS-systems have been treated within a scattering approach, focusing on the conductance, see e.g. Refs. 4, 53, 77, 115, 130, 148, 149, 153, 177, 178, the equilibrium Josephson current, see e.g. Refs. 39, 42, 70, 97, 98, 105, 117, 205, 243, 244, or the nonequilibrium Josephson current, see e.g. Refs. 72, 119, 120, 197–199, 233. It should be pointed out that NS and SNS systems have also been analyzed with other techniques, see e.g. Refs. 50, 150 for recent reviews, we however restrict our discussion to the scattering approach to the BdG equation.

In this chapter we outline the extension of the Landauer-Büttiker approach. We treat the case where one or two of the reservoirs are in the superconducting state. We assume here that all superconducting electrodes are at the same potential; a scattering theory for the case with a voltage applied between the superconductors is presented in Chapter 8. We first discuss the general modifications of the Landauer-Büttiker approach that have to be made to take into account superconducting reservoirs. Then the current transport in a NS-junction is considered, with emphasis on the Andreev reflection process. Thereafter a junction with a normal conductor connected to two superconducting reservoirs, an SNS-junction, is considered and the equilibrium Josephson current is studied. Finally, a junction with a normal conductor connected to two superconducting reservoirs and one normal reservoir, a three terminal SNS-junction, is studied, focusing on the Josephson current under nonequilibrium conditions created by quasiparticle injection from the normal reservoir. The scattering theory formulated in the last case is essentially a detailed discussion and extension of the theory presented in Ref. 198.

3.1 Superconductivity and the Bogoliubov-de Gennes equation.

We study the case with junctions consisting of a normal conductor connected to both superconducting and normal conducting reservoirs (see Fig. 3.1)

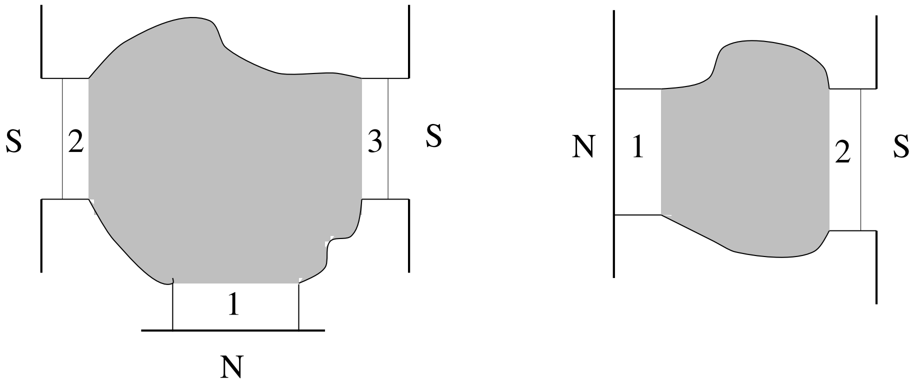

Figure 3.1: A schematic picture two junctions. Left: A mesoscopic scatter connected to one normal and one superconducting lead. Right: A mesoscopic scatter connected to one normal and two superconducting leads, the phases of the superconductors are ϕ_2 and ϕ_3.

It is assumed that the superconducting elements are all at the same potential, equal to zero. The mesoscopic structures containing superconducting elements are then described by the time independent Bogoliubov-de Gennes equation (BdG)[100]

$$\left[\begin{array}{cc} H_0 & \Delta \\ \Delta^* & -H_0^* \end{array}\right]\Psi = E\Psi,\; H_0 = \frac{1}{2m}(i\hbar\nabla + eA)^2 + U - E_F \tag{3.1}$$

where the wavefunction $\Psi = (\Psi_e, \Psi_h)$ has a two-component form. The BdG-equation consists of the Schrödinger equations for electrons and holes, coupled via the superconducting pair potential $\Delta(\mathbf{x})$. The solution to the BdG-equation at negative energies is given by $(-\Psi_h^*, \Psi_e)$. The superconducting pair potential, which in the general case has to be determined self-consistently, is a complex function with modulus Δ and a phase ϕ. It is given by[100]

$$\Delta(\mathbf{x}) = g(\mathbf{x}) \sum_{E>0} \Psi_h^*(\mathbf{x})\Psi_e(\mathbf{x})[1-2f(E)] \tag{3.2}$$

where g is the interaction constant of the BCS theory of superconductivity,[32] $f(E)$ is the Fermi-Dirac distribution function and E runs over all positive energies. The interaction constant is only nonzero in the superconductors and drops to zero over atomic distances in the normal conductor. We thus have $\Delta(\mathbf{x}) = 0$ in the normal conductor. Throughout this thesis we will consider the simplifying approximation for the pair potential in the superconductors, that the pair potential takes on it's bulk value everywhere in the superconductors, $\Delta(\mathbf{x}) = \Delta \exp(i\phi_j)$. This is in line with the assumption of the properties of reservoirs above: the electrodes are large bulk metal electrodes, not affected by the contact to the normal conductor.[158] One aspect of the so called proximity effect, the suppression of the pair potential in the superconductor close to the normal conductor, is thus neglected. The other aspect of the proximity effect, the influence of the superconductor on the properties of the normal conductor, is however fully taken into account by the scattering approach. The magnitude of these induced electron-hole correlations is given by Eq. (3.2), dividing out the interaction constant g.

The presence of a magnetic field has to be taken into account more carefully in junctions containing superconducting electrodes. In general, the problem becomes fully two dimensional (see e.g. Refs. 111, 155), but here we consider a simplified situation relevant to the junctions under discussion.

First, in the case with two superconductors and a Josephson current flowing, we assume that the Josephson self-screening length is much larger than the lateral dimensions of the junction (due to low current density in two dimensional junctions, see e.g Ref. 232); the magnetic field is then uniform across the whole junction and equal to the applied magnetic field.

Secondly, we neglect the variation of the superconducting phase along the NS-interface. The argument for this approximation is different for the two types of junctions studied in the thesis. The first type of junctions, studied in Chapter 4 and 5, contains a one- or two-dimensional ballistic normal conductor. In these junctions, the magnetic field is only used to control the phase difference by threading a magnetic flux, of order of one flux quantum, through a large superconducting loop connecting the two superconducting electrodes. In this case the magnetic field in the normal conductor, which has an area much smaller than the superconducting loop, can be neglected and the vector potential be put to zero in the entire conductor.

In the second type of junction, with the normal conductor consisting of a chaotic dot, the width W of the leads connecting the superconductors and the dot is much smaller than the lateral dimension L of the dot. Moreover, the applied magnetic field which is required to break time reversal symmetry corresponds to a a flux considerably less than one flux quantum through the dot. (see e.g. Ref. 48). The applied magnetic field is expelled from the superconductors due to the Meissner effect by screening currents at the surface of the superconductor. These currents are proportional to the superfluid momentum $p_s = \hbar\nabla\phi/2 - eA = e\lambda B \exp(-x/\lambda)$, where λ is the magnetic field penetration depth, of the order of the lateral size L of the conductor (see e.g. Ref. 232). The gauge invariant phase difference along the NS-interface in the contacts is thus $\gamma_i = \phi_i(y_i = W) - \phi_i(y_i = 0) - (2e/\hbar)\int A\, dl = 2p_s W\hbar = (2e/\hbar)W\lambda B = 2\pi W\lambda B/\Phi_0$, where $\int A\, dl$ is the line integral along the interface and $\Phi_0 = 2e/h$ is the superconducting flux quantum. In line with our assumptions, the magnetic flux $W\lambda B \ll L^2 B \leq \Phi_0$, and we can thus neglect the gauge invariant phase difference along the NS-interface. Equivalently, we can neglect magnetic field in the contacts.

Moreover, in the gauge $A_2 = 0$ and $A_3 = BL\hat{y}$ (i.e working with the gauge $A = Bx\hat{y}$ in the normal conductor, with the lead indices referring to Fig. 3.1), the same as for the normal conductor, the phases ϕ_2 and ϕ_3 can be taken constant. This follows from that, since $p_s \propto B = 0$, we have $\nabla\phi_i = 2e/\hbar A_i$, which gives ϕ_2 constant and $\phi_3 = 2eBLy/\hbar + const$, however, since $BLW \ll BL^2 \approx \Phi_0$, the y-dependent part of ϕ_3 can be neglected. In the case where the phase difference between the superconductors is controlled by threading a magnetic flux Φ' through a large superconducting ring connecting the electrodes, we have the phase difference $\phi_3 - \phi_2 = 2\pi\Phi'/\Phi_0$ (since the line integral $\int A\,dl$ between the superconductors is zero), which depends only on flux through the ring. Since the scattering matrix depends only on magnetic field, the calculated current then depends only on gauge invariant quantities.

To conveniently solve the BdG-equation in the leads, we perform a gauge transformation in lead i,[100]

$$e^{-i\sigma_z\phi_i/2}\begin{bmatrix} H_0 & \Delta \\ \Delta^* & -H_0^* \end{bmatrix} e^{i\sigma_z\phi_i/2}e^{-i\sigma_z\phi_i/2}\Psi_i = Ee^{-i\sigma_z\phi_i/2}\Psi_i. \tag{3.3}$$

Under this transformation the Hamiltonian in the leads is changed

$$H_0 \to \bar{H}_0 = \frac{(i\hbar\nabla + eA + \hbar\nabla\phi_i/2)^2}{2m} + U - E_F = -\frac{\hbar^2\nabla^2}{2m} + U - E_F, \tag{3.4}$$

i.e the vector potential is transformed away since the superfluid momentum is zero in the contacts. The superconducting order parameter transforms as $\Delta\exp(i\phi_i) \to \Delta$ and the transformed wavefunction is

$$\bar{\Psi}_i = e^{-i\sigma_z\phi_i/2}\Psi_i. \tag{3.5}$$

The solution $\bar{\Psi}$ to the transformed BdG equation is discussed in detail below and Ψ is directly obtained from Eq. (3.5).

The superconducting reservoirs have to be treated in a somewhat different way than the normal reservoirs, because the contact between the normal lead and the superconductor cannot be considered as “reflectionless”. Incident electrons are reflected into outgoing holes, Andreev reflected, with a certain probability. To deal with this we insert a short clean superconducting lead, contacting the bulk superconductor, directly at the NS-interface (see Fig. 3.1). The contact between this superconducting lead and the superconducting reservoir is assumed to be “reflectionless”, in the same way as the contact between a normal lead and a normal reservoir. In a superconducting reservoir, this is equivalent to that the contribution to the total junction resistance from the scattering in the superconductor can be neglected, directly applicable e.g. when superconductors are in the clean limit (see discussion and references in Ref. 47). With this technical modification, which does not alter the physical results, the superconducting reservoirs have the same four properties as listed in Chapter 2 for the normal reservoirs.

In the clean leads, the solution to BdG has the form of plane waves,[54] in lead i and mode n given by $\bar{\Psi}_e \propto \tilde{u}\exp(iq_nx_i)$ and $\bar{\Psi}_h \propto \tilde{v}\exp(iq_nx_i)$. Inserting these trial functions into the BdG equation, the spectrum is directly given by

$$E^2 = \varepsilon_q^2 + |\Delta|^2,\ \varepsilon_q = \frac{\hbar^2 q_n^2}{2m} - E_F + E_n, \tag{3.6}$$

which is symmetric around Fermi energy. There are four possible solutions for the wavenumber, $\pm q_n^{\pm}$, with

$$q_n^{\pm} = \sqrt{(2m/\hbar^2)(E_F - E_n \pm \sqrt{E^2 - \Delta^2})}. \tag{3.7}$$

It follows from Eq. (3.6) that the spectrum of the superconductors has a gap, given by twice the modulus of the superconducting pair potential, 2Δ. We will therefore, as is standard, refer to Δ as the superconducting gap. The spectrum is plotted in Fig. 3.2, which also shows the spectrum in the normal conductor, both the electron and hole branch. Note that the value of Δ/E_F is exaggerated for clarity of the figure, in metal superconductors this value is of the order[100] of 10^{-3}. For energies within the superconducting gap, $|E| < \Delta$, the solutions to BdG become exponentially decaying and growing, the wavenumber acquiring an imaginary part $\sqrt{\Delta^2 - E^2}/(\hbar v_F)$. The upper and lower components $\tilde{u}$ and $\tilde{v}$, normalized as $|\tilde{u}|^2 + |\tilde{v}|^2 = 1$, are found by inserting the trial wavefunction into the BdG-equation. For energies $E > \Delta$ and wavenumber $q_n^{\pm}$, they are given by

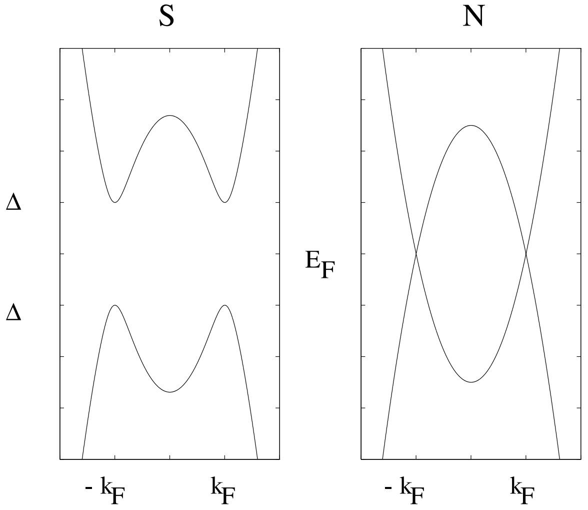

Figure 3.2: The spectrum for a superconductor (right) with a pair potential Δ and a normal metal ($\Delta = 0$), showing both the electron and hole branch. Note that the ratio Δ/E_F is chosen large for clarity.

$$\tilde{u}^2 = 1 - \tilde{v}^2 = \frac{1}{2}\left(1 \pm \frac{\sqrt{E^2 - \Delta^2}}{E}\right) \tag{3.8}$$

and similarly for energies $E < \Delta$, noting that for $|E| < \Delta$, the components are complex. With these definitions, the general solution to the BdG-equation in lead i, a sum of plane waves, can be written on the superconducting side, based on the gauge transformation discussed above,

$$\begin{aligned}\tilde{\Psi}_i &= \frac{1}{\sqrt{u^2 - v^2}} \sum_n \Theta_{in}(y_i) \left(\frac{1}{\sqrt{q_n^e}} \left[\tilde{a}_{in} \begin{pmatrix} u e^{i\phi_i/2} \\ v e^{-i\phi_i/2} \end{pmatrix} e^{i q_n^e x_i} + \tilde{b}_{in} \begin{pmatrix} u e^{i\phi_i/2} \\ v e^{-i\phi_i/2} \end{pmatrix} e^{-i q_n^e x_i} \right] \right. \\ &+ \left. \frac{1}{\sqrt{q_n^h}} \left[\tilde{c}_{in} \begin{pmatrix} v e^{i\phi_i/2} \\ u e^{-i\phi_i/2} \end{pmatrix} e^{i q_n^h x_i} + \tilde{d}_{in} \begin{pmatrix} v e^{i\phi_i/2} \\ u e^{-i\phi_i/2} \end{pmatrix} e^{-i q_n^h x_i} \right] \right). \end{aligned} \tag{3.9}$$

where the transverse wavefunction $\Theta_{2n} = \Theta_{1n}$, with Θ_{1n} given by Eq. (2.4). The wavenumbers are defined as

$$\begin{aligned} q_n^e &= \sqrt{(2m/\hbar^2)(E_F - E_n + \mathrm{sign}(E)\sqrt{E^2 - \Delta^2})} \\ q_n^h &= \sqrt{(2m/\hbar^2)(E_F - E_n - \mathrm{sign}(E)\sqrt{E^2 - \Delta^2})}. \end{aligned} \tag{3.10}$$

The plane-wave wavefunctions in (3.9) are of mixed electron-hole type, describing a quasiparticle. The quasiparticles are called electron(e)- or hole(h) like depending on whether they reduce to electrons or holes in the limit of $\Delta \to 0$ [$u \to 1$ and $v \to 0$]. For positive energies, the wavefunction components u and v are defined as

$$u(+), v(-) = \begin{cases} \sqrt{\frac{1}{2}\left(1 \pm \frac{\sqrt{E^2-\Delta^2}}{E}\right)} & E > \Delta \\ \sqrt{\frac{1}{2}\left(\frac{E}{\Delta} \pm i\frac{\sqrt{\Delta^2-E^2}}{\Delta}\right)} & E < \Delta \end{cases} \tag{3.11}$$

The components at negative energies are given by $u(-E) = u^*(E)$ and $v(-E) = -v^*(E)$. On the normal side the general solution is

$$\begin{aligned} \Psi_i &= \sum_n \Theta_{in}(y_i) \left(\frac{1}{\sqrt{k_n^e}} \left[a_{in} \begin{pmatrix} 1 \\ 0 \end{pmatrix} e^{ik_n^e x_i} + b_{in} \begin{pmatrix} 1 \\ 0 \end{pmatrix} e^{-ik_n^e x_i} \right] \right. \\ &+ \left. \frac{1}{\sqrt{k_n^h}} \left[c_{in} \begin{pmatrix} 0 \\ 1 \end{pmatrix} e^{ik_n^h x_i} + d_{in} \begin{pmatrix} 0 \\ 1 \end{pmatrix} e^{-ik_n^h x_i} \right] \right), \end{aligned} \tag{3.12}$$

where the wavenumbers for electrons and holes are given by

$$k_n^{e,h} = \sqrt{(2m/\hbar^2)(E_F - E_n \pm E)}. \tag{3.13}$$

Note that the normalization of the wavefunctions in Eqs. (3.9) and (3.12) is chosen such that each mode carries the same amount of quasiparticle probability current

$$j_p = \frac{\hbar}{m} \int dy_i \, \mathrm{Im}\left(\tilde{\Psi}_{ei}^* \frac{d}{dx} \tilde{\Psi}_{ei} - \tilde{\Psi}_{hi}^* \frac{d}{dx} \tilde{\Psi}_{hi} \right). \tag{3.14}$$

With this normalization, the scattering matrices of the NS-interfaces, describing the connection of wavefunction coefficients in the normal conductor and the superconductor, are unitary. The unitarity follows from that the BdG equation conserves probability current.[54] This is in contrast to the quasiparticle charge current

$$j_q = \frac{e\hbar}{m} \int dy_i \, \mathrm{Im}\left(\tilde{\Psi}_{ei}^* \frac{d}{dx} \tilde{\Psi}_{ei} + \tilde{\Psi}_{hi}^* \frac{d}{dx} \tilde{\Psi}_{hi} \right), \tag{3.15}$$

which is not conserved in the scattering (consider e.g. an Andreev reflection where an incoming electron is converted into an outgoing hole). In the normal region ($u = 1$) we have just $j_q = e j_p$, as expected.

We choose to work with all energies, both positive and negative, since this allows us, within the same approach, to treat both the equilibrium ground state properties, like the Josephson current, and the nonequilibrium effects. (see e.g. the discussion in Appendix B. in Ref.27). To treat the normal and superconducting reservoirs on equal footing, we assume that the normal reservoirs act as superconducting reservoirs with $\Delta = 0$.

This is similar to the so called generalized semiconductor scheme in Ref. 54, however, we choose the convention to display both electron and hole excitations, i.e solutions to BdG with positive energy, $E > 0$, *above* the Fermi energy. This taken together has two consequences worth pointing out.

1) In a normal reservoir in equilibrium at zero temperature, electrons it and holes below Fermi

energy are occupied with unity probability. Applying a positive voltage at the reservoir, the distribution of electrons (holes) is shifted upwards (downwards).
2) Twice as many particles are injected from the normal reservoirs as in the purely normal case treated above, and to correct for this we do not multiply the current by a factor of two for spin degeneracy, as was done in Eq. (2.14). Note that from the superconductors, only quasiparticles with energies outside the gap are injected.

With these clarifications we can proceed in the same way as with the normal junctions and construct a scattering theory for the transport in the normal conductor-superconductor junctions. The wavefunction amplitude of the electrons is matched at the conductor with the scattering matrix, as described by Eq. (2.7). We see from the BdG-equation, Eq. (3.1), in the normal conductor ($\Delta = 0$), that $\Psi_h^*(-E)$ is a solution to the electron Schrödinger equation [By taking the complex conjugate of the hole Schrödinger equation and changing $E \rightarrow -E$]. Complex conjugation of the wavefunction turns an incoming wave into an outgoing, and vice versa, but hole waves travel in the opposite direction compared to electron waves with the same wave number (see Fig. 3.2 and note that the group velocity $\hbar v = dE/dk$ has the same direction as the probability current), so that the scattering matrix for holes is related to the scattering matrix for electrons as $S_h(E) = S_e(-E)^*$, such that

$$c^h_{out} = S^*(-E)c^h_{in}. \tag{3.16}$$

The last difference between purely normal junctions and junctions with superconducting reservoirs, is that we also have to take the scattering at the NS-interfaces into account. This is done by directly matching the wavefunctions on both sides, further discussed below. This finally gives us the scattering states and from them the charge current, via Eq. (3.15). To avoid problems with the charge current not being conserved in the superconductors, we choose to calculate the current on the normal side of the NS-interfaces or directly on the superconducting side. Below we discuss charge current only, just referring to it as current, since the charge current is the physical quantity measured in experiment.

We first study the two-terminal NS-junction. We then discuss the scattering approach to the Josephson effect in an SNS-junction. Finally, we extend the discussion to a three-terminal Josephson junction, with an additional normal reservoir connected to the normal part of the SNS-junction.

3.2 NS-junction and Andreev reflection

Consider the two terminal junction shown in Fig. 3.1. Electrons and holes are injected from the normal reservoir 1 and electron-like and hole-like quasiparticles from the superconducting reservoir 2. To find the scattering states, and from them the current, we have to match the wavefunctions at the conductor and at the NS-interface in lead 2. At the normal conductor, the amplitudes of the electron and hole wave functions are matched like

$$\begin{pmatrix} b_1 \\ a_2 \end{pmatrix} = S(E)\begin{pmatrix} a_1 \\ b_2 \end{pmatrix}, \quad \begin{pmatrix} c_1 \\ d_2 \end{pmatrix} = S^*(-E)\begin{pmatrix} d_1 \\ c_2 \end{pmatrix} \tag{3.17}$$

The relation between the wavefunction amplitudes at both sides of the NS-interface in lead 2 can be found straightforwardly by matching the wavefuctions over the NS-interface. It is however useful to discuss this procedure in more detail.

At energies within the superconducting gap, $|E| < \Delta$, the electrons and holes incident from the normal lead can not enter into the superconductor, due to the gap Δ in the quasiparticle spectrum. One could then naively expect that the electrons instead would be backreflected. This is however not the case, instead, the electron is back reflected as a hole at the same energy, a process termed Andreev reflection[14] after Andreev who first pointed out this phenomena in a paper on heat transport through NS-interfaces. (equivalently, holes are back reflected as electrons). This is schematically shown in Fig. 3.3 The reflection amplitude can be obtained formally by matching the electron and hole wavefunctions on the normal side to the decaying solutions of the BdG-equation on the superconducting side, giving, the same for each transverse mode,

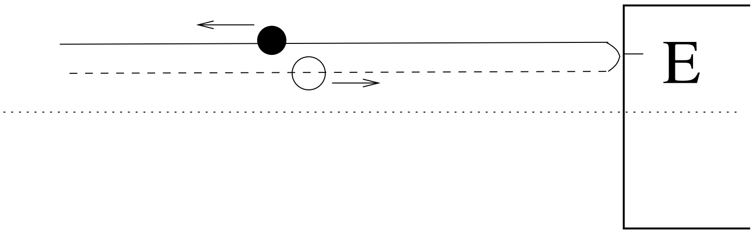

Figure 3.3: A schematic picture of hole (white) being back reflected as an electron (black), an Andreev reflection

$$\begin{aligned} c_2 &= v/ue^{-i\phi_2}a_2, \\ b_2 &= v/ue^{i\phi_2}d_2. \end{aligned} \tag{3.18}$$

From Eq. (3.18) it follows that an electron (hole) Andreev reflected into a hole (electron) picks up a phase $\arg(v/u)$ [a phase since $|v/u| = 1$ for $|E| < \Delta$, see Eq. (3.11)], and in addition the negative (positive) phase of the superconductor ϕ_i. One can note that in real space, all momentum components are reversed, and Andreev reflection is consequently also called retroreflection.

In obtaining the relations in Eq. (3.18), terms of order $\Delta/(E_F - E_n)$, which gives the amplitude for normal back reflection from a perfect NS-interface, have been neglected (sometimes referred to as the Andreev approximation or quasiclassical approximation). For the modes with high transverse mode energies $E_n \leq E_F$, this approximation is no longer accurate, but these modes constitute only a small fraction of all modes, and can be neglected.

For energies outside the gap $|E| > \Delta$, one get the relations

$$\begin{aligned} \begin{pmatrix} b_2 \\ \tilde{d}_2 \end{pmatrix} &= \begin{pmatrix} v/ue^{i\phi_2} & \sqrt{u^2-v^2}/ue^{i\phi_2/2} \\ \sqrt{u^2-v^2}/ue^{i\phi_2/2} & -v/u \end{pmatrix} \begin{pmatrix} d_2 \\ \tilde{b}_2 \end{pmatrix}, \\ \begin{pmatrix} c_2 \\ \tilde{a}_2 \end{pmatrix} &= \begin{pmatrix} v/ue^{-i\phi_2} & \sqrt{u^2-v^2}/ue^{-i\phi_2/2} \\ \sqrt{u^2-v^2}/ue^{-i\phi_2/2} & -v/u \end{pmatrix} \begin{pmatrix} a_2 \\ \tilde{c}_2 \end{pmatrix} \end{aligned} \tag{3.19}$$

i.e there is a finite probability for quasiparticles incident from the normal conductor to escape out into the superconductor.

Andreev reflection is thus the microscopic mechanism for charge transport through NS-interfaces, converting quasiparticle current in the normal conductor into supercurrent in the superconductors. Conversely, this also means that Andreev reflection is the mechanism for the proximity effect, i.e the process that induces superconducting correlations into the normal metal. The total scattering matrix for the NS-junction, connecting amplitudes in lead 1 and in the superconducting part of lead 2, can be written on the general form

$$\begin{pmatrix} b_1 \\ c_1 \\ \tilde{a}_2 \\ \tilde{d}_2 \end{pmatrix} = S_{NS} \begin{pmatrix} a_1 \\ d_1 \\ \tilde{b}_2 \\ \tilde{c}_2 \end{pmatrix}, \; S_{NS} = \begin{pmatrix} r_{11}^{ee} & r_{11}^{he} & t_{21}^{ee} & t_{21}^{he} \\ r_{11}^{eh} & r_{11}^{hh} & t_{21}^{eh} & t_{21}^{hh} \\ t_{12}^{ee} & t_{12}^{he} & r_{22}^{ee} & r_{22}^{he} \\ t_{12}^{eh} & t_{12}^{hh} & r_{22}^{eh} & r_{22}^{hh} \end{pmatrix} \tag{3.20}$$

where the $N \times N$ matrix amplitudes $r_{jj}^{\sigma,\nu}$ and $t_{ji}^{\sigma,\nu}$ are the amplitudes for σ-type quasiparticles, injected in lead j, to reflect (transmit) as ν-type quasiparticles to lead $j(i)$. These amplitudes are possible to derive from the matching equations (3.17)-(3.19), but it turns out that not all of these amplitudes are needed in calculating the current.

For convenience the current is calculated in lead 1 (see Fig. 3.1). The wavefunction for a quasiparticle at energy E in lead i resulting from an σ-like particle injected in lead j and mode q is written $\Psi_i^{nj\sigma}(E)$. The scattering state is analogously labeled $\{Ejq\sigma\}$, i.e an additional index describing the type of quasiparticle is needed to label the state compared to the normal case. The current from a given scattering state flowing in lead i, $I_i^{jq\sigma}(E)$, is given by inserting the scattering state wavefunction into Eq. (3.15) (and performing the integration over y_i),

$$I_i^{jq\sigma}(E) = \frac{e\hbar}{n} \sum_n \left(|a_{in}^{jq\sigma}(E)|^2 - |b_{in}^{jq\sigma}(E)|^2 + |c_{in}^{jq\sigma}(E)|^2 - |d_{in}^{jq\sigma}(E)|^2 \right). \tag{3.21}$$

The amplitudes of the incident electron-(hole-)like quasiparticles from the superconductors are given by $\sqrt{q_q^{e(h)}}\sqrt{u^2 - v^2}$ and from the normal reservoirs by $\sqrt{k_q^{e(h)}}$, both weighted with the respective quasiparticle distribution functions of the reservoirs The potential of the superconductor assumed to be zero, $V_2 = 0$, and the potential at the normal reservoir is set to $V_1 = V$. The current I, calculated in lead 1 and summed over all types of injected quasiparticles in all modes in both leads is then given by

$$I = \int dE \sum_{j,\sigma} i_1^{j,\sigma}(E) f_j^{\sigma}(E), \tag{3.22}$$

where $i_1^{j,\sigma}(E)$ is the current density in lead 1 due to σ-like quasiparticles injected from reservoir j, summed over injection modes, just as in Eq. (2.14), and the distribution functions f_j^e and f_j^h are the Fermi-Dirac distributions for electrons and holes respectively, $f_j^{e(h)} = (1 + \exp[E \mp eV_j])^{-1}$. Since no current flows in equilibrium, $V = 0$, the current expression can be simplified as

$$I = \int dE \left(i_1^{e,1}(E)[f_1^e(E) - f(E)] + i_1^{h,1}(E)[f_1^h(E) - f(E)] \right), \tag{3.23}$$

where $f(E)$ is the Fermi-Dirac distribution at $V = 0$ and the spectral current densities are given by[147]

$$\begin{aligned} i_1^{e,1}(E) &= \frac{e}{h}\left[N - \mathrm{tr}\left(r_{11}^{ee}(r_{11}^{ee})^\dagger - r_{11}^{eh}(r_{11}^{eh})^\dagger \right) \right], \\ i_1^{h,1}(E) &= -\frac{e}{h}\left[N - \mathrm{tr}\left(r_{11}^{hh}(r_{11}^{hh})^\dagger - r_{11}^{he}(r_{11}^{he})^\dagger \right) \right]. \end{aligned} \tag{3.24}$$

The definition of the distribution functions f_j^e and f_j^h shows that the electron- and hole distributions are shifted in opposite directions for an applied potential V, as discussed above. What determines the current density is thus just the scattering amplitudes for injected electron or holes injected from the normal reservoir to be reflected back as electrons or holes. These amplitudes can be expressed conveniently in terms of the scattering amplitudes of the normal conductor and the Andreev reflection amplitudes, like[163]

$$\begin{aligned}
r_{11}^{ee} &= r(E)+\alpha^2 t'(E)r'^*(-E)[1-\alpha^2 r'(E)r'^*(-E)]^{-1}t(E), \\
r_{11}^{hh} &= r^*(-E)+\alpha^2 t'^*(-E)r'^*(-E)[1-\alpha^2 r'^*(-E)r'(E)]^{-1}t^*(-E), \\
r_{11}^{eh} &= \alpha e^{-i\phi_2/2}t'(E)[1-\alpha^2 r'^*(-E)r'(E)]^{-1}t^*(-E), \\
r_{11}^{he} &= \alpha e^{i\phi_2/2}t'^*(-E)[1-\alpha^2 r'(-E)r'^*(-E)]^{-1}t(E),
\end{aligned} \tag{3.25}$$

where we have introduced the scattering phase from the Andreev reflection

$$\alpha = \frac{v}{u} = \begin{cases} (E-\mathrm{sign}(E)\sqrt{E^2-\Delta^2}) = \exp[-\mathrm{arccosh}(E/\Delta)] & |E|>\Delta \\ (E-i\sqrt{\Delta^2-E^2}) = \exp[-i\arccos(E/\Delta)] & |E|<\Delta \end{cases} \tag{3.26}$$

The form in (3.25) is useful since it allows one to find the NS-conductance once the scattering properties of the normal conductor is known. It also shows the electron-hole symmetry relation $i_1^{e,1}(E) = -i_1^{h,1}(-E)$ which allows us to write the current on the form

$$I = \int dE i_1^{e,1}(E)[f_1^e(E)-f_1^h(E)]. \tag{3.27}$$

At low voltages and temperatures, $eV, kT \ll \Delta$, all quasiparticles injected from the normal conductor are contributing to the current, but have to low energy to transmit into the superconductor, i.e $|E| < \Delta_0$, and are inevitably Andreev reflected at the NS-interface. Then, due to probability conservation tr $(r_{11}^{ee}(r_{11}^{ee})^\dagger + r_{11}^{eh}(r_{11}^{eh})^\dagger) = N$, and the current density takes on the simplified form[44, 147, 163, 227]

$$i_1^e(E) = \frac{2e}{h}\mathrm{tr}\left(r_{11}^{eh}(r_{11}^{eh})^\dagger\right). \tag{3.28}$$

For $eV, kT = 0$, the conductance dI/dV becomes, ($\alpha = -i$ for $E = 0$)

$$G_{NS} = \frac{4e^2}{h}\mathrm{tr}\left[t'^\dagger t'(1+r'r'^*)^{-1}t^*t^T(1+r^\dagger r'^T)^{-1}\right]. \tag{3.29}$$

The forms in Eqs. (3.28) and (3.29) are the standard starting expressions for studies of different aspects of the subgap NS-conductance using the scattering approach.

3.3 Equilibrium Josephson current

We now turn to the situation with a normal conductor connected to two equipotential superconducting reservoirs (see Fig. 3.4) at $V_1 = V_2 = 0$, representing an SNS-junction in equilibrium. Both superconductors are assumed to have the same magnitude of the superconducting gap Δ, but the phases ϕ_1 and ϕ_2 may be different. This junction is qualitatively different from the NS-junction studied above, in the sense that an equilibrium current, a Josephson current, can flow between the superconductors if the phase difference $\phi = \phi_2 - \phi_1$ is nonzero. Since the normal conductor is connected to two superconducting reservoirs, quasiparticles with energies inside the gap, $|E| < \Delta$, are trapped in the SNS-well and bound states are formed. For energies outside

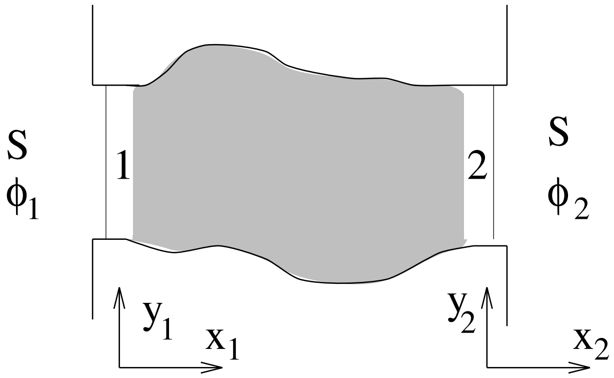

Figure 3.4: A schematic picture of a mesoscopic SNS-junction, a conductor connected to two superconducting reservoirs via ideal leads. The superconductors have phases ϕ_1 and ϕ_2.

the gap, $|E| > \Delta$, the quasiparticles have a finite probability to escape out into the superconductors, and the states form a continuum, just as in the NS-case. The Josephson current is carried both by the bound states and the continuum states,

$$I = I^b + I^c = \sum_n i_n^b(E_n)f(E_n) + \left(\int_{-\infty}^{-\Delta} + \int_{\Delta}^{\infty}\right) dE i^c(E)f(E), \tag{3.30}$$

where we, in line with our approach sum over all states with both positive and negative energies. The bound state current is related to the bound state spectrum in a simple way[39, 214]

$$i_n^b(E_n) = \frac{2e}{\hbar}\frac{dE_n}{d\phi} \tag{3.31}$$

i.e proportional to the derivative of the bound state energy with respect to phase difference ϕ. The continuum current can be calculated within the scattering approach derived earlier, by summing up the current from the scattering states from quasiparticles injected for both superconductors. As further discussed below, it is also possible to relate the continuum and bound state currents to the scattering density of states.

To find the equation for the bound states, the wavefunctions on the normal side of the leads, Ψ_1 and Ψ_2, are first matched across the normal conductor. The matching conditions, given in Eq. (3.17), can be put on a convenient matrix form in line with Ref. 39,

$$\begin{pmatrix} b_1 \\ a_2 \\ c_1 \\ d_2 \end{pmatrix} = S_N \begin{pmatrix} a_1 \\ b_2 \\ d_1 \\ c_2 \end{pmatrix}, \; S_N = \begin{pmatrix} S(E) & 0 \\ 0 & S^*(-E) \end{pmatrix} \tag{3.32}$$

where the block diagonal form of S_N shows that the normal conductor does not mix electrons and holes. The Andreev reflection at the NS-interfaces relates the wavefunction coefficients,

$$\begin{aligned} a_1 = \alpha e^{i\phi_1} c_1, \; d_1 = \alpha e^{-i\phi_1} b_1, \\ b_2 = \alpha e^{i\phi_2} d_1, \; c_2 = \alpha e^{-i\phi_1} a_2, \end{aligned} \tag{3.33}$$

which can be written on a similar matrix form,

$$\begin{pmatrix} a_1 \\ b_2 \\ d_1 \\ c_2 \end{pmatrix} = S_A \begin{pmatrix} b_1 \\ a_2 \\ c_1 \\ d_2 \end{pmatrix}, \; S_A = \alpha \begin{pmatrix} 0 & r_A \\ r_A^* & 0 \end{pmatrix} \tag{3.34}$$

where, with the definition $\phi_1 = -\phi/2$ and $\phi_2 = \phi/2$,

$$r_A = \begin{pmatrix} e^{i\phi/2} & 0 \\ 0 & e^{-i\phi/2} \end{pmatrix}. \tag{3.35}$$

Combining Eqs. (3.32) and (3.34) gives

$$(1 - S_N S_A) \begin{pmatrix} b_1 \\ a_2 \\ c_1 \\ d_2 \end{pmatrix} = 0, \tag{3.36}$$

and thus the bound state equation[39] becomes

$$\det(1 - S_N S_A) = \det(1 - \alpha^2 S(E) r_A S^*(-E) r_A^*) = 0, \tag{3.37}$$

where we have used the determinant relation

$$\det \begin{pmatrix} a & b \\ c & d \end{pmatrix} = \det(ad - aca^{-1}b), \tag{3.38}$$

which holds if $\det(a) \neq 0$. From this bound state equation it is in principle possible to find the bound state energies expressed in terms of the phase difference ϕ, from which the bound state current is given by Eq. (3.31).

The continuum current is calculated by summing up the currents from electron- and hole quasiparticles injected from both sides of the junction. To calculate the continuum current it is convenient first to find the scattering matrix of the total SNS-junction, S_{SNS}, relating the in- and outgoing states in the leads on the superconducting sides of the NS-interfaces. The current is then most easily calculated directly at the superconducting side of the NS-interfaces. It follows that the continuum current density calculated in lead 1, is given by,

$$i^c(E) = i_1^{e,1} + i_1^{h,1} + i_1^{e,2} + i_1^{h,2} \tag{3.39}$$

where the partial current density is given by

$$\begin{aligned} i_1^{e,1} &= \frac{e}{h}\frac{1}{u^2 - v^2}\left[N - \mathrm{tr}\left(r_{11}^{ee}(r_{11}^{ee})^\dagger - r_{11}^{eh}(r_{11}^{eh})^\dagger\right)\right], \\ i_1^{h,1} &= -\frac{e}{h}\frac{1}{u^2 - v^2}\left[N - \mathrm{tr}\left(r_{11}^{hh}(r_{11}^{hh})^\dagger - r_{11}^{he}(r_{11}^{he}))^\dagger\right)\right], \\ i_1^{e,2} &= \frac{e}{h}\frac{1}{u^2 - v^2}\mathrm{tr}\left(t_{21}^{eh}(t_{21}^{eh})^\dagger - t_{21}^{ee}(t_{21}^{ee}))^\dagger\right), \\ i_1^{h,2} &= -\frac{e}{h}\frac{1}{u^2 - v^2}\mathrm{tr}\left(t_{21}^{he}(t_{21}^{he})^\dagger - t_{21}^{hh}(t_{21}^{hh}))^\dagger\right), \end{aligned} \tag{3.40}$$

where the scattering amplitudes $r_{ii}^{\sigma,\nu}$ and $t_{ij}^{\sigma,\nu}$ are defined similarly as in the NS-case in Eq. (3.20). Note that the prefactor $1/(u^2 - v^2) = (1 + \alpha^2)/(1 - \alpha^2) = |E|/\sqrt{E^2 - \Delta^2}$ is just the superconducting density of states. The total continuum current density can then be written, using the unitarity of the scattering matrix S_{SNS},

$$i^c(E) = \frac{e}{2h}\frac{1}{u^2 - v^2}\mathrm{tr}\left(S_{SNS}^\dagger \sigma_z S_{SNS} \sigma_z'\right) \tag{3.41}$$

where $\sigma_z = \mathrm{diag}(1,1,-1,-1)$, the Pauli-matrix in electron-hole space, and $\sigma_z' = \mathrm{diag}\{1,-1,1,-1\}$. The expression for the scattering matrix S_{SNS} in terms of the scattering matrix S of the normal conductor and the Andreev scattering amplitudes can be found in the following way. Matching the wavefunctions at the NS-interfaces gives the following wavefunction coefficient relations, like in Eq. (3.19), on matrix form

$$\begin{pmatrix} a_1 \\ b_2 \\ d_1 \\ c_2 \end{pmatrix} = \frac{u}{\sqrt{u^2-v^2}} \begin{pmatrix} \sqrt{r_A} & 0 \\ 0 & \sqrt{r_A^*} \end{pmatrix} \tilde{c}_{in} + \frac{v}{\sqrt{u^2-v^2}} \begin{pmatrix} 0 & \sqrt{r_A} \\ \sqrt{r_A^*} & 0 \end{pmatrix} \tilde{c}_{out} \tag{3.42}$$

and

$$\begin{pmatrix} b_1 \\ a_2 \\ c_1 \\ d_2 \end{pmatrix} = \frac{u}{\sqrt{u^2-v^2}} \begin{pmatrix} \sqrt{r_A} & 0 \\ 0 & \sqrt{r_A^*} \end{pmatrix} \tilde{c}_{out} + \frac{v}{\sqrt{U^2-v^2}} \begin{pmatrix} 0 & \sqrt{r_A} \\ \sqrt{r_A^*} & 0 \end{pmatrix} \tilde{c}_{in} \tag{3.43}$$

where the coefficient vectors $\tilde{c}_{in} = [\tilde{a}_1, \tilde{b}_2, \tilde{d}_1, \tilde{c}_2]$ and $\tilde{c}_{out} = [\tilde{b}_1, \tilde{a}_2, \tilde{c}_1, \tilde{d}_2]$. Combining these equation with the matching equation at the conductor, the complete scattering matrix, defined from $\tilde{c}_{out} = S_{SNS}\tilde{c}_{in}$, is found to be

$$\begin{aligned} S_{SNS} &= \begin{pmatrix} \sqrt{r_A} & 0 \\ 0 & \sqrt{r_A^*} \end{pmatrix} (1 - S_N S_A)^{-1} (1 - S_A^\dagger S_N^\dagger) S_N \begin{pmatrix} \sqrt{r_A^*} & 0 \\ 0 & \sqrt{r_A} \end{pmatrix} \\ &= \begin{pmatrix} \sqrt{r_A} & 0 \\ 0 & \sqrt{r_A^*} \end{pmatrix} (1 - M)^{-1} (1 - M^\dagger) S_N \begin{pmatrix} \sqrt{r_A^*} & 0 \\ 0 & \sqrt{r_A} \end{pmatrix} \end{aligned} \tag{3.44}$$

where we have introduced $M = S_N S_A$. The scattering matrix S_{SNS} is unitary, which follows upon noting that $MM^\dagger = M^\dagger M = \alpha^2$.

The expression for the continuum current density is then obtained by inserting the expression for the scattering matrix into Eq. (3.41). Noting the anti commutation relation $M\sigma_z + \sigma_z M = 0$, the current density can be written

$$i^c(E) = \frac{e}{2h} \frac{1}{u^2-v^2} \mathrm{tr} \left[\tilde{\sigma}_z (1+M)(1+M^\dagger)^{-1}(1-M^\dagger)(1-M)^{-1} \right]. \tag{3.45}$$

where $\tilde{\sigma}_z = \sigma_z \sigma_z' = \mathrm{diag}\{1,-1,-1,1\}$. Some further matrix algebra, using the fact that M is traceless, i.e tr $(M) = 0$, gives the final expression for the continuum current density

$$i^c(E) = \frac{2e}{h} \mathrm{Re} \left(\mathrm{tr}\, [\tilde{\sigma}_z (1-M)^{-1}] \right) = \frac{2e}{h} \mathrm{Re} \left(\mathrm{tr}\, [\tilde{\sigma}_z (1 - S_N S_A)^{-1}] \right). \tag{3.46}$$

One can note that in the (short dwell-time) regime where the scattering matrix S is independent of energy on the scale of Δ, i.e $S(-E) = S(E)$, the continuum current is zero. This follows from the fact that the matrix expression

$$\begin{aligned} \mathrm{tr}\, [\tilde{\sigma}_z (1 - S_N S_A)^{-1}] &= \mathrm{tr}\, [\sigma_z (1 - \alpha^2 S r_A S^* r_A^*)^{-1} - \sigma_z (1 - \alpha^2 S^* r_A^* S r_A)^{-1}] \\ &= i \mathrm{Im}\, \mathrm{tr}\, [\sigma_z (1 - \alpha^2 S r_A S^* r_A^*)^{-1}] \end{aligned} \tag{3.47}$$

is purely imaginary, i.e. the continuum current density in Eq. (3.46) is zero. Note that we have used that $[1 - \alpha^2 S^* r_A^* S r_A]^* = [1 - \alpha^2 S r_A S^* r_A^*]$ since α is real at $|E| > \Delta$.

3.3.1 Free energy approach and scattering density of states

It is interesting to relate the scattering state approach to the Josephson current, to the free energy approach, discussed in Refs. 33, 39, 42, 43. In the free energy approach, the total Josephson current follows from the general thermodynamical relation[13]

$$I = \frac{2e}{\hbar}\frac{dF}{d\phi}, \tag{3.48}$$

where F is the free energy of the junction. Within our model of the junction, the free energy is given by,[33,43,100]

$$F = -2k_BT\sum_{E>0}\ln[2\cosh(E/k_BT)] + \phi - \text{indep. terms}, \tag{3.49}$$

where the sum runs over all positive energies. Inserting this expression for the free energy into the relation (3.48) for the Josephson current and changing to summation over both positive and negative energies, one get the expression for the current

$$\begin{aligned} I &= \frac{2e}{\hbar}\sum_n \frac{dE_n}{d\phi} f(E_n) \\ &+ \frac{2e}{\hbar}k_BT\left(\int_{-\infty}^{-\Delta} + \int_{\Delta}^{\infty}\right) dE\,\ln[\cosh(E/2k_BT)]\frac{d\rho}{d\phi}, \end{aligned} \tag{3.50}$$

where the sum over the excitation energies has been written as a discrete sum over the bound state energies and an integral over the continuum states, weighted by the continuum density of states $\rho(E)$. The continuum density of states for the SNS-junction is given by the same general formula, Eq. (2.38), as in the purely normal case

$$\rho(E) = \frac{-i}{2\pi}\frac{d}{dE}\ln\left[\det(S_{SNS})\right]. \tag{3.51}$$

Inserting the expression (3.44) for the scattering matrix S_{SNS} into Eq. (3.51), one gets

$$\rho(E) = -\frac{1}{\pi}\frac{d}{dE}\mathrm{Im}\left[\ln\left\{\det(1-M)\right\}\right] + \phi - \text{indep. terms}. \tag{3.52}$$

Inserting this into Eq. (3.50) for the current and performing a partial integration for the continuum current, we get

$$I^c = -\frac{2e}{\hbar\pi}\left(\int_{-\infty}^{-\Delta} + \int_{\Delta}^{\infty}\right) dE \frac{d}{d\phi}\mathrm{Im}\left(\ln\left[\det(1-M)\right] f(E)\right) \tag{3.53}$$

which is on the same form as Eq. (3.30). The continuum current density, identified from Eq. (3.53), can be rewritten as

$$\begin{aligned} i^c(E) &= -\frac{2e}{\hbar\pi}\frac{d}{d\phi}\mathrm{Im}\left[\ln\left\{\det(1-M)\right\}\right] = -\frac{4e}{h}\frac{d}{d\phi}\mathrm{Im}\left[\mathrm{tr}(\ln[1-M])\right] \\ &= -\frac{4e}{h}\mathrm{Im}\left(\mathrm{tr}\left[\frac{dM}{d\phi}(1-M)^{-1}\right]\right) = \frac{4e}{h}\mathrm{Re}\left[\mathrm{tr}\left(\sigma_z'(1-S_NS_A)^{-1}\right)\right] \end{aligned} \tag{3.54}$$

where $\ln(1-M)$ is defined in terms of the series expansion and we have used that $dS_A/d\phi = i/2\check{\sigma}_z S_A$. The second step follows from the identity, using the diagonalization $M = U\lambda U^{-1}$ and that $\det(UV) = \det(U)\det(V)$,

$$\begin{aligned}\ln[\det(1-M)] &= \ln\left[\det(U[1-\lambda]U^{-1})\right] = \ln\prod_n(1-\lambda_n) = \sum_n \ln(1-\lambda_n)\\ &= \mathrm{tr}(\ln[1-\lambda]) = \mathrm{tr}(\ln[1-M]).\end{aligned}\tag{3.55}$$

The current density expression in Eq. (3.54) is precisely the same as found by the scattering approach above in Eq. (3.46), showing that both approaches are equivalent.

Moreover, as was discussed in the preceding chapter, the scattering density of states of an open conductor also gives the bound states of the closed conductor, when adding a small positive imaginary part to the energy,[85] i.e performing an analytic continuation. The same relation holds between the continuum state current and the bound state current of a Josephson junction,[65] which can be seen from the following expression for the continuum current density at energies $|E+i0^+| < \Delta$ (performing a pole expansion)

$$\begin{aligned}i^c(E+i0^+) &= -\frac{4e}{h}\mathrm{Im}\left(\frac{d}{d\phi}\det(1-M)\left[\frac{d}{dE}\det(1\text{-M})(E+i0^+-E_n)\right]^{-1}\right)\\ &= -\frac{4e}{h}\mathrm{Im}\left(\frac{d}{d\phi}\det(1-M)\left[\frac{d}{dE}\det(1\text{-M})\right]^{-1}\frac{1}{\pi}\delta(E-E_n)\right)\\ &= \frac{2e}{\hbar}\sum_n\frac{dE_n}{d\phi}\delta(E-E_n),\end{aligned}\tag{3.56}$$

which intergrated over energy directly gives the result in Eq. (3.30). Using that the current density $e/(\hbar\pi)d/d\phi[\mathrm{Im}(\ln[\det(1-S_N S_A)])]$ is an odd function of energy (follows from that $\det[1-S_N(-E)S_A(-E)] = \det[1-S_N(E)S_A(E)]^*$), the total equilibrium current can then be written

$$I = \frac{e}{\hbar\pi}\frac{d}{d\phi}\int_{-\infty+i0^+}^{\infty+i0^+} dE\,\mathrm{Im}(\ln[\det(1-S_N S_A)])\tanh(E/2kT).\tag{3.57}$$

Generally it holds that scattering matrices are analytic in the upper half complex energy plane (see e.g Ref. 37), and we can therefore close the integration contour (3.57) in the upper half of the plane. The integrand then has poles only at the Matsubara frequencies $\omega_n = (2n+1)i\pi kT$. Summing over the residues one finds

$$I = -\frac{e}{\hbar}2kT\frac{d}{d\phi}\sum_{n>0}\ln(\det[1-S_N(i\omega_n)S_A(i\omega_n)]).\tag{3.58}$$

From the the expression in Eq. (3.57), it can be shown that for conserved time reversal symmetry, i.e $S = S^T$, the current density is an odd function of phase difference. This can be seen in the following way: From Eq. (3.37) we have $\det(1-S_N S_A) = \det(1-\alpha^2 S(E)r_A S^*(-E)r_A^*)$. Moreover, we know that $r_A^T = r_A$, $\det(1-UV) = \det(1-VU)$ and that $\det(U^T) = \det(U)$. For $\phi \to -\phi$, using $r_A(-\phi) = r_A^*(\phi)$, we find

$$\begin{aligned}&\det(1-\alpha^2 S(E)r_A S^*(-E)r_A^*) \to \det(1-\alpha^2 S(E)r_A^* S^*(-E)r_A)\\ &= \det(1-\alpha^2 r_A S^*(-E)r_A^* S(E)) = \det(1-\alpha^2 S(E)r_A S^*(-E)r_A^*),\end{aligned}\tag{3.59}$$

i.e $\det(1-S_NS_A)$ is unchanged. The expression $\det(1-S_NS_A)$ is thus an even function of the phase difference ϕ and accordingly, the current density, proportional to the first derivative with respect to phase difference, is an odd function of ϕ.

To sum up the result of this section, the Josephson current of an SNS-junction with arbitrary normal conductor can be calculated from Eq. (3.57) [or equivalently Eq. (3.58)], as long as the scattering matrix for the normal conductor is known.

3.4 Nonequilibrium Josephson current

With a scattering theory derived for the three cases normal, NS and SNS-junctions, we are ready to proceed to the multiterminal SNS-junctions which constitute the largest part the of the studies presented in this thesis. In the present chapter we study a three terminal junction, shown in Fig. 3.5. This type of junction is analyzed in papers I,II (single mode ballistic),III (wide ballistic) and IV (chaotic). The generalization to e.g. four terminal junctions, studied in paper II, is straightforward. When an SNS-junction is coupled to an additional normal reservoir, the bound states of the SNS-junction are changed into scattering states; therefore the problem of calculating the current in a three terminal junction is conceptually a scattering problem. Since the current flowing through the conductor is conserved, i.e $I_1+I_2=I_3$, there are in principle only two currents to calculate. It is then natural to divide the question of the current flowing in the junction, into two parts. i) what is the current I_1 injected into the junction; ii) What is the net current $(I_2+I_3)/2$ flowing between the superconductors.

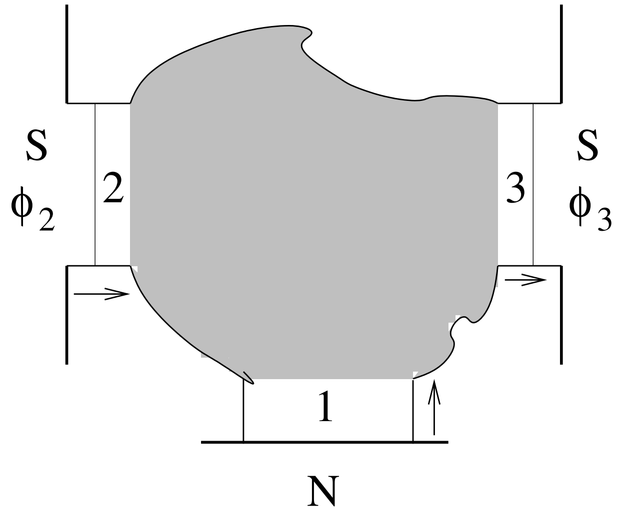

Figure 3.5: A schematic picture of a three terminal mesoscopic SNS-junction, a conductor connected to two superconducting reservoirs and one normal r4eservoir, via ideal leads. The superconductors have phases ϕ_2 and ϕ_3 and the black arrows show the defined positive direction of current flow.

The first problem is similar to finding the current flowing in an NS-junction, with the difference that the current in a three terminal SNS-junction becomes dependent on the phase difference $\phi=\phi_3-\phi_2$ between the superconductors. Experimental studies of this phase dependence in metallic wire junction[188,189] showed that the phase dependent part of the conductance was much larger than predicted in early theoretical work.[7,219] This was one of the reasons for the large interest shown over the last years in these so called Andreev interferometers.

Since no current flows in equilibrium in the lead 1 connected to the normal reservoir, the injection lead, the current in lead one, is given on the same form as the expression as Eq. (3.23),

$$\begin{aligned} I_1 &= \int dE \left(i_1^{e,1}(E)[f_1^e(E) - f(E)] + i_1^{h,1}(E)[f_1^h(E) - f(E)] \right) \\ &= \int dE \left(i_1(E)[f_1^e(E) - f_1^h(E)] \right), \end{aligned} \tag{3.60}$$

where we have defined $i_1(E) = i_1^{e,1}(E) = -i_1^{e,1}(-E)$, with the current densities $i_1^{e,1}$ and $i_1^{h,1}$ given by by Eqs. (3.24); however the expressions for the reflection amplitudes, derived below, are different from the NS-case.

The main focus in this section is on the current flowing between the superconductors. It is most convenient to calculate this current in the normal parts of the leads 2 and 3. In equilibrium $f_1^e = f_1^h = f$, no current flows in the injection lead, and the equilibrium current flowing between the superconductors can be written as

$$I_{eq} = \int dE i_{eq} f(E) \tag{3.61}$$

with the equilibrium current density, given by summing up electron- and hole-like quasiparticles injected from the normal reservoir and from both superconductors at energies outside the gap, $|E| > \Delta$,

$$i_{eq} = (i_2^{1,e} + i_2^{1,h} + i_2^{2,e} + i_2^{2,h} + i_2^{3,e} + i_2^{3,h}) = (i_3^{1,e} + i_3^{1,h} + i_3^{2,e} + i_3^{2,h} + i_3^{3,e} + i_3^{3,h}), \tag{3.62}$$

where we have suppressed the energy notation for the current densities. It follows from current conservation, which holds for every energy, that we can write the total current densities in lead 2 and 3 as

$$\begin{aligned} i_2^{e(h),1} &= (i_2^{e(h),1} + i_3^{e(h),1})/2 - i_1^{e(h)}/2 \\ i_3^{e(h),1} &= (i_2^{e(h),1} + i_3^{e(h),1})/2 + i_1^{e(h)}/2. \end{aligned} \tag{3.63}$$

We introduce the sum and difference current densities

$$\begin{aligned} i^+ &= [i_2^{e,1} + i_3^{e,1} + i_2^{h,1} + i_3^{h,1}]/2 \\ i^- &= [i_2^{e,1} + i_3^{e,1} - (i_2^{h,1} + i_3^{h,1})]/2 \end{aligned} \tag{3.64}$$

and note that one can rewrite

$$(i_2^{e,1} + i_3^{e,1})f_1^e + (i_2^{h,1} + i_3^{h,1})f_1^h = i^+(f_1^e + f_1^h) + i^-(f_1^e - f_1^h). \tag{3.65}$$

The current flowing in the leads $j = 2, 3$ connected to the superconductors, is then given by

$$\begin{aligned} I_{2(3)} &= \int_{-\infty}^{\infty} dE \left(i_{2(3)}^{1,e} f_1^e + i_{2(3)}^{1,h} f_1^h + \left[i_{2(3)}^{2,e} + i_{2(3)}^{2,h} + i_{2(3)}^{3,e} + i_{2(3)}^{3,h} \right] f \right) \\ &= \int_{-\infty}^{\infty} dE \left[\frac{i^+}{2}(f_1^e + f_1^h - 2f) + \frac{i^-}{2}(f_1^e - f_1^h) + i_{eq} f \pm \frac{i_1}{2}(f_1^e - f_1^h) \right] \\ &\equiv I^+ + I^- + I_{eq} \pm I_1/2 \end{aligned} \tag{3.66}$$

where $+(-)$ denotes lead 3(2). With these manipulations, the total current in the three leads are written on a form where each term has a clear physical meaning. The injection current I_1 is the current flowing in lead 1. The current flowing between the superconductors, $I_2 + I_3$, is separated into three currents: I_{eq}, the current flowing in equilibrium, and the two nonequilibrium currents, I^+ and I^-. The reason for dividing the non-equilibrium current into two separate parts is that it is possible to identify I^+ (at $eV < \Delta$) as the *nonequilibrium population* of the states carrying the current in equilibrium. This is clear from Eqs. (3.62) and(3.64), where one sees that the current density $i^+(E)$ is equal to the equilibrium current density $i_{eq}(E)$ for energies within the gap $|E| < \Delta$, where no quasiparticles are is injected from the superconductors. The remaining part of the nonequilibrium current, I^-, has a less transparent physical origin, but it can be described as a quantum interference contribution to the Josephson current, only present in nonequilibrium. It has quantum interference character, since it depends manifestly on the phases of the scattering amplitudes, discussed in detail below. Accordingly, in single mode junctions, as discussed in the next chapter, this current has the same magnitude as all other current components, and dominates the current in certain situations. In large junctions with sufficiently complex scattering, this current is of the order of the single mode current, as discussed in chapter 6, but gives rise to unexpectedly large sample-to-sample fluctuations of the nonequilibrium Josephson current.

In the following section we will calculate the wavefunction coefficients and the resulting current densities, and then rewrite the current expressions in a form convenient for further evaluation.

3.4.1 Wavefunction coefficients and current densities

The electron wavefunction amplitudes are matched at the normal conductor with the scattering matrix as (the direction of positive current flow is shown in Fig. 3.5)

$$\begin{pmatrix} b_1 \\ b_2 \\ a_3 \end{pmatrix} = S(E) \begin{pmatrix} a_1 \\ a_2 \\ b_3 \end{pmatrix}, \; S = \begin{pmatrix} r_{11} & t_{12} & t_{13} \\ t_{21} & r_{22} & t_{23} \\ t_{31} & t_{32} & r_{33} \end{pmatrix}. \tag{3.67}$$

The hole wavefunction amplitude are matched using $S^*(-E)$, just as in Eq. (3.17). It is convenient for subsequent calculations to introduce the following matrices containing parts of the total electron and hole scattering matrices,

$$\bar{S}_N = \begin{pmatrix} \bar{S}_0(E) & 0 \\ 0 & \bar{S}_0^*(-E) \end{pmatrix}, \; \bar{S}_0 = \begin{pmatrix} r_{22} & t_{23} \\ t_{32} & r_{33} \end{pmatrix}, \tag{3.68}$$

$$\mathcal{T} = \begin{pmatrix} t_{12}(E) & t_{13}(E) & 0 & 0 \\ 0 & 0 & t_{12}^*(-E) & t_{13}^*(-E) \end{pmatrix}, \tag{3.69}$$

$$\mathcal{T}' = \begin{pmatrix} t_{21}(E) & 0 \\ t_{31}(E) & 0 \\ 0 & t_{21}^*(-E) \\ 0 & t_{31}^*(-E) \end{pmatrix}, \tag{3.70}$$

and

$$\mathcal{R} = \begin{pmatrix} r_{11}(E) & 0 \\ 0 & r_{11}^*(-E) \end{pmatrix}. \tag{3.71}$$

These matrices are related by the following identities, resulting from the unitarity of S,

$$\begin{aligned} \mathcal{R}\mathcal{T}'^{\dagger} &= -\mathcal{T}\bar{S}_N^{\dagger}, & \mathcal{R}^{\dagger}\mathcal{T} &= -\mathcal{T}'^{\dagger}\bar{S}_N, \\ \mathcal{T}'\mathcal{T}'^{\dagger} &= 1-\bar{S}_N\bar{S}_N^{\dagger}, & \mathcal{T}^{\dagger}\mathcal{T} &= 1-\bar{S}_N^{\dagger}\bar{S}_N \\ \mathcal{R}\mathcal{R}^{\dagger}+\mathcal{T}\mathcal{T}^{\dagger} &= 1, & \mathcal{R}^{\dagger}\mathcal{R}+\mathcal{T}'^{\dagger}\mathcal{T}' &= 1, \end{aligned} \tag{3.72}$$

which are useful in the following discussion. The matching equations at the NS-interfaces can be written, just as in Eq. (3.34), as

$$\begin{pmatrix} a_2 \\ b_3 \\ d_2 \\ c_3 \end{pmatrix} = S_A \begin{pmatrix} b_2 \\ a_3 \\ c_2 \\ d_3 \end{pmatrix}. \tag{3.73}$$

Since the current from the injected quasiparticles can be calculated independently, we first study the current density arising from quasiparticles injected from the normal reservoir.

For the current flowing in lead 1, we need, as is clear from Eq. (3.23), the reflection amplitudes for injected electrons and holes. These are most conveniently expressed in terms of the scattering matrix S' that connects incoming and outgoing electrons and holes at the normal reservoir. It can be found by first writing the outgoing amplitudes b_1 and c_1, from Eq. (3.68) and the corresponding equation for holes,

$$\begin{pmatrix} b_1 \\ c_1 \end{pmatrix} = \mathcal{R}\begin{pmatrix} a_1 \\ d_1 \end{pmatrix} + \mathcal{T}\begin{pmatrix} a_2 \\ b_3 \\ d_2 \\ c_3 \end{pmatrix}. \tag{3.74}$$

Then, from the same equations, writing

$$\begin{pmatrix} b_2 \\ a_3 \\ c_2 \\ d_3 \end{pmatrix} = \bar{S}_N \begin{pmatrix} a_2 \\ b_3 \\ d_2 \\ c_3 \end{pmatrix} + \mathcal{T}'\begin{pmatrix} a_1 \\ d_1 \end{pmatrix} \tag{3.75}$$

and combining this equation with the matching equation at the NS-interfaces, Eq. (3.73), one gets

$$\begin{pmatrix} b_2 \\ a_3 \\ c_2 \\ d_3 \end{pmatrix} = (1-\bar{S}_N S_A)^{-1}\mathcal{T}'\begin{pmatrix} a_1 \\ d_1 \end{pmatrix}. \tag{3.76}$$

Eqs. (3.73), (3.74) and (3.76) straightforwardly gives the scattering matrix S' connecting incoming and outgoing amplitudes from the normal reservoir,

$$S' = \begin{pmatrix} r_{11}^{ee} & r_{11}^{he} \\ r_{11}^{eh} & r_{11}^{hh} \end{pmatrix} = \mathcal{R} + \mathcal{T}(S_A^{\dagger}-\bar{S}_N)^{-1}\mathcal{T}' \tag{3.77}$$

where the same sub- and superscript notation has been used as in Eq. (3.20). Using the same form as in Eq. (3.24), the injection current density i_1 is then given by

$$i_1(E) = i_1^e(E) = -i_1^h(-E) = \frac{e}{h}\left[N - \mathrm{tr}(S'^{\dagger}\sigma_z S'\sigma_{10})\right], \tag{3.78}$$

where $\sigma_{10} = \mathrm{diag}(1,0)$. One can note that at energies far outside the gap, the current density is just the normal current density $(e/h)[N - \mathrm{tr}(r_{11}^\dagger r_{11})]$. At energies within the gap the current density expression simplifies, since the complete Andreev reflection at the NS-interfaces makes S' unitary, and becomes

$$\begin{aligned}
i_1(E) &= \frac{e}{h}\mathrm{tr}[(r_{11}^{eh})^\dagger r_{11}^{eh}] = \frac{e}{h}\mathrm{tr}\left(S^{'\dagger}\sigma_{01}S^{'}\sigma_{10}\right) \\
&= \frac{e}{h}\mathrm{tr}\left(\mathcal{T}'^\dagger(S_A - \bar{S}_N^\dagger)^{-1}\mathcal{T}^\dagger\sigma_{01}\mathcal{T}(S_A^\dagger - \bar{S}_N)^{-1}\mathcal{T}'\sigma_{10}\right) \\
&= \frac{e}{h}\mathrm{tr}\left[(1-\bar{M}^\dagger)^{-1}\sigma_{10}(1-\bar{M}^\dagger\bar{M})(1-\bar{M})^{-1}\sigma_{10}(1-\bar{M}\bar{M}^\dagger)\right],
\end{aligned}$$

where $\sigma_{01} = \mathrm{diag}(0,1)$, $\bar{M} = \bar{S}_N S_A$ and we in the last step have used the matrix identities in Eq. (3.73).

We now turn to the current flowing in the leads 2 and 3 connected to the superconductors, due to quasiparticles injected from the normal reservoir. The matching equations in (3.73)-(3.76) provide an expression for the wavefunction coefficients in lead 2 and 3 in terms of the amplitudes of injected quasiparticles in lead 1. After some matrix algebra, the sum and difference current densities, defined in Eq. (3.64), become

$$\begin{aligned}
i^+(E) &= \frac{e}{2h}\frac{1}{|u|^2}\mathrm{tr}\left(\mathcal{T}^{'\dagger}(1-S_A^\dagger\bar{S}_N^\dagger)^{-1}\sigma_z'(1-\bar{S}_N S_A)^{-1}\mathcal{T}'\right) \\
&= \frac{e}{h}\frac{1}{|u|^2}\mathrm{Re}\left(\mathrm{tr}\left[\sigma_z'(1-\bar{S}_N S_A)^{-1}\right]\right) = \frac{e}{h}\frac{1}{|u|^2}\mathrm{Re}\left(\mathrm{tr}\left[\sigma_z'(1-\bar{M})^{-1}\right]\right) \qquad (3.79)
\end{aligned}$$

and

$$\begin{aligned}
i^-(E) &= \frac{e}{2h}\frac{1}{|u|^2}\mathrm{tr}\left(\mathcal{T}^{'\dagger}(1-S_A^\dagger\bar{S}_N^\dagger)^{-1}\sigma_z'(1-\bar{S}_N S_A)^{-1}\mathcal{T}'\sigma_z\right) \\
&= -\frac{e}{h}\frac{1}{|u|^2}\mathrm{tr}\left(\tilde{\sigma}_z(1+\bar{S}_N S_A)^{-1}(S_A^\dagger\bar{S}_N^\dagger - \bar{S}_N S_A)(1-\bar{S}_N S_A)^{-1}\right) \\
&= -\frac{e}{h}\frac{1}{|u|^2}\mathrm{tr}\left(\tilde{\sigma}_z(1+\bar{M})^{-1}(\bar{M}^\dagger - \bar{M})(1-\bar{M})^{-1}\right)
\end{aligned}$$

where in the second step the matrix identities in Eq. (3.73) have been used. These current density expressions hold for all energies, both inside and outside the gap, and one notes that for energies far outside the gap $|E| \gg \Delta$, where $\bar{M} = 0$, both the sum and difference current densities vanishe. Using the relation $\bar{M}(E) = \sigma_x\bar{M}(-E)\sigma_x$ it is straightforward to show the energy symmetries $i^+(E) = -i^+(-E)$ and $i^-(E) = i^-(-E)$.

Finally we consider the current density due to injected quasiparticles from the superconductors. This current density contributes only to the equilibrium current density, given by Eq. (3.62). Since the equilibrium current density in leads 2 and 3 is the same, it is most convenient to express the contribution from the superconductors, denoted i^s as the halfsum $(i_2 + i_3)/2$ of the current densities in lead 2 and 3,

$$\begin{aligned}
i^s &= \frac{1}{2}(i_2^{2,e} + i_2^{2,h} + i_2^{3,e} + i_2^{3,h} + i_3^{2,e} + i_2^{2,h} + i_2^{3,e} + i_2^{3,h}) \\
&= \frac{e}{2h}\frac{1}{u^2 - v^2}\mathrm{tr}\left(\bar{S}_{SNS}^\dagger\sigma_z\bar{S}_{SNS}\hat{\sigma}_z\right) \qquad (3.80)
\end{aligned}$$

i.e this current density can, just as in the SNS-junction case, be directly expressed in terms of the scattering matrix $\bar{S}_{SNS}$, connecting wavefunction amplitudes in the two superconductors.

The only difference is that the scattering matrix connecting the wavefunction amplitudes in the normal part of the leads 2 and 3, i.e $\bar{S}_N$ defined in Eq. (3.68), is no longer unitary, due to the coupling to the normal reservoir. The scattering matrix $\bar{S}_{SNS}$ is thus given by the same expression as S_{SNS} in Eq. (3.44), with S_N substituted by $\bar{S}_N$. The equilibrium current density in Eq. (3.62), for energies $|E| > \Delta_0$, can then be written, adding the current densities in (3.79) and (3.80), i.e

$$i_{eq} = i^s + i^+. \tag{3.81}$$

With this result, all current densities appearing in the current expressions in Eq. (3.66) have been expressed in terms of scattering matrix elements and Andreev scattering amplitudes, which provides the basis for further analytical and numerical analysis.

3.4.2 Connection to scattering density of states approach

Before turning to such analysis, it is interesting to note that also the sum and difference current densities are possible to express in terms of the scattering matrix for the injected quasiparticles from the normal reservoir. Using the derivative of the scattering matrix with respect to phase difference

$$\frac{d}{d\phi}S' = \frac{i}{2}\mathcal{T}(S_A^\dagger - \bar{S}_N)^{-1}S_A^\dagger\sigma_z'(S_A^\dagger - \bar{S}_N)^{-1}\mathcal{T}'. \tag{3.82}$$

we obtain for the sum current density for energies $|E| < \Delta$

$$\begin{aligned} i^+(E) &= \frac{e}{h}\mathrm{tr}\left[\mathcal{T}'^\dagger(S_A - \bar{S}_N^\dagger)^{-1}\sigma_z'(S_A^\dagger - \bar{S}_N)^{-1}\mathcal{T}'\right] \qquad (3.83) \\ &= \frac{e}{h}\mathrm{tr}\left(\mathcal{T}'^\dagger\left[-\bar{S}_N + (S_A - \bar{S}_N^\dagger)^{-1}(1 - \bar{S}_N^\dagger\bar{S}_N)\right](S_A^\dagger - \bar{S}_N)^{-1}S_A^\dagger\sigma_z'(S_A^\dagger - \bar{S}_N)^{-1}\mathcal{T}'\right) \\ &= \frac{e}{h}\mathrm{tr}\left[\mathcal{R}^\dagger\mathcal{T}(S_A^\dagger - \bar{S}_N)^{-1}S_A^\dagger\sigma_z'(S_A^\dagger - \bar{S}_N)^{-1}\mathcal{T}'\right. \\ &+ \left.\mathcal{T}'^\dagger(S_A - \bar{S}_N^\dagger)^{-1}\mathcal{T}^\dagger\mathcal{T}(S_A^\dagger - \bar{S}_N)^{-1}S_A^\dagger\sigma_z'(S_A^\dagger - \bar{S}_N)^{-1}\mathcal{T}'\right] = \frac{i2e}{h}\mathrm{tr}\left(S'^\dagger\frac{d}{d\phi}S'\right). \end{aligned}$$

This is just the same form as for the continuum current density for the equilibrium Josephson current in Eq. (3.54), and follows from the general relation between the scattering density of states and phase derivative of the scattering matrix discussed above.[2] Along the same lines, the difference current density becomes

$$i^-(E) = \frac{e}{h}\mathrm{tr}\left[\mathcal{T}'^\dagger(S_A - \bar{S}_N^\dagger)^{-1}\sigma_z'(S_A^\dagger - \bar{S}_N)^{-1}\mathcal{T}'\sigma_z\right] = -\frac{i2e}{h}\mathrm{tr}\left(S'^\dagger\frac{d}{d\phi}S'\sigma_z\right). \tag{3.84}$$

In conclusion, we have expressed all current densities entering the nonequilibrium current in terms of the scattering matrix S' for injected electrons and holes from the normal reservoirs. Together with the expression for the equilibrium current we now have all information needed to study the current transport in the three terminal SNS-junction. This study will be performed in the subsequent chapters for systems where either the exact scattering matrix or a statistical distribution for the scattering matrix are known.

CHAPTER 4

Nonequilibrium Josephson current in quantum ballistic junctions

When there is a nonequilibrium quasiparticle population in the normal part of the junction, the properties of the equilibrium Josephson current are very different from the properties of the nonequilibrium Josephson current. The effect of a nonequilibrium quasiparticle distribution in the normal part of SNS junctions was first studied experimentally[241] and theoretically[25,156,250] at the end of the seventies and the beginning of the eighties. These early studies were focused on nonstationary effects of electromagnetic irradiation or applied ac-voltage in long SNS junctions, where nonequilibrium leads to enhancement of the critical current at finite temperature. More recently, a similar problem was studied in classical and quantum superconducting point contacts where the dc Josephson current can be suppressed and even reversed under nonequilibrium.[102,213]

During the nineties it became possible to construct mesoscopic multiterminal SNS-junctions and to study nonequilibrium in the normal part of the junction due to current injection. The effect of the suppression and the reversal of the Josephson current under current injection in multiterminal SNS junctions was first studied theoretically by Van Wees et al.[233] in ballistic junctions and by Volkov[237] in diffusive junctions. Thereafter, there has been a number of theoretical studies regarding different aspects of the nonequilibrium Josephson current, both in ballistic[72,119,120,198,199] and diffusive[240,246,247] systems.

Suppression of the Josephson current due to injection has been experimentally demonstrated in both ballistic[183,207] and diffusive SNS junctions.[175] Very recently, Baselmans et. al.[35] were able experimentally to reverse the direction of the Josephson current. One should also note that an increase of the Josephson current above the equilibrium current was recently demonstrated experimentally by Kutchinsky et al,[146] although it appears that the effect is a result of an assymetric splitting of the phase dependent injection current, an effect originally discovered by Volkov and Pavlovskii.[238] This phase dependent injection current effect was very recently clearly demonstrated experimentally.[211]

Josephson junctions in which the transport in the normal part of the junction is ballistic, are interesting both from theoretical and experimental point of view. Ballistic SNS-junctions are relatively simple to model and study theoretically, and they clearly display the basic physical phenomena associated with the nonequilibrium Josephson effect. The equilibrium (see e.g.

Refs.27, 34, 38, 69, 96, 98, 108, 124, 140, 143, 195, 222, 223, 248, 249) and nonequilibrium (see e.g. Refs.72, 119, 120, 198, 199, 233 Josephson effect as well as the conductance (see e.g. 172, 177, 178, 226) in ballistic Josephson junctions has been studied in a large number of theoretical works.

Also experimentally, over the last years there have been several studies of equilibrium (see e.g. Refs. 1, 112, 176, 182, 193, 206, 228, 229) and nonequilibrium[183, 207] Josephson effects, as well as conductance[173, 174] in ballistic Josephson junctions. The agreement between experiment and theory in ballistic structures has, however, in general not been as good as in diffusive structures. One reason for this is that the theoretical models used have often been to simple to quantitatively describe the structures studied in the experiments. Another reason is that the understanding and controllability of the properties of the interfaces between the normal ballistic conductor and the superconductors still needs improvement.

In this chapter we study in detail both the equilibrium and nonequilibrium Josephson current, as well as briefly the conductance in the most basic ballistic structure, a quantum, single mode junction. This case is from an experimental point of view, having semiconductor heterostructures in mind, somewhat artificial, although there is a continuous strive towards smaller structures. However, the Josephson effect has very recently been studied in truly one dimensional systems like e.g atomic point contacts.[101] Besides the possible direct connection to experiments, a careful study of this single mode junction is, from the point of view of providing physical understanding of the microscopic mechanisms responsible for the current transport, highly rewarding. The contents in the present chapter is essentially a discussion of the results in paper II and III. The nonequilibrium Josephson effect in wide ballistic junctions is studied in the next chapter.

4.1 Spectrum and equilibrium Josephson current in the closed junction

We start by considering a single-mode ballistic normal conductor, with length L and width $W < \lambda_F/2$, placed between two superconducting electrodes, shown in Fig. 4.1. The interfaces between the superconducting electrodes and the normal ballistic junction are assumed to be

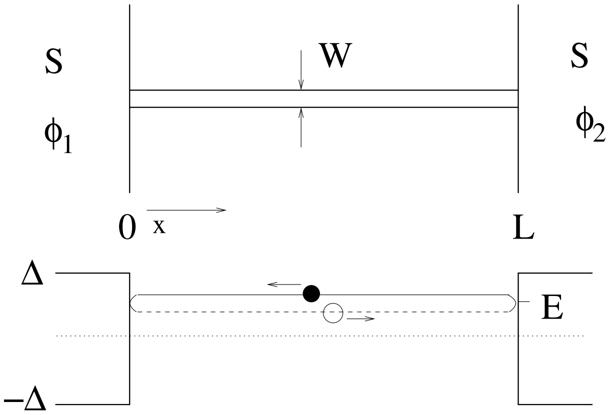

Figure 4.1: Upper part: a schematic figure of a ballistic, single mode SNS-junction. Lower part: An Andreev bound state at energy E, formed by a quasiparticle trapped in the SNS-well. The quasiparticle traverse the junction alternating as a leftgoing electron and a right going hole, transporting current from right to left

ideal, therefore quasiparticles at energies $|E| < \Delta$ Andreev reflect with unit probability at the NS-interfaces. Since quasiparticles with energies within the gap, $|E| < \Delta$, cannot escape out into the superconductors, they are trapped in the SNS-well, forming bound Andreev states. The process where a quasiparticle traverses the junction as a leftgoing electron, Andreev reflect into a hole, traverses the junction back as a hole and finally Andreev reflects back as an electron, is shown schematically in Fig. 2.1. Note that with the chosen hole energy-axis convention, discussed in the previous chapter, it is clear that Andreev reflection is a process that conserves energy, i.e an incident electron at energy E is converted to an outgoing hole with the same energy, and vice versa.

The energy of the bound state is found by the Bohr-Sommerfeld quantization rule, equating the phase picked up traversing the junction one closed cicuit with $2n\pi$. The phases picked up are given by Eq. (3.18), which gives the bound state equation[140]

$$\frac{2EL}{\hbar v_F} + 2\arccos(E/\Delta) \pm \phi = 2n\pi \tag{4.1}$$

where we have expanded th emomentum around Fermi energy, $k^e - k^h = 2E/(\hbar v_F)$, and put the phase difference $\phi = \phi_2 - \phi_1$ ($\pm$ for left/right going electrons). In the short junction limit, $L \ll \hbar v_F/\Delta$, the bound state energy becomes $E = \Delta\cos(\phi/2)$, i.e there is a single bound state at positive energies $E > 0$ and a mirror image of the state at the opposite side of the Fermi energy, $E < 0$. In the long junction limit, $L \gg \hbar v_F/\Delta$, for $E \ll \Delta$, the bound state equation instead become[15] $E = \hbar v_F/L(n\pi \pm \phi)$. Examples of bound state spectra as a function of phase difference ϕ in the long and short limits (with normal scattering in the junction) is shown in Fig. 4.2.

The levels in long junctions come in pairs, with the upper and lower states corresponding to the $\pm\phi$ dependence in the bound state equation. Thus, there are in total $\mathrm{Int}[L/\xi_0]$ pairs of bound states, where the coherence length $\xi_0 = \hbar v_F/L$. This means that the level density, $2L/(\hbar v_F \pi)$ is twice as high as in a corresponding normal quantum well. This holds generally for the spectrum of the BdG-equation 3.1, which takes into account both electrons and holes.

These basic properties of the spectrum does not change if we take into account normal scattering in the junction. The simplest case of normal scattering is to consider a pointlike impurity somewhere in the normal conductor,[27] effectively constituting a potential barrier. The case with normal scattering at the NS-interfaces is studied in the next chapter, in connection with wide ballistic junctions. The spectrum in the case with normal scattering can not be simply found by the Bohr-Sommerfeld argument, but instead we must turn to the general form presented in Eq. (3.37). After some algebra, the bound state equation becomes[27,248]

$$\cos 2\theta = R\cos\chi + D\cos\phi, \tag{4.2}$$

where we, in line with paper II, have introduced the essential phase parameters characterizing the junction

$$\theta = \arccos(E/\Delta) - EL/(\hbar v_F) \tag{4.3}$$

$$\chi = 2El/(\hbar v_F) \tag{4.4}$$

where l is the distance of the impurity measured from the middle of the junction, describing the asymmetry, and D is the transmission probability through the impurity. The bound state spectrum as a function of phase difference is shown for different length limits in Fig. 4.2 One

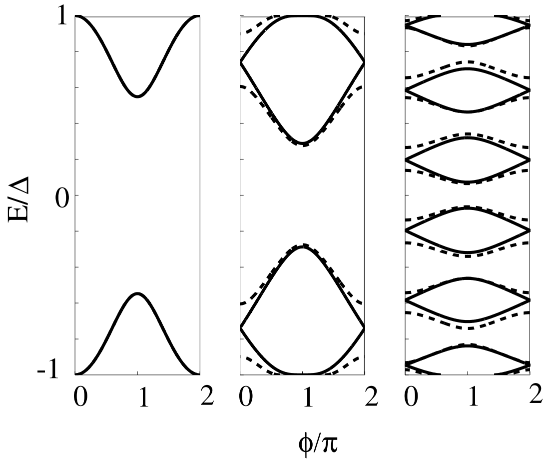

Figure 4.2: Andreev bound state energies as a function of phase difference ϕ for different lengths $L = 0$ (left), L ξ_0 (middle) and L ξ_0 (right) of the junction with $D = 0.7$. Solid lines are for a symmetric junction $l = 0$, dashed for an asymmetric one. A gap opens up in the spectrum at $\phi = 0$ due to the asymmetry.

can note that the spectrum is 2π-periodic and symmetric with respect to phase difference. In a short junctions, the spectrum takes the simple form[96, 144]

$$E = \Delta\sqrt{1 - D\sin^2(\phi/2)}. \tag{4.5}$$

For phase difference $\phi = \pi$, a gap $E_g = \Delta\sqrt{1-D}$ opens up due to the normal scattering. Also for a long junction with a symmetrically placed impurity, $l = 0$, there is a gap at $\phi = \pi$, of size $E_g = (\pi\hbar v_F/2L)\arccos(1-2D)$. Moreover, the spectrum is degenerate at $\phi = 0$, a degeneracy broken for finite asymmetry $l \neq 0$ (see Fig. 4.2). For energies outside the gap, $|E| > \Delta$, the quasiparticles can escape out in the superconductors and the spectrum becomes continuous. Both the bound states and the continuum states carry Josephson current, given by the equation Eq. (3.30), with the bound state current determined directly from the derivative of the bound state energies with respect to phase difference in Eq. (3.31). In the short limit, $L \ll \xi_0$, this derivative is simply

$$dE/d\phi = \Delta\frac{D\sin(\phi)}{4\sqrt{1 - D\sin^2(\phi/2)}} \tag{4.6}$$

while in the long limit, $L \gg \xi_0$, the result becomes

$$\frac{dE^{\pm}}{d\phi} = \pm\frac{\hbar v_F}{L}\frac{\sqrt{D}\sin(\phi)}{4|\sin(\phi/2)|\sqrt{1 - D\sin^2(\phi/2)}}. \tag{4.7}$$

This last expression holds everywhere [with accuracy $O(1/L^3)$] except close to the gap edge, $\Delta - E_n \sim (\hbar v_F/L)(\xi_0/L)$, a distance much smaller than the energy distance $\pi\hbar v_F/L$ between the pairs of levels. Therefore, equation (4.7) can be used for calculation of the currents of all levels except the last pair of levels closest to the energy gap; this will be useful in the following discussion.

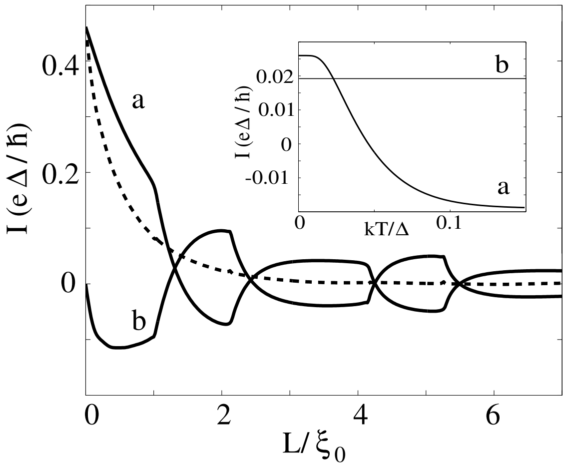

Figure 4.3: The equilibrium bound state (a) and continuum (b) currents and their sum (dashed) as a function of length L for finite $kT = 0.2\Delta$, $D = 0.8$ and $\phi = 3\pi/4$. Inset: The equilibrium bound state and continuum currents as a function of temperature for a long junction $L = 15\xi_0$ with $D = 0.8$ and $\phi = 3\pi/4$.

The continuum current is exactly zero in the short limit, as pointed out in connection to Eq. (3.46), but finite in junctions of finite length. For a symmetrically placed impurity, $l = 0$, the continuum current is given by Eq. (3.46), which after some algebra becomes

$$I^c_{eq} = \frac{e}{h}\left(\int_{-\infty}^{-\Delta} + \int_{\Delta}^{\infty}\right) dE f(E) \frac{4D\sin\phi\sin\beta\sinh 2\gamma_c}{(\cos\beta\cosh 2\gamma_c - R - D\cos\phi)^2 + (\sin\beta\sinh 2\gamma_c)^2}, \tag{4.8}$$

where we have introduced $\gamma_c = \operatorname{arccosh}(E/\Delta)$ in line with paper II. Since the bound state current, in contrast to the continuum current, can be strongly modified under nonequilibrium conditions caused by current injection in the normal part of the junction, it is interesting to study the bound state and continuum parts of the currents separately. In Fig. 4.3, the bound state and continuum currents for a symmetric junction, $l = 0$, are plotted as functions of length. From the figure one sees how the bound state and continuum currents oscillate, to large extent in anti-phase, with a period of oscillation in L of order ξ_0. This behavior is explained by the fact that for increasing junction length, new bound states successively form out of the continuum, starting to contribute to the bound state current instead of the continuum one. The total equilibrium current, however, dies monotonically with increased length, and goes to zero for $kT \gg \hbar v_F/L$.

It is also interesting to study the behavior of the separate currents as a function of temperature for a long junction, shown in the inset in Fig. 4.3. The bound state current decreases from $I^b_{eq}(T = 0)$ to $-I^c_{eq}$, when the temperature is increased from zero to $kT \ll \hbar v_F/L$, while the continuum current is unaffected in this temperature regime, since it is carried by states at energies of order Δ away from Fermi energy. At these temperatures, small compared to Δ, only the states at energies within $\hbar v_F/L$ away from Fermi energy are effected, and one can thus study the effect of temperature on the total Josephson current by just considering the thermal redistribution of the quasiparticle close to Fermi energy, i.e only consider the bound state current.

As discussed in the preceding chapter, the bound state current can be found from the continuum current, by integrating between $-\Delta$ and Δ while adding a small imaginary part to the energy $E \to E + i0^+$, giving the total equilibrium current I_{eq}, written as a sum of Matsubara

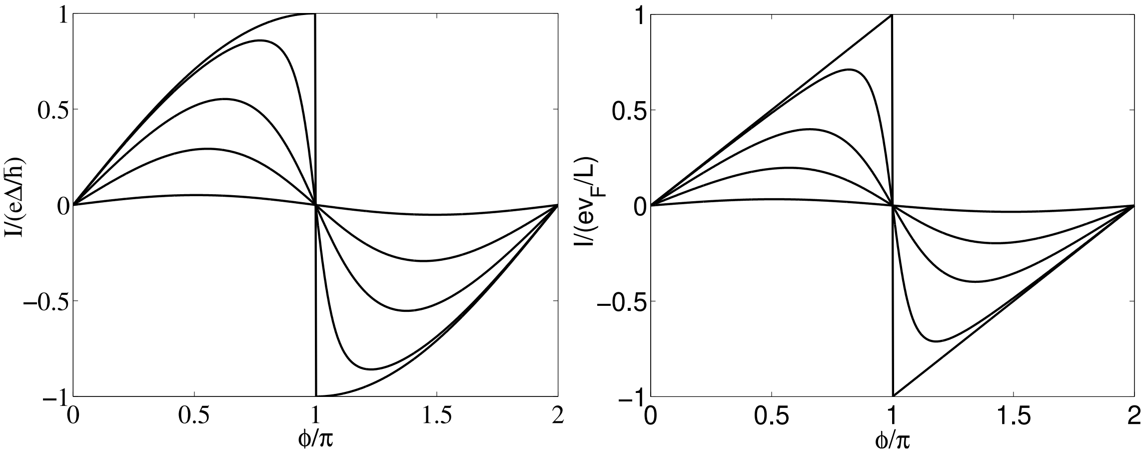

Figure 4.4: The current phase relation for a short (left panel) and long (right panel) junction for different barrier transparencies $D = 0.1, 0.5, 0.8, 0.98$ and $D = 1$. The temperature is zero.

frequencies $\omega_p = (2p+1)i\pi kT$,[222]

$$I_{eq} = I_{eq}^c + I_{eq}^b = \frac{e}{h} 4kT\pi D \sin\phi \times \sum_{p=0}^{\infty} \left\{ \left[\frac{\omega_p}{\Delta} \cosh\left(\frac{\omega_p L}{\hbar v_F}\right) + \sqrt{1+\left(\frac{\omega_p}{\Delta}\right)^2} \sinh\left(\frac{\omega_p L}{\hbar v_F}\right) \right]^2 + 1 - D\sin^2(\phi/2) \right\}^{-1} \quad (4.9)$$

In short junctions, the total current is just given by the bound state current of the single Andreev level, since the continuum current is zero, and one finds the well known[23,96,108,252] relation

$$I_{eq} = \frac{e\Delta}{\hbar} \frac{D\sin\phi}{2\sqrt{1-D\sin^2(\phi/2)}} \tanh\left(\Delta\sqrt{1-D\sin^2(\phi/2)}/2kT\right). \quad (4.10)$$

However, in the long junction, the continuum contributes to the current, and one can find analytical expressions for the two temperature regimes $kT \ll \hbar v_F/L$ and $kT \gg \hbar v_F/L$. For low temperatures the total current monotonously decays with increasing length as $1/L$,[124,222,248]

$$I_{eq}(T=0) = \frac{e}{\hbar}\frac{\hbar v_F}{L} \frac{\sqrt{D}\sin(\phi)\arccos(R + D\cos\phi)}{2\pi|\sin(\phi/2)|\sqrt{1-D\sin^2(\phi/2)}}. \quad (4.11)$$

When the temperature increases, the total current decreases with temperature and becomes exponentially small for $kT \gg \hbar v_F/L$,[140,222]

$$I_{eq}(kT \gg \hbar v_F/L) = \frac{e}{\hbar} 8kTD\sin\phi e^{-2\pi L/\xi_T}, \quad (4.12)$$

where $\xi_T = \hbar v_F/kT$ is the so called normal-metal coherence length. The current phase relation for short and long junctions at zero temperature, for different junction transparencies D, is shown in Fig. 4.4. Note that in the tunnel limit, $D \ll 1$, both the long and short junction currents have a sinusoidal current phase relation, which can be straightforwardly found by taking the $D \ll 1$ limit of Eqns. (4.10) and (4.11).

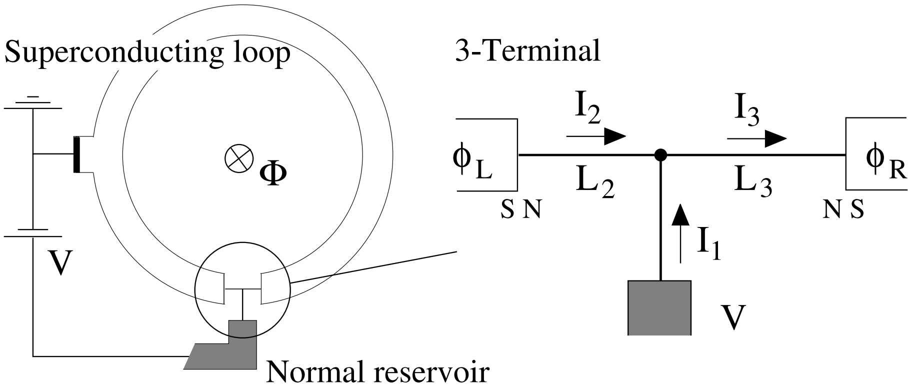

Figure 4.5: A schematic picture of a 3-terminal SNS junction setup, with a normal reservoir attached to the normal part of the junction. The normal reservoir is connected to the superconducting loop (grounded) via a voltage source biased at V. The right figure shows a close-up of the junction area with the arrows showing the direction of the current flow in the junction

4.2 Nonequilibrium Josephson current in three terminal junctions

After this brief presentation of the equilibrium Josephson current in closed two-terminal junctions, we now turn to the situation when the normal part of the junction is connected to a third, normal, reservoir. This system was originally studied by van Wees et al.[233] and has over the last years been extensively studied by several authors.[72,119,120,198] A schematic picture of the junction, with a suggestion of a phase-controlling experimental setup, is given in Fig. 4.5. It should be pointed out that in this section we will only focus on the current as a function of a given phase difference. From an experimental point of view it is cumbersome, although not impossible,[134] to study the current as a function of phase difference, therefore in most experiments the critical nonequilibrium current is the object of study. The critical current is given by the largest possible current one can push between the superconductors, without having a voltage drop over the junction, the phase difference ϕ being allowed freely to adjust to maximize the current (One then normally has a setup which only consists of the broken loop part of the setup shown in the inset in Fig. 4.5). However, as was pointed out in the last section of the preceding chapter, the definition of the critical current is ambiguous in open junctions under injection. A detailed discussion of the critical current and related problems will be given in the next chapter.

The general expressions for the currents flowing in a three terminal junction was derived in the last section of the preceding chapter; in this chapter we just introduce the single mode results, following in a straightforward manner from the general current expression after some algebra.

When a normal reservoir is coupled to the normal part of the junction, the system is open and the current flowing is entirely carried by scattering states, i.e there are only continuum states and no bound states. In the limit where the normal reservoir is weakly coupled to the normal part of the junction, discussed in detail below, the states at energies within the gap $|E| < \Delta$ have a small width $\propto \varepsilon$, where ε is the coupling strength, defined below in Eq. (4.13). In this limit, the current transport in the junction can be described in terms of resonant transport through broadened Andreev levels, where the properties of the resonant Andreev levels to large extent can be found from the properties of the bound Andreev state.

There is however one important exception from this rule, which was the main discovery in paper I. As discussed in the preceding chapter, in nonequilibrium, the I^- current contains a

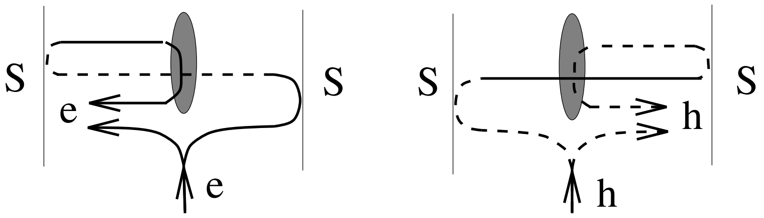

Figure 4.6: Two lowest order paths for an injected electron (solid) or a hole (dashed) at a resonance. The grey ellipse denotes the effective scatterer due to the three lead connection. The difference of the currents due to these processes is proportional to $\mathrm{Im}(rd^*)\sin\phi$, the first order term of the anomalous current

part, in this chapter called the anomalous current I_a, which depends manifestly on the properties of the contact of the third normal reservoir to the junction, and can thus not be expressed in terms of the two-terminal bound state current. The single-mode, three-terminal junction, is a very convenient model to study the anomalous current and to understand it's basic properties. Qualitatively, one can understand the origin of the anomalous current by considering the lowest order quasiparticle giving rise to the current.

Consider a resonant state where the most of the electrons move to the left and the holes to the right, only a fraction of them travelling in the opposite direction due to normal scattering at the connection point, described by reflection and transmission amplitudes r and d, defined below in Eq. (4.13). An injected electron gives rise to a leftgoing electron in lead 2 with the amplitude $1+e^{i\phi_3}d^*e^{-i\phi_2}r$ with $\phi=\phi_3-\phi_2$ (not taking into account electron and hole dephasing or the energy dependent phase picked up when Andreev reflecting) thus giving a contribution to the current of order $1+RD+\mathrm{Re}(rd^*e^{i\phi})$ (see inset in Fig. 4.6). Correspondingly, an injected hole gives rise to a rightgoing hole in lead 3 with amplitude $1+e^{-i\phi_L}de^{i\phi_R}r^*$ and a contribution to the current of order $1+RD+\mathrm{Re}(rd^*e^{-i\phi})$ (see right figure in inset in Fig. 4.6). The difference between the currents from injected electrons and holes thus contains a part proportional to $\mathrm{Re}[rd^*(e^{i\phi}-e^{-i\phi})]=2\mathrm{Im}(rd^*)\sin(\phi)$, which is the leading term in the anomalous current. At a resonant state where the particles move in opposite directions, i.e the electrons to the right and the holes to the left, we find from the same arguments that the anomalous current is again proportional to $2\mathrm{Im}(rd^*)\sin(\phi)$, *with the same sign*. The anomalous current thus flows in the same direction for all resonances, in contrast to the equilibrium Josephson current which changes sign from one level to the next, as further discussed below. In the limit of weak coupling the IVC for I_a is thus a staircase, saturating at $eV>\Delta$ due to the absence of sharp resonances for energies above the superconducting gap. This has a dramatic effect in long junctions, $L\gg\xi_0$, which has many Andreev levels but a small equilibrium current.

To quantitatively study the current, we introduce the phenomenological scattering matrix[67] for the three lead coupling point, assuming energy independent scattering amplitudes,

$$S=\begin{pmatrix}\sqrt{1-2\varepsilon} & \sqrt{\varepsilon} & \sqrt{\varepsilon}\\ \sqrt{\varepsilon} & r & d\\ \sqrt{\varepsilon} & d & r\end{pmatrix}, \tag{4.13}$$

where r and d are complex reflection and transmission amplitudes for scattering between lead 2 to lead 3, and $\sqrt{\varepsilon}$ is the scattering amplitude from the injection lead 1 to leads 2 or 3 (see Fig. 4.5). Due to unitarity of S, the scattering amplitudes obey the relations $Re(rd^*)=-\varepsilon/2$ and $D+R=1-\varepsilon$ ($D=|d|^2, R=|r|^2$). The coupling parameter is thus limited $0\leq\varepsilon\leq0.5$. Moreover, $\mathrm{Im}(rd^*)=\sigma\sqrt{RD-\varepsilon^2/4}$, with $\sigma=\pm1$ dependent on the phase of the scatterer. For simplicity the coupling parameter ε is chosen real and positive. The total scattering matrix for the ballistic junction, which is the scattering matrix entering the general current expressions, is then found in a straightforward way, since the quasiparticles propagate ballistically between the connection point and the NS-interfaces. It should be emphasized that the scattering matrix in (4.13) differs from the scattering matrix used in other studies[72,119,120,233] in the sense that the scattering amplitudes r and d are complex, i.e. include scattering phase shifts. This turns out to be crucial for the observation of the anomalous current, as discussed further below.

We now define, in line with paper *II*, the additional energy dependent phases $\gamma = \arccos(E/\delta)$ and $\beta_{2,3} = 2EL_{2,3}/(\hbar v_F)$, noting that the asymmetry parameter is $l = L_3 - L_2$. The current densities of the scattering states in leads 2 and 3 from electrons $i^e_{2,3}$ and holes $i^h_{2,3}$ are then given by

$$\begin{aligned} i_2^{e,h} \;=\; & -\frac{e}{h}\frac{\varepsilon}{Z}\Big\{2D\sin\phi\sin 2\theta \pm \Big[\sigma 2\sqrt{RD-\varepsilon^2/4}\sin\phi(\cos\chi-\cos 2\theta) \\ & +\varepsilon\left[1-\cos(2\gamma-\beta_2)+\cos\phi(\cos\chi-\cos 2\theta)\right]\Big]\Big\} \end{aligned} \tag{4.14}$$

$$\begin{aligned} i_3^{e,h} = \;& -\frac{e}{h}\frac{\varepsilon}{Z}\Big\{2D\sin\phi\sin 2\theta \pm \Big[2\sigma\sqrt{RD-\varepsilon^2/4}\sin\phi(\cos\chi-\cos 2\theta) \\ & -\varepsilon\left[1-\cos(2\gamma-\beta_3)+\cos\phi(\cos\chi-\cos 2\theta)\right]\Big]\Big\} \end{aligned} \tag{4.15}$$

with the superscript $e(h)$ related to $+(-)$ and where

$$Z = [(1-\varepsilon)\cos 2\theta - R\cos\chi - D\cos\phi]^2 + \varepsilon^2\sin^2 2\theta. \tag{4.16}$$

From Eqs. (4.14) and (4.15) it follows that the sum of the electron and hole current densities, $i^+ = i^e + i^h$, are equal in leads 2 and 3, giving the sum current density

$$i^+ = i_3^+ = i_2^+ = -\frac{4e}{h}\frac{\varepsilon}{Z}\left\{D\sin\phi\sin 2\theta\right\}. \tag{4.17}$$

The difference between the current density due to injected electrons and holes in leads 2 and 3 are not equal, however. We therefore define the anomalous current density i_a as that part of the difference current density which survives in the limit $\varepsilon \to 0$,

$$i_a = -\sigma\frac{4e}{h}\frac{\varepsilon}{Z}\left\{\sqrt{RD-\varepsilon^2/4}\sin\phi(\cos\chi-\cos 2\theta)\right\} \tag{4.18}$$

The injection current density $i_{inj} = i_3^- - i_2^-$, denoted i_1 in the general derivation in Eq. (3.60), is given by,

$$i_{inj} = \frac{4e}{h}\frac{\varepsilon^2}{Z}\left\{\sin^2\chi + (\cos\chi+\cos\phi)(\cos\chi-\cos 2\theta)\right\} \tag{4.19}$$

and splits asymmetrically between the two horizontal arms 2 and 3,

$$i_{inj2,3} = \pm\frac{2e}{h}\frac{\varepsilon^2}{Z}\left\{1-\cos(2\theta-\beta_{2,3})+\cos\phi(\cos\chi-\cos 2\theta)\right\} \tag{4.20}$$

This gives the connection to the difference current density i^-, defined in Eq. (3.64), as $i^- + i_{inj}/2 = i_a + i_{inj3}$ and thus $i^- - i_{inj}/2 = i_a - i_{inj2}$. From the relations $i^+(E) = -i^+(-E)$ and $i^-(E) = i^-(-E)$ one can calculate the current densities for all energies inside the gap $|E| < \Delta$.

The corresponding current densities, for energies $|E| > \Delta$, is calculated in the same way. However, in the following discussion we focus on the weak coupling limit, for which the continuum contributions take on a simple form, further discussed below. The full formulas for the continuum current density for a symmetric junction $l = 0$ are presented in Appendix A in paper II.

The total current is thus divided into four different currents, I_{eq}, I^+, I_a and I_{inj}, with distinctly different physical behavior. To make connection to the notation in paper *II*, we will refer to the sum current, I^+, as the regular current I_r.

4.2.1 Weak coupling limit

As discussed above, in the limit of weak coupling, $\varepsilon \ll 1$, the injection current can be neglected, and the part of i^- flowing between the superconductors is exactly i_a. Moreover, the current densities i_a and i^+ for energies outside the gap are negligible, due to the absence of sharp resonances; the only continuum contribution arises from the quasiparticles injected from the superconductors, which is just the equilibrium continuum current, given in Eq. (4.8). In the following discussion on the nonequilibrium current we focus on this weak coupling limit and only discuss the large coupling limit in connection with the injection current separately treated below.

In the limit of small coupling to the reservoir, $\varepsilon \ll 1$, the Andreev resonances are very sharp, and the current densities can be calculated by evaluating the expression ε/Z appearing in the Eqs. (4.17)-(4.19), in the limit $\varepsilon \to 0$, which gives

$$\lim_{\varepsilon \to 0} \frac{\varepsilon}{Z} = \sum_{n,\pm} \frac{\pi}{D|\sin\phi \sin 2\theta|} \left| \frac{dE}{d\phi} \right| \delta(E - E_n^{\pm}). \tag{4.21}$$

Here $E_n^{\pm}$ are the energies of the bound Andreev states ($\pm$ labeling upper ($+$) and lower ($-$) level in the pair, see Fig. 4.2). To calculate the current densities, information about the bound state energies in Eq. (3.37) as well as about the derivative of the energy with respect to phase difference is thus needed. One can note that the bound state energies are given by the zeros of the denominator Z [given in Eq. (4.16)] at $\varepsilon = 0$. Inserting the expression (4.21) into Eq. (4.17), the equilibrium bound state current density is given by the expression in Eq. (3.56), which after integration over energy gives Eqs. (3.31) and (3.30). The regular current is similarly given by

$$I_r = \frac{e}{\hbar} \sum_{n,\pm} \frac{dE_n^{\pm}}{d\phi} \left[f^e(E_n^{\pm}) + f^h(E_n^{\pm}) - 2n_F(E_n^{\pm}) \right]. \tag{4.22}$$

The anomalous current density i_a is obtained by inserting Eq. (4.21) into (4.18), which after integration over energy results in the anomalous current

$$I_a = -\sigma \frac{e}{\hbar} \mathrm{sgn}(\sin\phi) \sqrt{RD} \sum_{n,\pm} \frac{\cos\chi - \cos\phi}{|\sin 2\theta|} \left| \frac{dE_n^{\pm}}{d\phi} \right| \left[f^e(E_n^{\pm}) - f^h(E_n^{\pm}) \right], \tag{4.23}$$

having the form of a sum over bound state contributions, since it turns out that the anomalous continuum current density is exactly zero in the weak coupling limit. Note that the anomalous current, in contrast to the regular current, is proportional to the modulus $|dE/d\phi|$, i.e proportional to the modulus of the current carried by each Andreev level. As is also seen in Eq. (4.23), the anomalous current is proportional to $\sigma\sqrt{RD} = \mathrm{Im}(rd^*)$ and is thus exactly zero if one consider a phenomenological scattering matrix with only real scattering amplitudes, as discussed above in connection with Eq. (4.13).

The injection current I_{inj} goes to zero for $\varepsilon \ll 1$. We approximate the injection current in the weak coupling limit by the first order term in ε, obtained by inserting the expression for ε/Z in the zero coupling limit into Eq. (4.21)

$$I_{inj} = \varepsilon\frac{8e}{\hbar}\sum_{n,\pm}\frac{\sin^2\chi + D(\cos\chi - \cos\phi)^2}{|\sin 2\theta|}\left|\frac{dE_n^{\pm}}{d\phi}\right|\left[f^e(E_n^{\pm}) - f^h(E_n^{\pm})\right] \tag{4.24}$$

which, just as the anomalous current, is proportional to the modulus $|dE/d\phi|$.

4.2.2 Short junction limit

For a short junction, $L, l \ll \xi_0$, the equilibrium current is given by Eq. (4.10). The regular current, describing the nonequilibrium population of the Andreev levels, is given by

$$I_r = \frac{e\Delta}{\hbar}\frac{D\sin\phi}{4\sqrt{1 - D\sin^2(\phi/2)}}g(E_0), \tag{4.25}$$

where $g(E) = \tanh[(E+eV)/2kT] + \tanh[(E-eV)/2kT] - 2\tanh(E/2kT)$, and where E_0 is the bound state energy given by Eq. (4.5). The anomalous current follows from Eqs. (4.23) and (4.6)

$$I_a = \frac{e}{\hbar}\frac{\sigma D\sqrt{R}\sin\phi|\sin(\phi/2)|}{1 - D\sin^2(\phi/2)}h(E_0), \tag{4.26}$$

where $h(E) = \tanh[(E-eV)/2kT] - \tanh[(E+eV)/2kT]$. At zero temperature and zero applied bias, only the level with negative energy $-E_0$ is populated. For an applied a voltage bias $V > 0$, the electron (hole) population is shifted upwards (downwards) in energy. When the voltage $eV = E_0$, the resonant level becomes populated and there is an abrupt jump of the current. The regular part of the current, I_r, jumps an amount $\delta I_r = -I_{eq}$, thus cancelling the equilibrium Josephson current, a feature which has recently been observed in experiments in wide, short ballistic junctions[207] The anomalous current jumps by the amount

$$\delta I_a = \sigma\frac{e\Delta}{2\hbar}\frac{\sqrt{R}D\sin\phi|\sin\phi/2|}{1 - D\sin^2(\phi/2)}. \tag{4.27}$$

and thus constitutes the total current of the junction. This is shown in Fig. 4.7. The effect of finite temperature in a short junction is merely to smear the steps in the IVC. From this result one can draw the conclusion that in single mode junctions, the anomalous current, strongly dependent on the phases of the scattering amplitudes, is crucial for a correct understanding of the total current. One can extend the discussion to a symmetric $l = 0$ junction in the tunnel limit $D \ll 1, \beta/2 \gg \sqrt{D}$, with two Andreev levels at positive energy (see Fig. 4.2). In this limit, the individual levels carry currents of order $\sqrt{D}$, while the equilibrium current is of order D, which allows for a nonequlibrium current $\sqrt{D}$ larger than the equilibrium current, a so called giant Josephson effect.[243]

4.2.3 Josephson current of a long junction

We now focus on the Josephson current in a long ($L \gg \xi_0$) symmetric ($l = 0$) junction. In principle, the junction length is limited by the requirement that the injected quasiparticles must not scatter inelastically in the junction, $L \ll \varepsilon l_i$, where l_i is the inelastic scattering length.

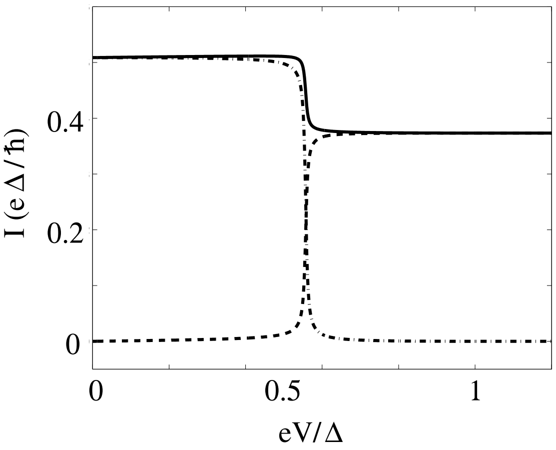

Figure 4.7: The currents $I_{eq}+I_r$ (dash-dotted), I_a (dashed) and the total Josephson current $I_{eq}+I_r+I_a$ (solid) in the horizontal leads 2 and 3 as a function of voltage V at $T=0$ for a short junction $L=0$ with $D=0.8, \phi=3\pi/4, \varepsilon=0.01$ and $\sigma=$ (1. The total current is I_{eq} for $eV<E_0$ and δI_a for $eV>E_0$.

The equilibrium current is presented for the two limiting temperature cases, $kT \ll \hbar v_F/L$ and $kT \gg \hbar v_F/L$, in Eqs. (4.11) and (4.12). To get the regular current, we need the derivative of energy with respect to phase, given by Eq. (4.7) which holds for all energy levels except the pair of levels closest to the gap Δ. Treating this pair of levels on a separate footing, we get the regular current

$$I_r = \frac{e}{\hbar}\frac{\hbar v_F}{2L}\frac{\sqrt{D}\sin(\phi)}{2|\sin(\phi/2)|\sqrt{1-D\sin^2(\phi/2)}}\sum_{n=0}^{N-1}[g(E_n^-)-g(E_n^+)]+\frac{i^*}{2}g(\Delta). \qquad (4.28)$$

where $E_n^\pm$ are the bound state energies given by Eq. (3.37) and i^* is the current carried by the last pair of levels. The regular current I_r jumps up or down every time $eV=E_n^\pm$ [see Fig. 4.8], and the sum of the regular and equilibrium currents, I_r+I_{eq}, changes sign at each jump. This change of sign of the current due to nonequilibrium population of the Andreev levels is the microscopic mechanism underlying the so called π-junction behavior, recently observed in diffusive wire junctions[35] and in line with theoretical predictions for diffusive junctions.[237,240,246,247] In an earlier experiment[175] on a similar structure, only a gradual suppression of the current with injection voltage was observed, presumably due to heating effects from inelastic scattering. This π-junction behavior has not yet been observed in ballistic junctions, most probably due to the fact that only short junctions have been studied experimentally.[206,207]

From Fig. 4.8 it is clear that the oscillations of the current are suppressed by temperatures $kT \gg \hbar v_F/L$. At zero temperature one finds from Eq. (4.28) that each current jump has the magnitude

$$\delta I_r = \frac{e}{\hbar}\frac{\hbar v_F}{L}\frac{\sqrt{D}\sin(\phi)}{2|\sin(\phi/2)|\sqrt{1-D\sin^2(\phi/2)}} \qquad (4.29)$$

At voltages $eV>\Delta$, the regular current is the sum of all states in the range $0<E<\Delta$, which is just $-i^*$, since the current from each pair of levels $\{n,\pm\}$ is zero, with an accuracy of order $1/L^3$, as is clear from Eq. (4.7). The current i^* is thus, with the same accuracy, equal to the zero temperature bound state current.

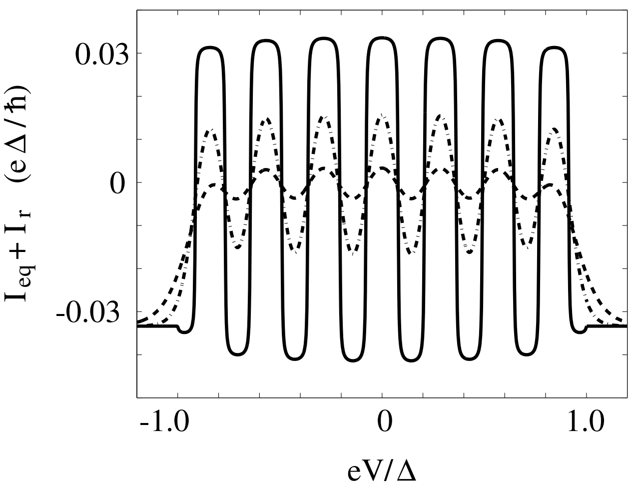

Figure 4.8: The equilibrium current I_{eq} plus the regular current I_r vs voltage. $L = 10\xi_o$, $\phi = \pi/2$, $D = 0.8$, $\varepsilon = 0.05$. Solid line - $T = 0$, dashed-dotted - $kT = 0.04\Delta$, dashed - $kT = 0.07\Delta$. The regular current jumps alternating by ŁδI_r every time the voltage is equal to the energy of an Andreev resonance. For $kT \quad \hbar v \quad _F/L$ and $eV > \Delta$ the current $I_{eq} + I_r = I^c_{eq}$

It is interesting to study the sum $I_{eq} + I_r$, plotted in Fig. 4.8, at temperatures $kT \gg \hbar v_F/L$. In this temperature regime the equilibrium current is exponentially small, and also the regular current steps in the IVC in Fig. 4.8 are suppressed. For a voltage $eV \sim \Delta$, the last level, carrying the major part (i^*) of the bound state current, is populated and the current $I_{eq} + I_r$ jumps to I^c_{eq}, the value of the continuum current, since all bound states are populated. This current I^c_{eq} is of the order of $1/L$ and the current $I_r + I_{eq}$ *increases* at $eV \sim \Delta$ from zero to a finite value $\sim 1/L$.

In connection to the discussion of the nonequilibrium Josephson current in long junctions, one can note that another phenomenon, not describable by the nonequilibrium population of the Andreev levels, (i.e not derivable from the regular current), was recently observed in experiment,[146,211] namely the increase of the current flowing between the superconductors due to current injection. This is deliberately not called the Josephson current, because the mechanism is instead an asymmetric splitting of the phase dependent injection current, thoroughly discussed in Refs. 210, 238, 240. Since we are considering the weak coupling limit, in our case the injection current is small and this effect is not present. However, starting from the full current density expression for arbitrary coupling to the normal reservoir in Eqs. (4.17) -(4.20), one can obtain this effect also in single mode ballistic junctions.

4.2.4 Anomalous current

The anomalous current is obtained by inserting Eq. (4.7) into Eq. (4.23),

$$I_a = -\sigma \frac{e}{\hbar}\frac{\hbar v_F}{4L}\frac{\sqrt{RD}\sin\phi}{1 - D\sin^2(\phi)}\sum_{n=0}^{N-1}[h(E_n^+) + h(E_n^-)], \tag{4.30}$$

where we have neglected the current from the last level close to $E = \Delta$ [the currents of all levels add up and the current from the last level is negligible, as discussed in connection to Eq. (4.23)]. The IVC at zero temperature looks like a staircase, as shown in Fig. 4.9. The magnitude of the

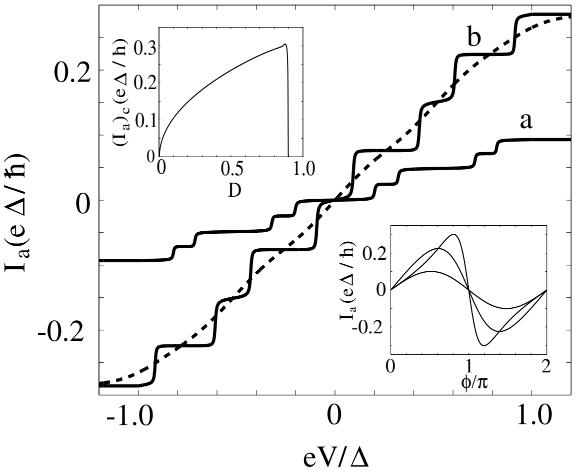

Figure 4.9: The anomalous current as a function of voltage V for (a) $\phi = \pi/4$ and (b) $\phi = 3\pi/4$ for $L = 10\xi_0$, $D = 0.8$, $\varepsilon = 0.05$ and $\sigma = (1$. Temperature $T = 0$ (solid) and $T = 0.1\Delta$ (dashed line). Upper inset: The critical anomalous current at $eV = \Delta$ as a function of transparency D for coupling constant $\varepsilon = 0.1$. Lower inset: The anomalous current $I_a(eV = \Delta, kT \quad \hbar v \quad _F/L)$ as a function of phase difference ϕ for different transparencies $D = 0.1, 0.5$ and 0.9. The highest amplitude corresponds to the highest transparency and vice versa.

current step at zero temperature is given by

$$\delta I_a = \frac{e}{\hbar}\frac{\hbar v_F}{2L}\frac{\sqrt{RD}\sin\phi}{1 - D\sin^2(\phi/2)}. \tag{4.31}$$

At temperatures larger than the interlevel distance, $kT \gg \hbar v_F/L$, the staircase IVC is smeared out to a straight slope, as shown in Fig. 4.9. The exact position of each level becomes irrelevant, and we can write the sum over bound states in (4.30) as an integral, noting that the expression $dE/dn = \pi\hbar v_F/L$ holds for all levels in the sum (4.30),

$$\sum_{n=0}^{N}[h(E_n^+) + h(E_n^-)] \approx \frac{2L}{\pi\hbar v_F}\int_0^{\Delta} dE[\tanh(E + eV) - \tanh(E - eV)] = \frac{4L}{\hbar v_F \pi} f(V,T) \tag{4.32}$$

where

$$f(V,T) = kT\ln\left(\frac{\cosh(\Delta + eV)/kT}{\cosh(\Delta - eV)/kT}\right), \tag{4.33}$$

and the anomalous current takes the simple form

$$I_a = -\sigma\frac{e}{\hbar}\frac{\sqrt{RD}\sin\phi}{\pi[1 - D\sin^2(\phi/2)]}f(V,T). \tag{4.34}$$

In the limit $\hbar v_F/L \ll kT \ll \Delta$, $f(V,T) = \min(eV, \Delta)$: the anomalous current thus scales linearly with applied voltage up to Δ. It follows from Eq. (4.34) that I_a is independent of the length of the junction, being the sum of $N \sim L$ levels which each carries a current $I_n \sim 1/L$. This gives that the anomalous current roughly is equal to the total equilibrium current of the short junction. The critical anomalous current is plotted with respect to transparency in the inset in Fig. 4.9. In the limit $D \ll 1$ it is given by $(I_a)_c = (e/\hbar)(\sqrt{D}/\pi)f(V,T)$. It is proportional to the first power of Δ for T close to T_c, therefore surviving up to $kT \approx \Delta$. The anomalous current-phase relation (see inset in Fig. 4.9) is 2π periodic and resembles that of the equilibrium Josephson current. The direction of the anomalous current is however proportional to σ, i.e dependent on the phase of the scatterer at the connection point, which is not the case for the equilibrium Josephson current.

From this discussion it is clear that the anomalous current is the dominating current in long single mode ballistic junctions. One can then ask why the predicted behavior of the anomalous current has not been observed in experiments in neither ballistic or diffusive junctions. The reason for this is that the anomalous current is proportional to $\mathrm{Im}(rd^*)$, i.e. dependent on the phases of the scattering amplitudes. This quantity will change sign every time passing an intrinsic resonance of the conductor, and in a large junction with many transverse modes and considerable intermode scattering, $\mathrm{Im}(rd^*)$ will be function rapidly oscillating around zero as a function of energy, thus averaging out the anomalous current to zero. However, as is discussed in Chapter 5, the anomalous current will have a profound effect on the sample to sample fluctuations in a mesoscopic conductor.

The anomalous current in asymmetric junctions is discussed in detail in Paper II, to where we refer the interested reader.

4.3 Injection current

There is, as discussed above, a large literature on the phase dependent differential conductance in so mesoscopic Josephson junctions (Andreev interferometers), both theoretical and experimental investigations of mostly diffusive, but also ballistic systems. A recent review is given in Ref. 150. The conductance in single or few mode ballistic junctions has been studied in Refs. 53, 53, 72, 119, 120, 130, 177, 178, 197, 198, 226, and provide a physical picture that can be used to understand the injection current and conductance in more complicated junctions. Here we present the discussion in line with Paper II.

4.3.1 Symmetric injection

We start by discussing symmetric junctions, $l = 0$. Focusing on the properties of the injection current at subgap voltages $eV < \Delta$, an explicit expression for this current[178] is given by inserting Eq. (4.19) into Eq. (3.60),

$$I_{inj} = \varepsilon^2 \frac{4e^2}{h} \int_{-\Delta}^{\Delta} dE (n_e - n_h) \frac{2\cos^2(\phi/2)\sin^2\theta}{[(1-\varepsilon)\cos 2\theta - R - D\cos\phi]^2 + \varepsilon^2 \sin^2 2\theta}. \tag{4.35}$$

For voltages above the gap $eV > \Delta$, the injection current oscillates smoothly, due to the broadening of resonances, around a straight line with the slope corresponding to the normal conductance $G_N = 4\varepsilon e^2/h$.

From the expression in Eq. (4.35) one can make some observations regarding the differential conductance, $G = dI_{inj}/dV$, at zero temperature. The maximum magnitude of G is found for voltages satisfying $1 - \cos[\theta(eV) = D[1 - \cos(\phi)]/\sqrt{1-2\varepsilon}$, i.e at resonance with an Andreev level. The conductance at resonance is independent of ε and equal to $4e^2/h$, a property noticed in Ref. 72. At voltages far away from resonance, the conductance is proportional to ε^2, and thus considerably smaller in the weak coupling limit. This leads to that the amplitude of the conductance oscillates strongly as a function of voltage.

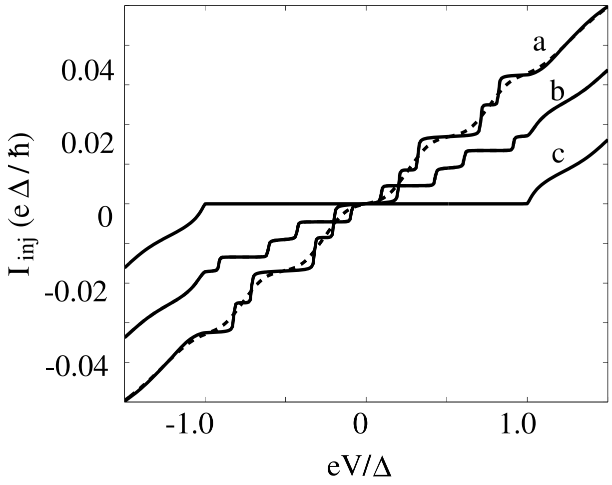

Figure 4.10: The injection current in lead 1 as a function of voltage for (a) $\phi = \pi/4$, (b) $\phi = 3\pi/4$ and (c) $\phi = \pi$. Zero T (solid lines) and $T = 0.05\Delta$ (dashed line) with $D = 0.8$, $L = 10\xi_0$ and $\varepsilon = 0.05$. For $eV > \Delta$ the slope of the IVC approaches the value of a normal junction.

This resonant property has a profound effect on the oscillations of the conductance as a function of phase difference. This most convenientelly discussed in the weak coupling limit, where the injection current is given by, using the relation in (4.21),

$$I_{inj} = \varepsilon \frac{e}{\hbar} \frac{|\cos(\phi/2)|}{\sqrt{D}\sqrt{1 - D\sin^2(\phi/2)}} \sum_{n,\pm} \left| \frac{dE_n^{\pm}}{d\phi} \right| \left[n^e(E_n^{\pm}) - n^h(E_n^{\pm}) \right]. \tag{4.36}$$

From this expression one notices that the injection current, just as the anomalous current, is proportional to $|dE/d\phi|$, i.e the modulus of the current carried by each Andreev level, and thus that the IVC has a step-like character, with current plateaus and onsets, shown in Fig. 4.10. In the limit of zero length of the junction, with a single Andreev level, the magnitude of the step at zero temperature is

$$\delta I_{inj} = \varepsilon \frac{e}{\hbar} \frac{\sqrt{D}}{2} \frac{|\sin(\phi/2)|\cos^2(\phi/2)}{1 - D\sin^2(\phi/2)}, \tag{4.37}$$

while for long junctions $L \gg \xi_0$, the current step is

$$\delta I_{inj} = \varepsilon \frac{e}{\hbar} \frac{\hbar v_F}{L} \frac{\cos^2(\phi/2)}{1 - D\sin^2(\phi/2)}. \tag{4.38}$$

The properties of the conductance in the long junction limit changes from current plateau to plateau. For example, in junctions with finite transmissivity $D \neq 1$, there is a current plateau at zero voltage and therefore the amplitude of the current-phase oscillations is small, while it dramatically increases at $D = 1$ when the Andreev resonance approaches the Fermi level. This giant enhancement of the conductance oscillations has been discussed by Kadigrobov et al.[130]

There is a π-shift of the conductance oscillations as a function of phase when moving from one current plateau to another. Such a crossover has been found in Ref. 153 by numerical simulations of multimode SNS-junctions with arbitrary impurity concentration. In the diffusive limit, a similar phenomenon, π-shift of the conductance oscillations when the voltage passes the Thouless energy, has been discussed by Volkov and Zaitsev.[239] This effect has been experimentally observed in various structures.[84,110,174] Within our model, the crossover phenomenon has

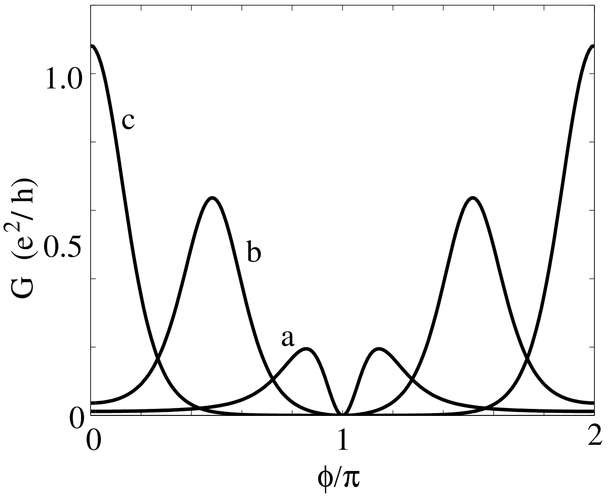

Figure 4.11: The conductance as a function of ϕ for different voltages (a) $eV = 0$, (b) $eV = 0.075\Delta$ and c) $eV = 0.15\Delta$ at zero temperature $T = 0$. $D = 0.9$, $\varepsilon = 0.05$ and $L = 20\xi_0$. The conductance maximum shifts from $\phi\ \ \pi$ to $\phi = 0$ upon increasing voltage. There is an absolute minimum at $\phi = \pi$.

a very simple explanation which follows from the phase dependence of the Andreev resonances presented in Fig. 4.2. At a given voltage, the magnitude of the conductance depends on the distance to the nearest Andreev resonance: the closer the resonance the bigger the conductance. As is clear from the figure, when the phase difference changes from zero to π, the distance between the Andreev resonances confining the odd current plateaus (the first plateau is at zero voltage) decreases, while the distance between the resonances confining the even plateaus increases. As a result, the conductance at the odd plateaus has a maximum around π, while the conductance at the even plateaus has a maximum at zero phase difference. Similar arguments hold for the phase dependence of the conductance in diffusive junctions below and above the Thouless energy, which plays the role of the first Andreev resonance. The conductance as a function of phase for different voltages is plotted in Fig. 4.11. At finite temperature, the step structure in the IVC in Fig. 4.10 is smeared. This effect is most interesting in long junctions, where the temperature can be much larger than the distance between the Andreev levels, $kT \gg \hbar v_F/L$ without suppressing superconductivity itself, $kT \ll \Delta$. The expression for the current in this temperature limit is obtained by inserting Eq. (4.7) into (4.36) and then converting the sum over Andreev levels into an integral, just as for the anomalous current, see Eq. (4.32). The current is then given by

$$I_{inj} = \varepsilon \frac{4e}{h} \frac{\cos^2(\phi/2)}{1 - D\sin^2(\phi/2)} f(V,T). \tag{4.39}$$

where $f(V,T)$ is given by Eq. (4.33). The IVC becomes linear for $eV < \Delta$, with the slope independent of the length of the junction and the temperature. The current is thus a true long range current. From Eq. (4.39) it is clear that the conductance has a maximum at $\phi = 0$ and a minimum at $\phi = \pi$ for all applied voltages $eV < \Delta$. This is different from the phase dependence of the conductance at odd current plateaus at zero temperature, and therefore at these plateaus the current-phase oscillations undergoes a π-shift as a function of temperature at $kT \sim \hbar v_F/L$. The conductance as a function of phase difference is plotted for different temperatures in the inset in Fig. 4.12. Such a crossover has recently been observed in quasi ballistic junctions by Dimoulas et al.[84] and also a similar crossover has been observed in diffusive junctions at the Thouless temperature.[17] It is interesting to point out that the information on the conductance

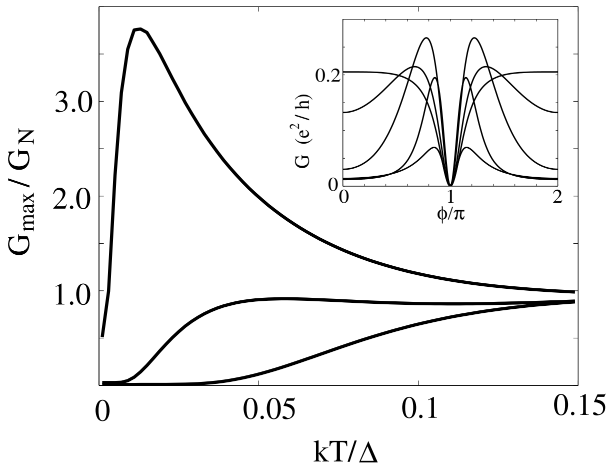

Figure 4.12: The maximum conductance G_{max}/G_N as a function of T for zero voltage for different junction transparencies, (a) $D = 0.94$, (b) $D = 0.9$ and (c) $D = 0.1$ and $\varepsilon = 0.01$. The maximum conductance saturates at a constant value $G_{max} = G_N$ for $kT \quad \hbar v \quad _F/L$, independent on D. Inset: The conductance as a function of ϕ for different temperatures $kT = 0, 0.01\Delta, 0.025\Delta, 0.05\Delta$ and 0.1Δ at zero voltage $V = 0$. Increasing temperature from bottom to top at $\phi = 0$. $D = 0.9$, $\varepsilon = 0.05$ and $L = 20\xi_0$.

as a function of phase difference was used recently by Baselmans et al.[35] to determine the direction of the Josephson current. One should however note that in a loop geometry a large current circulating in the loop may change the applied external flux vs phase dependence, thus modifying the phase dependence of the conductance.

When discussing symmetric junctions, it is also worth noting that the effect discussed by Volkov and Pavlovskii[238] does not exist in these junctions because the injection current is equally distributed between the left and the right arms of the junction [see Eq. (4.20)].

It is found in Paper II that in long junction with large asymmetry $L \gg l \gg \xi_0$, there is a cross over from 2π to π periodic behavior of the injection current with increasing temperature, occurring at $kT \sim \hbar v_F/l$. The discussion about the periodicity of the conductance oscillations with respect to phase goes back to the early eighties. A π-periodic contribution to the weak localization correction to the conductance in a SNS junction was predicted by Spivak et al[219] and later Altshuler et al.[7] It has been shown in numerical simulations for a structure similar to ours that the full conductance, i.e not only the weak localization contribution, might become π-periodic at finite temperatures.[115,149] A large π-periodic conductance oscillation with phase was also observed in diffusive samples.[188] Whether the explanation for the crossover from 2π to π periodicity with increased temperature discussed above can account for these observations remains to be investigated.

CHAPTER 5

Nonequilibrium Josephson current in two-dimensional ballistic junctions

While the last chapter was devoted to single mode, quantum junctions, convenient objects for studying the basic microscopic properties of the equilibrium and nonequilibrium Josephson effect, we now turn to two-dimensional ballistic junctions, with the aim to provide a more quantitative theoretical description of junctions studied in experiments, see e.g. Refs. 1, 111, 112, 182, 183, 206, 207, 228, 229.

We first discuss the properties of the equilibrium Josephson current, especially taking into account the effect of normal scattering at the NS-interfaces. Then, a three terminal junction, where the normal conductor is connected to a normal electron reservoir, is considered, and the nonequilibrium Josephson current is studied, with the focus on the critical current as a function of injection voltage. The discussion is essentially an extension of paper III

5.1 Equilibrium Josephson current

A schematic picture of the junction under study is presented in Fig. 5.1. A ballistic two-dimensional normal region, with width W and length L, is connected to two superconducting electrodes. The junction differs from the single mode junction in Fig. 4.1 only in the sense that it is effectively two dimensional, $W \gg \lambda_F$. The transparency Γ of the interfaces between the normal conductor and the superconductor is assumed to be the same for both interfaces and the phase difference between the superconductors is ϕ. It is assumed that the width is constant along the whole sample and that the separation between the electrodes L is constant along the width. In this case the ballistic conductor is just a long lead, in the sense discussed in Chapter 3, with $N = \mathrm{Int}(2W/\lambda_F)$ transverse modes. Moreover, the normal scattering at the NS-interfaces is assumed to be specular, i.e no scattering between the modes, which makes it possible to treat the junction as consisting of N independent single mode junctions. It is assumed throughout the chapter that the junction is classically wide, i.e. $N \gg 1$.

The single mode currents calculated in the preceding chapter, can then be used, with the modification that the mode dependence has to be taken into account, entering via the mode dependence of the Fermi velocity v_F (or, equivalently, the Fermi wave number, k_F), as $v_F \to v_{Fn} = v_F\sqrt{1-(n/N)^2}$. In the continuum limit, the current in the wide junction can thus be

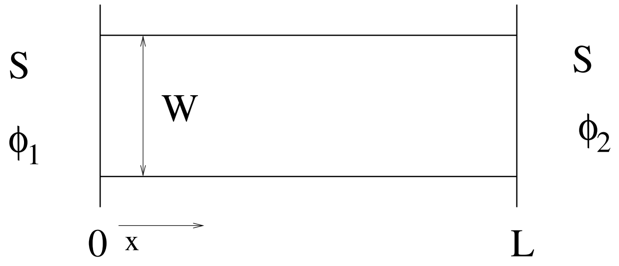

Figure 5.1: A schematic picture of the wide ballistic junction.

found as

$$I = \sum_{n=1}^{N} I(v_{Fn}) \approx N \int_0^1 d(n/N) I(v_{Fn}). \tag{5.1}$$

5.1.1 Ideal NS-interfaces

First consider the case with no normal scattering at the NS-interfaces. In the short junction case, $L \ll \xi_0$, there is no mode dependence in the expression for the Josephson current, and the total current is just a sum over the single mode currents in Eq. (4.10). In the opposite long case, $L \gg \xi_0$, it is useful for the physical intuition to formulate the integral in Eq. (5.1) in terms of the effective length of each mode $s_n = L/\sqrt{1-(n/N)^2}$, possible since the mode dependence only enters in v_F which appears in all current expressions divided by the physical length L. The total current can thus be written

$$I = N \int_L^\infty ds\, I(s) P(s), \tag{5.2}$$

where the distribution of effective lengths $P(s)$ is just given by

$$P(s) = \frac{d(n/N)}{ds} = \frac{L^2}{s^3} \frac{1}{\sqrt{1-(L/s)^2}}. \tag{5.3}$$

This distribution is just an effect of the hard wall boundary conditions, and it is strongly peaked around the physical length L, which implies that the total current will be dominated by the current carried by the modes with effective lengths s close to the physical length L, an important message for the discussion below in connection with the nonequilibrium Josephson current.

The equilibrium Josephson current in the long junction limit can be found straightforwardly in the low, $kT \ll \hbar v_F/L$, and high $kT \gg \hbar v_F/L$, temperature limits, by performing the integration over effective lengths of the current expressions in Eqs. (4.11) and (4.12) respectively, assuming perfect transparency ($D = 1$), which gives the result originally found in Refs. 124, 222, 223. One can note that the length dependence of the current is the same as that of the single mode junction, i.e $I \propto 1/L$ for $kT \ll \hbar v_F/L$ and $I \propto \exp(-2\pi L/\xi_T)$ for $kT \gg \hbar v_F/L$.

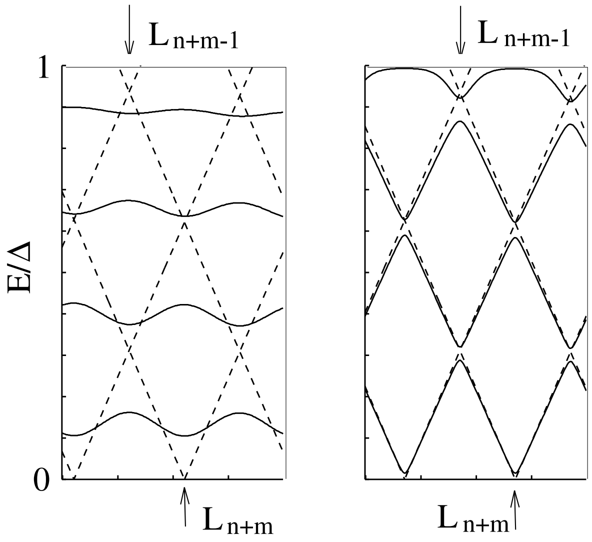

Figure 5.2: The Andreev levels (solid) and the normal electron and hole resonances (dotted) as a function of length L of the junction with four Andreev levels in (a) weak resonance limit Γ 1 (b) strong resonance limit Γ 1. The lengths of two subsequent intersections of normal resonances L_{n+m} and L_{n+m-1} are shown with arrows

5.1.2 Barriers at the NS-interfaces

Potential barriers at the NS-interfaces are almost always present in semiconductor-superconductor heterostructures, due to Fermi velocity mismatch and/or Schottky barriers, as discussed in Chapter 2. These barriers modify the transport properties of the junction in the normal state, giving rise to Breit-Wigner resonances in the normal conductance. These resonances also affect the Josephson current, giving rise to a Josephson current that oscillates as a function of length, with a period of the Fermi wavelength λ_F. This phenomenon has been studied theoretically[73, 105, 136, 139, 195, 198, 205] as well as experimentally.[74, 229]

In the case with barriers at the NS-interfaces, one can not directly use the argument with effective lengths in Eq. (5.1), since the mode dependence now also enters via the Fermi wave number k_F, which appears multiplied with the length L, as shown below.

In the absence of the superconducting leads (a NININ-junction), the two barriers give rise to normal Breit-Wigner resonances for the electrons and holes. Understanding the properties of these resonances turns out to be crucial for describing the behavior of Andreev levels and current transport. The energies of the electron and hole resonances for a single mode are given by

$$E_n^e = -2E_F\left[1-\frac{\pi(n-\nu)}{k_F L}\right], \qquad E_m^h = 2E_F\left[1-\frac{\pi(m-\nu)}{k_F L}\right], \tag{5.4}$$

where $r_b = \sqrt{1-\Gamma}e^{i\nu\pi}$ and $n(m)$ are integers denoting the index of the electron (hole) resonances. The intersection between electron and hole resonances ($E_n^e = E_m^h$) is given by $L_{n+m} = \lambda_F/4(m+n-2\nu)$ with the Fermi wavelength $\lambda_F = 2\pi/k_F$. These normal resonances are plotted in Fig. 5.2. For simplicity, we put the phase $\nu = 0$, which only has the effect of shifting the electron and hole resonances, as is seen by Eq. (5.4). For junctions with superconducting leads, one can derive an equation for the bound Andreev states from Eq. (3.37), with the result

$$\begin{aligned}&\Gamma^2\cos\phi + 2(1-\Gamma)\cos\beta - \cos(2\gamma-\beta) - (1-\Gamma)^2\cos(2\gamma+\beta)\\ &-4(1-\Gamma)\sin^2\gamma\cos(2k_F L) = 0.\end{aligned} \tag{5.5}$$

One can draw some qualitative conclusions about how the Andreev levels are related to the normal resonances by looking at Fig. 5.2. In the limit of high barrier transparency $\Gamma \sim 1$, the Andreev levels are weakly modified by the barriers. In the opposite limit $\Gamma \ll 1$, the Andreev levels get pinned at the normal resonances, but there are no level crossings at the points where the normal electron and hole resonances intersect.

The main difference between the Andreev levels and the normal resonances is that the normal resonance move very quickly through the junction when the length L increases, while the Andreev levels oscillate up and down. Considering Andreev state energies close to the Fermi level, $E \ll \Delta$, one can derive a simplified dispersion relation,[130]

$$\sin^2(\beta/2) = \frac{\Gamma^2\cos^2(\phi/2) + 4(1-\Gamma)\sin^2(k_F L)}{(2-\Gamma)^2}. \tag{5.6}$$

Using this relation we can study the bound state current in different length limits.

In the short limit, $L \ll \xi_0$ there are two cases to be considered. For nearly transparent barriers $\Gamma \sim 1$, and thus broad resonances with a width $\Gamma\hbar v_F/L \gg \Delta$, one can neglect dephasing (putting $\beta = 0$) and just get the total transparency of the junction $D = \Gamma^2/(\Gamma^2 + 4(1-\Gamma)\sin^2(k_F L))$ to be put into the standard zero length junction equilibrium current formula. In the strong barrier case $\Gamma \ll 1$ the resonances are sharp, with a width $\Gamma\hbar v_F/L \ll \Delta$ and one can not neglect the dephasing. Assuming that the resonance is close to the Fermi energy ,$E^{e,h} \ll \Delta$, we can put $\beta \ll 1$ in (5.6) and obtain[41,244]

$$E = \pm\sqrt{\left(\frac{\Gamma\hbar v_F}{L}\right)^2\cos^2(\phi/2) + (E^{e,h})^2}. \tag{5.7}$$

When the resonance is exactly at the Fermi energy $E^{e,h} = 0$, the Josephson current is given by

$$I = \frac{e\Gamma v_F}{L}\sin(\phi/2)\tanh\left(\frac{\Gamma\hbar v_F}{L}\frac{\cos(\phi/2)}{2kT}\right). \tag{5.8}$$

The critical current at low temperatures ($kT \ll \Gamma$) is thus smaller than the critical current of a short, clean junction by a factor $\Gamma\hbar v_F/L\Delta$.

For a long junction $L \gg \xi_0$ we can calculate the derivative of energy with respect to phase,

$$\frac{dE}{d\phi} = \pm\frac{\hbar v_F}{2L}\frac{\Gamma^2\sin\phi}{\sqrt{(2-\Gamma)^4 - [\Gamma\cos\phi - 4(1-\Gamma)\cos(2k_F L)]^2}}, \tag{5.9}$$

In the weak barrier limit $\Gamma \sim 1$, this just causes oscillations with length around the clean junction ($\Gamma = 1$) result. In the strong barrier limit $\Gamma \ll 1$, one can distinguish two limits: When the length of the junction is very different from the length L_{n+m} where the electron and hole resonances intersect, the junction is out of resonance. The second term in Eq. (5.9) is then negligible and the current from the individual levels thus becomes

$$I = \pm\frac{ev_F}{4L}\Gamma^2\sin\phi. \tag{5.10}$$

It is proportional to Γ^2 and thus strongly suppressed. In the opposite limit, when the length of the junction $L = L_{n+m} = \lambda_F(m+n)/4$, the junction is in resonance. When $n+m$ is even we get the current carried by each level

$$I = \pm\frac{ev_F}{L}\frac{\Gamma\sin\phi}{4|\cos(\phi/2)|} \tag{5.11}$$

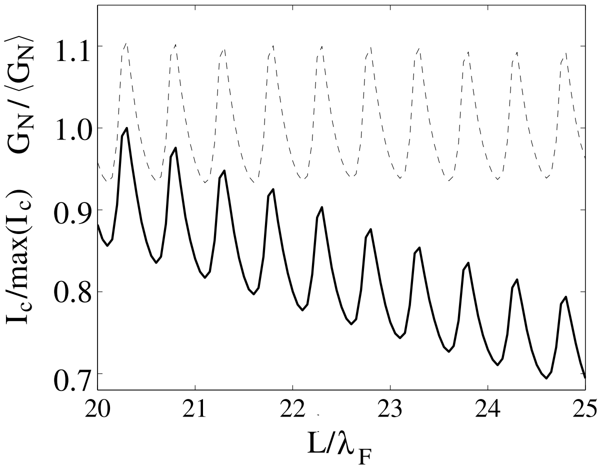

Figure 5.3: The critical Josephson current, normalized with the maximum value (thick solid) and the normalized normal state conductance $G_N/$

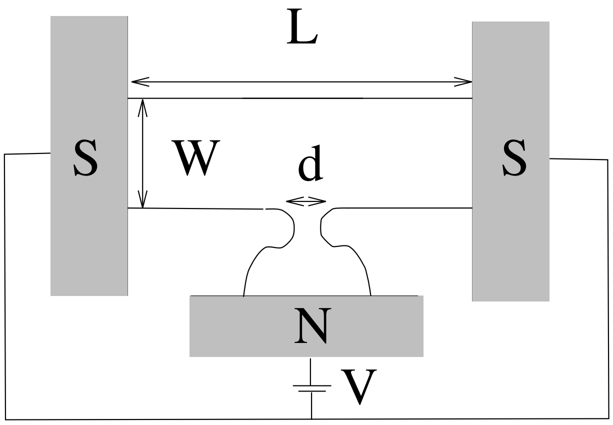

Figure 5.4: A schematic picture of the junction.

reservoir. In experiment with wide injection contact,[183] this has been shown to be a good approximation for junction widths up to several micrometers. In wider junctions, there will be transverse modes that are not coupled to the normal reservoir and thus only carry the equilibrium Josephson current.

It is also assumed that the scattering at the point contact itself does not mix transverse modes, i.e. that each transverse mode only couples to the modes in the point contact. Scattering between the modes at the injection contact gives rise to a technically much more complicated problem, however at the moment it is not fully clear whether it substantially changes the physical properties of the junction. As found below, inter-mode scattering at the NS-interfaces does not change the result considerably, which indicates that the qualitative result found is not very sensitive to scattering between the modes at the injection point.

Moreover, we assume that the coupling is weak, so that the weak coupling results derived in the previous chapter can be used. This implies that the injected current is small and the current flowing between the superconductors is only the nonequilibrium Josephson current. The effect on the critical current due to asymmetric splitting of the injected current,[146, 210, 211, 238, 240] discussed above, is thus neglected. It is important, however, to remember that the coupling must be large enough so that the injected quasiparticles do not scatter inelastically before leaving the junction. Under these assumptions, the distribution of the injected electrons and holes are governed by the applied voltage at the normal reservoir.

As discussed in Chapter 3, the total Josephson current in the weak coupling limit is naturally partioned into the equilibrium current I_{eq} and the sum and difference current, I^+ and I^-, present in nonequilibrium. The final simplifying assumption is that we neglect the difference, what we call in the anomalous current. This current is sensitive to the phases of the scattering amplitudes, and is assumed to be small in large junctions, for which it is reasonable to assume that the quasiparticles scattering in different modes pick up different scattering phases. With this assumption, we can write the total Josephson current as

$$I \equiv I_{eq} + I^{+} = \int_{-\infty}^{\infty} dE\, i_{eq}(E)\, f(E) + \int_{-\infty}^{\infty} dE \left[\frac{i^{+}(E)}{2}\left(f_1^e(E) + f_1^h(E) - 2f(E)\right)\right]. \quad (5.13)$$

For applied voltages $eV < \Delta$ and small temperatures $kT \ll \Delta$, only the current density $i^{+}(E)$ for energies $|E| < \Delta$ is important for determining the current. However, for these energies $i^{+} = i_{eq}$ and the current density $i_{eq}(E)$ directly determines the nonequilibrium Josephson current. This current density will thus be the staring point for the discussions below.

We will focus on long junctions studied are in the long limit, $L \gg \xi_0$, the short junction result trivially is N times the single mode result studied in the previous chapter, since the current in short junctions is the same for each mode.

5.2.1 Perfectly transmitting NS-interfaces

We first consider the case when there is perfect Andreev reflection at the NS-interfaces, i.e no normal reflection. For the low-energy levels, $E \ll \Delta$, the bound state energies are given by Eq. (4.1) generalized to many modes

$$E_{p,n}^{\pm} = \frac{\hbar v_{Fn}}{2L}\left[(2p+1)\pi \pm \phi\right], \quad (5.14)$$

where the index n denotes the transverse mode and where the indices p and $\pm$ label the Andreev levels for a given mode. The current density for each Andreev level is given by inserting the expression (5.14) into Eq. (3.31). The total current density is then obtained by first summing over the modes n, i.e integrating over angles as in Eq. (5.2), and then summing over $p, \pm$, giving

$$i^{+}(E) = N\frac{e}{\hbar}\frac{\hbar v_F}{L}\sum_{p,\pm}\frac{\pm E^2 \theta(E_{p0}^{\pm} - E)}{(E_{p0}^{\pm})^2\sqrt{(E_{p0}^{\pm})^2 - E^2}}, \quad (5.15)$$

where θ is the Heavyside stepfunction and $E_{p0}^{\pm}$ is given by Eq. (5.14) with $n = 0$. The current density for phase differences $\phi = \pi/4$ and $3\pi/4$ is plotted in Fig. 5.5. The current density consists of alternating positive and negative peaks[20] at the phase dependent energies $E_{p0}^{\pm}$. The peaks arise from the square root singularities of the current density in Eq. (5.15) and the amplitude of the peaks decreases with increasing energy. One can thus conclude that wide junctions have an equilibrium current density very similar to single mode junctions, with an effective broadening of the single mode peak due to the large number of modes. This is a consequence of the sharp distribution of effective lengths in Eq. (5.3), with large weight of lengths close to the physical length L. One can also note that the repeated peak structure with slowly decaying amplitude is different from diffusive junctions[246,247] where there is only one peak around the Thouless energy (which corresponding to $\hbar v_F/L$ in ballistic junctions).

The expression for the equilibrium part, I_{eq}, of the Josephson current in Eq. (5.13) is discussed in the previous section. The nonequilibrium part, I^{+}, is straightforwardly calculated from Eqs. (5.15) and (5.13). In the limit of $eV, kT \ll \Delta$, using that $i^{+}(-E) = -i^{+}(E)$, we get

$$I^{+} = N\frac{ev_F}{2L}\sum_{p,\pm}\int_0^{\Delta} dE \frac{\pm E^2/\left(E_{p0}^{\pm}\right)^2 \theta(E_{p0}^{\pm} - E)}{E_{p0}^{\pm}\sqrt{1 - E^2/(E_{p0}^{\pm})^2}} g(E) \quad (5.16)$$

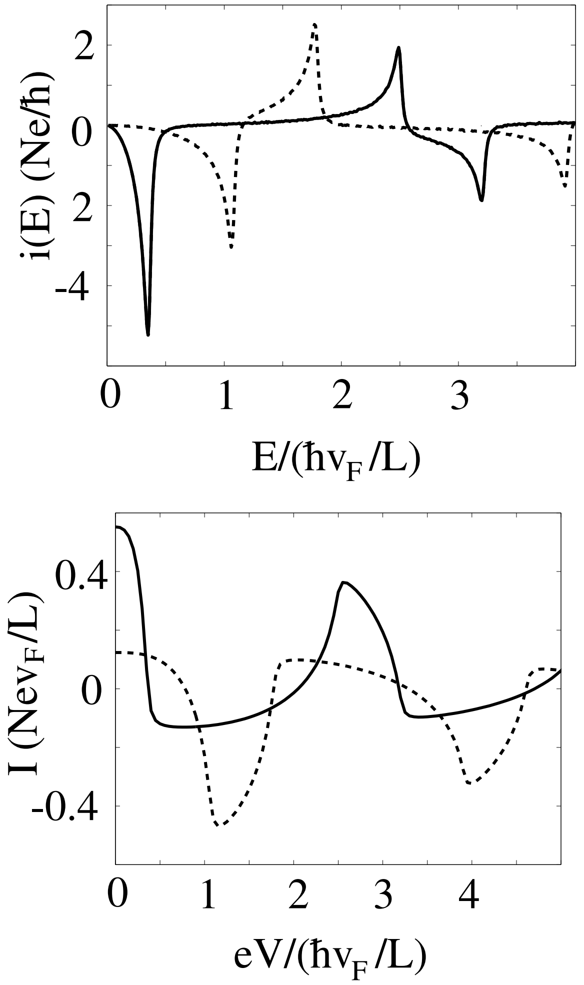

Figure 5.5: Upper: The current density as a function of energy. Lower: The total current as a function of voltage for zero temperature. The phase difference $\phi = \pi/4$ (dashed)and $3\pi/4$ (solid) and $L = 10\xi_0$

with $g(E) = \tanh[(E+eV)/2kT] + \tanh[(E-eV)/2kT] - 2\tanh(E/2kT)$. From the shape of the current density, see Fig. 5.5, it is clear that the current will oscillate as a function of voltage between maximas around $eV = E^+_{p0}$ and minimas around $eV = E^-_{p0}$. The period of oscillation is thus $\pi\hbar v_F/L$. Evaluating the integral at a maximum, $eV = E^+_k$, for $T = 0$ we get the maximum current

$$I^{max}_k = N\frac{ev_F}{2L}\frac{\sqrt{D}\sin\phi}{|\sin\phi/2|\sqrt{1-D\sin^2\phi/2}}\sum_{l,\pm}\pm\left[\arcsin(eV/E^\pm_l) - \frac{eV}{E^\pm_l}\sqrt{1-\left(\frac{eV}{E^\pm_l}\right)}\right], \tag{5.17}$$

where $E^+_l = eV + (\hbar v_F/L)l\pi$ and $E^-_l = eV + (\hbar v_F/L)[l\pi + \phi]$. For voltages $eV \gg \hbar v_F/L$, the amplitude of the current oscillations can be approximated as

$$\delta I^{max} \propto \left(\frac{\hbar v_F}{LeV}\right)^{3/2}. \tag{5.18}$$

For finite temperatures the amplitude of the voltage oscillations decreases, and the oscillations are completely washed out for $kT \gg \hbar v_F/L$. The total current, $I_{eq} + I^+$, is plotted in Fig. 5.5, showing the oscillation of the current as a function of applied voltage as well as the decaying amplitude of the oscillations.

The equilibrium current I_{eq} is always positive for phase differences $0 < \phi < \pi$ and negative for $-\pi < \phi < 0$, as can bee seen from the current phase relation for the single mode junction in Fig. 4.4. In nonequilibrium, the total current for a given phase difference $I(\phi)$ changes sign as a function of applied voltage, i.e the junction becomes a so called π-junction.[35,237] This can bee seen from the current-phase relationship $I(\phi)$, shown in Fig. 5.6 for different voltages. It can be noted that for certain voltages, the current-phase relationship has several local current minima and maxima.

The critical current is defined as the maximum possible current for any phase difference in the range $-\pi < \phi < \pi$. To study the π-junction behavior, the critical current multiplied by the sign of the critical phase difference ϕ_c, $\mathrm{sgn}(\phi_c)I_c$, is shown in Fig. 5.6 for different temperatures. The critical current multiplied by the critical phase difference $\mathrm{sgn}(\phi_c)I_c$ oscillates

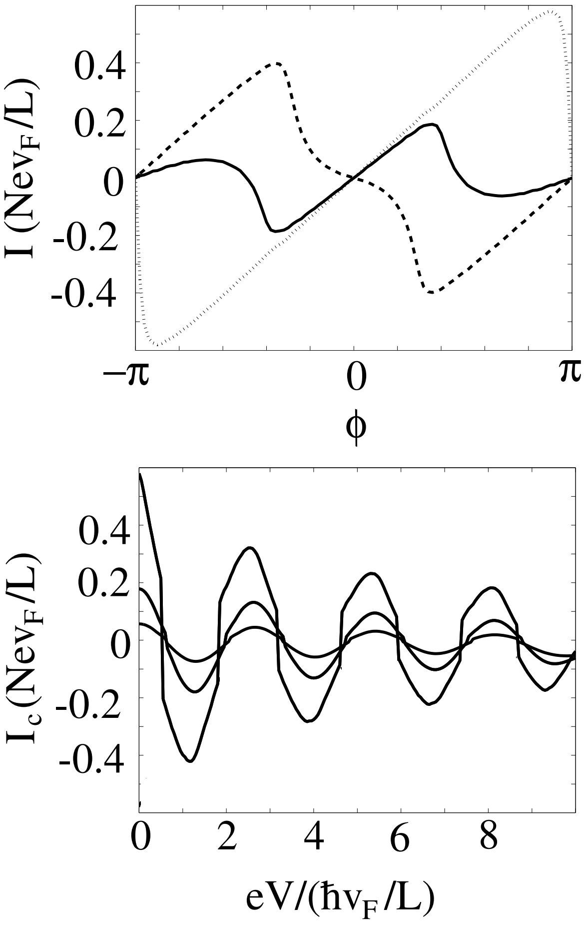

Figure 5.6: Upper: The current phase relationship for different voltages $eV = 0$ (dotted), $eV = \hbar v_F/L$ (dashed) and $eV = 2\hbar v_F/L$ (solid), temperature $T = 0$. Lower: The critical current multiplied by the sign of the critical phase difference $\mathrm{sgn}(\phi_c)I_c$ as a function of applied voltage for different temperatures, $kT = 0, 0.3, 0.5\hbar v_F/L$, with decaying amplitude for increasing temperature.

between positive and negative values as a function of voltage, with period $\pi\hbar v_F/L$, i.e it shows typical π-junction behavior. The amplitude of the oscillations decreases with increasing voltage, just as does the current for a given phase difference, as shown in Eq. (5.18). It can be noted that for zero temperature there are, for certain voltages, jumps between the branches of positive and negative critical current, i.e the critical current I_c never becomes zero. This can be understood from the current-phase relationship in Fig. 5.6, where for certain voltages, the critical phase difference ϕ_c jumps between positive and negative values, changing the sign of $\mathrm{sgn}(\phi_c)I_c$.

5.2.2 Normal reflection at the NS-interfaces

Normal scattering at the NS-interfaces is taken into account by introducing interface barriers with transmission probability Γ. We consider analytically the case with specular normal scattering at the NIS-interfaces, i.e no scattering between the modes; the case with mode-dependent scattering is treated numerically below. The low lying bound states energies, $E \ll \Delta$, are given by Eq. (5.6)

$$E^{\pm}_{p,n} = \frac{\hbar v_{Fn}}{2L}\left[2p\pi \pm \mathrm{acos}\left(\frac{4(1-\Gamma)\cos(2k_{Fn}L) - \Gamma^2\cos\phi}{(2-\Gamma)^2}\right)\right]. \tag{5.19}$$

The bound state energies oscillate rapidly as a function of length of the junction, due to the term $\cos(2k_{Fn}L)$ in Eq. (5.19). The corresponding rapid oscillations of the current density are averaged out when summing over the transverse modes, and we assume that the junction length $L \gg \lambda_F$ so that the length dependence of the critical current on the scale of λ_F, shown in Fig. 5.3, can be neglected. The total current density, summed over n and $p, \pm$, is then given by

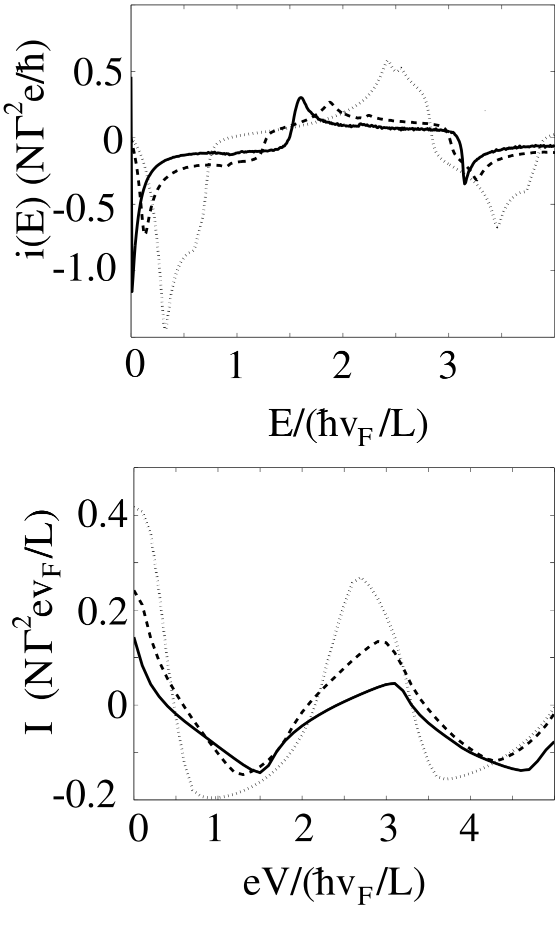

Figure 5.7: Upper: The current density as a function of energy. Lower: The total current as a function of appled voltage. The barrier barrier transparencies $\Gamma = 0.1$ (solid), 0.5 (dashed) and 0.9 (dotted). The phase difference $\phi = 3\pi/4$ and the length $L = 10\xi_0$

$$i = \frac{e}{\hbar}\frac{2\Gamma^2\sin\phi}{\pi}\int_0^N dn \frac{\mathrm{sgn}[\sin(2EL/\hbar v_{F_n})]}{\sqrt{16(1-\Gamma)^2-[(2-\Gamma)^2\cos(2EL/\hbar v_{F_n})+\Gamma^2\cos\phi]^2}}. \tag{5.20}$$

The current density as a function of energy is plotted for different barrier transparencies Γ in Fig. 5.7. The current density has a shape with alternating positive and negative peaks, similar to the current density for the junction without barriers at the NS-interfaces, shown in Fig. 5.5. The effect of the NIS-barriers, apart from the overall decreased current density amplitude, is that each current density peak is shifted towards lower energies, as is seen in Fig. 5.7.

The total current I as a function of voltage, for fixed phase difference, thus oscillates with the same period $\pi\hbar v_F/L$ both with and without barriers at the NS-interfaces, and with a decreasing amplitude of the oscillations for increasing voltage (see Fig. 5.7). The π-junction behavior is thus present also in junctions with low-transparent NIS-barriers. The critical current has not been studied explicitly in this work.

5.2.3 Dirty NS-interfaces

It is reasonable to assume that in the general case there is some dirt at the NS-interfaces from the junction processing, leading to scattering between the different modes at the interfaces. For very dirty interfaces, the scattering is in principle diffusive and one can assume that an incoming electron in a given mode is back-scattered with equal probability in all modes. This situation is modeled by introducing phenomenological random scattering matrices, describing the scattering between the modes. The details of this modeling in found in paper III and since the next chapter is devoted to the theory of random matrices, we here merely present the result. The current density is plotted in Fig. 5.8 for different barrier transparencies Γ. The main result is that the peak-like structure of the current density is not substantially changed compared the corresponding specular barrier case in Fig. 5.7. From this result one can draw the conclusion that the effect of diffusive scattering at the NS-interfaces does not qualitatively modify the nonequilibrium Josephson current. The result that the current for a fixed phase difference oscillates periodically with applied voltage is still valid. Whether rough 2DEG-sidewalls, giving rise to diffusive boundary scattering, have a more profound effect on the current, remains to be investigated.

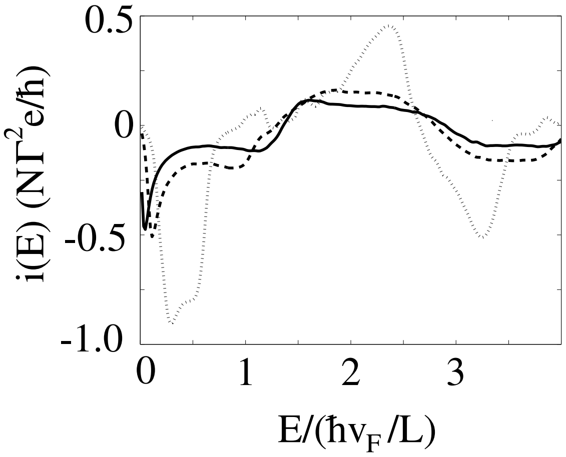

Figure 5.8: The current density as a function of energy for different barrier transparencies $\Gamma = 0.1$ (solid), 0.5(dashed) and 0.9(dotted). The current density has been calculated by generating 1000 random matrices of dimension $N = 15$. The phase difference $\phi = 3\pi/4$ and the length $L = 10\xi_0$

As a conclusion, the π-junction behavior predicted and observed in diffusive junctions (with $E_{Th} \ll \Delta$), should be possible to observe also in long wide ballistic junctions. The effect is predicted to be stronger since the smearing of current density features due to impurity scattering in diffusive junctions is not present in ballistic junctions.

CHAPTER 6

Random matrix theory of chaotic quantum dots

The junctions studied in the preceding chapter were systems where the scattering matrix of the conductor was assumed to be known a priori. In most realistic experimental situations, however, this is not the case. Boundary scattering or presence of impurities are some sources of additional scattering that are normally present and not included in the models in the preceding chapters. In certain situations, the scattering is so chaotic that it is impossible to get any information about the scattering matrix. Then it is instead possible to apply a statistical theory for the scattering matrix, allowing one to calculate average quantities as well as sample-to-sample fluctuations around the average. This is based on the theory of random matrices, RMT, that was originally developed in the beginning of the fifties (see e.g. the monograph by Mehta, Ref. 166), to explain scattering data from nuclear physics experiments.

In this chapter we briefly present the original ideas of RMT and then describe how to apply them to calculate transport properties in mesoscopic system. The main emphasis is on chaotic quantum dots, i.e small effectively zero-dimensional semiconductor dots or metallic particles, with the adjective "quantum" because the transport in the dot is quantum mechanically phase coherent and chaotic due to that the classical motion in the dot is chaotic. The chapter is to large extent a short summary of what is presented in recent reviews on the subject, Refs. 5, 48, 104, 221, in order to make the presentation in the thesis more self contained. The concepts discussed are then applied in Chapters 7 and 9 to calculate the current in chaotic Josephson junctions.

6.1 Closed systems; Random Matrix Theory of spectral statistics

6.1.1 Wigner-Dyson statistics

Originally, RMT was constructed in the early fifties to explain results from experiments in nuclear physics. The object of study was the high lying energy levels in heavy atomic nuclei, investigated in scattering experiments. This was well before any rigorous theory for nuclear interactions was known, but it was assumed that these energy levels, far away from the ground state, had such a complex structure that it was impossible to describe them exactly. However, experimental data from different samples displayed a number of common features, e.g. that the distribution of the distances between nearest neaigbouring enery levels, the level spacings, had an almost universal form. The naive guess, that this distribution would be Poissonian, i.e the level spacing distribution resulting from completely randomly distributed energy levels (see Fig. 6.1) was not a good description of the experimental findings. This was however not surprising, since it was known from the early days of quantum mechanics that energy levels had a tendency to repel each other, giving a smaller statistical weight to small spacings, which was also observed.

Wigner made a conjecture to explain the observed spacing distribution, anmely that the Hamiltonian of the system could be described by a large, random Hermitian matrix, with the matrix elements being independently, Gaussian distributed numbers. The running average, i.e the average over a large number of subsequent energy levels of the physical system, is equivalent to an average over the ensemble of Hamiltoninans, with the eigenvalues of the Hamiltonians corresponding to the energy levels. This was a new idea to statistical physics, where statistical quantities normally were obtained by considering the distribution of a system in position-momentum space, i.e phase space. It turned out, however, that the spacing distribution derived from Wigners conjecture gave an excellent fit to the existing data (see Fig. 6.1). Dyson[86]

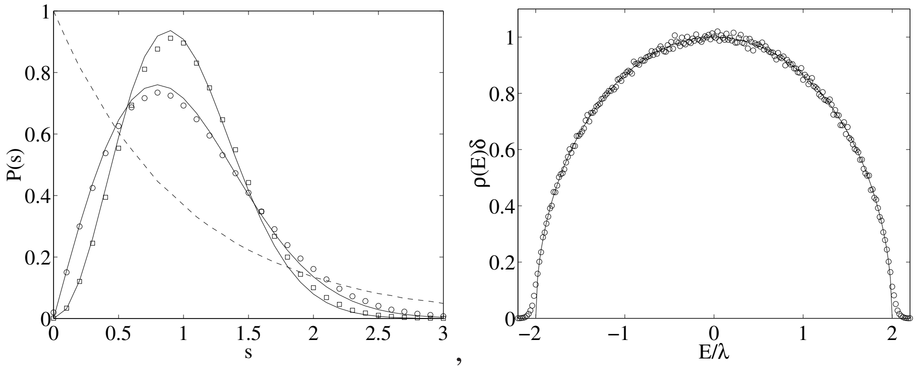

Figure 6.1: Left: The distribution of level spacings. Shown are numerical results for a random Hamiltonian distributed according to Eq. (6.1), for GOE (circles) and GUE (squares). The corresponding Wigner surmise (solid) and the Possin distribution (dashed) are shown for comparison. Right: The numerical result for the average density of states (circles) and the Wigner semi-circle (solid). In both figures, 10000 Hamiltonians of size $M = 100$ have been generated.

found, using group-theoretical arguments, that there were three generic symmetry classes that the Hamiltonian could belong to, with conserved time and spin-rotation symmetry ($\beta = 1$), with broken time reversal symmetry ($\beta = 2$) and with conserved time reversal but broken spin rotation symmetry ($\beta = 4$), respectively. The index $\beta = 1, 2, 4$ corresponds to the number of degrees of freedom of the matrix elements, real, complex or real quaternion. The three Gaussian ensembles of Hamiltonians are called Gaussian Orthogonal Ensemble (GOE) for $\beta = 1$, Gaussian Unitary Ensemble (GUE) for $\beta = 2$ and Gaussian Symplectic Ensemble (GSE) for $\beta = 4$, due to that the distribution $P(H)$ is invariant under transformations $H \to UHU^{-1}$ where U is a orthogonal, unitary or symplectic matrix respectively. In this thesis we will not consider the last class, GSE, relevant for mesoscopic systems with strong spin orbit scattering. The distribution of the Hamiltonian, i.e the joint distribution of the matrix elements, is thus given by

$$P(H) \propto \exp\left[-\frac{1}{\beta}\frac{M}{4\lambda^2}\mathrm{tr}(H^2)\right] = \exp\left[-\frac{1}{\beta}\frac{M}{4\lambda^2}\sum_{i,j}|H_{ij}|^2\right] \tag{6.1}$$

where λ has the dimension energy. The quantity $P(H)dH$ is thus the probability to find a matrix H whose elements are in an interval dH_{ij} around H_{ij} (where for $\beta = 1$, $dH = \prod_{i \leq j} dH_{ij}$).

From the distribution in (6.1), it is possible to derive the distribution of the eigenvalues $\{E_i\}$. Due to the fact that the distribution in Eq. (6.1) depends on the Hamiltonian as $\mathrm{tr}(H^2)$, it is a function of the eigenvalues only, since any Hermitian matrix can be diagonalized $H = UEU^\dagger$. To get the complete distribution of the eigenvalues one must also find the Jacobian from the variable transformation $\{H_{ij}\} \to \{E_i, p_i\}$, where the variables $\{p_i\}$ parameterize U. It was found[191] that the Jacobian is a product of functions of the two sets of parameters $J = f_E(\{E_i\})f_p(\{p_i\})$, with $f_E = \prod_{i<j}|E_i - E_j|^\beta$, giving

$$P(\{E_i\}) \propto \prod_{i \leq j}|E_i - E_j|^\beta \exp\left[-\frac{1}{\beta}\frac{M}{4\lambda^2}E_i^2\right]. \tag{6.2}$$

From this result one can first obtain the average density of states, i.e the inverse mean level spacing, in the limit $M \gg 1$, same for all β,

$$\langle\rho(E)\rangle = \langle\sum_m \delta(E - E_m)\rangle = \frac{M}{\pi\lambda}\sqrt{1 - [E/(2\lambda)]^2}, \tag{6.3}$$

where $\langle..\rangle$ denotes ensemble average. This is known as the Wigner semicircle law for the density of states (see Fig. 6.1) For energies far away from the edges of the spectrum, $E \ll \lambda$, the mean level spacing is given by $\delta = \pi\lambda/M$. This is the region of universality of RMT, where the correlation between different energy levels derived from Eq. (6.2), scaled with δ, only depend on the symmetry index β. The density of states δ is thus not predicted by RMT but has to be found by other means and introduced into the distribution in Eq. (6.1). It should thus be pointed that the density of states predicted by the Wigner semicircle does not describe the density of states of any known physical system.

From Eq. (6.2) one can also find the universal distribution of level spacings $s_i = E_{i+1} - E_i$ in the limit of $M \gg 1$. Wigner did not find the exact expression (found later by Mehta and Gaudin[166]) but he surmised that the result was on the form given by the $M = 2$ result of Eq. (6.2),

$$P(s) \propto (s)^\beta e^{-c_\beta s^2}, \tag{6.4}$$

where $c_\beta = \pi/4$ for $\beta = 1$ and $4/\pi$ for $\beta = 2$. This turned out to be very close to the truth, as is shown in Fig. 6.1. It is interesting to note that the exponential term in the distribution does not arise from the exponential term in Eq. (6.2), but instead from the Jacobian term. This means that the correlations arise from the so called geometrical correlations between matrix elements in large random matrices, and the exact distribution $P(H)$ is not important. This is one feature of the universality of RMT.

6.1.2 Applications to mesoscopic physics

The first period of development of RMT took place in the fifties and sixties and it was almost only used as a tool in nuclear physics. It was however clear that the basic concepts were very general and could perhaps be applied to other fields. In 1965 Gorkov and Eliashberg[103] conjectured that Wigner-Dyson statistics should also apply to the spectral properties of small metallic grains, to explain experiments with microwave absorption by granular metals.

This conjecture was proven in 1982 by Efetov[87,88] who showed, using a so called supersymmetric non-linear σ model, that the spectral properties of a small diffusive grain obeys Wigner-Dyson statistics. Shortly after, another very general conjecture appeared. In 1984 Bohigas, Giannoni and Schmit[57] conjectured that Wigner Dyson statistics applies generically to systems where the classical motion is chaotic. Until today there is no complete proof of this conjecture,[104] although there is a large number of numerical and theoretical studies supporting it. However, very recently Andreev et al[16] were able to show that Wigner-Dyson statistics applies to classically chaotic ballistic systems, chaotic billiards.

Taken together, this implies that at the present stage there is microscopic justification for the Gaussian distribution of the Hamiltonian in Eq. (6.1) for quantum dots which are chaotic due to scattering from either impurities or boundaries. These systems, connected to external leads, are schematically shown in Fig. 6.2. In what follows we will not care about what makes the motion chaotic and simply talk about chaotic quantum dots. In real physical systems the range of universality of RMT is determined by the time (or energy) of ergodicity τ_{erg} (E_{erg}), effectively the time it takes for the electrons in the dot to be randomized. On shorter time scales $t < \tau_{erg}$ (energy differences $|E - E'| > E_{erg}$), deviations from RMT appear.[9,18] The ergodic energy is approximately given by the Thouless energy of the closed system, $E_{erg} \approx \hbar v_F / L^2 \min(l, L)$, i.e the inverse time of flight through the system.

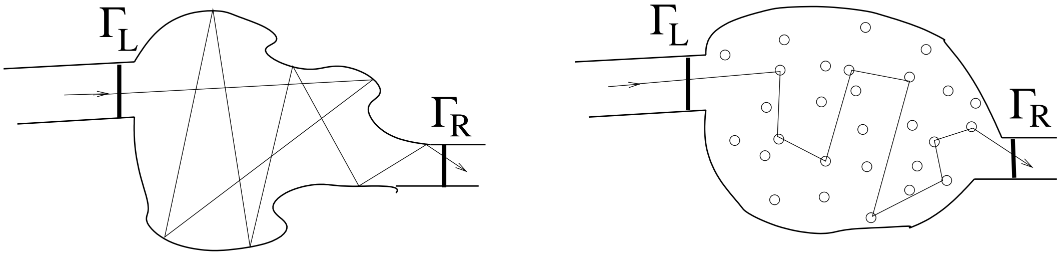

Figure 6.2: Schematic pictures of the two types of dots with chaotic classical dynamics. Left, the chaotic motion is due to irregularly shaped dot boundaries, right due to impurity scattering. The dots are connected to reservoirs via contacts with mode independent tunnel barriers Γ_L and Γ_R.

It should be pointed out that the second extensively studied mesoscopic object in RMT is quasi-one dimensional diffusive wires. Many of the results discussed in this chapter for chaotic quantum dots have analogues in diffusive wires, and we will sometimes present the results for a diffusive wire for comparison. However, due to the limited scope of the thesis, we will put the emphasis on chaotic dots and the interested reader is referred to e.g. Refs 48, 221 for comprehensive reviews.

6.1.3 Transition between ensembles

The ensembles GUE and GOE discussed above are appropriate for physical situations where time reversal symmetry is completely broken or conserved. It is often interesting to study the transition between the two ensembles, i.e situations where time reversal symmetry is partially broken by an applied magnetic field. This can be done by considering a Hamiltonian[165,186]

$$H = H_0 + i\gamma H_1 \tag{6.5}$$

where H_0 is a real, symmetric and H_1 is a real, anti symmetric $M \times M$ matrix, independently distributed with the same Gaussian distribution, and γ is the symmetry breaking parameter. The resulting distribution of H is given by the so called Pandey-Metha distribution

$$P(H) \propto \exp\left(-\frac{M(1+\gamma^2)}{4\lambda^2}\sum_{i,j=1}^{M}[\mathrm{Re}(H_{ij})^2+\frac{1}{\gamma^2}\mathrm{Im}(H_{ij})^2]\right), \tag{6.6}$$

This distribution interpolates between GOE for $\gamma = 0$ and GUE for $\gamma = 1$. One can note that in this intermediate regime, the eigenvalues $\{E_i\}$ and the eigenvectors in U are no longer independently distributed. It is possible to relate the parameter γ to the magnetic flux through the dot[58, 93]

$$\gamma \simeq \frac{\Phi}{\Phi_0}\sqrt{\frac{E_{erg}}{M\delta}} \tag{6.7}$$

where $\Phi_0 = h/e$ is the flux quantum. The GOE-GUE transition is effectively completed on an energy scale E if $\Phi/\Phi_0 > \sqrt{E/E_{erg}}$, i.e in a dot where the level spacing $\delta \ll E_{erg}$, time reversal symmetry is already broken on the energy scale δ for a magnetic flux $\simeq \Phi_0\sqrt{\delta/E_{erg}}$, much smaller than a flux quantum through the dot, since the ergodic energy is much larger than the mean level spacing.

6.2 Open systems; Random Matrix Theory of the scattering properties

When the chaotic quantum dot is connected to one or several electron reservoirs, the system is open. In the discussion below we will for simplicity consider a dot connected to two electron reservoirs via leads, to study transport through the dot. Each lead has N transverse modes and contain tunnel barriers with mode independent transmission probabilities Γ_L and Γ_R (see Fig. 6.2). Generalizations to more leads, different number of transverse modes in the leads or mode independent tunnel barrier transparencies are straightforward.

The bound states of the dot get broadened due to the coupling to the reservoirs, with a width of order E_{Th}. It is known that charging effects become important[141, 212] if the dot is weakly coupled to the reservoirs, $G \ll 2e^2/h$, i.e the broadening of the levels is smaller than the level spacing, $E_{Th} < \delta$. In Fig. 6.3 the density of states, given by Eq. (2.40), for the two opposite limits $E_{Th} \ll \delta$ and $E_{Th} \gg \delta$ are plotted. A large number of studies have been devoted to the effect of chaotic dynamics in this so called Coulomb blockade regime, see Refs. 5, 48, 104 for reviews. In this thesis we always assume that the condition for Coulomb blockade is not fulfilled, and we thus neglect charging effects. The quasiparticles injected into the dot from the reservoirs spend a certain time in the dot before scattering out of the dot into one of the reservoirs. The dwell time τ_w averaged over all the injected modes is given by Eq. (2.41), and the ensemble averaged dwell time $\langle\tau_w\rangle$ is simply related to the mean level spacing as $\langle\tau_w\rangle = \hbar\pi/(2N\delta)$. As was mentioned in Chapter 2, the relevant quantity for our studies is the average time $\langle\tau_d\rangle$ the quasiparticle dwells in the dot after having been injected, sometimes referred to as the escape time. This time is related to the dwell time simply as $\langle\tau_d\rangle = \langle\tau_w\rangle/(\Gamma_L+\Gamma_R)$, i.e only divided by the probability to enter the dot. The corresponding Thouless energy E_{Th} is given by

$$E_{Th} = \frac{N(\Gamma_L+\Gamma_R)\delta}{\pi} \tag{6.8}$$

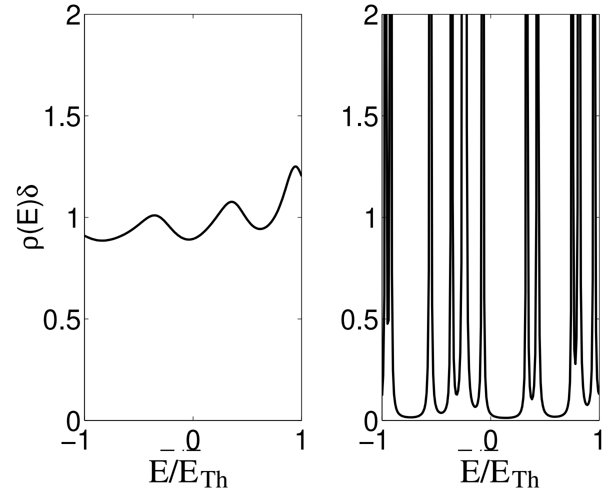

Figure 6.3: The normalized density of states as a function energy in the regimes where the broadening of the states is much larger, E_{Th} δ, (left) and smaller E $_{Th}$ δ (right) than the mean level spacing, for one given random Hamiltonian drawn from GOE.

It is important to note that the Thouless energy of the open dot, E_{Th} is much smaller than the Thouless energy of the closed dot (approximately equal to the ergodic energy E_{erg}), roughly by a factor of the area of the openings in the dot divided by the total area of the dot multiplied by the tunnel probability to escape out through the openings.

6.2.1 Theoretical and experimental studies of quantum dots

The distributions for the Hamiltonians presented above in Eq. (6.1) and (6.6), together with the relation between the scattering matrix and the Hamiltonian of the closed dot in Eq. (2.32), are in principle enough to study the transport through the open dot. A large number of theoretical studies of different transport properties of chaotic quantum dots have been carried out, for a review see e.g. Refs. 5, 48, 104.

In the major part of the transport experiments carried out on chaotic dots, see e.g. Refs 71, 116, 131, 161, 184, good agreement is found with the theoretical predictions of RMT, if one takes into account temperature effects and dephasing.[30,61,66] However, in the Coulomb blockade regime, the results are more ambiguous.[187,215–217] As an example, the distribution of the level spacings is found to deviate strongly from the theoretically predicted Wigner-Dyson distribution (Fig. 6.1). The reason for these discrepancies is assumed to be electron-electron interactions, which makes the independent particle picture inappropriate and leads to a different statistical distribution of the level spacings.

The theoretical calculations have been performed with a number of different approaches, semi-classical or fully quantum mechanical RMT methods, where the latter are usually starting from the Hamiltonian ensemble in Eq. (6.1), applying diagrammatic approaches or the so called nonlinear σ-model (see e.g references in 5, 48, 104). The path taken in this thesis is however different. In 1995 Brouwer[60] showed that it is possible, starting from the Gaussian ensemble of Hamiltonians, directly to find the distribution of the scattering matrix S in Eq. (2.32), which in many cases simplifies calculations considerably. In this thesis we will only use the Hamiltonian ensemble for numerical calculations, and do not discuss any analytical techniques for the averaging over the Hamiltonian ensemble.

6.2.2 Distribution of the scattering matrix

As was shown in Ref. 60 it is possible, starting from the Gaussian ensemble of Hamiltonians, to find the distribution of the scattering matrix S in Eq. (2.32). The distribution of S is given by the so called Poisson kernel

$$P(S) \propto |\det(1-\langle S\rangle^{\dagger} S)|^{-\beta(2N-1+2/\beta)}. \tag{6.9}$$

where the average scattering matrix at $E \ll \lambda$ for $M \to \infty$ is[235]

$$\langle S\rangle = \frac{M\delta - \pi^2 W^{\dagger}W}{M\delta + \pi^2 W^{\dagger}W} = \begin{pmatrix} \sqrt{1-\Gamma} & 0 \\ 0 & -\sqrt{1-\Gamma} \end{pmatrix}. \tag{6.10}$$

Note that the distribution of S in Eq. (6.9) has physical relevance for any number of modes N, i.e. one does not have to take the limit $N \to \infty$ to make contact to a physical system, since a dot with two mode contacts makes perfect sense. The second equality in Eq. (6.10) allows us to write the eigenvalues w_n of the Hermitian matrix $W^{\dagger}W$ in terms of Γ as

$$w_n = \frac{M\delta}{\pi^2\Gamma}(2-\Gamma \pm 2\sqrt{1-\Gamma}) \tag{6.11}$$

noting that Γ does not determine w_n uniquely. Since the distribution of S depends on $\langle S\rangle$ only, via the Poisson kernel in Eq. (6.9), any averaged quantity can only depend on the w_n's. We can thus without any loss of generality choose the matrix elements of W as $W_{nm} = \delta_{nm}\sqrt{w_n}$.

The distribution in Eq. (6.9) holds for each energy, but provides no information on how scattering matrices at different energies are correlated. To find this information, further discussed below, one has to turn to the underlying Hamiltonian ensemble in (6.1). However, in many cases, like transport properties on Fermi energy, the energy dependence of the scattering matrix is not necessary, and one can use the distribution given in (6.9). Moreover, Brouwer et al.[64] have developed a scattering matrix approach to deal with a parameter dependence of the scattering matrix, like energy or magnetic field, equivalent to the Hamiltonian approach.

The most important message for practical calculations in Eq. 6.9 is that for perfect leads connecting the dot, i.e $\Gamma = 1$, the average scattering matrix is zero, $\langle S\rangle = 0$. This means that $P(S) = 1$, and thus that S is uniformly distributed in the group of unitary matrices, only subject to the global symmetries ($\beta = 1, 2$ or 4). The resulting ensembles of unitary matrices are known as the Circular Orthogonal Ensemble (COE) ($\beta = 1$), Circular Unitary Ensemble (CUE) ($\beta = 2$) and Circular Symplectic ensemble (CSE) ($\beta = 4$), where "circular" comes from the fact that the eigenvalues are uniformly distributed on the complex unit circle and "orthogonal", "unitary" and "symplectic" have the same origin as for the corresponding Gaussian ensembles, discussed above.

These ensembles were introduced already by Dyson[86] as a more elegant tool to model the spectral statistics discussed above, since for the unitary group there is no need to impose an external weight on the elements [like $\exp(-M/(4\beta\lambda^2)H^2)$ in Eq. (6.1)] to get convergent integrals when performing an average over the group.

6.3 Averages over the unitary group

The technical aspect of the problems discussed in this thesis concerns the ensemble averaging of a given transport quantity, expressed as a function of the scattering matrix of the dot. The average of a function of the scattering matrix over the Poisson kernel in Eq. (6.9) for dots connected to nonideal leads is in general difficult to carry out directly; in most cases it is convenient to decompose the scattering matrix of the dot with the tunnel barriers into the separate scattering matrices of the barriers and the dot without barriers, as in Eq. (2.28). One can then concentrate on performing the average over a function of the unitary group, over COE or CUE depending on the presence or absence of a time reversal symmetry(TRS)-breaking magnetic field.

Several studies have been performed on averaging over the unitary group,[19,62,82,168,196] also of importance in other fields of physics. Here we just present the general approach to parameterize the scattering matrix, mostly useful for problems where the scattering matrix has a small number of modes, as well as an outline of the diagrammatic approach presented by Brouwer and Beenakker[62] (see also ref. 19), especially convenient for the opposite limit of a large number of modes $N \gg 1$.

6.3.1 Averaging over the variables parametrizing S

The uniformity of the distribution of S is defined with respect to the measure $d\mu(S)$[109] in matrix space, such that $d\mu(S)$ is invariant under multiplication with fixed unitary matrices U, V as $S \to USV$ (where $V = U^T$ for $\beta = 1$ to preserve the symmetry of S), in other words that all matrices in the the unitary group have the same statistical weight. This invariance property is enough[86] to completely determine the distribution of S (in contrast to the Hamiltonian ensemble discussed above).

The distribution of S is related to a given distribution of variables $\{x_n\}$ that parameterizes S, like

$$P(\{x_n\}) \prod_i dx_i = 1/\mathcal{V} d\mu(S) \tag{6.12}$$

where $\mathcal{V} = \int d\mu(S)$ is the volume of the matrix space. The general method to calculate the distribution $P(\{x_n\})$ is first to consider the infinitesimal change dS related to an infinitesimal change dx_i in the parameterizing variables. A so called metric tensor g_{ij} is defined as

$$g_{ij} = \mathrm{yr}\left(\frac{dS}{dx_i}\frac{dS^\dagger}{dx_j}\right) \tag{6.13}$$

from which one obtains $\rho(\{x_n\}) \propto |\det\,(g)|^{1/2}$. As an example, consider the 2×2 symmetric ($\beta = 1$) scattering matrix S, which can be parametrized as

$$S = \begin{pmatrix} \sqrt{1-D}e^{i\psi_r} & \sqrt{D}e^{i\psi_t} \\ \sqrt{D}e^{i\psi_t} & -\sqrt{1-D}e^{2\psi_t-\psi_r} \end{pmatrix}, \tag{6.14}$$

with T, ψ_r and ψ_t free parameters. The derivatives in (6.13) are then given by

$$\frac{dS}{dT} = \begin{pmatrix} -\frac{1}{2\sqrt{1-D}}e^{i\psi_r} & \frac{1}{2\sqrt{D}}e^{i\psi_t} \\ \frac{1}{2\sqrt{D}}e^{i\psi_t} & \frac{1}{2\sqrt{1-D}}e^{i(2\psi_t-\psi_r)} \end{pmatrix}, \tag{6.15}$$

$$\frac{dS}{d\psi_r} = \begin{pmatrix} i\sqrt{1-D}e^{i\psi_r} & 0 \\ 0 & -i2\sqrt{1-D}e^{i(2\psi_t-\psi_r)} \end{pmatrix}, \tag{6.16}$$

$$\frac{dS}{d\psi_t} = \begin{pmatrix} 0 & \sqrt{D}e^{i\psi_t} \\ \sqrt{D}e^{i\psi_t} & -i2\sqrt{1-D}e^{i(2\psi_t-\psi_r)} \end{pmatrix}. \tag{6.17}$$

From these derivatives, taking the traces in Eq. (6.13) gives the elements of g,

$$g = \begin{pmatrix} \frac{1}{2\sqrt{D(1-D)}} & 0 & 0 \\ 0 & 2(1-D) & -2(1-D) \\ 0 & -2(1-D) & 2(2-D) \end{pmatrix} \tag{6.18}$$

and the determinant $\det(g) = 2/D$. With proper normalization, the joint probability distribution becomes $\rho(D,\psi_t,\psi_r) = 1/(8\pi^2\sqrt{D})$, independent of the scattering phases. In the case of broken time reversal symmetry ($\beta = 2$), the same procedure, now with the additional free parameter ψ_t', gives the distribution $\rho(D,\psi_t,\psi_r,\psi_t') = 1/(8\pi^3)$, i.e a constant, independent on any of the parameterizing variables. The average over a function $f(S)$ of the symmetric scattering matrix ($\beta = 1$) is thus written

$$\langle f(S)\rangle_S = \frac{1}{\mathcal{V}}\int f(S)d\mu(S) = \frac{1}{8\pi^2}\int_{-\pi}^{\pi} d\psi_r \int_{-\pi}^{\pi} d\psi_t \int_0^1 dD \frac{1}{\sqrt{D}} f(D,\psi_r,\psi_t) \tag{6.19}$$

and the average over the scattering matrix not subjected to the symmetry constraint ($\beta = 2$) is given analogously.

6.3.2 Diagrammatic technique for averaging over the unitary group

The method to perform the average via the parameterizing variables becomes in general awkward for large scattering matrices, $N \gg 1$. In this limit, it is often more convenient to perform the average over the unitary matrix directly, applying the diagrammatic technique of Brouwer an Beenakker.[62] One can then obtain a perturbative expression for the averaged quantity in terms of the small parameter $1/N$, giving to leading order the "classical" result, $O(N)$ and to sub-leading order the quantum corrections $O(1)$. Here we will only present the approach to calculate the leading order contributions, used in the last chapter of the thesis.

The quantities to be averaged over (discussed in detail below) will be traces of products of unitary and fixed matrices. To illustrate the technique we will consider the three functions [largely the same as in Ref. 62] $f = \mathrm{tr}(AUBU^\dagger)$, $g = \mathrm{tr}(AUBUCU^\dagger DU^\dagger)$ and $h = \mathrm{tr}(A(1-UB)^{-1}UCU^\dagger(1-DU^\dagger)^{-1}) = \sum_{n,m}\mathrm{tr}(A[UB]^n UCU^\dagger[DU^\dagger]^m)$ where A, B, C and D are fixed matrices. The different elements of the trace are represented by the diagrammatic symbols shown in Fig. 6.4 The three traces can then be diagrammatically shown as in Fig. 6.5 , where for

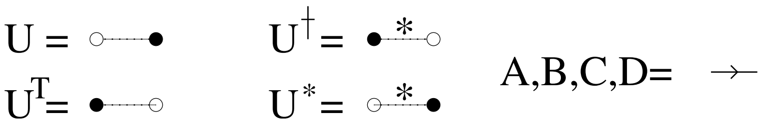

Figure 6.4: Diagrammatic representation of the different matrices in the functions to be averaged

the function h only one term in the expansion is shown. To calculate the average, we sum up the contributions to highest order in $1/N$ from all possible diagrams that can be constructed according to the following rules:

1) For CUE, connect black dots attached to U or U^T to black dots attached to U^* or $U^\dagger$ with thin lines. Do the same for white dots (In COE, black dots can also be connected to white dots

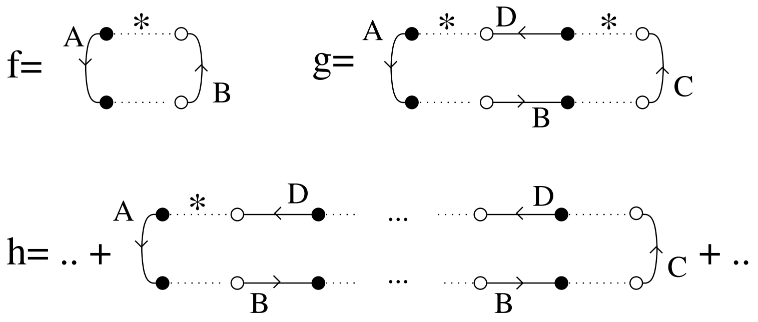

Figure 6.5: Diagrammatic representation of the different functions f, g and h

and vice versa). The lines must be drawn in such a way that they do not cross (crossing lines are associated with lower order contributions).

2) Each closed cycle of alternating thick lines (corresponding to a matrix A, B, C or D) and thin lines correspond to a trace of the product of the matrices in the order traversed in the cycle. A matrix traversed opposite to it's direction (shown as the thick line arrow) appears transposed in the trace.

3) Every closed cycle of alternating dotted lines (corresponding to the unitary matrices U) and thin lines contain $2j$ dotted lines and is attributed a weight $1/N^j$.

4) The total value of the diagram is given by the product of the traces of matrices A, B, C and D from 2) and the weights from 3).

The diagrammatic contributions from the three functions f, g and h are shown in Fig. 6.6 (the same for CUE and COE in these cases). It follows from the diagrammatic rules that the

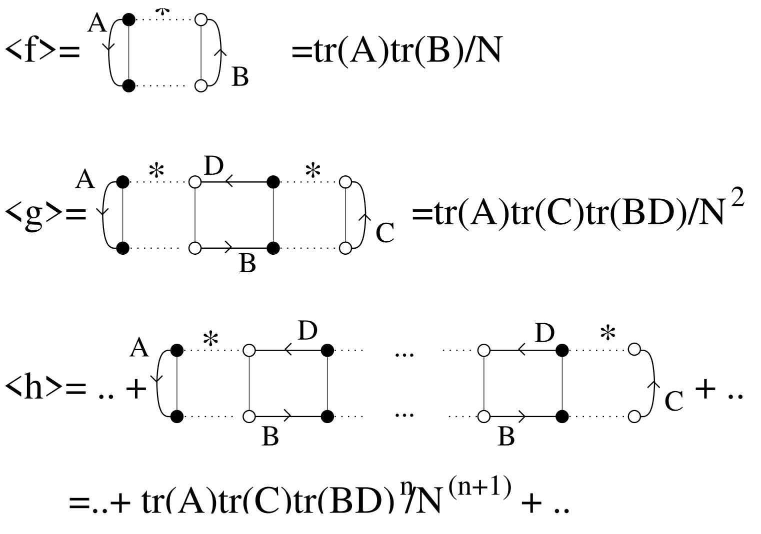

Figure 6.6: Diagrammatic representation of the different matrices in the functions to be averaged

number of complex conjugated (U^* and $U^\dagger$) and not complex conjugated (U and U^T) matrices in the matrix product must be the same in order to get a nonzero contribution from the average. To get the total average of h, one has to sum up all the averaged terms, obtaining

$$\langle h\rangle = \sum_{n\geq 0} \mathrm{tr}(A)\mathrm{tr}(C)\mathrm{tr}(BD)^n/N^{n+1} = N\frac{\mathrm{tr}(A)\mathrm{tr}(C)/N^2}{1-\mathrm{tr}(BD)/N^2} \tag{6.20}$$

which is of order N since each trace has a value of order N. It should be noted that the three example functions f, g and h are particularly simple to average, already the average of e.g $(1-$

$UBU^{\dagger}U)^{-1}$ with U in COE, leads to a self-consistent, Dyson equation-like, result. The simple averages of the type discussed above are however the only ones appearing in the calculations in this thesis.

As an example of Eq. (6.20), one can straightforwardly calculate the average conductance of a dot with non-ideal leads. It follows from Eq. (2.28) that the conductance of the dot, given by the Landauer formula in Eq. (2.17), is

$$\begin{aligned} G &= \frac{2e^2}{h}\mathrm{tr}(tt^{\dagger}) = \frac{2e^2}{h}\mathrm{tr}(\sigma_{01}S\sigma_{10}S^{\dagger}) \\ &= \frac{2e^2}{h}\mathrm{tr}(\sigma_{01}\tilde{r}\sigma_{10}\tilde{r}^{\dagger} + \sigma_{01}\tilde{t}'S_0(1-\tilde{r}'S_0)^{-1}\tilde{t}\sigma_{01}\tilde{t}^{\dagger}(1-S_0^{\dagger}\tilde{r}'^{\dagger})^{-1}S_0^{\dagger}\tilde{t}'^{\dagger} \\ &+ \sigma_{01}\tilde{r}\sigma_{10}\tilde{t}^{\dagger}(1-S_0^{\dagger}\tilde{r}'^{\dagger})^{-1}S_0^{\dagger}\tilde{t}'^{\dagger} + \sigma_{01}\tilde{t}'S_0(1-\tilde{r}'S_0)^{-1}\tilde{t}\sigma_{10}\tilde{r}^{\dagger}) \end{aligned} \tag{6.21}$$

where $(\sigma_{10})_{ij} = 1$ if $i = j \leq N$ and zero otherwise and $\sigma_{01} = 1 - \sigma_{10}$. The matrix S_0 is the scattering matrix of the dot without barriers, uniformly distributed in the unitary group, and we can perform the average of G directly over S_0. The two last terms in Eq. (6.21) has a zero average, since they only contain S_0 or $S_0^{\dagger}$, while the first term is exactly zero, since $\tilde{r}$ is diagonal. Thus, only the second term contribute to the average, and is given directly by Eq. (6.20), noting that S_0 has the dimension $2N \times 2N$

$$\langle G\rangle = \frac{2e^2}{h}2N\frac{\mathrm{tr}(\tilde{t}'^{\dagger}\sigma_{10}\tilde{t}')\mathrm{tr}(\tilde{t}^{\dagger}\sigma_{01}\tilde{t})/(2N)^2}{1-\mathrm{tr}(\tilde{r}'\tilde{r}'^{\dagger})/(2N)} = \frac{2e^2}{h}N\frac{\Gamma_L\Gamma_R}{\Gamma_L+\Gamma_R}, \tag{6.22}$$

which is just the classical conductance of two tunnel barriers in series.

6.4 Linear statistics and the transmission eigenvalue distribution

6.4.1 Average of a linear statistic

For a large number of transport quantities where $N \gg 1$, it is not necessary to perform the average of the desired quantity employing the full diagrammatic machinery. As an example, the linear response conductance in Eq. (2.17) can be written in terms of the eigenvalues D_n of the Hermitian matrix product $tt^{\dagger} = UDU^{\dagger}$, where $D = \mathrm{diag}(D_1, ...D_N)$, as

$$G = \frac{2e^2}{h}\sum_{n=1}^{N} D_n. \tag{6.23}$$

It thus suffices to know the distribution of the eigenvalues D_n, called the transmission eigenvalues, to calculate the average conductance. This can be calculated, starting from the uniform distribution of the scattering matrix. The first step is to use the fact that the scattering matrix can be decomposed according to the so called polar decomposition[164, 167]

$$S = \begin{pmatrix} U & 0 \\ 0 & V \end{pmatrix}\begin{pmatrix} \sqrt{1-D} & \sqrt{D} \\ \sqrt{D} & -\sqrt{1-D} \end{pmatrix}\begin{pmatrix} U' & 0 \\ 0 & V' \end{pmatrix}, \tag{6.24}$$

where U, U', V, V' are unitary matrices. For a symmetric scattering matrix, $U' = U^T$ and $V' = V^T$. The scattering matrix S can be parametrized by the $D_n's$ and a number of additional variables parameterizing U, U', V and V'. Baranger and Mello[29] and Jalabert et al[126]found the Jacobian relating the two sets of variables, giving the relation to the invariant measure in Eq. (6.12),

$$d\mu(S) = \prod_{n<m} |D_n - D_m|^\beta \prod_k D_k^{-1+\beta/2} \prod_i dD_i d\mu(U) d\mu(U') d\mu(V) d\mu(V') \tag{6.25}$$

i.e. that the matrices U, U', V, V' are themselves uniformly distributed in the group of unitary matrices (CUE), while the transmission eigenvalues have the distribution

$$P(\{D_n\}) = \prod_{n<m} |D_n - D_m|^\beta \prod_k D_k^{-1+\beta/2} \tag{6.26}$$

One can note that the transmission eigenvalues contain the same "repulsion" factor $\prod_{n<m} |D_n - D_m|^\beta$ as the distribution of eigenenergies in the Hamiltonian ensemble in Eq. (6.2). This shows that there is a similar strong correlation between the transmission eigenvalues. For $N = 1$ one immediatly recovers the result in Eq. (6.19), when the scattering angles have been integrated out. This is plotted in Fig. 6.7. A further simplification can be found for the large number of transport quantities, like the linear response conductance, which are so called linear statistics of the transmsission eigenvalues,

$$A = \sum_n a(D_n) \tag{6.27}$$

where the "linear" indicates that the function $a(D_n)$ does not contain any products of different $D_n's$, while $a(D_n)$ can be any function of the single eigenvalue D_n. It is then clear that the average over this linear statistic can be found from

$$\begin{aligned} \langle A \rangle &= \sum_n \int P(\{D_i\}) a(D_n) \prod_i dD_i = \sum_n \int a(D_n) \left[\int P(\{D_i\}) \prod_{i \neq n} dD_i \right] dD_n \\ &= \int \rho(D) a(D) dD, \end{aligned} \tag{6.28}$$

where

$$\rho(D) = \langle \sum_n \delta(D - D_n) \rangle \tag{6.29}$$

is the transmission eigenvalue density. In the limit of large number of modes $N \gg 1$ it is possible to find both the leading and sub-leading order contribution to the transmission eigenvalue density[29, 126]

$$\rho(D) = \frac{N}{\pi} \frac{1}{\sqrt{D(1-D)}} - \frac{1}{4}(1 - 2/\beta)[\delta(D) - \delta(1-D)]. \tag{6.30}$$

This convenient form allows direct calculations of the average of any linear statistic, the leading order "classical" term as well as the quantum correction. Note that the leading order term is the same for COE and CUE, while the quantum correction depends on β.

As an example, the conductance in Eq. (6.23) becomes

$$\langle G \rangle = \frac{2e^2}{h} \left[\frac{N}{2} + \frac{1}{4} \left(1 - \frac{2}{\beta} \right) \right], \tag{6.31}$$

where the leading order term coincides with the result in Eq. (6.22) for $\Gamma_L = \Gamma_R = 1$. This result can be qualitative understood by realizing that the chaotic dot is chaotic just in the sense that half of the injected quasiparticles scatter back through the injection contact, while the other half scatter out through the other contact, giving a "classical" conductance $N/2$. The subleading order, the weak localization correction to the conductance, is zero for broken TRS ($\beta = 2$) but finite and negative, $-e^2/2h$ for conserved TRS. (One can note that this is very close to the well known result for a diffusive wire, where the weak localization correction is $-2e^2/3h$ for conserved TRS.) The conductance in Eq. (6.23) is only one transport quantity that is a linear statistic. Another example is the zero frequency shot noise, $P = P_0 \sum_{n=1}^{N} D_n(1-D_n)$; more linear statistics are presented below in connection to transport in chaotic dot-superconductor proximity structures.

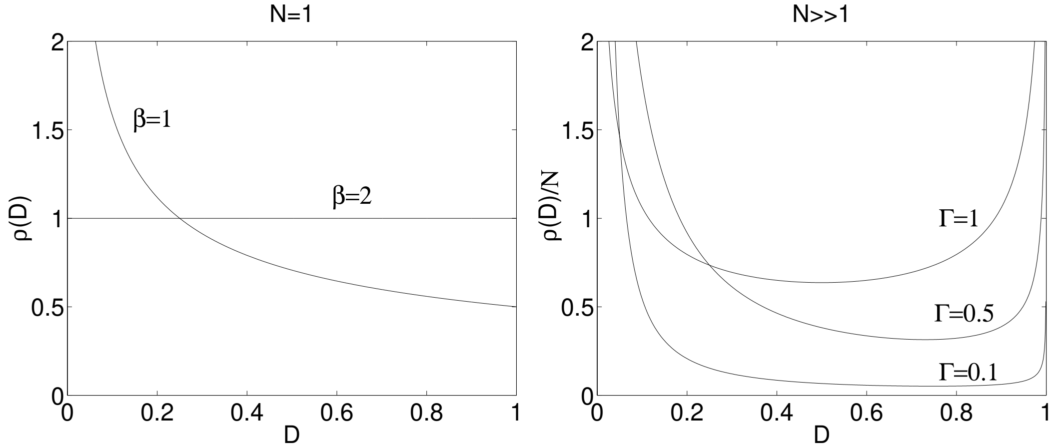

Figure 6.7: Transmission eigenvalue distribution $\rho(D)$ for a single mode dot, $N = 1$, with conserved ($\beta = 1$) and broken ($\beta = 2$) time reversal symmetry (Left panel) and a dot with a large number of modes N 1 with different barrier transparency $\Gamma = 1, 0.5$ and 0.1 (Right panel).

This makes it interesting to study the transmission eigenvalue distribution for other systems than the chaotic dot coupled to ideal leads, presented in Eq. (6.30). Brouwer and Beenakker[62] calculated the eigenvalue distribution for arbitrary barrier transparency for tunnel barriers in the leads, which for similar barriers, transparency Γ, in both leads becomes

$$\rho(D) = \frac{N}{\pi} \frac{\Gamma(2-\Gamma)}{[\Gamma^2 + 4D(1-\Gamma)]\sqrt{D(1-D)}}. \tag{6.32}$$

This distribution is plotted in Fig. 6.7 for different Γ. A very general and powerful circuit approach to calculate the transmission eigenvalue distribution in mesoscopic conductors has been presented by Nazarov,[181] allowing one to calculate the transmission eigenvalue distribution for any combination of mesoscopic scattering elements like diffusive wires, tunnel barriers and point contacts.

6.4.2 Variance of a linear statistic

Using the diagrammatic approach above, one can also study the sample-to-sample fluctuations of a function f of the scattering matrix S, given by the variance

$$\mathrm{var}(f) = \langle f^2 \rangle - \langle f \rangle^2 \tag{6.33}$$

This general approach is not studied in this thesis; we instead focus on the variance of a linear statistic. In contrast to the average quantities of a linear statistic, it does not suffice to know the density of transmission eigenvalues to calculate the variance. This is clear since the average $\langle A^2 \rangle$ contains cross products of different transmission eigenvalues. One therefore also needs the so called two-point correlation function $K(D,D') = \langle \sum_{i,j} \delta(D-D_i)\delta(D-D_j) \rangle - \rho(D)\rho(D')$, in principle possible to find from the full distribution of the transmission eigenvalues in Eq. (6.26).

Beenakker found,[45] using a method of functional derivatives, an expression for this correlation function, and showed that it was possible to write the variance of a linear statistic like

$$\mathrm{var}(A) = -\frac{1}{\beta\pi^2}\int_0^1 dD \int_0^1 dD' \frac{da(D)}{dD}\frac{da(D')}{dD'} \ln \left| \frac{\sqrt{D'}\sqrt{1-D}-\sqrt{D}\sqrt{1-D'}}{\sqrt{D'}\sqrt{1-D}+\sqrt{D}\sqrt{1-D'}} \right| . \tag{6.34}$$

The variance of the conductance in Eq. (6.23) becomes

$$\mathrm{var}(G/[2e^2/h]) = \frac{1}{8\beta}. \tag{6.35}$$

Thus, the fluctuation of the conductance is an order N smaller than the average conductance, which can be seen as a result of the strong correlation between the transmission eigenvalues, pointed out below Eq. (6.26). Completely uncorrelated transmission eigenvalues would instead give a variance $\sim N$. This strong correlation is therefore, just as the correlation between the eigenvalues of the Gaussian ensembles in Eq. (6.1), a consequence of that the transport beeing completely phase coherent but also of the fact that the quasiparticles are randomized by the chaotic scattering in the dot. It can be noted that the value in Eq. (6.35) is, just like the weak localization correction, very close to the well known[8,154] value for the universal conductance fluctuations in a diffusive wire, given by $2/15\beta$.

6.5 Correlations between scattering matrix elements at different energies and magnetic fields

A problem often encountered is to find the correlation between scattering matrix elements at different energies, e.g. in normal conductor-superconductor systems discussed below. Moreover, when studying systems with finite applied magnetic field not large enough to break time reversal symmetry, it also generally appears the problem of calculating the correlation function between scattering matrix elements at different magnetic fields. Both these problems appear in the last chapter of the thesis.

The correlator to study is

$$C_{X,\delta X} = \mathrm{tr}(\langle S(X)S^*(X+\delta X)\rangle) - \mathrm{tr}(\langle S(X)\rangle\langle S^*(X+\delta X)\rangle), \tag{6.36}$$

with X being energy or magnetic field. Several other type of correlators have been studied, e.g. the conductance autocorrelation function,[89,94] which can be immediately measured in experiments.

The correlator in Eq. (6.36) is plotted as a function of energy difference δE normalized with the Thouless energy for unity transparencies $\Gamma_L = \Gamma_R = 1$, the case discussed in this thesis, in Fig. 6.8. The result does not depend on the absolute value of the energy E. Only the result for scattering matrices in COE are shown, the result for CUE is similar. One notes that the result is in good agreement with the semi-classical result[56,235] $C_{E,\delta E} = 1/[1+i\delta E/(4E_{Th})]$ for

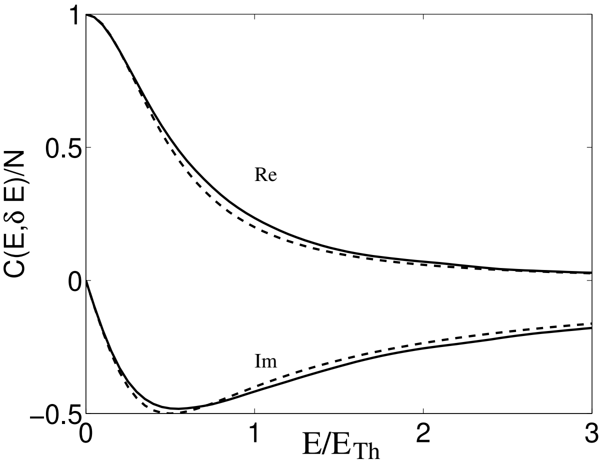

Figure 6.8: The numerical result for the real and imaginary part of the normalized correlation function $C_{E,\delta E}/N$ as a function of energy. The matrix dimensions are $N = 10$ and $M = 400$ and 1000 random Hamiltonians have been generated. The semi-classical result is shown as a comparison (dashed line).

ideal contacts. The correlation between scattering matrix elements, $|C_{0,\delta E}|$, thus decays as a Lorentzian with increasing energy difference, on an energy scale of order E_{Th}. This means that the correlation between matrix elements at energy differences $\delta E \gg E_{Th}$ is zero and that the scattering matrices $S(E)$ and $S(E+\delta E)$ are statistically independent.

For a magnetic field the situation is somewhat different. By applying a magnetic field, the time reversal symmetry is successively broken and there is a corresponding transition between the ensembles COE and CUE. In open systems, the critical magnetic field B_c on which scale the transition is completed is given by[48, 89, 94]

$$B_c \simeq \frac{\Phi_0}{A}\sqrt{\frac{\hbar}{\tau_{erg}E_{Th}}} \tag{6.37}$$

and we can thus relate the symmetry breaking parameter γ for $\gamma \ll 1$ in Eq. (6.6) to the applied magnetic field as $\gamma = B/B_c\sqrt{2\pi M/N}$.

The correlator $C_{0,\delta B}$ in Eq. (6.36) is plotted as a function of magnetic field difference δB divided by the critical magnetic field B_c for ideal leads $\Gamma_L = \Gamma_R = 1$ in Fig. 6.8. The result is compared to the theoretical result,[63, 125] $C_{0,\delta B} = 1/(1+\delta B/2B_c)^2$. The correlation between scattering matrix elements, $|C_{B,\delta B}|$ decays monotonically with increasing magnetic field difference, on an magnetic field scale of order B_c. This means that the correlation between matrix elements at energy differences $\delta B \gg B_c$ is zero, independent of B, and that the scattering matrices $S(B)$ and $S(B+\delta B)$ are statistically independent. This result is utilized in the last chapter.

6.6 Applications to chaotic dot-superconductor systems

In this thesis we are mainly interested in the Josephson effect in junctions where a chaotic dot is coupled to two superconducting electrodes, a so called chaotic Josephson junction. When a chaotic quantum dot is put in contact with a superconductor, it's spectral properties are dramatically changed.[6, 95, 118, 135, 159, 170, 171, 203] A gap of magnitude $E_g \sim \min(\Delta, E_{Th})$ opens up in the spectrum around Fermi energy. The induced gap is a generic feature of all chaotic conductors put in contact with superconductors and is in stark contrast to the situation when a

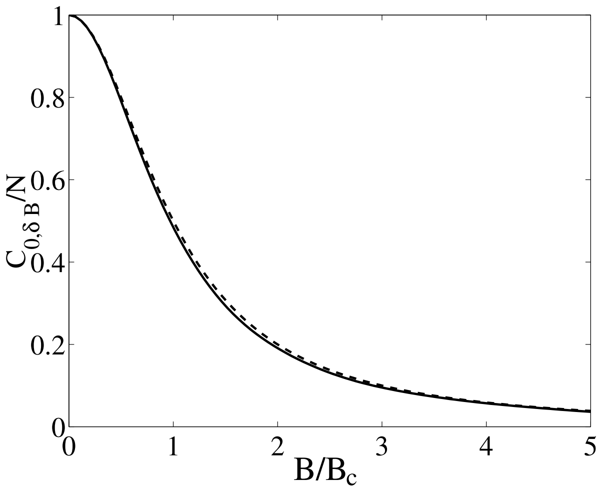

Figure 6.9: The numerical result for the normalized correlation function $C_{B=0,\delta B}/N$ as a function of magnetic field δB. The matrix dimensions are $N = 10$ and $M = 400$ and 1000 random Hamiltonians have been generated. The semi-classical result is shown as a comparison (dashed line).

conductor with integrable motion is connected to a superconductor.[170] In an integrable conductor, the density of states instead increases as a power law in energy (similar to e.g. the Josephson current density in wide ballistic junctions, studied in the previous chapter, noting that $i(E) \propto d\rho(E)/d\phi$). In the case when the chaotic dot is connected to two superconducting reservoirs with different phases, the gap becomes phase-dependent.[170,171] In the limit $E_{Th} \ll \Delta$, the gap is closed by a magnetic field[171] $B \gg B_c$, i.e the same field required to break time reversal symmetry in the dot, given in Eq. (6.37). (One can note that these features are qualitatively the same as has been discussed in diffusive normal metal-superconductor proximity systems, see e.g. Ref. 49.)

Several aspects of the conductance of the dot coupled to one or two superconducting reservoirs has been studied in Refs. 62,63,75. The equilibrium current in chaotic Josephson junctions has been studied by Brouwer and Beenakker.[65] The next chapter in this thesis is devoted to the study of the nonequilibrium Josephson current and current fluctuations, and the last chapter concerns the current transport through a voltage biased chaotic Josephson junction.

6.6.1 Linear statistics in normal conductor-superconductor systems

In normal conductor-superconductor systems electrons and holes are coupled via Andreev reflection, and the transport quantities will contain scattering amplitudes for both electrons and holes. Since the scattering matrix for holes is related to the scattering matrix of electrons as $S^*(-E)$, as given in Eq. (3.16), the calculation of the transport quantities includes taking into account the correlation between scattering amplitudes at different energies, and it is in general not possible to write the transport quantity as a linear statistic.

However, for transport at the Fermi energy, i.e $E = 0$, or in the short dwell time regime $E_{Th} \gg \Delta$, where the scattering matrix is independent on energy on the scale of Δ, this obstacle is overcome and one can express the transport quantities as linear statistics, assuming that TRS is conserved.

One example is the NS-conductance in Eq. (3.29) for small voltages and temperatures $eV, k_BT \ll \min(E_{Th}, \Delta)$. It can be found by inserting the polar decomposition in Eq. (6.24) into

Eq. (3.29), giving[44]

$$G_{NS} = \frac{4e^2}{h}\sum_{n=1}^{N}\frac{D_n^2}{(2-D_n)^2}. \tag{6.38}$$

Another quantity is the equilibrium Josephson current in Eq. (3.57) in the short dwell time regime, furter studied in the next chapter, giving at temperatures much less than the superconducting gap[39]

$$I_{eq} = \frac{e\Delta}{\hbar}\sum_{n=1}^{N}\frac{D_n\sin\phi}{2\sqrt{1-D_n\sin^2(\phi/2)}}. \tag{6.39}$$

These forms of transport quantities in NS- systems enables one directly to employ the statistical information for the normal dot in calculating the N-dot-S conductance and the Josephson current. More examples of linear statistics in NS- systems will be given in Chapter 7 and 9.

6.6.2 N-dot-S conductance

As an example illustrating the discussion above, with connection to the calculation in the last chapter, we can consider the subgap conductance of an N-chaotic dot-S junction, following the discussion in Ref.62. Assuming that the applied potential drops equally at the contacts between the dot and the reservoirs and inserting the polar decomposition in Eq. (6.24) in the expression for the subgap conductance in Eq. (3.29) one obtains

$$\begin{aligned} G_{NS}(V,B) &= \frac{2e^2}{h}\mathrm{tr}\left(D_+\left[1-\alpha^2 u_+\sqrt{1-D_-}u_-^*\sqrt{1-D_+}\right]^{-1}u_+D_-\right.\\ &\times \left. u_+^\dagger\left[1-1/\alpha^2\sqrt{1-D_+}u_-^T\sqrt{1-D_-}u_+^\dagger\right]^{-1}\right), \end{aligned} \tag{6.40}$$

where $D_\pm = D(\pm eV/2)$ and $u_\pm = V'(\pm eV/2)V(\mp eV/2)^*$ and α is evaluated at $E = eV$. The matrices U and U' drop out of the expression for the conductance.

We consider several different cases analytically, assuming that the number of transverse modes $N \gg 1$ and only considering the contribution to leading order in N.

In the short dwell time regime, $E_{Th} \gg \Delta$, one can neglect the energy dependence of the scattering matrix and thus drop the ± subscripts. Moreover, in this limit it is only sensible to consider zero magnetic field, since an applied magnetic field destroys superconductivity in the electrodes before breaking TRS in the dot. Due to symmetry of the scattering matrix, $S = S^T$, we have $V' = V^T$ and thus $u_\pm = 1$, giving the conductance as a linear statistic

$$G_{NS} = \sum_{n=1}^{N}\frac{2e^2}{h}\frac{D_n^2}{1+(1-D_n)^2-2(1-D_n)(2[eV/\Delta]^2-1)}, \tag{6.41}$$

which for $eV \ll \Delta$ is just the result in Eq. (6.38). The average conductance can be obtained simply by integrating over the transmission eigenvalue density in Eq. (6.30). Note that the non-averaged conductance becomes equal to $2G_N$ for $eV = \Delta$, i.e perfect Andreev reflection.

In the long dwell time regime we have the four different cases:

1) $B \ll B_c$ and $eV \ll E_{Th}$, i.e TRS is conserved and we can neglect the difference in energy dependence between the electron and hole scattering amplitudes. This gives the same result as

in the short dwell time regime with $\alpha = i$, i.e the result in Eq. (6.38). The average conductance becomes, after integrating with the transmission eigenvalue density

$$\langle G_{NS} \rangle = N \frac{2e^2}{h}(1 - 1/\sqrt{2}) \tag{6.42}$$

i.e. a value well below the normal conductance $G_N = N/2$. This can be contrasted to the value of a diffusive NS-contact, where the corresponding conductance is exactly equal to the normal conductance,[22,44] the so called re-entrance of normal conductance.

2) $B \gg B_c$ and $eV \ll E_{Th}$, i.e TRS is broken but we can still neglect the difference in energy dependence between the electron and hole scattering amplitudes, dropping the ± subscripts on u and D. Since the unitary matrices V and V' are uniformly and independently distributed in the unitary group, so is also the product $u = VV'^{*}$ in the conductance expression (6.40). We can thus average the conductance directly over u, using the diagrammatic technique discussed in the section above. The expression is very similar to the function h, with the average in Eq. (6.20), and we get

$$\langle G_{NS} \rangle_u = 2N \frac{2e^2}{h} \frac{\mathrm{tr}(D)/N}{2 - \mathrm{tr}(D)/N}. \tag{6.43}$$

Remaining is then the average over the function of the linear statistics $\mathrm{tr}(D) = \sum_n D_n$. Since the variance of a linear statistic A is of order 1, while the average is of order N, we can write $A = \langle A \rangle + \delta A$, where δA is of order 1. This means that to leading order we can write the average of a function $f(A)$ of linear statistics as

$$\langle f(A) \rangle_D = f(\langle A \rangle_D), \tag{6.44}$$

i.e a function of the averages of the individual linear statistics. We can thus straightforwardly perform the average over the transmission eigenvalues in Eq. (6.43), where $\langle \mathrm{tr}(D) \rangle = N/2$, giving

$$\langle G_{NS} \rangle = \frac{N}{3} \frac{2e^2}{h}. \tag{6.45}$$

This value is slightly larger than the conductance with conserved TRS, but still smaller that the normal conductance. One can also note that in this limit there is no voltage dependence of the conductance, an effect of that we have no barriers in the contacts between the dot and the reservoirs.

3) $B \ll B_c$ and $eV \gg E_{Th}$, i.e conserved TRS but we have to take into account the difference in energy dependence between the electron and hole scattering amplitudes. Due to TRS, the matrix $V' = V^T$, but in this high voltage limit, the matrices $V(-eV)$ and $V(+eV)$ are independently distributed and thus $u_+ = u_-^{\dagger}$ is uniformly distributed in the unitary group. The average of the conductance in Eq. (6.40) can thus be performed directly over u_+, giving in the same way as in 2)

$$\langle G_{NS} \rangle_{u_+} = 2N \frac{2e^2}{h} \frac{\mathrm{tr}(D_-)\mathrm{tr}(D_+)/N^2}{\mathrm{tr}(D_-)/N + \mathrm{tr}(D_+)/N - \mathrm{tr}(D_-)\mathrm{tr}(D_+)/N^2} \tag{6.46}$$

Once again, we can use Eq. (6.44) and write the average over the function of the linear statistics as function of the averages of the individual linear statistics. However, in contrast to Eq. (6.43), one has to take into account the dependence of the average $\langle \mathrm{tr}(D_\pm) \rangle$ on voltage, but since this average is independent of energies on the large scale of the Fermi energy, we can neglect the voltage dependence and get once again the average conductance in Eq. (6.45).

4) $B \gg B_c$ and $eV \gg E_{Th}$, i.e both broken TRS and a difference in the energy dependence between the electron and hole scattering amplitudes. In this limit all four matrices $V(\pm eV)$ and $V'(\pm eV)$ are independently distributed in the unitary group and thus also u_+ and u_-. We can perform the average in two steps, first over u_+ and then over u_-. The average of the expression in (6.40) over u_+ is exactly on the form in Eq. (6.20), giving

$$\langle G_{NS}\rangle_{u_+} = N\frac{\mathrm{tr}(D_-)\mathrm{tr}(D_+)/N^2}{1-\mathrm{tr}[(1-D_-)u_-^*(1-D_+)u_-^T]/N}. \tag{6.47}$$

The same arguments that hold for the variance of a linear statistics above, hold for the trace of a function g of unitary matrices, i.e $\mathrm{tr}[g(U)] = \langle \mathrm{tr}[g(U)]\rangle + O(1)$, and one gets to leading order

$$\langle f(\mathrm{tr}[g(U)])\rangle_U = f(\langle(\mathrm{tr}[g(U)]\rangle_U). \tag{6.48}$$

It is therefore possible to perform the average of Eq. 6.48 over u_- directly over the trace in the denominator, just the same as the average of the function g above. The averaged expression is simply given by Eq. 6.46 and thus the resulting conductance, averaged over the transmission eigenvalues, is given by Eq. (6.45).

Therefore, to leading order the cases with either $eV \gg E_{th}$ or $B \gg B_c$ or both, gives the same average conductance. As is shown in Ref. 62, the weak localization corrections to the leading order result are different in the different cases. In contrast to normal conductors, discussed above, the weak localization corrections in NS-systems are not suppressed by applying a magnetic field $B \gg B_c$: one has simultaneously to apply a voltage $eV \gg E_{Th}$ to suppress these corrections. We plot the numerical result for the N-dot-S conductance in Fig. 6.10, and find good agreement with the theoretical results presented in the section, with deviations due to weak localization corrections, since the number of modes N in the numerics is limited. It should be noted that the conductance for arbitrary magnetic field and $E_{Th} \ll \Delta$, has recently been considered by Clerk et al,[75] for a junction with arbitrary tunnel barriers in the contacts between the dot and the reservoirs. Their results are further discussed in the last chapter.

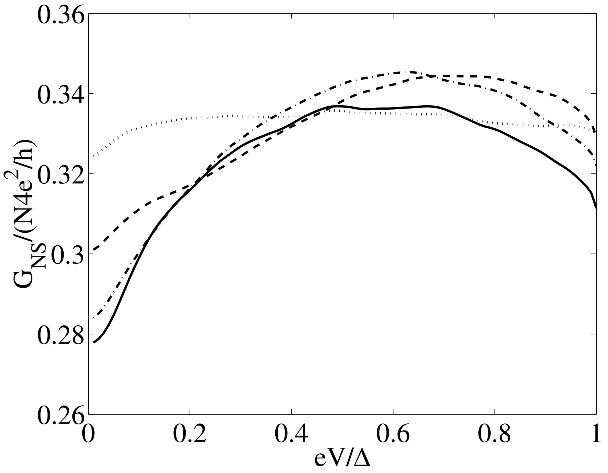

Figure 6.10: The subgap conductance of the N-dot-S junction as a function of voltage for different magnetic fields $B = 0$ (solid), $1.2B_c$ (dash-dotted), $2.4B_c$ (dashed) and $B \quad B \quad _c$ (dotted). The Thouless energy $E_{Th} = 0.1\Delta$, dimensionalities are $N = 15$ and $M = 300$ and 1000 Hamiltonians have been generated.

CHAPTER 7

Nonequilibrium current and current fluctuations in a chaotic Josephson junction

One of the remarkable discoveries[8,154] during the study of mesoscopic systems in the eighties was that the conductance of diffusive metallic wires with different configurations of impurities, i.e different "samples", varied from sample to sample, with a universal magnitude of the sample-to-sample fluctuations of order e^2/h, the so called universal conductance fluctuations. The different samples were obtained in experiments by varying the magnetic field or the Fermi energy in the wire, effectively producing new impurity configurations. The universality has two aspects, first that the amplitude of the fluctuations is of order e^2/h, second that the amplitude is exactly halved if time reversal symmetry is broken by a magnetic field. An intuitive explanation for the universality of the conductance fluctuations in terms of universality of the statistics of the transmission eigenvalues (similar to the discussion in the preceding chapter for a chaotic dot), was proposed by Imry (see e.g. Ref. 122)

Later, Altshuler and Spivak[10] studied the sample to sample fluctuations of the Josephson current in a long diffusive SNS-junction, $E_{Th} \ll \Delta$, and found that the sample-to-sample fluctuations of the critical current were of the order $eE_{Th}/\hbar$, again halved by breaking time reversal symmetry. They also pointed out that since the averaged Josephson current is exponentially small for broken time reversal symmetry, the total current is determined by the fluctuating part. In contrast to the conductance fluctuations, the magnitude of the Josephson current fluctuations in long SNS-junctions is non-universal, since it depends on the material dependent Thouless energy E_{Th}.

In 1991 Beenakker[39,46] studied the Josephson current fluctuations in a diffusive junction in the opposite, short limit $E_{Th} \gg \Delta$, and found that in this limit the magnitude of the critical current sample-to-sample fluctuations is indeed universal, of order $e\Delta/\hbar$. Since it was found by Beenakker that the Josephson current in the short junction limit is a linear statistic of the transmission eigenvalues [see Eq. (6.39)], it is clear from Eq. (6.34) that one can calculate the magnitude of the fluctuations for any mesoscopic Josephson junction as soon as the statistics of the transmission eigenvalues of the normal conductor is known.

Good qualitative agreement with the theoretical predictions were obtained by Takayanagi et al. in an experiment with a diffusive semiconductor SNS-junction,[230] where new samples were effectively produced by varying the Fermi energy via an electrostatic gate. In the light of the recent studies on nonequilibrium Josephson effects discussed in the previous chapters, with especially the discussion of the scattering phase dependent anomalous current in mind, it is interesting to study the sample-to-sample fluctuations of the nonequilibrium Josephson current. In this chapter we study the nonequilibrium Josephson current and current fluctuations in a three-terminal chaotic SNS-junction, to a large extent a detailed presentation of the work performed together with H. Schomerus in the short paper IV.

7.1 Equilibrium Josephson current and current fluctuations

The equilibrium Josephson current in junctions containing a chaotic dot coupled to two superconducting reservoirs is in the general case found from Eq. (3.58). The averaged current in junctions with wide contacts, i.e number of transverse modes $N \gg 1$, has been studied by Brouwer and Beenakker,[62] who averaged the current expression directly over the Hamiltonian ensemble in (6.1). Their results are briefly discussed below for the long dwell time regime. The results are also valid in the short dwell-time regime, where the scattering matrix is independent of energy on the scale of Δ, but in this regime the current can be found for both wide and narrow contacts, i.e $N \gg 1$ and $N = 1$ respectively, by integrating the short junction result in Eq. (6.39) directly over the distribution of transmission eigenvalues in Eq. (6.32).

7.1.1 Short dwell time regime

In the short dwell time regime, the calculations of the Josephson current is considerably simplified by the fact that the only contribution to the current comes from the bound states, i.e the continuum contribution to the current is zero. It is then possible to use the simplified expression of the Josephson current in Eq. (6.39), where the current is expressed in terms of the transmission eigenvalues. At temperatures much smaller that the superconducting gap, $k_B T \ll \Delta$, the current can be straightforwardly averaged over the distribution for transmission eigenvalues in the limiting cases $N = 1$ and $N \gg 1$.

In a single mode junction, $N = 1$, the distribution for ballistic leads ($\Gamma_1 = \Gamma_2 = 1$) is given by $\rho(D) = 1/(2\sqrt{D})$, and the averaged Josephson current becomes

$$\langle I_{eq}\rangle = \frac{G_N\Delta}{e}\frac{3\pi}{4}\frac{\cos(\phi/2)}{\sin^2(\phi/2)}(\phi - \sin\phi), \tag{7.1}$$

where the normal conductance is $G_N = [2e^2/h]/3$.

For a large number of modes, the transmission eigenvalue distribution to leading order in N is given by Eq. (6.6). For ballistic leads the average current becomes[45]

$$\langle I_{eq}\rangle = \frac{G_N\Delta}{e}\frac{\pi\sin(\phi)}{2} 2F_1\left(\frac{1}{2},\frac{3}{2};2;\sin^2(\phi/2)\right), \tag{7.2}$$

where $2F_1$ is the hyper-geometric function and G_N, the normal conductance, follows from the general expression $G_N = G_0(N\Gamma/2)$ for junctions $N \gg 1$. In the tunnel regime, $\Gamma = \Gamma_1 = \Gamma_2 \ll 1$, the averaged current becomes

$$\langle I_{eq}\rangle = \frac{G_N\Delta}{e}\sin(\phi)K[\sin(\phi/2)], \tag{7.3}$$

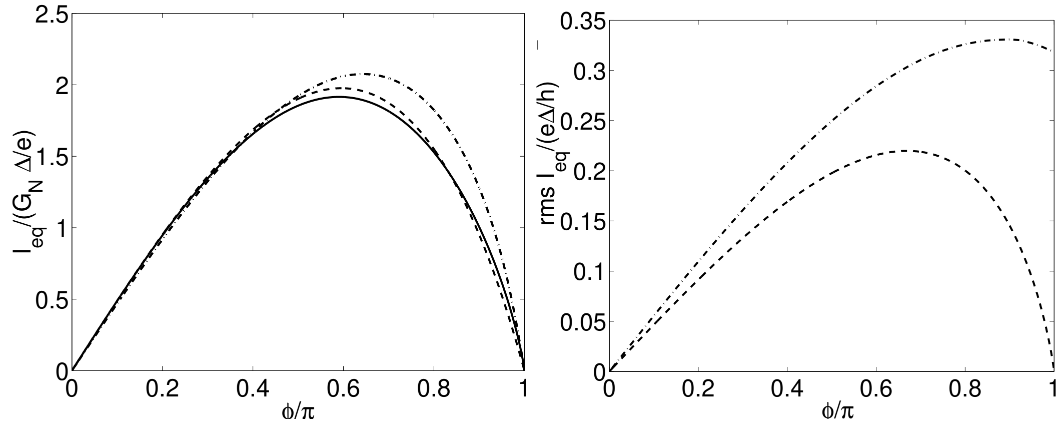

Figure 7.1: Left: The equilibrium Josephson current as a function of phase difference for a single mode junction, $N = 1$ (dashed) and a junction with many modes, N 1 with ideal leads, $\Gamma = 1$, (dash-dotted) and with tunnel barriers in the leads Γ 1 (solid). Right: The root mean square fluctuations of the equilibrium Josephson current as a function of phase difference for a single mode junction $N = 1$ (dashed) and a ballistic junction with a large number of modes N 1 and ideal leads $\Gamma = 1$ (dash-dotted).

where K is the complete elliptic integral of the first kind. The equilibrium currents as a function of phase difference are plotted in Fig. 7.1 It is interesting to note that all three curves, normalized with the normal conductance, almost fall upon each other. The current-phase dependence is almost sinusoidal, with a critical current of order $I_c \approx 2G_N\Delta/e$ for a phase difference $\phi_c \approx 0.6\pi$. These values for the critical current are between the known values for the ballistic point contact[143] and pure tunnel junction,[11] close to the value of a diffusive point contact.[142]

7.1.2 Sample-to-sample fluctuations of the current

It is also possible to find the magnitude of the sample-to-sample fluctuations of the Josephson current in the short dwell-time regime. For a single-mode junction, one simply calculates the average second moment, $\langle I_{eq}^2\rangle$, by integrating with the distribution $\rho(D)$, which gives

$$\begin{aligned}\langle I_{eq}^2\rangle &= \left(\frac{e\Delta}{\hbar}\right)^2 \frac{\cos^2(\phi/2)}{|\sin(\phi/2)|^3} \\ &\quad \times \left[\operatorname{atanh}(|\sin(\phi/2)|) - |\sin(\phi/2)|(1+\sin^2(\phi/2)/3)\right]. \qquad (7.4)\end{aligned}$$

Together with the average of the first moment in Eq. (7.1), one obtains the variance $\mathrm{var}(I_{eq}) = \langle I_{eq}^2\rangle - \langle I_{eq}\rangle^2$. For a junction with many modes, the average of the product I_{eq}^2 is no longer possible to calculate directly, since it contains products of different transmission eigenvalues. One instead has to use the formula for the variance of a linear statistic in Eq. 6.34, which holds for ideal leads, $\Gamma = 1$. The variance can not be evaluated explicitly but can be found[46] in the limits $\phi \ll 1$ and $\phi \to \pi$ where it becomes $\mathrm{var}(I_{eq}) = (e\Delta/\hbar)^2(\phi/32)$ and $\mathrm{var}(I_{eq}) = (e\Delta/\hbar)^2(1/\pi^2)$ respectively. The root mean square, the square-root of the variance, for both single and many mode junctions is plotted in Fig. 7.1.

The interesting feature is that the sample-to-sample fluctuations are of the same magnitude for the single-mode junction and the junction with a large number of modes, although the average current is an order N larger in the junction with a large number of modes. The reason for this is the strong correlation between the transmission eigenvalues in junctions with a large number of modes. Moreover, the magnitude of the fluctuations are independent of any junction parameters, being only a numerical constant of order unity multiplied by $e\Delta/\hbar$. This is thus the Josephson current analogue of the universal conductance fluctuations.

In the same way the critical current can be calculated. In single-mode junctions, the critical current at zero temperature is given simply by maximizing the current in Eq. (4.10) with respect to phase difference, giving

$$I_c = \frac{e\Delta}{\hbar}\sqrt{2 - D - 2\sqrt{1-D}}. \tag{7.5}$$

It can be noted that from this result one can calculate the full critical current distribution $\rho(I_c) = dD/dI_c\rho(D)$. We however only need the two first moments. The average critical current is again found by integrating over the transmission eigenvalue distribution, giving

$$\langle I_c\rangle = \frac{e\Delta}{2\hbar}\left(2 - \frac{\pi}{2}\right). \tag{7.6}$$

In the same way the variance is found via the second moment, giving the root mean square

$$\text{rms } I_c = \frac{e\Delta}{\hbar}\sqrt{\frac{2}{3} - \frac{\pi^2}{16}} \approx 0.22\frac{e\Delta}{\hbar}. \tag{7.7}$$

The critical current for the junctions with a large number of modes has to calculated in a different way, since the phase difference ϕ_c, for which the Josephson current has a maximum, is itself a function of transmission eigenvalues (this is clear since ϕ_c is defined from $dI_{eq}/d\phi = 0$). However, since the Josephson current fluctuations are a factor of N smaller than the average current, and since it is clear from Fig. 7.1 that the fluctuations of the critical phase difference ϕ_c also are small compared to the critical phase difference of the ensemble averaged Josephson current $\langle\phi_c\rangle \approx 1.97$, the fluctuations of the critical Josephson current are the same as the fluctuations of the Josephson current for the averaged critical phase difference $\langle\phi_c\rangle$,[45]

$$\langle I_c\rangle = \langle I_{eq}(\langle\phi_c\rangle)\rangle, \tag{7.8}$$

which is a linear statistic. The root mean square can be found from Fig. 7.1,

$$\text{rms } I_c \approx 0.29\frac{e\Delta}{\hbar}, \tag{7.9}$$

i.e. slightly larger than the amplitude of the fluctuations in the single mode junction.

7.1.3 Long dwell time regime

In the long dwell time regime, $E_{Th} \ll \Delta$, one has to calculate the Josephson current, given by Eq. (3.58), from the underlying Hamiltonian ensemble in Eq. (6.1). This was done by Brouwer and Beenakker[65] for zero magnetic field (note that a time reversal symmetry breaking magnetic field has the effect of suppressing the Josephson current), in the limit of many transverse modes $N \gg 1$.

Their main result is that the Josephson current, for arbitrary barrier transparency, shows a logarithmic dependence on the superconducting gap Δ, with

$$\langle I_c\rangle \simeq \frac{G_N E_{Th}}{e}\ln(\Delta/\max[E_{Tk}, k_B T]). \tag{7.10}$$

The logarithmic Δ-dependence arises because the current density $\langle i_{eq}(E)\rangle$ decays as $1/E$ for $E \gg E_{Th}$. For temperatures $k_B T \gg E_{Th}$ the critical current thus decays logarithmically with temperature. A similar logarithmic temperature dependence was found by Aslamasov, Larkin and Ovchinnikov[24] for a diffusive junction with tunnel barriers at the NS-interfaces. This can be put in contrast to the result for a long diffusive wire SNS-junction, where the critical current decays exponentially for $k_B T \gg E_{Th}$, since the current density decays exponentially for $E \gg E_{Th}$[246, 247]

The sample to sample fluctuations of the Josephson current in a chaotic Josephson junction in the long dwell time regime has not been studied and constitutes an interesting object for further investigations.

7.2 Nonequilibrium Josephson current and current fluctuations

We now turn to the three terminal SNS-junction, pictured in Fig. 3.5, to study how the average Josephson current and current fluctuations are affected by nonequilibrium conditions. A tunnel barrier with mode independent transparency Γ is present in the lead connecting the conductor to the normal reservoir. As discussed in Chapter 3, the current flowing between the superconductors can be divided into equilibrium and nonequilibrium parts, in a way described in Eq. (3.66). The equilibrium part is modified due to the coupling to the normal reservoir, and approaches the equilibrium current of the two terminal SNS-junction in the limit of vanishingly small coupling, $\Gamma \ll 1$, to the normal reservoir. The nonequilibrium current can be further divided into the sum and difference currents, I^+ and I^-, and the injection current I_1.

As discussed in Chapter 4, this division of the difference current and the injection current is artificial, and becomes meaningful only in the limit of vanishingly small coupling, where the injected current is negligiably small. For these reasons we will mainly focus our discussion on the weak coupling limit and not discuss the injection current at all. It should be noted, however, that since the coupling strength to the normal reservoir determines the dwell time of the injected quasiparticles at subgap energies $|E| < \Delta$, the dwell time must be smaller than the inelastic scattering time for the nonequilibrium to be preserved, this then puts a lower limit to the coupling to the normal reservoir.

In the weak coupling limit, $\Gamma \ll 1$, the sum and difference current densities i^+ and i^- at energies outside the gap are small, proportional to Γ, just as for the single mode junction discussed in Chapter 4. We therefore focus on i^+ and i^- at energies within the gap. To arrive at convenient expressions for i^+ and i^- for further evaluation, we will now go through several technical steps.

7.2.1 Current densities and matrix diagonalizations

We first rewrite the sum and difference current densities in Eqs. (3.79) and (3.80) on a more convenient form, by first diagonalizing the matrix $\bar{M} = \bar{S}_N S_A$,

$$\bar{M} = u\lambda u^{-1}, \tag{7.11}$$

where u is a matrix with linearly independent eigenvectors u_n and $\lambda = \mathrm{diag}(\lambda_n)$, with non-degenerate λ_n. Since in the weak coupling limit the bound state energies for the SNS-junction, given by Eq. (3.37), is $\det(1-\bar{M})$, the nondegeneracy assumption is essentially equivalent to the assumption that the bound states in the SNS-junction are non-degenerate. As discussed above, there is strong level repulsion in chaotic dots as well as in chaotic Josephson junctions, so that accidental level degeneracies can be neglected in calculating ensemble averaged quantities. We can write

$$\lambda = re^{i\chi} = \alpha re^{i\beta}, \; re^{i\beta} = u^{-1}\bar{S}_N S_A u/\alpha, \tag{7.12}$$

with $|r_n| \leq 1$ for all energies due to the subunitarity of $\bar{S}_N$ for a finite coupling to the normal reservoir. An important point is that since $\bar{M}$ has a block off-diagonal structure, it can also be diagonalized as

$$\bar{M} = -\sigma_z \bar{M} \sigma_z = \sigma_z u(-\lambda)u^{-1}\sigma_z. \tag{7.13}$$

That is, there is a matrix $\tilde{u} = \sigma_z u$ that diagonalizes $\bar{M}$, with the corresponding eigenvalues $-\lambda$. This means that for every eigenvalue λ_n with the corresponding eigenvector u_n, there is another eigenvalue $-\lambda_n$ with the eigenvector $\tilde{u}_n = (\sigma_z u)_n$. We can also take advantage of the energy symmetry of $\bar{S}_N$ and diagonalize

$$\bar{M}(E) = -\sigma_x \bar{M}^*(-E)\sigma_x = -\sigma_x u^*(-E)\lambda^*(-E)[u^*(-E)]^{-1}\sigma_x, \tag{7.14}$$

where σ_x is the Pauli matrix in electron-hole space. For every eigenvalue $\lambda_n(E)$ with the corresponding eigenvector $u_n(E)$, there is thus another eigenvalue $-\lambda_n^*(-E)$ with the eigenvector $\hat{u}_n = [\sigma_x u^*(-E)]_n$. For junctions in the short dwell time regime, $\bar{S}_N$ is independent of energy and the eigenvalues of $\bar{M}$ thus come in groups of four, like $\lambda_n = \pm\alpha r_n \exp(\pm i\beta_n)$.

Inserting the diagonalized expression for $\bar{M}$ into the current density expressions in Eq. (3.79) and (3.80), one gets

$$i^+ = \frac{2e}{h}\mathrm{Re}\,\mathrm{tr}\left[u^{-1}\sigma_z' u(1-\lambda)^{-1}\right], \tag{7.15}$$

$$i^- = -\frac{4e}{h}\mathrm{Re}\,\mathrm{tr}\left[u^\dagger \sigma_z' u(1-\lambda)^{-1}\lambda u^{-1}\sigma_z(u^\dagger)^{-1}(1-\lambda^*)^{-1}\right]. \tag{7.16}$$

The current densities have poles at energies E_{np} in the complex energy plane (due to the finite coupling to the normal reservoir), given by the pole equation,

$$1-\lambda_n = 0 \;\Rightarrow\; \sin(\chi_n/2) = 0 \;\Rightarrow\; \chi_n = 2\pi p. \tag{7.17}$$

In both current density expressions (7.15) and (7.16) the expressions $(1-\lambda)^{-1}$ and $(1-\lambda^*)^{-1}$ can be evaluated by pole expansion, using the fact that any function can be written as sum over it's poles and the residue at these poles. The residue of the function $(1-\lambda_n)^{-1}$ is given by

$$\mathrm{Res}\frac{1}{1-\lambda_n} = -\left(\frac{dE_n}{d\lambda_n}\right), \tag{7.18}$$

and we can write the pole expansion, summing over the pole index p.

$$\frac{1}{1-\lambda_n} = -\sum_p \left(\frac{dE_{np}}{d\lambda_n}\right)\frac{1}{E-E_{np}}. \tag{7.19}$$

7.2.2 Weak coupling limit

Turning to the limit of weak coupling to the normal reservoir, all matrix quantities can be expanded to first order in Γ, as

$$\bar{S}_N = \bar{S}_N(\Gamma = 0) + \Gamma \left.\frac{d\bar{S}_N}{d\Gamma}\right|_{\Gamma=0} \equiv S_{N0} + \delta S_N. \tag{7.20}$$

Since S_A is independent on Γ, we write

$$\bar{M} = S_{N0}S_A + \delta S_N S_A \equiv M_0 + \delta M, \tag{7.21}$$

where we note that M_0 is unitary. In the same way we can expand the eigenvalue and eigenvector matrices like

$$u = u(\Gamma = 0) + \Gamma \left.\frac{du}{d\Gamma}\right|_{\Gamma=0} \equiv u_0 + \delta u, \tag{7.22}$$

where u_0 is unitary, and

$$\lambda = \lambda(\Gamma = 0) + \Gamma \left.\frac{d\lambda}{d\Gamma}\right|_{\Gamma=0} \equiv \lambda_0 + \delta\lambda, \tag{7.23}$$

with the elements λ_{0n} having modulus unity. From Eq. (7.12) we can expand

$$\lambda = e^{i\chi_0} + \Gamma \left[\left.\frac{dr}{d\Gamma} e^{i\chi}\right|_{\Gamma=0} + i \left.\frac{d\beta}{d\Gamma} e^{i\chi}\right|_{\Gamma=0} \right] \equiv (1 + \Gamma c) e^{i\chi_0}, \tag{7.24}$$

with $c = c_R + ic_I$ just a complex number,

$$c_R = \left.\frac{dr}{d\Gamma}\right|_{\Gamma=0}, \; c_I = \left.\frac{d\beta}{d\Gamma}\right|_{\Gamma=0}. \tag{7.25}$$

It is useful to write down the expansion for the inverse of u, like

$$u^{-1} = [u_0 + \delta u]^{-1} = [u_0(1 + u_0^\dagger \delta u)]^{-1} = u_0^\dagger - u_0^\dagger \delta u u_0^\dagger. \tag{7.26}$$

By identification of the terms of the same order in Γ, expanding Eq. (7.13), we find

$$M_0 = u_0 \lambda_0 u_0^\dagger \tag{7.27}$$

and

$$\delta M = \delta u \lambda_0 u_0^\dagger + u_0 \delta\lambda u_0^\dagger - u_0 \lambda_0 u_0^\dagger \delta u u_0^\dagger. \tag{7.28}$$

The pole equation in Eq. (7.17) becomes

$$1 - \lambda_{0n} - \delta\lambda_n = 0 \Rightarrow e^{-i\chi_{0n}} = 1 + \Gamma c. \tag{7.29}$$

The effect of the finite Γ is that the pole energy is shifted from the real axis out into the lower half of the complex energy plane, as $E_{0np} \to E_{0np} + \varepsilon$, where ε is a complex number (The indices $[n, p]$ on ε and accordingly on c are suppressed for simplicity). Expanding Eq. (7.19) to first order in Γ in the denominator and putting $E_{np} = E_{0np}$ and $\Gamma = 0$ in the numerator (not strongly dependent on E or Γ), we get

$$\frac{1}{1-\lambda_n} \approx i \sum_p \left(\frac{dE_{0np}}{d\chi_{0n}}\right) \frac{1}{E - E_{0np} + \varepsilon_R + i\varepsilon_I}. \tag{7.30}$$

The shift of the pole along the real axis is not important and can be neglected for $\Gamma \to 0$. The shift away from the real axis due to ε_I is however crucial. Taking the limit $\Gamma \to 0$ gives

$$\lim_{\Gamma \to 0} \frac{1}{E - E_{0np} + i\Gamma c_R (d\chi_{0n}/dE_{0np})} = P\left(\frac{1}{E - E_{0np}}\right) + i\pi\delta(E - E_{0np}) \tag{7.31}$$

where P denotes the principal part and where we have used the δ-function identity $\delta(f(x))|df/dx| = \delta(x)$. This result can be used directly for i^+ but i^- must be treated somewhat differently due to the product of the two terms with poles on different sides of the real energy axis.

Before turning to the evaluation of the current densities, we point out that the energies E_{0np} are just the bound state energies, since the equation for the bound states is given by, as in Eq. (3.37),

$$\det(1 - M_0) = 0, \tag{7.32}$$

where we can write, using the matrix diagonalization in Eq. (7.27),

$$\begin{aligned} \det(1 - M_0) &= \det(1 - \lambda_0) = \prod_n (1 - \lambda_{0n}) \\ &= -2i \prod_n e^{i\chi_{0n}/2} \sin(\chi_{0n}/2) = 0. \end{aligned} \tag{7.33}$$

The bound state equation can thus be expressed as an equation for the eigenphases χ_{0n},

$$\sin(\chi_{0n}/2) = 0, \ \Rightarrow \ \chi_{0n} = p2\pi \ \Rightarrow \ \beta_{0n} = \arccos(E/\Delta) + p2\pi, \tag{7.34}$$

where $p = 0, \pm 1, \pm 2..$ and $\arccos(E/\Delta)$ is the phase of α, the Andreev reflection amplitude. This equation is satisfied for the energy E_{0np}, where n and p are the quantum number labeling the bound state. In the short junction limit, $E_{Th} \gg \Delta$, there are only two bound states per scattering matrix mode n (i.e $2N$ bound states), symmetrically around Fermi energy and we can drop the p quantum number ($p = 0$). The eigenenergies are then directly given from

$$E_{0n} = \pm\Delta \cos(\beta_{0n}), \tag{7.35}$$

since β_{0n} is independent of energy in this limit. There are however $4N$ distinct eigenvalues λ_n. The reason for that they only give rise to $2N$ bound states is that for every bound state obtained from $\lambda_{0n}(E_{0n}) = 1$, there is a bound state equation $-\lambda_{0n} = 1$ without solution, since β_{0n} is energy independent and $\arccos(E_{0n}/\Delta)$ can only take on values between 0 and π.

7.2.3 Sum current density

We now turn to the expression of the sum current density in Eq. (7.15). Taking the trace, we can write

$$i^+ = \frac{2e}{h} \mathrm{Re} \sum_n \left[(u^{-1}\sigma_z' u)_{nn} (1 - \lambda_n)^{-1}\right]. \tag{7.36}$$

This expression is now expanded to first order in Γ. The first term is given by

$$u^{-1}\sigma_z' u \approx (u_0^\dagger - u_0^\dagger \delta u u_0^\dagger)\sigma_z'(u_0+\delta u). \tag{7.37}$$

The leading order term for the diagonal matrix element is finite and real, given by

$$(u_0^\dagger \sigma_z' u_0)_{nn} = \sum_m (\sigma_z')_n |u_{0nm}|^2. \tag{7.38}$$

The sub-leading order terms can then be neglected, and we get in the weak coupling limit, using the pole expanded expression in Eq. (7.31),

$$i^+ = -\frac{2e\pi}{h}\sum_{n,p}\left[(u_0^\dagger\sigma_z'u_0)_{nn}\left(\frac{dE_{0np}}{d\chi_{0n}}\right)\delta(E-E_{0np})\right]. \tag{7.39}$$

This can be compared to the general expression for the sum current density in Eq. (3.31), from which we can identify

$$2(u_0^\dagger\sigma_z'u_0)_{nn}\left(\frac{dE_{0np}}{d\chi_{0n}}\right) = \frac{dE_{onp}}{d\phi}. \tag{7.40}$$

7.2.4 Difference current density

We now turn to the expression for the difference current density in Eq. (7.16). Taking the trace, we can write

$$\begin{aligned} i^- = -\frac{4e}{h}\mathrm{Re}\sum_{nm}\Big[&(u^\dagger\sigma_z'u)_{nm}(1-\lambda_m)^{-1}(\lambda u^{-1}\sigma_z(u^\dagger)^{-1})_{mn} \\ &\times(1-\lambda_n^*)^{-1}\Big]. \end{aligned} \tag{7.41}$$

Two observations can be made from this equation. First, since the difference current density expression has poles on both sides of the real energy axis, the total current can not be calculated in the same way as the equilibrium sum current, by closing an integration contour in the upper half energy plane and write the current as a sum over Matsubara frequencies. Second, since the current density expression contains a "squared delta function", it must also be proportional to a term of order Γ, to give a physically reasonable result.

Inserting the pole expansion expression [given in Eq. (7.19)], we get

$$\begin{aligned} i^- = -\frac{4e}{h}\mathrm{Re}\sum_{nm}\sum_{pk}\Big[&(u^\dagger\sigma_z'u)_{nm}(\lambda u^{-1}\sigma_z(u^\dagger)^{-1})_{mn} \\ &\times\left(\frac{dE_{np}}{d\lambda_n}\frac{dE_{mk}}{d\lambda_m^*}\right)\frac{1}{E-E_{np}}\frac{1}{E-E_{mk}^*}. \end{aligned} \tag{7.42}$$

From Eq. (7.42) it is clear that only the terms with $\{np\}=\{mk\}$ give a finite result, since all other terms contains the product $\delta(E-E_{0np})\delta(E-E_{0mk})$ in the limit $\Gamma\to 0$. Only in the case when there is a degeneracy in bound state energies, $E_{0np}=E_{0mk}$, we would have to take these terms into account, but degeneracies are neglected, as discussed above. We then perform the expansion to first order in Γ and note that

$$\frac{1}{1-\lambda_n}\frac{1}{1-\lambda_n^*} \approx -\left(\frac{dE_{0np}}{d\chi_{0n}}\right)\frac{1}{(E-E_{0np})^2+\varepsilon_I^2}, \tag{7.43}$$

where we have neglected the small pole shift along the real axis (the same for both terms) and assumed a weak energy dependence of χ_{0n} around E_{0np}.

The first matrix product term in the current density expression, Eq. (7.42), is finite and real to leading order, $(u^\dagger\sigma_z' u)_{nn} \approx (u_0^\dagger\sigma_z' u_0)_{nn}$, which is the same as for the sum current density term in Eq. (7.39). We thus expect the leading order term in the second matrix product term to be zero. It can be expanded like

$$\begin{aligned} \lambda u^{-1}\sigma_z(u^\dagger)^{-1} &= (\lambda_0+\delta\lambda)(u_0^\dagger - u_0^\dagger\delta u u_0^\dagger)\sigma_z(u_0 - u_0\delta u^\dagger u_0) \\ &= -2\mathrm{Re}(u_0^\dagger\sigma_z u_0\delta u^\dagger u_0)_{nn}, \end{aligned} \tag{7.44}$$

where the last step was found after some matrix algebra, using Eq. (7.13). The resulting expression in (7.44) is proportional to Γ, via δu, just as anticipated above. Collecting the results, the difference current density is given by

$$\begin{aligned} i^- = \frac{8e}{h}\sum_{np}\Big[&(u_0^\dagger\sigma_z' u_0)_{nn}\mathrm{Re}(u_0^\dagger\sigma_z u_0\delta u_0^\dagger u_0)_{nn} \\ &\left(\frac{dE_{0np}}{d\chi_{0n}}\right)\frac{\Gamma}{(E-E_{0np})^2+\Gamma^2[c_R(d\chi_{0n}/dE_{0np})]^2}\Big], \end{aligned} \tag{7.45}$$

where we have put $\delta u = \Gamma\delta u_0$ to have the same order of all terms in the matrix expressions. We can now safely take the limit $\Gamma \to 0$, for which the the last term in Eq. (7.45) becomes

$$\lim_{\Gamma\to 0}\frac{\Gamma}{(E-E_{0np})^2+\Gamma^2[c_R(d\chi_{0n}/dE_{0np})]^2} = \frac{\pi}{c_R(d\chi_{0n}/dE_{0np})}\delta(E-E_{0np}). \tag{7.46}$$

Noting that

$$\left(\frac{dr}{d\Gamma}\bigg|_{\Gamma=0}\right)^{-1} = \frac{1}{\mathrm{Re}(\delta\lambda_{0n})} = \frac{1}{\mathrm{Re}(u_0^\dagger\delta S_N S_A u_0)}, \tag{7.47}$$

where we have introduced $\delta\lambda = \Gamma\delta\lambda_0$ and in the last step have used the expansion in Γ of Eq. (7.12), we can write the difference current

$$i^- = \frac{2\pi e}{h}\sum_{np}\frac{\mathrm{Re}(u_0^\dagger\sigma_z\delta S_N S_A u_0)_{nn}}{\mathrm{Re}(u_0^\dagger\delta S_N S_A u_0)_{nn}}\frac{dE_{0np}}{d\phi}\delta(E-E_{0np}), \tag{7.48}$$

where we also have used Eq. (7.28) and the relation between the scattering amplitudes and the bound state current density in Eq. (7.40). This expression is the starting point for further calculations.

After these formal perturbation expansion calculations, the final expressions for the sum and difference current densities have been put on a convenient and physically transparent form. The sum current density is just given by the sum over the current density of the bound Andreev states. The current I^+ thus describes the nonequilibrium population of the existing, current carrying states, effectively a depopulation. The difference current density i^- in Eq. (7.48) is proportional to the sum current density, with the proportionality factor $\mathrm{Re}(u_0^\dagger\sigma_z\delta S_N S_A u_0)_{nn}/\mathrm{Re}(u_0^\dagger\delta S_N S_A u_0)_{nn}$. This is qualitatively the same result as was found above for the single mode junction. However, from the full analysis it is clear that this proportionality factor depends on δS_N, which, as will be discussed in detail below, can not be expressed in terms of S_{N0}, the scattering matrix of the decoupled junction. This means that i^- depends manifestly on the properties of the contact between the normal reservoir and the conductor.

7.3 Short dwell-time regime

So far the discussion has been valid for any type of mesoscopic scatterer. In order to investigate the mesoscopic fluctuations of the nonequilibrium current in more detail we now apply the theory to a chaotic SNS junction in the short dwell time regime, which is possible to study analytically. The opposite long dwell time regime is not studied, and constitutes an interesting object of further investigation.

The scattering matrix S of the conductor is symmetric due to conserved time reversal symmetry and distributed according to the Poisson kernel in Eq. (6.9). Moreover, we assume that the lead connecting the normal reservoir and the conductor only contains one mode, $N_1 = 1$. The temperature is assumed to be much smaller than the superconducting gap, $k_B T \ll \Delta$. In this limit, it is convenient to use the energy symmetries $i^+(E) = -i^+(-E)$ and $i^-(E) = i^-(-E)$, to write the total current

$$\begin{aligned} I &= -\sum_{E_n > eV} I_n^+ + \sum_{E_n < eV} I_n^- \\ I_n^+ &= \frac{2e}{\hbar}\frac{dE_n}{d\phi},\; I_n^- = R_n I_n^+, \end{aligned} \tag{7.49}$$

as a sum over the currents I_n^+ and I_n^- carried by the individual Andreev levels with positive energies E_n, where

$$R_n = \frac{\mathrm{Re}(u_0^\dagger \sigma_z \delta S_N S_A u_0)_{nn}}{\mathrm{Re}(u_0^\dagger \delta S_N S_A u_0)_{nn}}, \tag{7.50}$$

The physical picture provided by Eq. (7.49) is transparent: in equilibrium all Andreev levels carry the currents I_n^+. Increasing the voltage, the Andreev levels one by one switch from I_n^+ to I_n^- when the voltage is passing through $eV = E_n$. At $eV \geq \Delta$, all levels carry the current I_n^-.

As shown in Eq. (6.39), the sum current density can conveniently be expressed in terms of the transmission eigenvalues D_n of the scattering matrix S_0 of the closed junction. The statistics of the transmission eigenvalues are given by Eq. (6.30), and the average current as well as the fluctuations can be calculated, as was discussed in the preceding sections.

However, the difference current density also contains δS_N, which cannot be expressed in terms of the closed junction scattering matrix. To calculate the average current $\langle I^- \rangle$ and the fluctuations, the problem is to express the difference current density in terms of scattering quantities with statistical properties which can be derived from the statistical distribution of the complete three terminal scattering matrix S in Eq. (3.67).

7.3.1 Parametrization of the contact scattering amplitudes

The tunnel barrier between the normal reservoir and the scatterer is characterized by a fixed scattering matrix

$$S_T = \begin{pmatrix} -\mu\sqrt{1-\Gamma} & \nu\sqrt{\Gamma} \\ \nu\sqrt{\Gamma} & (\mu^2/\nu)\sqrt{1-\Gamma} \end{pmatrix}. \tag{7.51}$$

with μ and ν beingphase factors. Writing the scattering matrix $\tilde{S}$ of the dot without barriers

$$\tilde{S} = \begin{pmatrix} \tilde{R} & \tilde{T}^T \\ \tilde{T} & \tilde{R}' \end{pmatrix}, \tag{7.52}$$

where the matrices $\tilde{R}, \tilde{R}'$ and $\tilde{T}$ are of dimensions $1 \times 1, 2N \times 2N$ and $2N \times 1$ respectively, we can write the total scattering matrix S of the dot with the tunnel barrier as [using the matrix composition expression in Eq. (2.28)]

$$S = \begin{pmatrix} \frac{\Gamma \tilde{R}}{1+\sqrt{1-\Gamma}\tilde{R}} & \frac{\sqrt{\Gamma}\tilde{T}^T}{1+\sqrt{1-\Gamma}\tilde{R}} \\ \frac{\sqrt{\Gamma}\tilde{T}}{1+\sqrt{1-\Gamma}\tilde{R}} & \tilde{R}' - \frac{\sqrt{1-\Gamma}\tilde{T}\tilde{T}^T}{1+\sqrt{1-\Gamma}\tilde{R}} \end{pmatrix}. \tag{7.53}$$

In Eq. (7.53) the scattering phases μ and ν have for simplicity been absorbed into S by a unitary transformation, which does not change the distribution of S [see Eq. (6.9)]. This shows that the result is independent of the scattering phases of the tunnel barrier. In the weak coupling limit, the scattering matrix $\bar{S}_0$ that connects wave function amplitudes in lead 2 and 3 expanded to first order in Γ gives

$$\bar{S}_0 = \tilde{R}' - \frac{\tilde{T}\tilde{T}^T}{1+\tilde{R}} + \frac{\Gamma}{2}\frac{\tilde{T}\tilde{T}^T}{(1+\tilde{R})^2} \equiv S_0 + \delta S_0, \tag{7.54}$$

from which can construct S_{N0} and δS_N in Eq. (7.20) as $S_{N0} = \mathrm{diag}\,(S_0, S_0^*)$ and $\delta S_N = \mathrm{diag}\,(\delta S_0, \delta S_0^*)$.

We want to find a convenient expression for the ratio R_n in Eq. (7.49). This can be done in the following way. Decomposing the eigenvector $u_n^T = (v_n^T, w_n^T)$ in electron-hole space, then from the eigenvalue equation $S_{\mathrm{N}0} S_{\mathrm{A}} u_n = u_n$ (noting that the eigenvalues $\lambda_n = 1$) one obtains the relations

$$v_n = \alpha S_0 r_{\mathrm{A}} w_n, \quad w_n = \alpha S_0^* r_{\mathrm{A}}^* v_n. \tag{7.55}$$

Using the unitarity of $\tilde{S}$, one obtains after some matrix algebra

$$\delta S_0 S_0^* = -\frac{1}{2}\frac{\tilde{T}\tilde{T}^\dagger}{|1+\tilde{R}|^2}. \tag{7.56}$$

Hence, the ratio R_n takes the form, using $S_0 S_0^* = 1$,

$$R_n = \frac{\mathrm{Re}(v_n^\dagger \delta S_0 r_A w_n - w_n^\dagger \delta S_0^* r_A^* v_n)}{\mathrm{Re}(v_n^\dagger \delta S_0 r_A w_n + w_n^\dagger \delta S_0^* r_A^* v_n)} = \frac{|v_n^\dagger \tilde{T}|^2 - |w_n^\dagger \tilde{T}^*|^2}{|v_n^\dagger \tilde{T}|^2 + |w_n^\dagger \tilde{T}^*|^2}, \tag{7.57}$$

which clearly can only take on values between -1 and 1. Now we have to determine v, w and $\tilde{T}$. First v and w (dropping the n-index for simplicity) from the eigenvalue equations [following from Eq. (7.55)],

$$\alpha^2 S_0 r_{\mathrm{A}} S_0^* r_{\mathrm{A}}^* v = v, \qquad \alpha^2 S_0^* r_{\mathrm{A}}^* S_0 r_{\mathrm{A}} w = w. \tag{7.58}$$

We can then insert the polar decomposition [in Eq. (6.24)] of the unitary symmetric S_0 in Eq. (7.58), as

$$S_0 = \begin{pmatrix} U & 0 \\ 0 & V \end{pmatrix} \bar{S} \begin{pmatrix} U^T & 0 \\ 0 & V^T \end{pmatrix}, \; \bar{S} = \begin{pmatrix} \sqrt{1-D} & \sqrt{D} \\ \sqrt{D} & -\sqrt{1-D} \end{pmatrix}, \tag{7.59}$$

and introduce the new transformed vectors

$$\bar{v} = \begin{pmatrix} U^\dagger & 0 \\ 0 & V^\dagger \end{pmatrix} v, \quad \bar{w} = \begin{pmatrix} U^T & 0 \\ 0 & V^T \end{pmatrix} w, \quad \bar{T} = \begin{pmatrix} U^\dagger & 0 \\ 0 & V^\dagger \end{pmatrix} \tilde{T}. \tag{7.60}$$

The ratio R_n from Eq. (7.57) does not change form under these substitutions, and the eigenvalue equation for $\bar{v}$ and $\bar{w}$ is simplified to two-dimensional algebra,

$$\alpha^2 \begin{pmatrix} 1+D(e^{-i\phi}-1) & \sqrt{D(D-1)}(e^{i\phi}-1) \\ \sqrt{D(D-1)}(e^{-i\phi}-1) & 1+D(e^{i\phi}-1) \end{pmatrix} \bar{v} = \bar{v}, \tag{7.61}$$

with the solution

$$\bar{v} = \begin{pmatrix} \sqrt{1-D}\exp^{i\phi/2} \\ \sqrt{D}\cos\phi/2 - \sqrt{1-D\sin^2\phi/2} \end{pmatrix}, \quad \alpha = \sqrt{1-D\sin^2\phi/2} + i\sqrt{D}\sin\phi/2. \tag{7.62}$$

[Note that the eigenvalue expression is thus just another way of expressing the bound state condition for the short junction in Eq. (4.5)] From Eq. (7.55) we get

$$\bar{w} = \alpha \begin{pmatrix} \sqrt{1-D} & \sqrt{D} \\ \sqrt{D} & -\sqrt{1-D} \end{pmatrix} r_{\mathrm{A}}^* \bar{v}. \tag{7.63}$$

Now we turn to $\bar{T}$. Recognize that, from Eq. (7.54), after some algebra

$$S_0 \tilde{T}^* = -\frac{1+\tilde{R}^*}{1+\tilde{R}} \tilde{T} \equiv \chi \tilde{T}, \tag{7.64}$$

where χ is just a phase factor. We can eliminate the factor χ by $\tilde{T}' = \tilde{T}\chi^{1/2}$, so that $S_0\tilde{T}'^* = \tilde{T}'$, or for the transformed quantity

$$\bar{S}\bar{T}'^* = \bar{T}', \; \bar{T}' = \begin{pmatrix} U^\dagger & 0 \\ 0 & V^\dagger \end{pmatrix} \tilde{T}'. \tag{7.65}$$

Noting that we can diagonalize the symmetric and orthogonal $\bar{S}$ as $\bar{S} = X\bar{\lambda}X^T$, with

$$X = \frac{1}{\sqrt{2}\sqrt{1-\sqrt{1-D}}} \begin{pmatrix} \sqrt{D} & 1-\sqrt{1-D} \\ 1-\sqrt{1-D} & -\sqrt{D} \end{pmatrix}, \bar{\lambda} = \sigma_z, \tag{7.66}$$

we can write Eq. (7.65)

$$\bar{\lambda}(X\bar{T}')^* = (X\bar{T}'). \tag{7.67}$$

For the ansatz $X\bar{T}' \equiv O_1 = (a,b)^T$, we get the solution $a = a^*$ and $b = -b^*$. We can thus parameterize the normalized solution as $X\bar{T}' = (\cos 2\beta, i\sin 2\beta)^T$, where 2β instead of β is chosen for later convenience. This thus gives $\bar{T} = \chi^{-1/2}X\bar{\lambda}^{1/2}O_1$; written out,

$$\bar{T} = \chi^{-1/2}[2-2(1-D)^{1/2}]^{-1/2} \begin{pmatrix} \sqrt{D}\cos 2\beta + i(1-\sqrt{1-D})\sin 2\beta \\ (1-\sqrt{1-D})\cos 2\beta - i\sqrt{T}\sin 2\beta. \end{pmatrix}. \tag{7.68}$$

We can then finally insert $\bar{T}$, $\bar{v}$ and $\bar{w}$ in R_n in Eq. (7.49), which after some algebra gives (writing out n again)

$$R_n = \frac{\sin(\phi/2)\sqrt{1-D_n}}{\sqrt{1-D_n\sin(\phi/2)}} \sin\beta_n. \tag{7.69}$$

We have by this procedure parameterized the coupling of the conductor to the reservoir by a single parameter β_n. The final question, to be able to calculate the statistics within this parameterization, is thus what is the distribution of β_n.

7.3.2 Distribution of the parameterization amplitude

It is clear from the construction above, that the different β_n can be chosen independently. To determine the distribution of the β_n's, we first write the scattering matrix of the dot with the barriers in terms of the parameterization in Eq. (7.59) and (7.68), as

$$S = Q \begin{pmatrix} \frac{\Gamma\tilde{R}}{1+\sqrt{1-\Gamma}\tilde{R}} & \frac{\sqrt{\Gamma}}{1+\sqrt{1-\Gamma}\tilde{R}} O_1 \\ \frac{\sqrt{\Gamma}}{1+\sqrt{1-\Gamma}\tilde{R}} O_1^T & 1 + \frac{1-\sqrt{1-\Gamma}}{(1+\tilde{R}^*)(1+\sqrt{1-\Gamma}\tilde{R})} O_1 O_1^T \end{pmatrix} Q^T, \tag{7.70}$$

where

$$Q = \begin{pmatrix} 1 & 0 \\ 0 & \begin{pmatrix} U & 0 \\ 0 & V \end{pmatrix} X\bar{\lambda}^{1/2} \end{pmatrix}, \tag{7.71}$$

and we have used Eq. (7.54) to obtain an expression for $\tilde{R}'$ in terms of the parameterization. From the distribution of S, given by Eq. 6.9, it is clear that the matrix

$$S' = YSY^T = Q \begin{pmatrix} \frac{\Gamma\tilde{R}}{1+\sqrt{1-\Gamma}\tilde{R}} & \frac{\sqrt{\Gamma}}{1+\sqrt{1-\Gamma}\tilde{R}} \bar{O} O_1 \\ \frac{\sqrt{\Gamma}}{1+\sqrt{1-\Gamma}\tilde{R}} (\bar{O} O_1)^T & 1 + \frac{1-\sqrt{1-\Gamma}}{(1+\tilde{R}^*)(1+\sqrt{1-\Gamma}\tilde{R})} O_1 \bar{O} (\bar{O} O_1)^T \end{pmatrix} Q^T, \tag{7.72}$$

where

$$Y = \begin{pmatrix} 1 & 0 \\ 0 & \begin{pmatrix} U & 0 \\ 0 & V \end{pmatrix} X\bar{\lambda}^{1/2}\bar{O}\bar{\lambda}^{1/2}X^T \begin{pmatrix} U^T & 0 \\ 0 & V^T \end{pmatrix} \end{pmatrix}, \tag{7.73}$$

has the same probability as S, i.e $P(S)$ is invariant under the transformation $S \to YSY^T$, where the matrix $\bar{O}$ is an arbitrary orthogonal matrix. With the choice of Y in Eq. (7.73), the transformation $S \to S'$ is the most general transformation for which the matrix S' reduces to the same S_0 in the limit of $\Gamma \to 0$, i.e the matrix $\bar{O}$ parametrices the subgroup of the unitary group that reduces to S_0 in the weak coupling limit. Because all S' have the same probability, the matrix $\bar{O}$ is uniformly distributed in the group of orthogonal matrices. A general 2×2 orthogonal matrix can be written

$$\bar{O} = \begin{pmatrix} \cos(2\beta) & -\sin(2\beta) \\ \sin(2\beta) & \cos(2\beta) \end{pmatrix}, \tag{7.74}$$

where O_1 thus is the first column (we could just as well chosen the second column). In line with the discussion in Chapter 5 regarding the distribution of the variables in a given parameterization of a matrix in the unitary group [The orthogonal group is a subgroup of the unitary group], we find the metric tensor

$$g = \mathrm{tr}\left(\frac{dO}{d\beta}\frac{dO^T}{d\beta}\right) = 4[\cos^2(2\beta) + \sin^2(2\beta)] = 4. \tag{7.75}$$

The distribution of β, given by $\rho(\beta) \propto |\det(g)|$ is thus constant, independent of β, i.e β is uniformly distributed between 0 and 2π. Together with the fact the β's are independent, this is the statistical information we need to proceed with the calculation.

7.3.3 Average currents and current fluctuations

With this we turn to the calculation of the currents. Inserting the value for R_n in Eq. (7.69) together with the single mode current for a short junction in Eq. (4.10) into Eq. (7.49), we get

$$\begin{aligned} I_n^+ &= \frac{e\Delta}{\hbar}\frac{D_n \sin\phi}{2\sqrt{1-D_n\sin^2(\phi/2)}} \\ I_n^- &= \frac{e\Delta}{\hbar}\frac{\sin\beta_n D_n\sqrt{1-D_n}\sin^2(\phi/2)\cos(\phi/2)}{1-D_n\sin^2(\phi/2)}. \end{aligned} \tag{7.76}$$

Since the distributions of β_n and D_n are known, the average current as well as the sample-to-sample fluctuations for any number of transverse modes can be calculated. In the discussion below we focus on the limit of many transverse modes, $N \gg 1$, and ideal leads, $\Gamma = 1$.

From Eq. (7.76) it is clear that due to the uniform distribution of β, for a given phase difference ϕ, the average current $\langle I^- \rangle = 0$ is zero at any voltage. The average current is thus entirely given by $\langle I^+(eV)\rangle$, which describes the nonequilibrium population of the Andreev states carrying the current in equilibrium. Directly performing the ensemble average of the current density, the sum over bound states effectively turns into a continuum. Using the delta function identity $\delta(E-E_n) = \delta(D-D_n)|dD_n/dE_n|$, the bound state equation (4.5) relating E_n and D_n and the transmission eigenvalue density $\rho(D)$ in Eq. (6.30), the current density becomes

$$\begin{aligned} < i^+ > &= \frac{e\Delta}{\hbar}\int_0^1 dD\,\rho(D)\frac{\mathrm{sgn}(E) D\sin\phi}{2\sqrt{1-D\sin^2(\phi/2)}}\left|\frac{dD_n}{dE_n}\right|\delta(D-D_n) \\ &= \frac{Ne}{h}\frac{4\cos(\phi/2)}{\sin(\phi/2)}\sqrt{\frac{1-(E/\Delta)^2}{(E/\Delta)^2-\cos^2(\phi/2)}}. \end{aligned} \tag{7.77}$$

The averaged current density for three different phase differences and the corresponding averaged currents as functions of applied voltage are shown in Fig. 7.2 One notes that there is a gap in the current density, $E_g = \Delta\cos\phi$, the same as in the density of states, discussed above. It follows that the current is unaffected by a voltage $eV < E_g$. Moreover, the current density

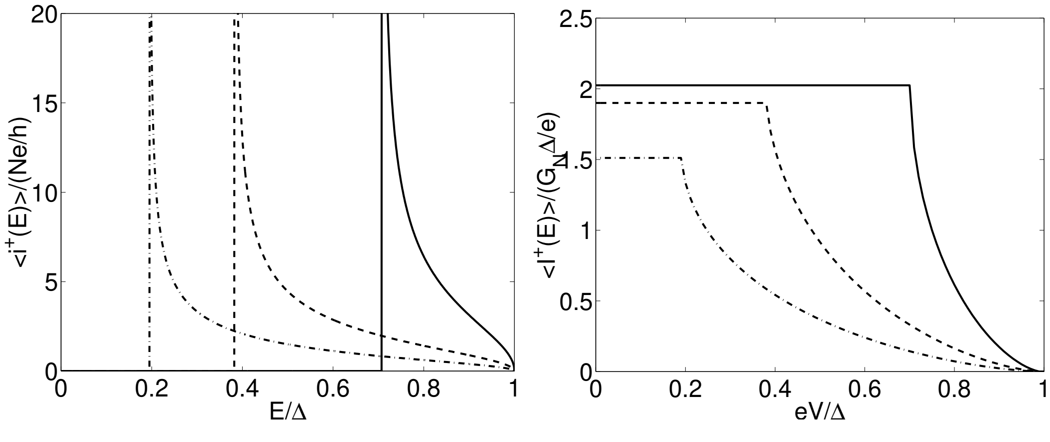

Figure 7.2: Left: The ensemble averaged sum current density as a function of energy (left) and the ensemble averaged current as a function of voltage (right) for phase difference $\phi = \pi/2$ (solid), $3\pi/4$ (dashed) and $7\pi/8$ (dash-dotted) and a large number of modes N 1.

has the same sign for all energies, leading to that the current is monotonically suppressed for increasing voltage, i.e. it does not change sign as a function of voltage (no π-junction behavior).

Although the average current $\langle I^- \rangle$ is zero, the fluctuations are not. At zero voltage, the fluctuations are just the equilibrium current fluctuations, plotted as a function of phase difference in Fig. 7.1. Increasing the voltage, the Andreev levels switch from carrying I_n^+ to I_n^-, and the fluctuations of I are determined by a combination of the sum and difference current fluctuations. At $eV \geq \Delta$, all levels are carrying I_n^- and the fluctuations are given by, since the average current $\langle I \rangle = \langle I^- \rangle$ is zero

$$\mathrm{Var}[I(eV \geq \Delta)] = \langle I^2 \rangle = \langle (\sum_n I_n^-)(\sum_m I_m^-) \rangle = \sum_{n,m} \langle I_n^- I_m^- \rangle. \tag{7.78}$$

Since the parametrizing variables β_n are independent, any average $\langle I_n^- I_m^- \rangle$ for $n \neq m$ is zero and only the terms with $n = m$ contribute to the fluctuations. The variance is thus given by

$$\begin{aligned}\mathrm{Var}(I) &= \langle \sum_n (I_n^-)^2 \rangle = \frac{e\Delta}{\hbar}\frac{1}{2\pi}\int d\beta \sin^2\beta \int dD\rho(D)\left(\frac{D\sqrt{1-D}\sin^2(\phi/2)\cos(\phi/2)}{1-D\sin^2(\phi/2)}\right)^2 \\ &= N\left(\frac{e\Delta}{2\hbar\tan\phi/2}\right)^2\left[\sin^2\frac{\phi}{2} + \frac{8\sin^2\phi/4}{\cos\phi/2} - 3\frac{\sin^2\phi/2}{\cos\phi/2}\right]. \end{aligned}\tag{7.79}$$

The result in Eq. (7.79) shows the surprising result that the magnitude of the fluctuations, rms I, are of order $\sqrt{N}e\Delta/\hbar$, i.e. $\sqrt{N}$ larger than the equilibrium fluctuations. This can be understood by that I^- is a sum of N independently fluctuating currents I_n^-, due to the fact that the β's are independent. Thus, the mechanism of strong correlations between the transmission eigenvalues, suppressing the fluctuations of the equilibrium current, is not present for the nonequilibrium current.

It is interesting to see whether this property of the nonequilibrium current for a given phase difference carries over to the critical current. Because $I(\phi) = -I(-\phi)$ it sometimes makes sense to restrict the phase to $0 < \phi < \pi$ and to consider the current which is largest in modulus; I_c can then be positive or negative. With this definition, the average critical current vanishes for $eV > \Delta$. In the following, however, we maximize over $-\pi < \phi < \pi$, hence I_c is always positive. This is more directly connected to an experimental situation, since the critical current obtained from the I/V characteristic in experiments is always positive, and the information about the phase difference for which this critical current is obtained must be found by other means, e.g from the conductance, as was done in Ref.35.

Since the critical phase difference ϕ_c for a given realization, i.e a given set of D_n and β_n, is itself a function of the D_n's and β_n's, the critical current is a complicated function of D_n and β_n, and can only be found numerically. The ensemble-averaged critical current and its fluctuations as a function of applied voltage eV, obtained by numerically generating 10^3 random scattering matrices with $N = 10$, are shown in Fig. 7.3. The result is compared to the contribution of I^+ alone, which only takes the nonequilibrium population of the Andreev levels into account.

For $0 \leq eV \leq 0.54\Delta$ the critical current is equal to its equilibrium value. This can be understood from that the Andreev levels carrying the critical equilibrium current, at a critical phase difference $\phi_\mathrm{c} \simeq 2$ all have energies $E_n > 0.54\Delta$ (i.e. a gap $E_g = 0.54\Delta$ in the current density $\langle i^+ \rangle$). In the range $0.54\Delta \leq eV \leq 0.98\Delta$ the critical phase is determined by the condition $\cos\phi_c/2 = eV/\Delta$, i.e at the phase difference where the applied voltage eV is equal to the current density gap edge. The fluctuations are however small due to the high density of transmission eigenvalues $D_n \approx 1$, which gives a large weight for the current density close to the gap (see Fig. 7.2). Hence the critical current is $I_c = I^{eq}(\phi_c)$. In this regime I^- does not play any role

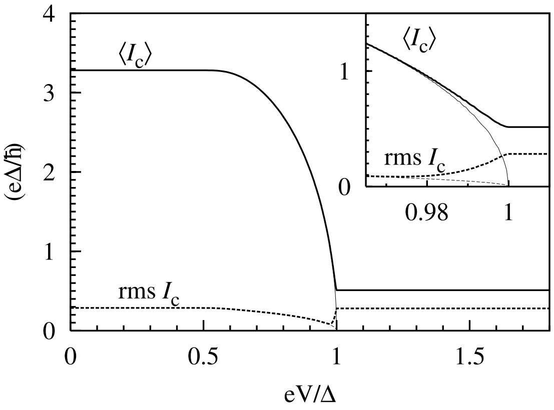

Figure 7.3: Ensemble-averaged critical current hI_ci (solid thick line) and the fluctuations rms I_c (dashed thick line) as a function of voltage V between the normal reservoir and the junction. The thin lines are the result with $I^- = 0$ in Eq. (7.49). The junction has $N = 10$ modes to each of the superconducting electrodes and $M = 1$ mode to the normal reservoir. Inset: the voltage range $0.965\Delta < eV < 1.01\Delta$. ($10^3$ random matrices S' have been generated).

because $\langle I^+ \rangle \gg$ rms I^-. For a voltage $eV \approx 0.98\Delta$ very close to the gap, I^+ and I^- are both of order $\sqrt{N}e\Delta/\hbar$, and the critical current starts to deviate from what one would expect from a pure nonequilibrium population of the Andreev levels. One can note that for increasing N the cross-over voltage $eV \to \Delta$. In parallel, the fluctuations of the critical current increase. The critical current remains constant for $eV \geq \Delta$, where it is given solely by I^-. We thus find

$$\text{rms } I_c \approx \langle I_c \rangle \approx \sqrt{N}\frac{e\Delta}{\hbar}. \tag{7.80}$$

for $eV \geq \Delta$. The critical current for $eV \geq \Delta$ and its fluctuations as a function of the number of junction modes N are shown in the upper panel of Fig. 7.4. The mean critical current is $\langle I_c \rangle \simeq 0.16\sqrt{N}e\Delta/\hbar$. The fluctuations are of the same order, rms $I_c \simeq 0.1\sqrt{N}e\Delta/\hbar$, which is a factor of about $\sqrt{N}/3$ larger than the equilibrium fluctuations. Hence the $\sqrt{N}$ dependence in Eq. (7.79) carries over to the average critical current and its fluctuations. One can note that due to that the critical current is defined as the largest possible current as a function of phase difference $-\pi < \phi < \pi$, the critical current itself is of order of $\sqrt{N}e\Delta/\hbar$ for $eV \geq \Delta$. That is, for every matrix realization, corresponding to every physical sample, there is a phase difference for which the current is positive, giving a nonzero averaged critical current of order $\sqrt{N}e\Delta/\hbar$, i.e of the same order as the fluctuations.

Finally let us consider the dependence of the critical current on the number of injection modes M. This number is significant because the current I^- depends manifestly on the coupling of the reservoir to the junction, in contrast to the current I^+ which only depends on properties of the decoupled junction. The lower panel of Fig. 7.4 shows that the critical current and its fluctuations at $eV \geq \Delta$ are suppressed when M is increased. The functional dependence is approximately $\propto M^{-1/3}$. The curves flatten out when M becomes larger than the total number $2N$ of modes connected to the superconductors. Thus, for an experimental observation of the large fluctuations predicted above, an injection contact with few modes is favorable. It is however an open question is if there is any type of scaling law for the fluctuations, i.e if the amplitude of the fluctuations vary as N^μ/M^ν. This would give additional information about in what range of experimental parameters this effect should be investigated.

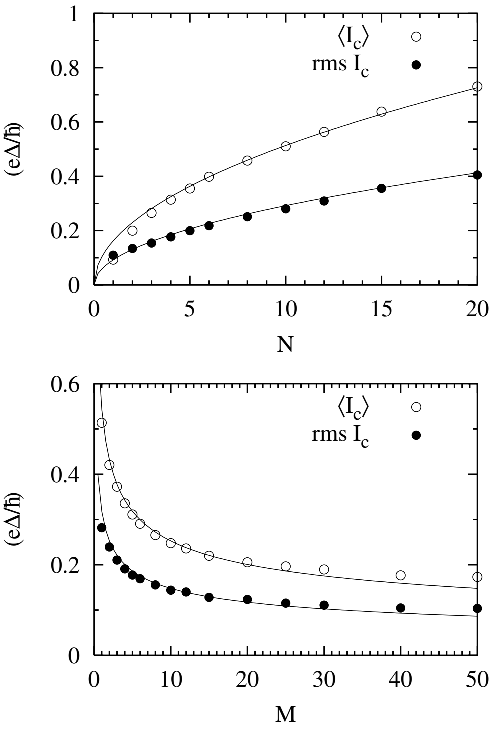

Figure 7.4: Ensemble-averaged critical current $\langle I_c \rangle$ (open circles) and the fluctuations rms I_c (full circles) as a function of the number of junction modes N for a single injection mode $M = 1$ (upper panel) and the number of injection modes M for $N = 10$ junction modes (lower panel). The curves are $\propto N^{1/2}$ (upper panel) and $\propto M^{-1/3}$ (lower panel).

CHAPTER 8

Current transport in voltage biased junctions:Multiple Andreev Reflection

The theoretical explanation of current transport in superconducting junctions was originally based on a tunnel Hamiltonian model.[76, 129] It predicted that the dc-current flowing between superconductors at finite applied bias would be exponentially small for $eV < 2\Delta$ and temperatures $kT \ll \Delta$. In early experiments by Taylor and Burstein,[231] it was found that the current in tunnel junctions was larger than predicted by the tunnel model at $eV < 2\Delta$, and had a sharp onset at $eV = \Delta$. This was explained by Schrieffer and Wilkins[204] in terms of second order tunneling processes, two-particle tunneling.

In later experiments on tunnel junctions with larger normal transparency and on weak links,[158] it was found that the current is finite at voltages $eV < 2\Delta$ and tends towards an excess value compared to the normal state current at large voltages $eV \gg 2\Delta$. Moreover, a rich current structure at $eV < 2\Delta$ was found, with clear conductance peaks at voltages equal to sub-multiples of the superconducting gap, $eV = 2\Delta/m$, so called Subharmonic Gap Structures (SGS).

The excess current was first given a microscopic explanation by Artmenko, Volkov and Zaitsev,[22] emphasizing the role of Andreev reflection. Attempts to explain the SGS by an extension of the two particle tunneling approach to higher orders, multi-particle tunneling, suffered from unphysical divergences. It was not until the work of Klapwijk, Blonder and Tinkham (KBT),[132] and later Octavio, Tinkham, Blonder and Klapwijk[185] (see also Ref. 91), that the subharmonic gap structure was given a simple and intuitive explanation in terms of Multiple Andreev Reflections (MAR). Quasiparticles, injected from the superconducting electrodes at energies below the gap, are accelerated by the electric field in the junction. They undergo Andreev reflections at the two superconducting electrodes and finally escape out into the superconductors at energies above the gap, effectively transporting current between the superconductors. At voltages $eV = 2\Delta/m$, a new process opens up with quasiparticles that effectively traverse the junction m times before escaping out into the superconducting electrodes, giving rise to the SGS at $eV = 2\Delta/m$.

The OTBK-approach is based on matching distribution functions and not wavefunctions, i.e. it a priori neglects the quantum coherence of the quasiparticles and the ac-Josephson effect. It has been shown in a number of experiments (see e.g. 36,92,113,114,133,138,145,208,225), that the OTBK approach nevertheless explains the qualitative features of the SGS. Moreover, it also predicts an excess current at voltages $eV \gg 2\Delta$ for high transparency junctions. However, the quantitative agreement between theory and experiment is in general rather poor, which suggests that coherent processes are important for the dc-current transport. Another contributing reason might be the effect of electron-electron interaction,[106] known to modify transport properties of the junction.[145]

A lot of theoretical work after OTBK has been directed towards finding a a complete coherent theory of Multiple Andreev Reflection. Arnold[21] first solved the full quantum problem of MAR for a one dimensional junction within a Green's function approach. Thereafter MAR in single mode junctions has been studied within a scattering approach to the BdG-equation.[26,59,214] Also the tunnel Hamiltonian approach was further developed in Ref. 78, curing the problem of the earlier encountered divergences. The full quantum single mode theory has been extraordinary successful in explaining the measured IV-curves in atomic point contacts in mechanically controllable break junctions,,[160,192,201] which illustrates the importance of quantum coherence in microscopic junctions. There has also been a continuous development the theory of current transport in mesoscopic junctions, based on the quasiclassical Green's function approach.[12,51,52,80,236,251,253,254]

In this chapter we outline a theory for current transport in voltage biased mesoscopic junctions, essentially a multi-mode[31] generalization of the coherent MAR-theory of Ref. 127. The theory is based on the scattering approach to the BdG-equation and allows us in principle to calculate the current in a voltage biased mesoscopic junction with arbitrary energy and magnetic field dependence of the scattering matrix of the normal part of the junction. This theory is then applied to a chaotic Josephson junction in the subsequent chapter. As is discussed in the subsequent chapter, it turns out that the OTBK-approach can be used to describe the transport in mesoscopic junctions with broken TRS. Therefore, in this chapter, we also briefly present the original OTBK-model and then extend it to treat scattering in the normal conductor, relevant for the discussion in the subsequent chapter.

8.1 Time independent Bogoliubov-de Gennes equation

We study the current transport through the two-terminal junction depicted in Fig. 3.4. To simplify notation, we denote the sides 1 and 2 as left (L) and right (R) respectively. Applying a voltage between the two superconducting electrodes leads to a fundamentally different problem compared to the case where the superconductors are equipotential. When the two superconductors are equipotential, or in the case with only one superconductor, it is always possible to choose the reference of energy to be the chemical potential of the superconductors. This is convenient, since one can then solve the BdG-equation without having to take into account the presence of electric potential in the superconductors, and the scattering scheme for calculating different transport quantities, discussed in Chapter 3, can be applied. A schematic picture of a biased junction in position-energy space is shown in Fig. 8.1. With a potential difference between the superconductors, there is no longer any natural reference of energy, and independently of choice of reference energy, i.e choice of gauge, there is an electric potential present in either of the superconductors. This leads to that we have to consider the BdG-equation in the presence of electrostatic potential. This is first discussed for a bulk superconductor, and then applied to a voltage biased Josephson junction, where the two superconducting electrodes are subjected to different electrostatic potentials. The full, timedependent BdG equation is,

$$\begin{bmatrix} H_0 & \Delta \\ \Delta^* & -H_0^* \end{bmatrix} \Psi = i\hbar\frac{\partial}{\partial t}\Psi,\ H_0 = \frac{(i\hbar\nabla + eA)^2}{2m} + U - E_F + e\varphi \tag{8.1}$$

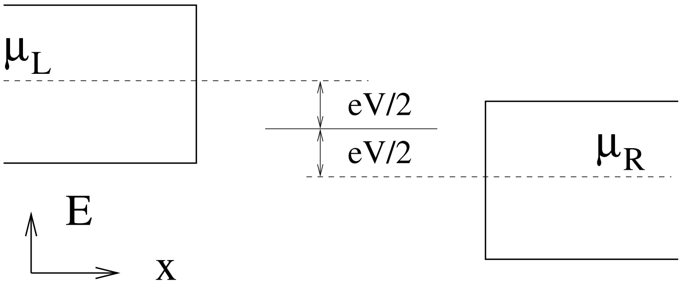

Figure 8.1: A schematic picture of junction, biased at eV with a symmetric gauge chosen.

where the wavefunction $\Psi = (\Psi_e, \Psi_h)$ has a two-component form and φ is the electrostatic potential due to the applied bias (U is the confining potential in the transverse direction). Just as in the time independent case in Chapter 3, we assume that the magnetic field is only present in the normal conductor, i.e. it is zero in the leads, and the vector potential A can be treated in the same way as in the time-independent case. The gauge invariant electric potential $\chi_i = e\varphi_i + (\hbar/2)\partial\phi_i/\partial t$, is assumed to be zero in the superconductors, due to the rapid spreading out of current in the bulk superconducting electrodes, in line with the reservoir approach.

The BdG-equation can be conveniently solved in a gauge where the phase of the superconductors is transformed away, as

$$e^{-i\sigma_z\phi_i/2}\left(\begin{bmatrix} H_0 & \Delta \\ \Delta^* & -H_0^* \end{bmatrix} - i\hbar\frac{\partial}{\partial t}\right) e^{i\sigma_z\phi_i/2}e^{-i\sigma_z\phi_i/2}\Psi = 0, \tag{8.2}$$

where σ_z is the Pauli matrix in electron-hole space. Under this transformation we find the Hamiltonian in the leads

$$H_0 \to \frac{(i\hbar\nabla + eA_i + \hbar\nabla\phi_i/2)^2}{2m} + U - E_F + e\varphi_i \tag{8.3}$$

and the time derivative

$$\frac{\partial}{\partial t} \to \frac{\partial}{\partial t} + \sigma_z\frac{i}{2}\frac{\partial\phi_i}{\partial t}. \tag{8.4}$$

The transformed BdG-equation in the leads is thus given by Eq. (8.2) with $H_0 \to \bar{H}_0$, where

$$\bar{H}_0 = -\frac{\hbar^2\nabla^2}{2m} + U - E_F, \tag{8.5}$$

which follows from the requirement that the gauge-invariant potential χ as well as the superfluid velocity $p_s = \hbar\nabla\phi - 2eA$ are zero in the leads. The superconducting order parameter transforms as $\Delta e^{\phi_i} \to \Delta$. The wavefunctions $\bar{\Psi}_i$ in this gauge are found in the same way as in Chapter 3, and the original wavefunctions are found by

$$\Psi_i = e^{-i\sigma_z\phi_i/2}\bar{\Psi}_i. \tag{8.6}$$

Due to the requirement that the gauge-invariant potential χ is zero, we get $e\varphi_i = -(\hbar/2)\partial\phi_i/\partial t$. Working in the convenient symmetric gauge, shown in Fig. 8.1, $\varphi_L = V/2, \varphi_R = -V/2$, we get $\phi_{L(R)} = \pm eVt/[2\hbar] + \phi^0_{L(R)}$, i.e the phase difference $\phi_R - \phi_L$ is rotating with the frequency $2eV/\hbar$, the Josephson frequency. The phases ϕ_i^0 in the time dependent case (compare to discussion in the time independent case in Chapter 3) is of no importance and can be neglected, since the total phases ϕ_i rotate in time.

One can note from the expression for the wavefunction in Eq. (8.6) that the electron and hole wavefunctions in the superconductors acquire different time-dependencies. This can be seen as a consequence of the electrons and holes having opposite charge and reacting oppositely to an electrostatic potential. From this different time dependence it follows that an applied voltage between the superconductors has a profound effect on the current transport, which is clearly displayed by considering a single Andreev reflection at a perfect NS-interface. The wavefunction matching equation for an incoming electron (at $x = 0$), written to get the same time dependence on the wavefunction components to be matched, is

$$\begin{pmatrix} 1 \\ 0 \end{pmatrix} e^{-iEt/\hbar} + \alpha \begin{pmatrix} 0 \\ 1 \end{pmatrix} e^{-i(E+eV)t/\hbar} = \begin{pmatrix} u(E+eV/2)e^{ieVt/[2\hbar]} \\ v(E+eV/2)e^{-ieVt/[2\hbar]} \end{pmatrix} e^{-i(E+eV/2)t/\hbar}. \quad (8.7)$$

This shows that the Andreev refleced hole has an energy $E+eV$, i.e eV more than the incoming electron, and that the Andreev reflection amplitude is $\alpha(E+eV/2) = v(E+eV/2)/u(E+eV/2)$.

Turning to the voltage biased Josephson junction, pictured in Fig. 8.1, the different chemical potentials in the two superconducting electrodes imply that the wavefunctions in the two superconducting electrodes have different time dependencies. This has the effect, considering the bias scenario in Fig. 8.1, that a left-moving electron in the normal part of the junction, at an energy E is Andreev reflected from the right superconductor into a hole with energy $E+eV$. Then traversing the junction from left to right, the hole is Andreev reflected back into an electron, at the energy $E+2eV$. Thus, after two subsequent Andreev reflections, the electron has gained an energy $2eV$. This process can continue, successively increasing the energy of the quasiparticle, until it eventually has gained enough energy to escape out into the superconducting electrodes at an energy outside the gap $E > \Delta$. This process, where the quasiparticle, by means of successive Andreev reflections, traverses the junction many times, alternating as electron and hole, each time gaining energy eV from the applied field, is called Multiple Andreev Reflections (MAR)..[132] It should be pointed out that backscattering in the normal conductor changes this picture, in the sense that it couples quasiparticles moving upwards and downwards in energy space. This will fully be taken into account in the quantitative discussion below.

The rather involved MAR-process can be illustrated conveniently by a sketch of the scattering process in energy-position space [noting that the energies are shown with respect to the Fermi energy in the superconductors and in the normal conductor] shown in Fig. 8.2. In this energy-position space figure, the superconductors are pictured at the same energy, and the scattering process for an injected electron quasiparticle below the gap is shown as a successive climbing in energy space, before the quasiparticle finally escapes out in the superconductors at an energy above the gap. It should also be pointed out in connection with this illustration that it differs from the way of illustrating the transport presented in the original works on MAR[132, 185] in two ways. First, since a local energy picture is chosen in our figure, the superconductors are aligned in energy, and not shifted in energy. Second, in line with our convention of displaying holes, (discussed in detail in Chapter 3) holes with positive excitation energy E are shown with positive energy in the figure.

The MAR-process thus couples quasiparticles at energies differing by meV where m is an integer, and one can conclude that the scattering state for an electron injected from one of the superconductors at energy E, will contain wavefunction amplitudes for electrons and holes at in principle all energies $E_m = E + meV$. To technically perform the wavefunction matching, we have to make an ansatz in both superconductors, consisting of a sum of plane waves at all energies $E_m = E + meV$. We adopt the convention, as depicted in Fig. 8.2, to count energies in each region with respect to the Fermi energy in the superconductors and the normal conductor

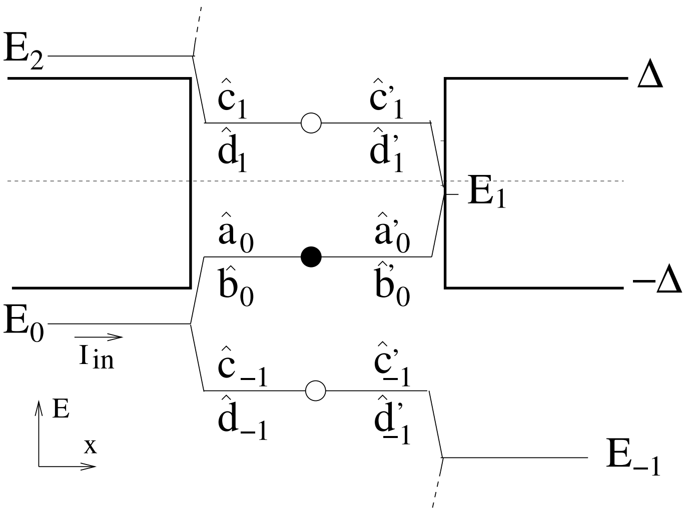

Figure 8.2: A picture of the MAR-ladder in a junction, biased at eV. Black (white) dots denote scattering of electrons (holes). The nonzero wavefunction coefficients of the wavefunction in Eq. (8.11) at each energy are shown.

respectively (this counting is not related to the gauge chosen, the gauge instead determines how the time dependence is introduced in the wavefunction ansatz). Following the same approach as in Chapter 3, we consider short superconducting segments on the superconducting sides of the NS-interface, where we make a formal wavefunction ansatz, similar to Eq. (3.9), with a sum over all energies E_m

$$\begin{aligned}\tilde{\Psi}_{SL} &= \frac{e^{-i\sigma_z eVt/(2\hbar)}}{\sqrt{u^2-v^2}}\sum_{m,n}\Theta_{1n}(y_1)\left(\frac{1}{\sqrt{q_n^e}}\left[\tilde{a}_{mn}\begin{pmatrix}u\\ v\end{pmatrix}e^{iq_n^e x_1}+\tilde{b}_{mn}\begin{pmatrix}u\\ v\end{pmatrix}e^{-iq_n^e x_1}\right]\right.\\ &+ \left.\frac{1}{\sqrt{q_n^h}}\left[\tilde{c}_{mn}\begin{pmatrix}v\\ u\end{pmatrix}e^{iq_n^h x_1}+\tilde{d}_{mn}\begin{pmatrix}v\\ u\end{pmatrix}e^{-iq_n^h x_1}\right]\right)e^{-iE_m t/\hbar}. \qquad (8.8)\end{aligned}$$

$$\begin{aligned}\tilde{\Psi}_{SR} &= \frac{e^{i\sigma_z eVt/(2\hbar)}}{\sqrt{u^2-v^2}}\sum_{m,n}\Theta_{1n}(y_2)\left(\frac{1}{\sqrt{q_n^e}}\left[\tilde{a}'_{mn}\begin{pmatrix}u\\ v\end{pmatrix}e^{iq_n^e x_2}+\tilde{b}'_{mn}\begin{pmatrix}u\\ v\end{pmatrix}e^{-iq_n^e x_2}\right]\right.\\ &+ \left.\frac{1}{\sqrt{q_n^h}}\left[\tilde{c}'_{mn}\begin{pmatrix}v\\ u\end{pmatrix}e^{iq_n^h x_2}+\tilde{d}'_{mn}\begin{pmatrix}v\\ u\end{pmatrix}e^{-iq_n^h x_2}\right]\right)e^{-iE_m t/\hbar}. \qquad (8.9)\end{aligned}$$

where the index n denotes transverse mode. The wavenumbers and transverse wavefunctions are the same as discussed in connection to Eq. (3.9). To be able to straightforwardly match the wavefunctions at the NS-interfaces, in line with Eq. (8.7), we make the ansatz on the normal side of the NS-interfaces as

$$\begin{aligned}\Psi_L &= e^{ieVt/(2\hbar)}\sum_{m,n}\Theta_{1n}(y_1)\left(\frac{1}{\sqrt{k_n^e}}\left[a_{mn}\begin{pmatrix}1\\ 0\end{pmatrix}e^{ik_n^e x_1}+b_{mn}\begin{pmatrix}1\\ 0\end{pmatrix}e^{-ik_n^e x_1}\right]\right.\\ &+ \left.\frac{1}{\sqrt{k_n^h}}\left[c_{mn}\begin{pmatrix}0\\ 1\end{pmatrix}e^{ik_n^h x_1}+d_{mn}\begin{pmatrix}0\\ 1\end{pmatrix}e^{-ik_n^h x_1}\right]\right)e^{-iE_m t/\hbar}. \qquad (8.10)\end{aligned}$$

$$\begin{aligned}\Psi_R &= e^{ieVt/(2\hbar)}\sum_{m,n}\Theta_{1n}(y_2)\left(\frac{1}{\sqrt{k_n^e}}\left[a'_{mn}\begin{pmatrix}1\\0\end{pmatrix}e^{ik_n^e x_2}+b'_{mn}\begin{pmatrix}1\\0\end{pmatrix}e^{-ik_n^e x_2}\right]\right.\\ &+ \left.\frac{1}{\sqrt{k_n^h}}\left[c'_{mn}\begin{pmatrix}0\\1\end{pmatrix}e^{ik_n^h x_2}+d'_{mn}\begin{pmatrix}0\\1\end{pmatrix}e^{-ik_n^h x_2}\right]\right)e^{-iE_m t/\hbar}. \qquad (8.11)\end{aligned}$$

To obtain the scattering state wavefunction for the complete junction and from this the current, we have to match the wavefunction at the NS-interfaces and across the normal conductor.

8.1.1 Current from scattering states

The scattering states can, just as in the cases without voltage bias, be labeled with the quantum numbers E, q, j and σ, where E is the energy of the incoming quasiparticle, q is the injection mode, j the injection lead (left or right) and σ is the quasiparticle type, electron- or hole like. With the ansatz above in Eq. (8.9)-(8.11) the matching equations at the left NS-interfaces connecting quasiparticles with the same time-dependence, can be written

$$\begin{pmatrix}\hat{a}_m\\ \hat{b}_m\end{pmatrix} = \begin{pmatrix}\alpha_m & 0\\ 0 & \alpha_m^{-1}\end{pmatrix}\begin{pmatrix}\hat{c}_{m-1}\\ \hat{d}_{m-1}\end{pmatrix}+\delta_{m0}\delta_{nq}(u^2-v^2)\begin{pmatrix}\delta_{\sigma,e}\sqrt{q_q^e}/u\\ -\delta_{\sigma,h}\sqrt{q_q^h}/v\end{pmatrix} \qquad (8.12)$$

where $\alpha_m = \alpha(E_m)$ and where we have introduced a vector notation, such that $\hat{a}_m, \hat{b}_m, \hat{a}'_m$ and $\hat{b}'_m$ are column vectors, length N, with entries of wavefunction coefficients $(\hat{a}_m)_n = \hat{a}_{mn}$ and similarly for $\hat{b}_m, \hat{a}'_m$ and $\hat{b}'_m$. Similarly at the right interface

$$\begin{pmatrix}\hat{c}'_m\\ \hat{d}'_m\end{pmatrix} = \begin{pmatrix}\alpha_m & 0\\ 0 & \alpha_m^{-1}\end{pmatrix}\begin{pmatrix}\hat{a}'_{m-1}\\ \hat{b}'_{m-1}\end{pmatrix}+\delta_{m0}\delta_{nq}(u^2-v^2)\begin{pmatrix}\delta_{\sigma,h}\sqrt{q_q^h}/u\\ -\delta_{\sigma,e}\sqrt{q_q^e}/v\end{pmatrix} \qquad (8.13)$$

The second terms in Eqs. (8.12) and (8.13) are source terms for the electron- and hole quasiparticles injected from left and right in mode q at energy $E = E_0$. In the vector notation adopted, δ_{nq} is thus a vector, length N, with element q equal to unity and the other elements zero. Across the normal conductor, the electron quasiparticles with the same time dependence are matched with the scattering matrix of the normal conductor as

$$\begin{pmatrix}\hat{a}'_m\\ \hat{b}_m\end{pmatrix} = S_m = S(E_m+eV/2)\begin{pmatrix}\hat{b}'_m\\ \hat{a}_m\end{pmatrix}. \qquad (8.14)$$

The hole wavefunction coefficients are matched as

$$\begin{pmatrix}\hat{d}'_m\\ \hat{c}_m\end{pmatrix} = S^*(-[E_m+eV/2])\begin{pmatrix}\hat{c}'_m\\ \hat{d}_m\end{pmatrix}, \qquad (8.15)$$

The equations (8.13)-(8.15) completely determines the scattering states, noting that the wavefunction coefficients approach zero for energies far outside the gap $|E| \gg \Delta$. From the scattering states, the time-dependent current density $i^{j,q,\sigma}(E,t)$ can be calculated, using the quantum mechanical formula for current in Eq. (2.9). The current is constant in the junction due to current conservation and we choose to calculate it on the normal side of the left NS-interface. Integrating the charge current expression in Eq. (3.15) over the transverse dimension y, the current density per unit energy [in line with Eq. (3.21)] can be written as a sum over Fourier components

$$i^{jq\sigma}(E,t) = \sum_k i_k^{jq\sigma}(E)e^{ikeVt/\hbar} \qquad (8.16)$$

with the current density components $i_k^{jq\sigma}(E)$ given by

$$i_k^{jq\sigma}(E) = \frac{e}{h}\frac{1}{q_q^\sigma(u^2-v^2)}\sum_{m=-\infty}^{\infty}(\hat{a}_m^\dagger \hat{a}_{m+k} - \hat{b}_m^\dagger \hat{b}_{m+k} + \hat{c}_m^\dagger \hat{c}_{m+k} - \hat{d}_m^\dagger \hat{d}_{m+k}) \qquad (8.17)$$

where the scattering state indices on the wavefunction amplitudes have been suppressed for notational convenience. The total current of each component is then found from summing over all injected quasiparticles in all leads and modes and then integrating over energy,

$$I_k = \int_{-\infty}^{\infty} dE \sum_{j,q,\sigma} i_k^{jq\sigma}(E) f(E). \qquad (8.18)$$

In the discussion below we focus on the time-independent dc-part, i.e the $k = 0$ component, and the index k is dropped in the following. Before solving the matching equations in (8.12)-(8.15) and finding the formal expressions for the scattering states, we introduce a conceptual simplification, based on the observation that half of the wavefunction coefficients in the normal part of the junction are zero for a given scattering state.

8.1.2 Energy space formulation and particle current decomposition

It is clear from Fig. 8.2, that for a left injected quasiparticle, $j = L$, the electron wavefunction coefficient with odd m and hole wavefunction with even m are zero. To get rid of the redundant coefficients we proceed in line with Johansson et al[128] and Ingerman et al[123] and introduce new coefficients, $\hat{c}_{m\pm}^{\uparrow(\downarrow)}$, which denote the wavefunction amplitudes for quasiparticles propagating upwards [↑] (downwards [↓]) in energy space. For m even we have on the left side $\hat{c}_{m+}^{\uparrow} = \hat{a}_m$, $\hat{c}_{m+}^{\downarrow} = \hat{b}_m$, $c_{m-}^{\uparrow} = \hat{c}_{m-1}$ and $\hat{c}_{m-}^{\downarrow} = \hat{d}_{m-1}$ and for m odd we have $\hat{c}_{m+}^{\uparrow} = \hat{c}'_m$, $\hat{c}_{m+}^{\downarrow} = \hat{d}'_m$, $\hat{c}_{m-}^{\uparrow} = \hat{a}'_{m-1}$ and $\hat{c}_{m-}^{\downarrow} = \hat{b}'_{m-1}$. Coefficients for right injected quasiparticles are introduced analogously.

This notation can be conveniently presented in a MAR-ladder corresponding to the one in Fig. 8.2, as shown in Fig. 8.3. In this notation, the matching equations at both NS-interfaces

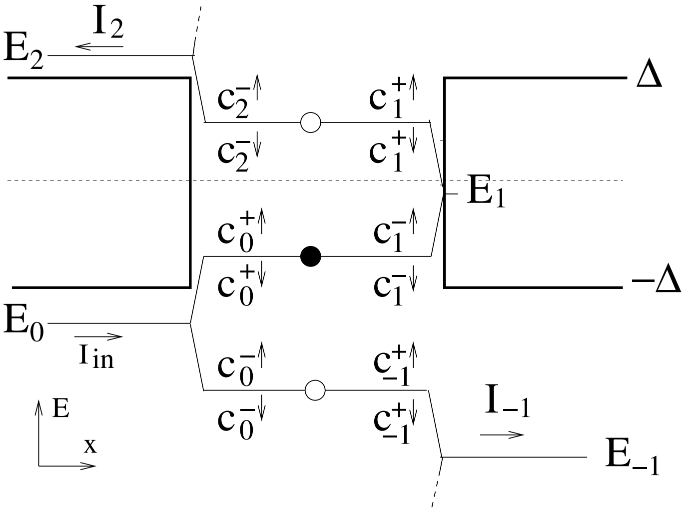

Figure 8.3: A picture of the MAR-ladder. The wavefunction coefficients $c_m^{\pm,\uparrow,\downarrow}$ at each energy are shown as well the m-particle current I_m leaking out at each energy. Black (white) dots denote electrons (holes).

for left injected quasiparticles in mode q can be written on a common form

$$\begin{pmatrix} \hat{c}_m^{\uparrow,+} \\ \hat{c}_m^{\downarrow,+} \end{pmatrix} = \begin{pmatrix} a_m & 0 \\ 0 & a_m^{-1} \end{pmatrix} \begin{pmatrix} \hat{c}_m^{\uparrow,-} \\ \hat{c}_m^{\downarrow,-} \end{pmatrix} + \delta_{m0}\delta_{nq}(u^2 - v^2) \begin{pmatrix} \delta_{\sigma,e}\sqrt{q_q^e}/u \\ -\delta_{\sigma,h}\sqrt{q_q^k}/v \end{pmatrix}. \quad (8.19)$$

The matching equations across the normal conductor becomes for electron wavefunction coefficients

$$\begin{pmatrix} \hat{c}_{2m}^{\downarrow,+} \\ \hat{c}_{2m+1}^{\uparrow,-} \end{pmatrix} = S(E_{2m} + eV/2) \begin{pmatrix} \hat{c}_{2m}^{\uparrow,+} \\ \hat{c}_{2m+1}^{\downarrow,-} \end{pmatrix} \quad (8.20)$$

and the hole wavefunction coefficients are matched as

$$\begin{pmatrix} \hat{c}_{2m}^{\uparrow,-} \\ \hat{c}_{2m-1}^{\downarrow,+} \end{pmatrix} = S^*(-[E_{2m} + eV/2]) \begin{pmatrix} \hat{c}_{2m}^{\downarrow,-} \\ \hat{c}_{2m-1}^{\uparrow,+} \end{pmatrix}. \quad (8.21)$$

The current density $i^L(E)$ summed over injection modes q and injected electron- and hole quasiparticles, can be written as [from Eq. 8.17]

$$i^L(E) = \sum_{q,\sigma} i^{Lq\sigma}(E) = \frac{e}{h} \sum_{m=-\infty}^{\infty} j_m^+ = \frac{e}{h} \sum_{m=-\infty}^{\infty} j_m^- \quad (8.22)$$

where, with suppressed scattering state index,

$$j_m^+ = \left[(\hat{c}_m^{\uparrow,+})^\dagger \hat{c}_m^{\uparrow,+} - (\hat{c}_m^{\downarrow,+})^\dagger \hat{c}_m^{\downarrow,+} \right] = j_{m+1}^- = \left[(\hat{c}_{m+1}^{\uparrow,-})^\dagger \hat{c}_{m+1}^{\uparrow,-} - (\hat{c}_{m+1}^{\downarrow,-})^\dagger \hat{c}_{m+1}^{\downarrow,-} \right] \quad (8.23)$$

since left-going holes carry charge current in the same direction as right-going electrons and current is conserved across the normal part of the junction. It is possible[128] to rewrite the charge current density in terms of the probability current density "leaking" out of of the MAR ladder at energies E_m (see Fig. 8.3) outside the superconducting gap. The probability current leaking out at energy E_m results from quasiparticles having traversed the junction effectively m times, which provides a link to the multi-particle tunneling picture[204]discussed above. This (by definition positive) current density is denoted I_m^p, with superscript p denoting particle currents. For the particle current flowing upwards in energy space, i.e. $m > 0$, we can write the corresponding charge current density $i_m^L(E)$ as

$$\begin{aligned} i_m^L(E) &= \frac{e}{h}\left[j_0^+ + j_1^+ + j_2^+ + \ldots \right] = \frac{e}{h}\left[j_0^+ - j_1^+ + 2j_1^+ - 2j_2^+ + 3j_2^+ \ldots \right] \\ &= \frac{e}{h}\left[(j_1^- - j_1^+) + 2(j_2^- - j_2^+) + 3(j_3^- - j_3^+) + \ldots \right] = \frac{e}{h} \sum_m m I_m^{pL}. \end{aligned} \quad (8.24)$$

where we thus have $I_m^{pL} \equiv j_m^- - j_m^+$. The same holds for particle currents flowing downwards in energy space, giving the total charge current density

$$i^L(E) = \frac{e}{h} \sum_{m \neq 0} m I_m^{pL}. \quad (8.25)$$

where we point out that particle currents flowing downwards in space ($m<0$) carry negative charge current, which is accounted for by that the index m in Eq. (8.25) is negative. The right injected quasiparticles can be treated analogously and the total dc-current is thus given by

$$I = \frac{e}{h}\int_{-\infty}^{\infty} dE \sum_{m\neq 0}\sum_{j} m I_m^{p,j} f_0(E) \tag{8.26}$$

This formulation of the current has the physical interpretation that the current is transported by quasiparticles with effective charge me. If this interpretation has any physical relevance, one would expect that the effective charge could be detected in the shot noise, known to be proportional to the effective charge carried[79,179] (in the tunnel limit). This has indeed been observed very recently in atomic size break junctions,[81] which suggests that the above formulation of the current presents a physically relevant picture.

As is clear from the discussion above, all states in the voltage biased Josephson junction are scattering states, i.e there are no bound states, since there is always a finite amplitude for a quasiparticle with an energy within the superconducting gap $|E|<\Delta$ to gain (lose) energy via multiple Andreev reflections and escape out in the superconductors at energies above (below) the gap. One could however argue that it is physically reasonable that at very low voltages, when the lifetime of the scattering states could be very long, there should be a clear connection to a Josephson junction without voltage bias, where a part of the current is carried by bound states, as discussed in Chapter 3. This is indeed the case, and the bridge between these two approaches, discussed in Ref. 26, is to consider Andreev bound states, slowly oscillating in time with the Josephson frequency, with Landau-Zener transitions between the different bound states giving rise to a finite net current. This approach is convenient for very low voltages $eV \ll \Delta$, [rigorously, for a single mode junction, the voltage $eV \ll R\Delta$, where R is the normal reflection probability of the junction], but since our focus in this thesis is on the regime with voltages of order $eV \sim \Delta$, we will use the full scattering approach to MAR.

8.1.3 Formal expression for scattering states

To calculate the current we need to have the scattering states expressed in terms of the scattering quantities of the junction, the scattering matrix and the Andreev reflection amplitudes. In a large number of works on MAR, the approach to calculating the current is to derive recurrency relations for the wavefunction coefficients. Here we however derive a formal solution of the wavefunction coefficients directly in terms of the scattering amplitudes. This has the advantage that each wavefunction coefficient can, in line with a general notion of a scattering approach, be straightforwardly expanded as a sum of matrix amplitudes, where each matrix amplitude corresponds to a path in energy position space, starting at the injection point. This turns out to be a very convenient formulation for the discussion in the subsequent chapter.

Consider quasiparticles injected from the left and study first the particle currents with positive m, i.e quasiparticles traveling upwards in energy space. The wavefunction amplitudes at different energies E_m and E_l, with $m>l>0$, are connected by the scattering matrix S_{ml}, such that

$$\begin{pmatrix} c_{l-}^{\downarrow} \\ c_{m+}^{\uparrow} \end{pmatrix} = S_{ml}\begin{pmatrix} c_{l-}^{\uparrow} \\ c_{m+}^{\downarrow} \end{pmatrix}, \quad S_{ml} = \begin{pmatrix} r_{lm} & t_{ml} \\ t_{lm} & r_{ml} \end{pmatrix} \tag{8.27}$$

where thus the first index on the scattering amplitudes t and r denotes the energy of the incident quasiparticle. The scattering matrix S_{ml} thus contains all information about the scattering between energies E_l and E_m. If any of the energies between E_{l+1} and E_{m-1} lies outside the superconducting gap, there is a certain probability for leakage of current at this energy and consequently the scattering matrix is nonunitary. The scattering matrix is most conveniently found from the corresponding transfer matrix M_{ml}, which connects wavefunction coefficients as

$$\left(\begin{array}{c} \hat{c}^{\uparrow}_{m-} \\ \hat{c}^{\downarrow}_{m-} \end{array} \right) = M_{ml} \left(\begin{array}{c} \hat{c}^{\uparrow}_{l+} \\ \hat{c}^{\downarrow}_{l+} \end{array} \right) \tag{8.28}$$

and is connected to the scattering matrix as, in line with Eq. (2.23),

$$M_{ml} = \left(\begin{array}{cc} t_{ml} - r_{lm} t_{lm}^{-1} r_{ml} & r_{lm} t_{lm}^{-1} \\ t_{lm}^{-1} r_{ml} & t_{lm}^{-1} \end{array} \right). \tag{8.29}$$

The transfer matrix has, as discussed in Chapter 2, a multiplicative property such that the transfer matrix M_{ml} is the product of all transfer matrices, alternating for the normal conductor T_m and the Andreev scattering U_m, as

$$M_{ml} = M_{ml} = T_{m-1} U_{m-1} T_{m-2} \ldots . T_l \tag{8.30}$$

where $U_m = \mathrm{diag}(\alpha_m, 1/\alpha_m)$ from Eq. (8.12) and T_m is the transfer matrix for alternating electrons and holes, such that $T_m = T(E_m + eV/2)$ for even m and $T_m = \sigma_x T^*(-[E_m + eV/2])^{-1} \sigma_x$ for odd m, where the matrix σ_x is the generalized Pauli matrix in left-right lead space. This allows us, by combining Eq. (8.28) and (8.19), to connect the wavefunction at the escape energy E_m with the coefficient at the injection energy E_0 as

$$M_{m0}^{-1} U_m^{-1} \left(\begin{array}{c} c^{\uparrow}_{m+} \\ c^{\downarrow}_{m+} \end{array} \right) = U_0 \left(\begin{array}{c} c^{\downarrow}_{0-} \\ c^{\downarrow}_{0-} \end{array} \right) + \delta_{m0} \delta_{nq} (u^2 - v^2) \left(\begin{array}{c} \delta_{\sigma,e} \sqrt{q^e_q}/u \\ -\delta_{\sigma,h} \sqrt{q^h_q}/v \end{array} \right). \tag{8.31}$$

Due to that there is only incoming quasiparticles at energy E_0, one can relate the wavefunction coefficients

$$c^{\uparrow}_{0-} = r_{0-} c^{\downarrow}_{0-}, \; c^{\downarrow}_{m+} = r_{m+} c^{\uparrow}_{m+}, \tag{8.32}$$

where r_{0-} and r_{m+} are the amplitudes for reflection from energies below E_0 and above E_m respectively, which can be expressed recursively for any $m \geq 0$

$$r_{m+} = r_{m,m+1} + \alpha_{m+1} t_{m+1,m} r_{m+1,+} \left(1 - \alpha^2_{m+1} r_{m+1,m} r_{m+1,+}\right)^{-1} t_{m,m+1} \tag{8.33}$$

and for any $l \leq 0$

$$r_{l-} = r_{l,l-1} + \alpha_{l-1} t_{l-1,l} r_{l-1,+} \left(1 - \alpha^2_{l-1} r_{l-1,l} r_{l-1,+}\right)^{-1} t_{l,l-1}. \tag{8.34}$$

This gives that the relation in Eq. (8.31) can be written

$$\begin{aligned} M_{m0}^{-1} U_m^{-1} \left(\begin{array}{cc} 1 & 0 \\ 0 & r_{m+} \end{array} \right) \left(\begin{array}{c} c^{\uparrow}_{m+} \\ c^{\uparrow}_{m+} \end{array} \right) &= U_0 \left(\begin{array}{cc} r_{0-} & 0 \\ 0 & 1 \end{array} \right) \left(\begin{array}{c} c^{\downarrow}_{0-} \\ c^{\downarrow}_{0-} \end{array} \right) \\ &+ \delta_{m0} \delta_{nq} (u^2 - v^2) \left(\begin{array}{c} \delta_{\sigma,e\to} \sqrt{q^e_q}/u \\ -\delta_{\sigma,h\to} \sqrt{q^h_q}/v \end{array} \right). \end{aligned} \tag{8.35}$$

This equation is straightforwardly solved, giving the wavefunction coefficient $c^{\uparrow}_{m+}$ for an injected electron in mode q

$$c^{\uparrow}_{m+} = -a_m G_{0m} \frac{u^2 - v^2}{u} \sqrt{q^e_q} \delta_{nq} \tag{8.36}$$

where we have introduced

$$G_{0m} \quad = \quad \left[(1 - \alpha_0^2 r_{0-} r_{0m}) t_{0m}^{-1} (1 - \alpha_m^2 r_{m0} r_{m+}) - \alpha_0^2 \alpha_m^2 r_{0-} t_{m0} r_{m+} \right]^{-1}. \tag{8.37}$$

From the expression for the wavefunction coefficients in Eqns. (8.36) and (8.38), one get the remaining coefficients. In the same way for an injected hole, conveniently solving Eq. (8.35) for $c^{\downarrow}_{m-}$, we get

$$c^{\downarrow}_{m-} = -a_0 a_m G_{0m} \frac{u^2 - v^2}{u} r_{0-} \sqrt{q^h_q} \delta_{nq}. \tag{8.38}$$

In Eq. (8.37) we have shifted back again from transfer to scattering matrix amplitudes, which is convenient for further evaluation. From the expression for the wavefunction coefficients in Eqs. (8.36) and (8.38), one gets the remaining coefficients via the matching equations in Eq. (8.19) and (8.32). Inserting these expression into the particle current density formula, one gets

$$I^{pL}_{m>0} = (1 - \alpha_0^2)(1 - \alpha_m^2) \mathrm{tr} \left[(1 + \alpha_m^2 r^{\dagger}_{m+} r_{m+}) G_{0m} (1 + \alpha_0^2 r_{0-} r^{\dagger}_{0-}) G^{\dagger}_{0m} \right] \tag{8.39}$$

where L denotes injection from left. We can proceed in the same way for particle current with negative m index, i.e leaking out at energies below the injection energy, and get the particle current

$$I^{pL}_{m<0} = (1 - a_0^2)(1 - a_m^2) \mathrm{tr} \left[(1 + \alpha_m^2 r^{\dagger}_{m-} r_{m-}) G'_{0m} (1 + \alpha_0^2 r_{0+} r^{\dagger}_{0+}) G'^{\dagger}_{0m} \right] \tag{8.40}$$

where

$$G'_{0m} = \left[(1 - \alpha_0^2 r_{0+} r_{0m}) t_{0m}^{-1} (1 - \alpha_m^2 r_{m0} r_{m-}) - \alpha_0^2 \alpha_m^2 r_{0+} t_{m0} r_{m-} \right]^{-1}. \tag{8.41}$$

and the reflection amplitudes r_0^+ and r_m^- are given recursively from Eqs. (8.33) and (8.34). Finally, to get the full formal solution, one has to consider right injected quasiparticles. Due to the notation adopted, the result can be immediately found from Eqs. (8.39) and (8.40), by transforming the scattering matrix of the normal conductor as $S \to \sigma_x S^*(-E) \sigma_x$, which is equivalent to interchanging left $\leftrightarrow$ right sides and electrons $\leftrightarrow$ holes in the scattering.

8.1.4 Total current and cancellations.

The general expression for the total dc-current is given by Eq. (8.18), and one could argue that although the particle current description provides an intuitive physical picture of the MAR-transport, we have merely rewritten the current density in a different form. However, in the case of conserved time reversal symmetry, or in a single mode junction,[127] it is possible to simplify the expression for the total current considerably.

By considering the Eqs. (8.39) and (8.40) for a particle current I^{pL}_m with m even, i.e when the injection and escape side both are the left side, one finds after explicit evaluation that the particle current with $m > 0$ is related to the particle current with $m < 0$ by a transformation of the scattering matrix $S \to S^T$, i.e

$$I_m^{pL}(E,S) = I_{-m}^{pL}(E+meV,S^T). \tag{8.42}$$

In the case with conserved time reversal symmetry, $S = S^T$ and the two currents are equal. This means that the particle current density flowing upwards in energy space from E_0 to E_m is exactly equal to the particle current flowing downwards in energy space from E_m to E_0. The net current flowing between energies E_0 and E_m is thus only proportional to the difference in occupation numbers. The same result is found for all particle currents, irrespectively of the injection and escape side. This allows us to write the total current $I = I_L + I_R$ as a sum over particle currents with positive m only on the simple form

$$\begin{aligned} I_{L(R)} &= \frac{e}{h}\sum_{m>0} m\left(\int_{-\infty}^{-\Delta-meV} dE[f(E)-f(E_m)]I_m^{pL(R)}\right. \\ &+ \left.\theta(meV-2\Delta)\int_{\Delta-meV}^{-\Delta} dE[2f(E)-1]I_m^{pL(R)}\right) = \sum_m I_m \end{aligned} \tag{8.43}$$

where we have defined I_m as the total m-particle current. At low temperatures compared to the superconducting gap, $kT \ll \Delta$, the Fermi distribution functions in Eq. (8.26) are exponentially close to unity in the interval of integration, and the current from left (right) injection becomes

$$I^{L(R)} = \frac{e}{h}\sum_{m>0} m\theta(meV-2\Delta)\int_{\Delta-meV}^{-\Delta} dE I_m^{pL(R)}. \tag{8.44}$$

This means that only real excitations through the gap contribute to the current. One can note that when time reversal symmetry is broken, this cancellation theorem does not hold, but there might be other more involved cancellation mechanisms in the game, enabling one to simplify the total current. This is an object of further study.

At a voltage $eV \gg \Delta$, only the single and two particle currents contribute to the total current. The single particle current density differs from the normal state current density only for injection energies close to $-\Delta$ or escape energies close to Δ, while the two particle current is nonzero only for the same energy region. The partition of the total current into particle current thus makes makes it straightforward to calculate the excess or deficit current compared to the normal state current at asymptotically large voltage. For temperature $kT \ll \Delta$ this current is

$$I_{exc} = \frac{e}{h}\int_{-\infty}^{-\Delta} dE[I_1^{pL}+I_1^{pR}+2(I_2^{pL}+I_2^{pR})]-I_N \tag{8.45}$$

where the normal state current I_N is found from Eq. (2.16).

8.2 Single mode junction

To exemplify the discussion above we study the simplest possible junction, a short,$L \ll \xi_0$, single mode junction. One could imagine that this simple case only could serve as a toy model for understanding the qualitative behavior, but this is not the case. Over the last decade there has been remarkable progress in the technique to fabricate mechanical break junctions, which now can be controlled with such a precision that a one atom contact can be systematically studied. These atomic size break-junctions have turned out to be perfect systems for the study of few mode voltage biased Josephson junctions,[160,192,201] and the agreement between the theory[26,59,78] without any fitting parameters and experiment has turned out to be extremely good.

The scattering matrix in the presence of time reversal symmetry is symmetric, with the elements independent on energy on the scale of Δ, due to the short limit. The matrices in the particle current density expressions in (8.39) and (8.40) reduce to numbers and the scattering phases drop out. It is possible to analyze the lowest order currents analytically in some detail as done in e.g Ref. 59, here we merely present the numerical results for some different junction transparencies D in Fig. 8.4. One can see how the individual particle currents I_m start contributing at $eV = 2\Delta/m$. The sub-harmonic gap structure is emphasized for low transparency, which is clearly seen in the differential conductance. At asymptotically large voltages $eV \gg \Delta$, the current has a magnitude in excess to the normal state current, given by Eq. (8.44), as,[78,214]

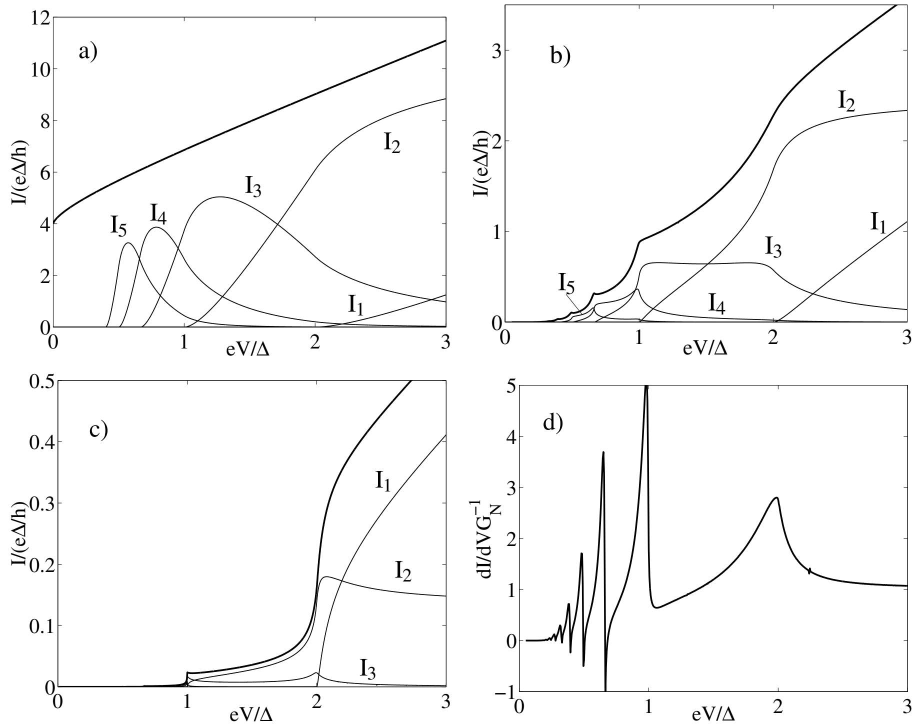

Figure 8.4: The current as a function of voltage of a short single mode junction, $L \quad \xi_0$ for transparency $D = 1$ (a), $D = 0.5$ (b) $D = 0.1$ (c). The first five individual particle currents I_1 to I_5 are shown [except in (c)]. The total differential conductance for $D = 0.5$ is shown in (d).

$$I_{exc} = \frac{e\Delta}{\pi\hbar}\frac{D^2}{1-D}\left[1 - \frac{D^2}{2\sqrt{1-D}(2-D)}\ln\left(\frac{1+\sqrt{1-D}}{1-\sqrt{1-D}}\right)\right] \tag{8.46}$$

This current is always positive and reduces to known results[185,252] in both the fully transparent limit $D = 1$, with $I_{exc} = 8e\Delta/(3\pi\hbar)$, and the tunnel limit $D \gg 1$, with $I_{exc} = e\Delta D^2/(\pi\hbar)$

8.3 Boltzman equation approach

The concept of multiple Andreev reflection, MAR, was introduced in two papers by Klapwijk, Blonder and Tinkham[132] (KBT) in 1982 and Octavio, Tinkham, Blonder and Klapwijk[185] (OTBK) in 1983. KBT studied an ideal SNS junction and showed that the current transport in voltage biased junctions could be explained in terms of multiple Andreev reflections. They also showed that at finite temperature, the IV-curve showed structures at voltages $eV = 2\Delta/m$, i.e the SGS discussed above, which provided a simple and intuitive explanation for these structures observed in several experiments. OTBK extended the KBT-model by introducing barriers at normal conductor-superconductor interfaces, a SINIS junction. They studied the distribution functions and the current in voltage biased Josephson junctions using a Boltzman equation approach and showed that in the presence of barriers at the NS-interfaces, the SGS was present already at zero temperature. A schematic figure of the junction is shown in Fig. 8.5. OTBK introduced distribution functions for subpopulations of electrons moving to the left ($\leftarrow$) and the right ($\rightarrow$) in the junction, $f_{\leftarrow}(E,x)$ and $f_{\rightarrow}(E,x)$. The distribution functions are evaluated in the normal conductor, right at the interfaces to the superconductors ($x = 0$ and $x = L$, see Fig. 8.5), and the energy E is calculated with respect to the chemical potential of the adjacent superconductor (the same as considered above). The distribution functions are matched across the junction as

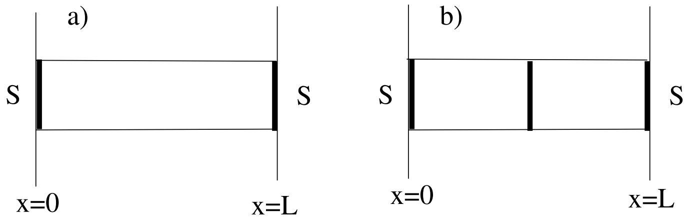

Figure 8.5: a) A schematic picture of OTBK-junction. b) A schematic picture of the modified OTBK-junction

$$f_{\rightarrow(\leftarrow)}(E,L) = f_{\rightarrow(\leftarrow)}(E-eV,0) \tag{8.47}$$

and at the left NIS-interface as

$$f_{\rightarrow}(E,0) = A(E)[1-f_{\leftarrow}(-E,0)] + B(E)f_{\leftarrow}(E,0) + T(E)f(E), \tag{8.48}$$

where $1-f_{\leftarrow}(-E,L)$ is the distribution of left moving holes, and at the right NIS-interface as

$$f_{\leftarrow}(E,L) = A(E)[1-f_{\rightarrow}(-E,L)] + B(E)f_{\rightarrow}(E,L) + T(E)f(E), \tag{8.49}$$

where f is the equilibrium Fermi distribution and $A(E) = |\tilde{a}(E)|^2$, $B(E) = |\tilde{b}(E)|^2$ and $T(E) = 1-A(E)-B(E) = C(E)+D(E)$ are the Andreev reflection probability and the normal reflection and transmission probabilities respectively. The amplitudes $\tilde{a}(E), \tilde{b}(E), \tilde{c}(E)$ and $\tilde{d}(E)$ are given by[54]

$$\begin{aligned}
\tilde{a}(E) &= \frac{\alpha}{1+(1-\alpha^2)Z^2}, \qquad \tilde{b}(E) = \frac{(1-\alpha^2)(Z^2+iZ)}{1+(1-\alpha^2)Z^2}, \\
\tilde{c}(E) &= \frac{\sqrt{1-\alpha^2}(1-iZ)}{1+(1-\alpha^2)Z^2}, \qquad \tilde{d}(E) = \frac{\alpha\sqrt{1-\alpha^2}iZ}{1+(1-\alpha^2)Z^2},
\end{aligned} \tag{8.50}$$

where the interface transparency Γ is related to the so called Z-parameter introduced in Ref. 54 as $\Gamma = 1/(1+Z^2)$. Using the electron-hole symmetry, it was shown later in Ref. 91 that electrons at $x = 0$ moving to the right have the same distribution as holes at $x = L$ moving to the left, i.e

$$f_{\rightarrow}(E,0) = 1-f_{\leftarrow}(-E,L) \tag{8.51}$$

Taken together, the equations (8.47)-(8.51) can be used to eliminate all but the distribution function for e.g. right-going quasiparticle [dropping position index since the left side and right side distributions are trivially related via Eq. (8.47], which then can be found from the recursive relation

$$f_{\rightarrow}(E) = A(E)f_{\rightarrow}(E-eV) + B(E)[1 - f_{\rightarrow}(-E-eV)] \tag{8.52}$$

From the distribution function, the current is readily obtained as

$$I = \frac{1}{eR_0}\int_{-\infty}^{\infty}[f_{\rightarrow}(E) - f_{\leftarrow}(E)] = \frac{1}{eR_0}\int_{-\infty}^{\infty}[2f_{\rightarrow}(E) - 1] \tag{8.53}$$

where R_0 is the normal state resistance of the junction without potential barriers. An example of the distribution function at $eV = \Delta$ and the differential conductance curve dI/dV is shown in Fig. 8.6 for $\Gamma = 0.5$. One clearly seen the SGS discussed above, however one should note that it is the second derivative (not shown) dI^2/d^2V that has a maximum at $eV = 2\Delta/n$, not the first derivative. The SGS become less and less pronounced for larger interface transparency Γ and it was shown by OTBK that at $\Gamma = 1$ the recursive relation in Eq. (8.52) reduces to the relation found by KBT for a clean SNS-junction.

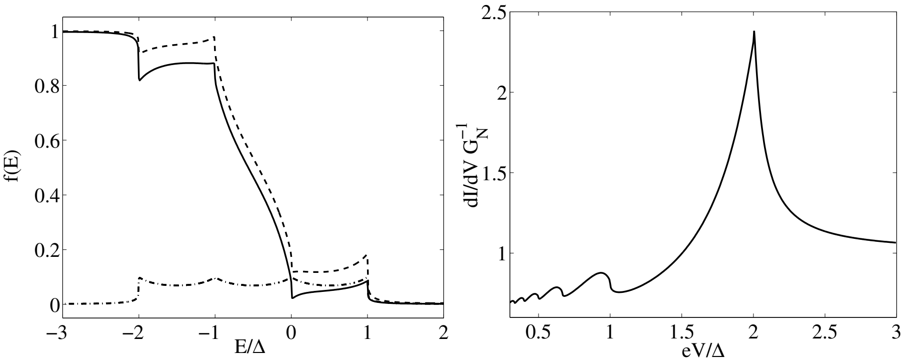

Figure 8.6: a) The OTBK-distribution function $f_{\rightarrow}(E)$ (solid), $f_{\leftarrow}(E)$ (dashed) and their difference (dash-dotted) at $eV = \Delta$. b) The differential conductance as a function of voltage. In both plots, the interface transparency $\Gamma = 0.5$.

In this context, it is interesting to note that the KBT-result is identical to the result for a single mode junction with perfect transparency ($D = 1$), calculated from the fully quantum mechanical approach.[26,59,78] However, as soon as normal scattering is introduced and quasiparticles moving up and down in energy space are coupled, there is a discrepancy between the fully quantum mechanical result and the OTBK-result, arising from that OTBK matches distribution functions, i.e effectively the modulus squared of wavefunctions, while in the fully quantum mechanical approach wavefunction amplitudes are matched. In the subsequent chapter, the relationship between the two approaches is studied further, and to perform this comparison it is useful to study a more generalized OTBK-model.

8.3.1 Generalized OTBK-approach

The distribution function approach taken by OTBK can straightforwardly be generalized by allowing for different transmission probabilities of the barriers,[113,138] $\Gamma_L \neq \Gamma_R$, which modifies the matching equations in (8.48) and (8.49), or by introducing additional barriers in the normal conductor, which would couple the left- and right going distributions in Eq. (8.47). It is clear that, if one is not interested in the distribution functions at certain positions inside the normal conductor (which are not relevant for calculating the current), all possible scattering inside the normal conductor can be accounted for by one single barrier with transparency $\mathcal{T}$ ($\mathcal{R} = 1 - \mathcal{T}$, not to confuse with matrices introduced in Chapter 3), such that the distribution functions at the interfaces, i.e at $x = 0$ and L are matched across the normal conductor as

$$\begin{aligned} f_{\leftarrow}(E,L) &= \mathcal{R} f_{\rightarrow}(E-eV,0) + \mathcal{T} f_{\rightarrow}(E,L) \\ f_{\rightarrow}(E-eV,0) &= \mathcal{T} f_{\rightarrow}(E-eV,0) + \mathcal{R} f_{\rightarrow}(E,L). \end{aligned} \tag{8.54}$$

This is thus, taken together with the possibility of different interface barriers, the most general model that can be treated within the OTBK-approach.

From the matching Eqns. (8.48), (8.49) and (8.54) one can derive recurrency relations for the distribution functions, similar to Eq. (8.52), and from these find the current via Eq. (8.53). Here, we do not derive such a relation. Instead, to make contact with the particle current decompositon of the quantum mechanical current above, we decompose the OTBK-current into particle currents along the same lines. This can be performed in the following way.

First we show that the injected quasiparticles can be treated independently. To do this it is convenient to also use the matching equations for the hole distribution functions at the NIS-interfaces, similarly to Eqns. (8.48)-(8.49), given by straightforward manipulation of the Eqns. (8.48)-(8.49) using that $A(-E) = A(E)$, $B(-E) = B(E)$, $T(-E) = T(E)$ and $f_0(E) = 1 - f_0(-E)$, as

$$1 - f_{\rightarrow}(-E,0) = A(E) f_{\leftarrow}(E,0) + B(E)[1 - f_{\leftarrow}(-E,0)] + T(E) f(E) \tag{8.55}$$

and

$$1 - f_{\leftarrow}(-E,L) = A(E) f_{\rightarrow}(E,L) + B(E)[1 - f_{\rightarrow}(-E,L)] + T(E) f(E). \tag{8.56}$$

We suppress the left/right indices on the scattering probabilities A, B and T for notational convenience. Combining the equations (8.48), (8.49) and (8.54)-(8.56), we can obtain a recurrency equation (not presented) that relates e.g the distribution function $f_{\rightarrow}(E,0)$ with the same distribution at energies $E \pm 2eV$ as well as the equilibrium distribution $f(E)$ at $E, E \pm eV$ and $E + 2eV$, i.e eliminating the hole distribution functions. This recurrency gives in principle an infinite system of linear equations, which can be written on a general matrix form

$$M_1 \hat{f}_{\rightarrow}(E,0) = M_2 \hat{f}(E) \tag{8.57}$$

where the matrices M_1 and M_2 are functions of A, B and T at different energies $E + meV$ and $\mathcal{T}$ and we have introduced infinite vectors $\hat{f}(E) = [...., f(E+eV), f(E), f(E-eV), ...]$. This system of equations is effectively truncated far outside the superconducting gap where all distribution functions $f(E \gg \Delta) = 0$ and $f(E \ll -\Delta) = 1$. The linear matrix equation (8.57) shows that the distribution function $f_{\rightarrow}(E,0)$ can be written as a sum over partial distribution functions related to quasiparticles injected at energies $E + meV$. Noting that $\det(M_1) \neq 0$, i.e that there are no “bound states”, all states are scattering states with non-infinite lifetime, as discussed above. The partial distribution functions are e.g. $f^m_{\rightarrow}(E',0)$ for right-going electrons at energy E' at the left side resulting from injected quasiparticles at energy $E' - meV$. In terms of these partial distribution functions, the total distribution function at energy E' is given by

$$f_{\rightarrow}(E',0) = \sum_m f^m_{\rightarrow}(E',0) \tag{8.58}$$

and similarly for the other total distribution functions.

To make contact with the wavefunction approach above, which expresses wavefunction amplitudes at an energy E_m, i.e. meV above the injection energy, we introduce a different set of partial distribution functions $f_{\uparrow,\downarrow}^{m\pm}$. These distribution functions are labeled in the same way as the wavefunctions in Eq. (8.19)-(8.21), i.e $f_\uparrow^{m+}$ is the distribution function for quasiparticles at energy E_m (resulting from quasiparticles injected at energy E) moving upwards in energy space and away from the NIS-interface in real space. (The corresponding notation for the wavefunctions is shown in Fig. 8.3.) There is thus a one to one correspondence between these partial distribution functions and the distribution functions in Eq. (8.58). Consider e.g. quasiparticles injected from the left side at energy E. At energy $E' = E + meV$, this results in partial distribution functions for left- and right moving electrons, $f_\leftarrow^m(E',0)$ and $f_\rightarrow^m(E',0)$ respectively. In the new notation, these distribution functions are denoted $f_\uparrow^{m+}$ and $f_\downarrow^{m+}$ if m is even or $f_\uparrow^{m-}$ and $f_\downarrow^{m-}$ if m is odd. The partial hole distribution functions $1 - f_\rightarrow^m(-E',0)$ and $1 - f_\rightarrow^m(-E',0)$ are denoted $f_\uparrow^{m-}$ and $f_\downarrow^{m-}$ if m is even or $f_\uparrow^{m+}$ and $f_\downarrow^{m+}$ if m is odd.

The partial distribution functions $f_{\downarrow,\uparrow}^{m\pm}$ are clearly related via the same matching equations as in Eqns. (8.48), (8.49) and (8.54-8.56), with the difference that the source term $T(E)f_0(E)$ is multiplied by a δ_{m0} since the injected quasiparticles are treated independently. In terms of the defined partial distribution functions, the partial current density flowing at energy E_m, defined in analogy with Eq. (8.23), is given by

$$\mathcal{J}_m^\pm = f_\uparrow^{m\pm} - f_\downarrow^{m\pm} \tag{8.59}$$

[Note the correspondence between the partial distribution functions $f_{\downarrow,\uparrow}^{m\pm}$ and the product of the wavefunction coefficients $(c_{\downarrow,\uparrow}^{m\pm})^\dagger c_{\downarrow,\uparrow}^{m\pm}$.] In the same way as in Eq. (8.24) we can thus define particle currents

$$I_m^p f(E) = \mathcal{J}^{m-} - \mathcal{J}^{m+} \tag{8.60}$$

It is thus possible to write the total current from the generalized OTBK-approach in Eq. (8.53) in terms of particle currents as (evaluated at the left side of the junction)

$$\begin{aligned} I &= \frac{1}{eR_0}\int_{-\infty}^{\infty} dE'[f_\rightarrow(E') - f_\leftarrow(E')] = \frac{1}{eR_0} dE' \int_{-\infty}^{\infty} \sum_m [f_\rightarrow^m(E') - f_\leftarrow^m(E')] \\ &= \frac{1}{eR_0}\int_{-\infty}^{\infty} dE \sum_{j,m} [f_{\uparrow,j}^{m\pm} - f_{\downarrow,j}^{m\pm}] = \frac{1}{eR_0}\int_{-\infty}^{\infty} \sum_{j,m\neq 0} m I_m^{p,j} f(E) \end{aligned} \tag{8.61}$$

where j denotes the injection side L/R. This expression is exactly the same as in Eq. (8.26). [One should note that the boundary conditions in Eqs. (8.48) and (8.49) incorporates directly both injected electrons and holes]

We want to express the particle currents in terms of the scattering probabilities of the NIS-interfaces $A(E), B(E)$ and $T(E)$ at different energies and also the scattering probabilities of the normal conductor $\mathcal{T}$ and $\mathcal{R}$. This can be done in terms of the formal solutions of the partial distribution functions, just as for the wavefunction matching above.

Considering first left-injected quasiparticles propagating up in energy space, $E_m > E_0$, we introduce the scattering matrix $\mathcal{S}_{0m}$ for the source free region between injection and escape energy E_0 and E_m, relating the partial distribution functions as

$$\begin{pmatrix} f_\downarrow^{0-} \\ f_\uparrow^{m+} \end{pmatrix} = \mathcal{S}_{m0} \begin{pmatrix} f_\uparrow^{0-}(E) \\ f_\downarrow^{m+}(E) \end{pmatrix}, \tag{8.62}$$

where

$$\mathcal{S}_{m0} = \begin{pmatrix} \mathcal{R}_{0m} & \mathcal{T}_{m0} \\ \mathcal{T}_{0m} & \mathcal{R}_{m0} \end{pmatrix} \tag{8.63}$$

and the reflection probabilities from below energy E_0 and above E_m, $\mathcal{R}_{0-}$ and $\mathcal{R}_{m+}$ respectively, relating the partial distribution functions as

$$\begin{aligned} f_{\uparrow}^{0-}(E) &= \mathcal{R}_{0-} f_{\downarrow}^{0-}(E), \\ f_{\downarrow}^{m+}(E) &= \mathcal{R}_{m+} f_{\uparrow}^{m+}(E). \end{aligned} \tag{8.64}$$

In terms of these quantities, the particle currents are straightforwardly found by performing a matching, similar to Eqs. (8.27)-(8.35), giving

$$\begin{aligned} I_m^{pL} &= \frac{(1-[A_0+B_0])(1-[A_m+B_m])}{(1-B_0\mathcal{R}_{0-})(1-B_m\mathcal{R}_{m+})} \\ &\times \frac{(1+[A_0-B_0]\mathcal{R}_{0-})(1+[A_m-B_m]\mathcal{R}_{m+})\mathcal{T}_{0m}}{(1-\mathcal{R}_{m0}F_m^{+})(1-\mathcal{R}_{0m}F_0^{-})-\mathcal{T}_{0m}\mathcal{T}_{m0}F_m^{+}F_0^{-}}, \end{aligned} \tag{8.65}$$

where

$$F_l^{\pm} = (B_l + [A_l^2 - B_l^2]\mathcal{R}_{l\pm})/(1 - B_l\mathcal{R}_{l\pm}). \tag{8.66}$$

The reflection and transmission probabilities $\mathcal{R}_{lm}$ and $\mathcal{T}_{lm}$ between the energies E_m and E_l are given by the recursive relations for $m > l$ (+) and for $m < l$ (-)

$$\begin{aligned} \mathcal{R}_{ml} &= \mathcal{R} + \frac{\mathcal{T}^2(B_{m\pm1}+[A_{m\pm1}^2-B_{m\pm1}^2]\mathcal{R}_{m\pm1,l})}{1-\mathcal{R}B_{m\pm1}-(B_{m\pm1}+\mathcal{R}[A_{m\pm1}^2-B_{m\pm1}^2])\mathcal{R}_{m\pm1,l}} \\ \mathcal{T}_{ml} &= \frac{\mathcal{T}A_{m\pm1}\mathcal{T}_{m\pm1,l}}{1-\mathcal{R}B_{m\pm1}-(B_{m\pm1}+\mathcal{R}[A_{m\pm1}^2-B_{m\pm1}^2])\mathcal{R}_{m\pm1,l}} \end{aligned} \tag{8.67}$$

with the boundary conditions $\mathcal{R}_{l,l\pm1} = \mathcal{R}$ and $\mathcal{T}_{l,l\pm1} = \mathcal{T}$ and from the infinities $\mathcal{R}_{l,\pm} = \mathcal{R}_{l,\pm\infty}$. Equations (8.65)-(8.67) completely determine the particle currents and from this the total current via Eq. (8.61). The particle currents from right injected quasiparticles are given by the same Eq. (8.65), just noting that odd (even) energy index m corresponds to the left (right) side of the junction. Moreover, since the cancellation theorem discussed above clearly holds for the generalized OTBK-approach, we only need particle currents for positive m. The total current from the generalized OTBK-approach is thus given by Eq. (8.43), with the particle current density given by Eq. (8.65).

It is sometimes convenient to express the scattering matrix elements in $\mathcal{S}_{m0}$ in terms of the corresponding transfer matrix

$$\mathcal{M}_{m0} = \frac{1}{\mathcal{T}_{m0}} \begin{pmatrix} \mathcal{T}_{m0}\mathcal{T}_{0m} - \mathcal{R}_{0m}\mathcal{R}_{m0} & \mathcal{R}_{m0} \\ -\mathcal{R}_{0m} & 1 \end{pmatrix} \tag{8.68}$$

since this transfer matrix is given by the products of transfer matrices $\mathcal{U}_m$ and $\mathcal{T}_m$ of the NIS-interfaces and the normal conductor respectively, similar to Eq. (8.30) as $M_{ml} = \mathcal{T}_m \mathcal{U}_{m-1} \ldots \mathcal{T}_l$. The individual transfer-matrices are given by, at the NIS-interfaces,

$$\mathcal{U}_n = \frac{1}{A_m} \begin{pmatrix} A_m^2 - B_m^2 & B_m \\ -B_m & 1 \end{pmatrix} \tag{8.69}$$

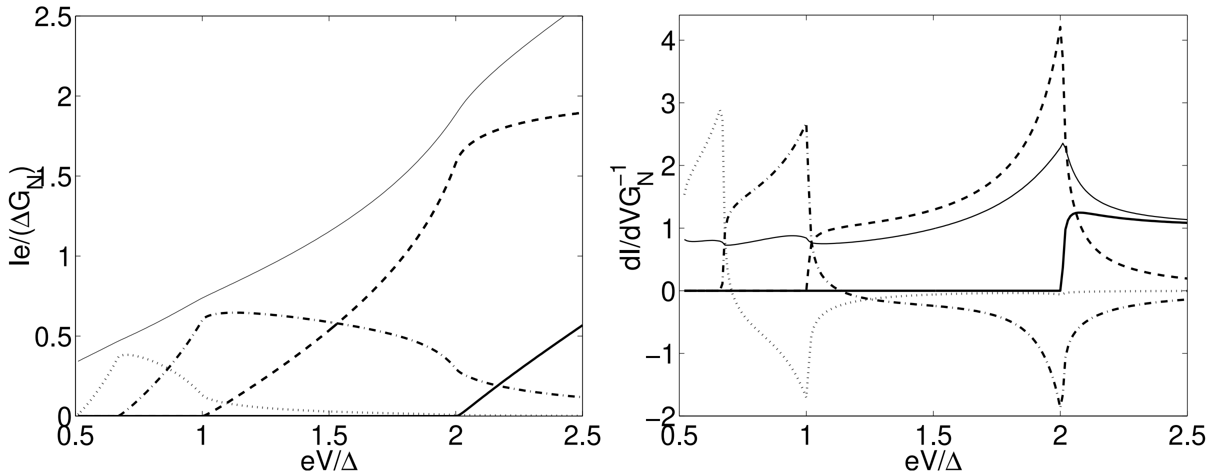

Figure 8.7: Left: The total current and the particle currents as a function of voltage. Right: The total differential conductance and the differential conductance for each individual particle current as a function of voltage. In both plots the total current is shown thin solid and the particle currents I_1 (solid), I_2 (dashed), I_3 (dash-dotted) and I_4 (dotted) for a junction with $\Gamma_L = \Gamma_R = 0.5$ and $\mathcal{T} = 1$

and across the normal conductor [using $\mathcal{R} + \mathcal{T} = 1$]

$$\mathcal{T}_m = \frac{1}{\mathcal{T}} \begin{pmatrix} \mathcal{T} - \mathcal{R} & \mathcal{R} \\ -\mathcal{R} & 1 \end{pmatrix}, \tag{8.70}$$

where we note that $\mathcal{T}_m$ is independent on energy E_m. The normal state conductance is directly found from the single particle current density I_1^p at injection and escape energies far outside the gap, $E_0 \ll -\Delta$ and $E_1 \gg \Delta$. At these energies $A_0 = A_1 = 0$ and for left injected quasiparticles (right injected gives the same final conductance) $B_0 = 1 - \Gamma_L$ and $B_1 = 1 - \Gamma_R$, which gives from Eq. (8.65)

$$G_N = \frac{1}{R_0} I_1^p = \frac{1}{R_0} \frac{\Gamma_L \Gamma_R \mathcal{T}}{\mathcal{T}(\Gamma_L + \Gamma_R) - \Gamma_L \Gamma_R (2\mathcal{T} - 1)} \tag{8.71}$$

where R_0 is the normal state resistance of the junction without barriers, i.e the resistance of a classical point contact. For the original OTBK-model, with $\mathcal{T} = 1$ we recover[113] $G_N = \Gamma_L \Gamma_R / (\Gamma_L + \Gamma_R - \Gamma_L \Gamma_R)$. It is interesting to note that the normal state conductance of the OTBK-model is not equal to the classical conductance of two tunnel barriers in series, $\Gamma_L \Gamma_R / (\Gamma_L + \Gamma_R)$, i.e only in the tunnel limit $\Gamma_L, \Gamma_R \ll 1$ the classical result is recovered. The current and the differential conductance of the original OTBK-model, shown in Fig. 8.7, is for comparison plotted separated into the different particle currents in Fig. 8.7.

There have been several studies that have focused on the effect of different interface barrier transparency[113] Γ_L and Γ_R. Here we briefly present some results for different transparencies of the middle barrier. In Fig. 8.8 the current and differential conductance are shown for the original OTBK-case, $\mathcal{T} = 1$ and $\mathcal{T} = 0.1$, with barrier transparency $\Gamma = \Gamma_L = \Gamma_R = 1.0$ and 0.1

One notes that the normal scattering from the barriers at the NS-interfaces provides strong SGS, while scattering from the middle barrier only produces very weak SGS. In fact, for no normal scattering at the NS-interfaces, $\Gamma_L = \Gamma_R = 1$ and very strong scattering at the middle barrier $T \ll 1$, the IV-curve just approaches Ohms law.

Finally, one should note that this approach is also very convenient for calculating the excess or deficit current at asymptotically large voltage $I_{exc} = \int dE (I_1^{pL} + I_1^{pR} + 2[I_2^{pL} + I_2^{pR}]) - I_N$,

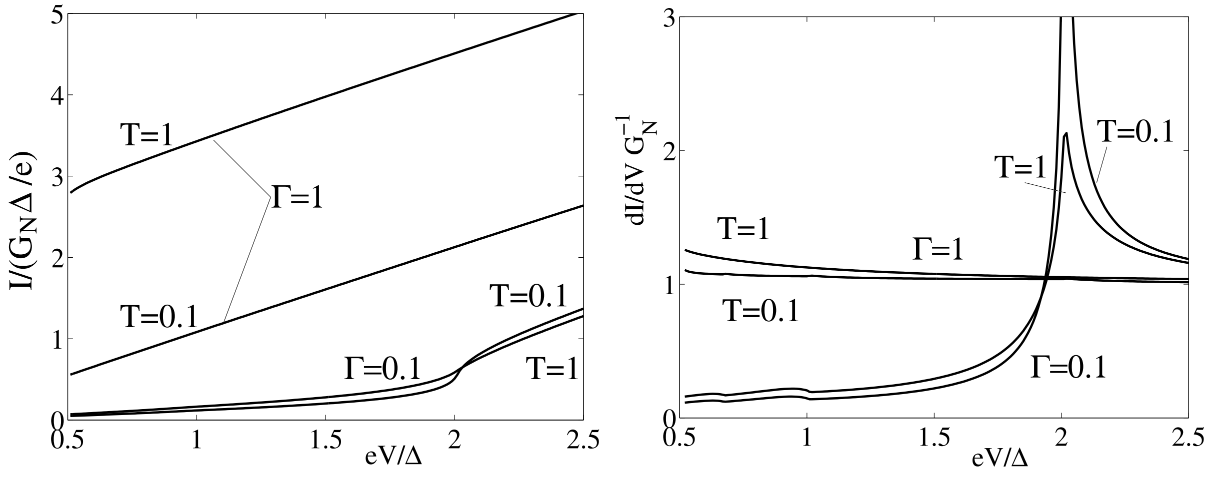

Figure 8.8: Left: The OTBK-current as a function of voltage. Right: The differential conductance as a function of voltage. The parameters are $\mathcal{T} = 1$ and $\mathcal{T} = 0.1$, with barrier transparency $\Gamma = \Gamma_L = \Gamma_R = 1.0$ and 0.1.

where the normal state current is $I_N = G_N V$. This current as a function of middle barrier transparency is plotted for different $\Gamma = \Gamma_L = \Gamma_R$ in Fig. 8.8. One notes that for no barriers at

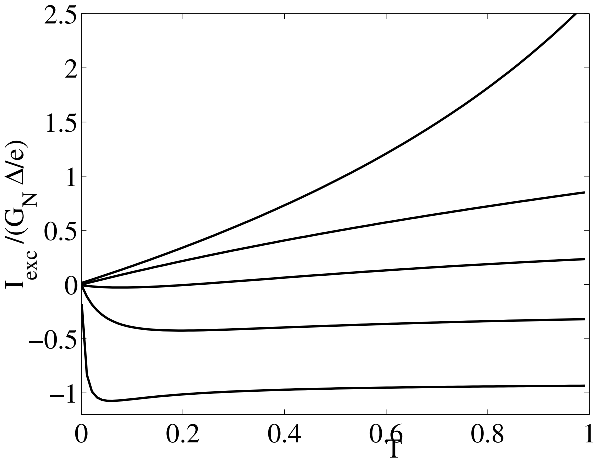

Figure 8.9: The excess current as a function of barrier transparency $\mathcal{T}$ of the middle barrier at asymptotically large voltage, for different NS-barrier transparencies $\Gamma = 1.0, 0.7, 0.5, 0.3$ and 0.1. Highest transparency corresponds to largest excess current.

the NS-interfaces, the asymptotic current is always an excess current, approaching the normal state current in the tunnel limit $\mathcal{T} \ll 1$. For moderate normal scattering at the NS-interfaces, $\Gamma = 0.5$, the current changes non-monotonically from deficit to excess as a function $\mathcal{T}$, while for NS-barriers in the low transparency limit $\Gamma = 0.1$ there is a deficit current for all $\mathcal{T}$. The values of the asymptotical current at $\mathcal{T}$ coincides with the OTBK-result, i.e goes from an excess current of $8G_N\Delta/(3e)$ to a deficit current $-4G_N\Delta/(3e)$ when Γ goes from 1 to $\ll 1$. We have not studied the analytical expression for the excess current in the general case; an expression for the case $\Gamma_G = \Gamma_R = \Gamma$ and $\mathcal{T} = 1/2$ is found in the subsequent chapter.

CHAPTER 9

Current transport in voltage biased chaotic Josephson junctions

The full quantum theory[21,26,59,78] for Multiple Andreev Reflection in voltage biased single mode junctions has been extremely successful in explaining the experiments[160,192,201] in atomic point contacts, as was discussed in the preceding chapter. Moreover, it was recently found[180] that the full quantum theory could be used to explain the current in disordered tunnel junctions. In general, in any mesoscopic junction in the short dwell-time regime, $E_{Th} \gg \Delta$, the scattering amplitudes are independent of energy on the scale of Δ. The current is thus, as was shown by Bardas and Averin,[31] a linear statistic of transmission eigenvalues, and can be calculated by integrating over transmission eigenvalues.

In mesoscopic junctions outside the short dwell-time regime, $E_{Th} \leq \Delta$, the current is no longer a linear statistic on transmission eigenvalues and one has to take into account the energy dependence of the scattering amplitudes. The full quantum theory for a single mode junction has been extended to resonant junctions[127] and recently to long junctions with a single impurity.[123] No results are however available for multi-mode junctions. Very recently, the case of a long, $E_{Th} \gg \Delta$, diffusive wire SNS- junction with no proximity coupling between the superconductors, and consequently no ac-current, was studied by Bezuglyi et al.[52] The found that the current showed the characteristic sub-harmonic gap structures at $eV = 2\Delta/m$, modified by the local proximity effect at the NS-interfaces.

It is interesting to relate this to the conductance in corresponding long diffusive NS-junctions which has been studied extensively (see e.g. Ref. 150). The conductance shows an anomaly at finite voltages $eV \approx E_{Th}$ for a perfect NS-interface. For a non-ideal interface, this anomaly is shifted towards lower voltages. At temperatures $kT \gg E_{Th}$ or in a magnetic field large enough to break time reversal symmetry, the conductance anomaly is suppressed. A similar behavior has been predicted in chaotic N-dot-S junctions,[75] which suggests that this is generic for mesoscopic scatterers with sufficiently complex scattering. This raises the question if there is any analogue to this bias anomaly in voltage biased SNS-junctions.

These observations taken together makes it interesting to systematically study the fully coherent current, using the general results derived in the previous chapter, in the transition from the short to long dwell-time regime, i.e from $E_{Th} \gg \Delta$ to $E_{Th} \ll \Delta$. Moreover, since the case with broken time reversal symmetry in NS-systems is particularly simple, this raises the question if there is any simple analogue in SNS-systems. It is also of interest to get a clearer picture to what extent the widely used OTBK-model can be rigorously justified in mesoscopic junctions.

In this chapter our aim is to clarify these issues. We study the current in a voltage biased chaotic Josephson junction, for which the distribution for the scattering matrix at arbitrary energies and magnetic fields is known, as was discussed in Chapter 6. We first discuss the short dwell time regime and calculate current voltage characteristics and the excess current at asymptotically large voltage. Thereafter, we turn to the opposite, long dwell-time regime and study the current as a function of magnetic field, from conserved to completely broken time reversal symmetry in the dot. Finally, we show that the current for completely broken TRS in the dot coincides with the current of the generalized OTBK-model with average transparency $\mathcal{T} = 1/2$ of the dot.

9.1 Short dwell-time regime

In the short dwell-time regime $\tau_{dwell} \ll \hbar/\Delta$, or equivalently $E_{th} \gg \Delta$, the scattering matrix is independent of energy on the scale Δ, and the current can be written as a sum of single mode currents.[31] This can be seen formally by decomposing the scattering matrix of the dot according to the polar decomposition in Eq. (6.24) and inserting the decomposed scattering amplitudes r, r', t, t', same for each energy, into the particle current expression in Eqs. (8.39) and (8.40). The unitary matrices U and V then drop out of all expressions which then become diagonal. Each of the particle currents are thus linear statistics of the transmission eigenvalues D_n and can be evaluated via Eq. (6.28), with the transmission eigenvalue distribution given in Eq. (6.32).

This short dwell time regime has been studied for diffusive junctions[31] and also for disordered tunnel junctions,[180] and the study for a chaotic junctions technically just differs because the distribution of transmission eigenvalues is different. One may note the interesting fact that the distribution of transmission eigenvalues for a chaotic dot connected to leads with a large number of modes $N \gg 1$ and with strong tunnel barriers in the leads ($\Gamma \ll 1$) is equivalent to the distribution for a ballistic double tunnel barrier junction[169] as well as a disordered tunnel junction.[202] The results for this limit, presented below, are thus the same as presented in Ref. 180.

We study the current in the limits of a single-mode junction without barriers in the leads, $N = 1$ and $\Gamma = 1$, and a junction with a large number of modes, $N \gg 1$, with arbitrary transparency Γ in the leads.

9.1.1 Single mode junction, $N = 1$

In the limit of a single transport mode the distribution of the transmission eigenvalues is given by $\rho(D) = 1/(2\sqrt{D})$ [given in Eq. (6.19)], assuming no barriers in the contacts connecting the dot and the superconductors ($\Gamma = 1$). The numerical result for the current and the differential conductance is presented in Fig. 9.1. Note that the normal conductance is $G_N = (2e^2/h)/3$. One clearly sees the sub-gap structure, both in the current voltage characteristics and the differential conductance. Since the single mode current at asymptotically large voltage $eV \gg \Delta$ is an excess current for all transparencies, see Eq. (8.46), we obviously get an ensemble averaged excess current $\langle I_{exc} \rangle$. It is calculated by integrating the expression in Eq. (8.46) over the transmission eigenvalue distribution $\rho(D)$, giving

$$\langle I_{exc} \rangle = \frac{e\Delta}{8\pi\hbar}(2[\psi'(1/8) + \psi'(3/8) + \psi'(5/8) + \psi'(7/8)] - 3 - 142c_c) \approx 0.13\frac{e\Delta}{\hbar}, \qquad (9.1)$$

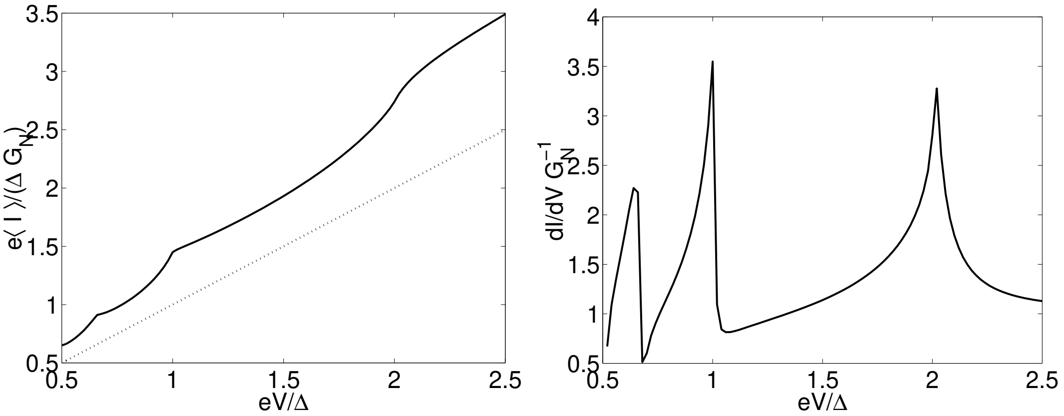

Figure 9.1: Left panel: The current of a single mode chaotic junction as a function of voltage (solid). For comparison, the normal state current $I_N = G_N V$ is shown (dotted). Right panel: The corresponding differential conductance.

where $\psi'(x)$ is the first derivative of the digamma function and $c_c \approx 0.916$ is the Catalan number. This is in good agreement with the numerical result.

9.1.2 Junction with large number of modes, $N \gg 1$

In the limit of large number of modes we can use the transmission eigenvalue distribution in Eq. (6.32) for arbitrary transparency. The numerical result for the current and the differential conductance is plotted in Fig. 9.2 for three different transparencies, $\Gamma = 1, 0.5$ and 0.1. The current voltage characteristics show SGS at applied voltage $eV = 2\Delta/m$ for all barrier transparencies, however, the features become stronger for smaller barrier transparencies. This can be understood by considering the distribution of transmission eigenvalues in Eq. (6.6): it is the small transmission eigenvalues that gives rise to the strong SGS and the bimodal distribution of the transmission eigenvalues (see Fig. 6.7) has a larger weight for eigenvalues close to zero for smaller barrier transparency.

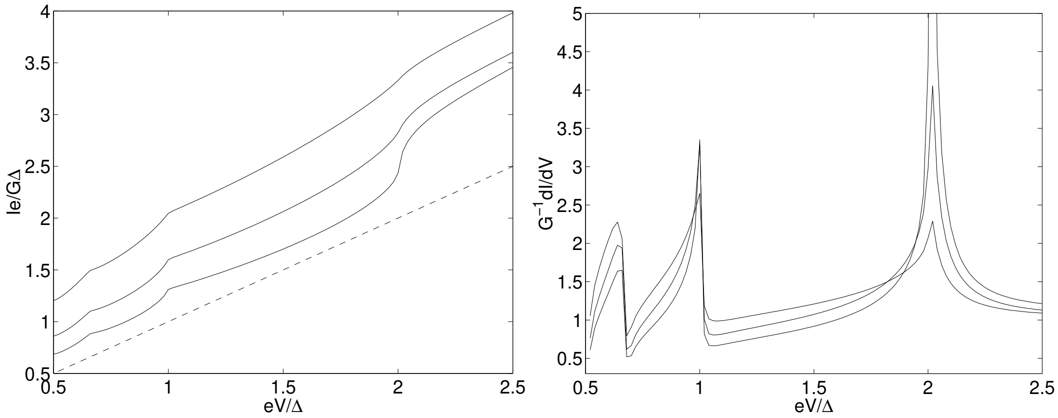

Figure 9.2: Left panel: The current voltage characteristics for barrier transparencies $\Gamma = 1, 0.5, 0.1$. For comparison, the normal state current $I_N = G_N V$ is shown (dotted). Right panel: The corresponding differential conductance for barrier transparencies.

It is clear, just as for the single mode junction, that the current at asymptotically large voltages $eV \gg \Delta$ is an excess current for all barrier transparencies. The excess current normalized with the normal conductance $G_N = 2e^2/h(N\Gamma/2)$ is weakly dependent on the barrier transparency Γ, again a consequence of the bimodal form of the transmission eigenvalue distribution function. In the two limiting cases, the ballistic limit $\Gamma = 1$ and the tunnel limit $\Gamma \ll 1$, the current can be found analytically,

$$\langle I_{exc}\rangle = \frac{G_N\Delta}{e}\begin{cases} \frac{16}{3}+\pi\left(\frac{9}{2}-4\sqrt{2}\right), & \Gamma = 1 \\ \frac{\pi}{4}(7-4\sqrt{2}), & \Gamma \ll 1 \end{cases} \tag{9.2}$$

It is interesting to compare the result in Eq. (9.2) with the result for a short, diffusive junction,[31] without NS-interface barriers, where the excess current is found to be $G_N\Delta/e(\pi^2/4-1)$. This corresponds to a chaotic junction with NS-barrier transparency of roughly one half, an effect of that the transmission eigenvalue distribution for a disordered wire compared to a chaotic cavity has a smaller weight for eigenvalues close to unity.

9.2 Long dwell-time regime

In the long dwell-time regime $\tau_{dwell} \gg \hbar/\Delta$, one has to take into account the energy dependence of the scattering matrix, calculating S directly from the Hamiltonian [see (2.32)]. It is a very difficult problem, if at all solvable, to analytically perform the average of the current density expression in Eq. (8.39) over the Hamiltonian ensemble in Eq. (6.1), for arbitrary applied voltage and magnetic field (already the expressions for the N-dot-S conductance in Ref. 75 are very cumbersome).

The complexity of the problem is a consequence of the coherent transport through the dot. First, electrons traversing the junction at different energies are correlated over an energy of order E_{Th} (as discussed in Chapter 5). Second, electrons and holes at energies of the order of E_{Th} from Fermi energy are correlated due to Andreev reflection, i.e an induced proximity effect in the dot. In principle, since we study applied voltages of order of the superconducting gap, the long dwell time limit also implies $eV \gg E_{Th}$, for which the correlation between electrons at different energies can be neglected. However, even in this limit, the full problem is very complicated and we instead study the current numerically, by generating a large number of random scattering matrices via the Hamiltonians, distributed according to the Pandey-Metha distribution in Eq. (6.5), to take into account magnetic field in the dot. From the scattering matrices at different energies and magnetic fields, the total current is then given from Eq. (8.26). It is however possible to simplify the numerical calculations considerably by noting the following symmetries.

9.2.1 Current density symmetries

As discussed in connection to the cancellation symmetries in the preceding chapter, the m-particle currents flowing upwards and downwards in energy space, between the same energies E_0 and E_m, are related by the transformation of the scattering matrix $S(E) \to S(E)^T$, i.e $I^{pL}_m(E,S) = I^{pL}_{-m}(E+meV,S^T)$. As discussed, for conserved TRS in the dot, the scattering matrix is symmetric $S = S^T$ and the equality $I^p_{-m}(E+meV) = I^p_m(E)$ holds for every realization, i.e. every scattering matrix. In the case with broken symmetry, this is no longer the case, and the currents flowing up and down in energy space between the same energies are in principle different.

However, as we now show, the equality holds for the ensemble averaged particle currents, $\langle I^{pL}_m(E,S)\rangle = \langle I^{pL}_{-m}(E+meV,S^T)\rangle$. From the expression for the scattering matrix in terms of the Hamiltonian, Eq. (2.32), it is clear that the transformation of the scattering matrix $S(E) \to S(E)^T$ is obtained by transforming the Hamiltonian in the same way, $H \to H^T$. Note that the Hamiltonian $H = H_0 + i\gamma H_1$, where H_0 and H_1 are real symmetric and antisymmetric Hamiltonians respectively, both distributed according to the same Gaussian Orthogonal Ensemble. The distribution $P(H)dH$ of the Hamiltonian in Eq. (6.6), is invariant under this transformation, [since it only depends on $\mathrm{tr}(H_0 H_0^T + H_1 H_1^T)$].

$$\begin{aligned}\langle I^p_{-m}(E+meV)\rangle &= \int dH I^p_{-m}(E+meV,H)P(H) = \int dH I^p_m(E,H^T)P(E,H)\\ &= \int dH^T I^p_m(H^T)P(H^T) = \langle I^p_m(E)\rangle,\end{aligned} \tag{9.3}$$

which shows the desired property. Due to this symmetry, we can use the cancellation between particle currents and work with the total current expression $\langle I\rangle = \langle I_L\rangle + \langle I_R\rangle$, similar to Eq. (8.44), for simplicity presented for $kT \ll \Delta$,

$$\langle I^{L(R)}\rangle = \frac{2e}{h}\sum_{m>0} m\theta(meV-2\Delta)\int_{\Delta-meV}^{-\Delta} dE\langle I_m^{pL(R)}\rangle. \tag{9.4}$$

This means that on average, only real excitations through the gap contribute to the current.

There is an additional symmetry in the case when the barriers on the left and right sides are equal, $\Gamma_L = \Gamma_R$. In this case, the particle current density $I_m^{pL}(E)$ for quasiparticles injected from the left is related to the particle current density for quasiparticles injected from the right $I_m^{pR}(E)$ by the transformation of the scattering matrix $S(E) \to \sigma_x S^*(-E)\sigma_x$. From the expression for the scattering matrix in terms of the Hamiltonian, Eq. (2.32), it is clear that the first transformation $S(E) \to S^*(-E)$ is obtained by transforming the Hamiltonian as $H \to -H^\dagger = -H$. The second transformation, $S^*(-E) \to \sigma_x S^*(-E)\sigma_x$ is obtained by first noting the matrix relation

$$\sigma_x W^\dagger = W^\dagger Q,\ Q = \begin{pmatrix}\sigma_x & 0\\ 0 & 1\end{pmatrix}, \tag{9.5}$$

where Q has the dimension $M \times M$ (Note that Q is unitary, $Q^2 = QQ^\dagger = 1$). The transformed scattering matrix then becomes

$$\begin{aligned}\sigma_x S\sigma_x &= 1 - i2\pi\sigma_x W^\dagger(E-H+i\pi WW^\dagger)^{-1}W\sigma_x\\ &= 1 - i2\pi W^\dagger Q(E-H+i\pi WW^\dagger)^{-1}QW\\ &= 1 - i2\pi W^\dagger(E-QHQ+i\pi WW^\dagger)^{-1}W.\end{aligned} \tag{9.6}$$

The corresponding transformation for the Hamiltonian is thus the transformation $H \to -QHQ^\dagger$ under which the distribution in Eq. (6.6) is invariant. We can thus write the average of the right injected particle currents

$$\begin{aligned}\langle I_m^{pR}(E)\rangle &= \int dH I_m^{pR}(E,H)P(H) = \int dH I_m^{pL}(E,-QHQ)P(H)\\ &= \int -dQHQ I_m^{pL}(E,-QHQ)P(-QHQ) = \langle I_m^{pL}(E)\rangle,\end{aligned} \tag{9.7}$$

which is the desired result.

9.2.2 Cross-over from conserved to broken TRS

Armed with these simplifying symmetries, we turn to the numerical study of the current. We only treat the case $N \gg 1$ and truncate the particle currents by putting the Andreev reflection at E_{m+1} and E_{-1} in the m-particle current to zero. This means that processes made up by quasiparticles Andreev reflecting at e.g energy E_{m+1}, normal reflecting from infinity and then again Andreev reflecting, i.e processes which have at maximum a probability $|\tilde{a}|^4$, are neglected. This is a good approximation for the rather high voltages $eV > 0.5\Delta$ considered in the numerics, since the neglected terms have at maximum the magnitude $|\tilde{a}(1.5\Delta)|^4 \approx 0.02$ (for ideal NS-interfaces, the approximation becomes better for barriers at the NS-interfaces).

In Fig. (9.3), the current for three different barrier transparencies, $\Gamma_L = \Gamma_R = 1.0, 0.6$ and 0.2, ranging from perfect to low transparency, are shown for the two limits $B = 0$ and $B \gg B_c$, i.e conserved and completely broken TRS. One can see that the current for conserved TRS is always larger than the current for broken TRS. Keeping the result for the short dwell time regime in mind (see Fig. 9.2), we can draw the conclusion that for large transparency of the NS-interfaces, the effect on the current of breaking TRS is not very strong. The curves with $B = 0$ and $B \gg B_c$ lie almost on top of each other and they are also very close to the current in the short dwell time regime. When the transparency of the NS-interfaces is decreased, the effect of breaking TRS becomes more strong, and for $\Gamma = 0.2$, there is a large difference between the I-V curves for conserved and broken TRS.

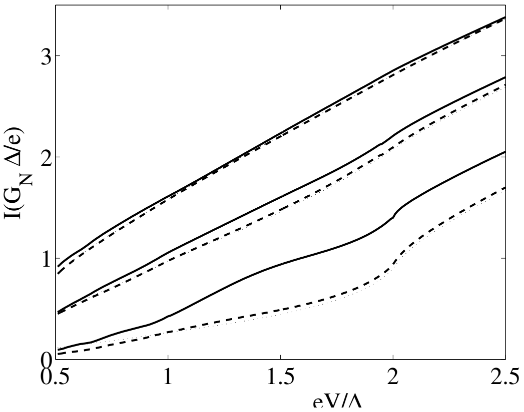

Figure 9.3: The current as a function of voltage for magnetic field $B = 0$ and B B_c and different barrier transparencies $\Gamma = 1.0, 0.6$ and 0.2. The Thouless energy $E_{Th} = 0.4\Delta$, the number of transverse channels $N = 10$ and 1000 Hamiltonians of size $M = 200$ have been generated for each curve. The corresponding OTBK-result is shown as a dashed line.

It is found from further numerical studies [not presented] that the current for broken TRS takes on a universal value, independent on E_{Th} and magnetic field. As is showed in detail below, the current in this universal limit coincides to leading order in $\Gamma_L N, \Gamma_R N$ with the current of the general OTBK-approach, discussed in the previous chapter, with transparency $\mathcal{T} = (\mathcal{R} =)1/2$, which is the average transparency of the dot without barriers at the NS-interfaces. The OTBK-result is shown as a reference in Fig. 9.3, which shows that the agreement between the analytical result an the numerics is good, the deviations are due to the limited dimension of N, i.e quantum corrections. In Fig. 9.4 the individual particle currents are plotted for high and low transparency. It is clear that the reason for the strong suppression of the current with broken time reversal symmetry is that the two particle current, I_2, i.e. the current from processes with one Andreev reflection, are stronly suppressed. These processes are essentially the same that contribute to the

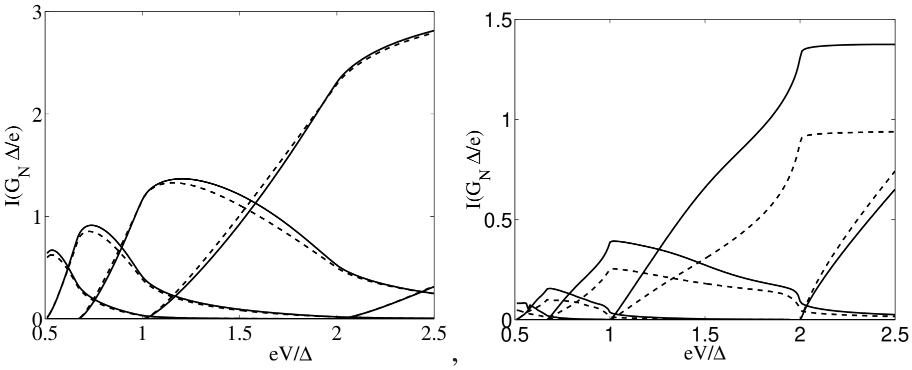

Figure 9.4: The different particle currents I_1 to I_5 as a function of voltage for magnetic field $B = 0$ (dashed) and $B \quad B \quad _c$ (solid), for barrier transparency $\Gamma = 1$ (left panel) and $\Gamma = 0.2$ (right panel). The parameters are the same as in Fig. 9.3.

current in the N-dot-S-case, which explains the suppression, since it is known[75] that breaking time reversal symmetry in the dot reduces the conductance to the series conductance of a normal point contact and a NIS-contact. Since the transparency of the NIS-contact is proportional to Γ^2 for energies $|E| \ll \Delta$, and thus much smaller than the normal point contact conductance $\propto \Gamma$, it determining the series conductance, giving a strong suppression of the total conductance.

To study the crossover from conserved to broken TRS, i.e from coherent to incoherent MAR, it is thus most interesting to focus on the low transparency limit, and to study the differential conductance. Guided by the knowledge[75] that the N-dot-S conductance shows most pronounced features for different barrier transparencies $\Gamma_L \neq \Gamma_R$, because small transparency of the contact connected to the normal reservoir resembles tunnel spectroscopy of the induced Thuless gap in the dot, we study the conductance for non-equal barrier transparencies $\Gamma_L = 0.1$ and $\Gamma_R = 0.3$, showed in Fig. 9.5. It is clear from Fig. 9.5 that the conductance shows anomalies around voltages $eV \approx \Delta \pm E_{Th}$. At low voltages $eV < 2\Delta/3$, where the current is carried by particle currents of order four and higher, the numerical result is less clear. For the interpretation of the result it is fruitful first to study the result at voltages $eV > \Delta$ in larger detail, shown in Fig. 9.6. For comparison, the corresponding differential conductance for the N-dot-S junction is also plotted. For these parameters, the conductance anomaly is clearly pronounced as a peak

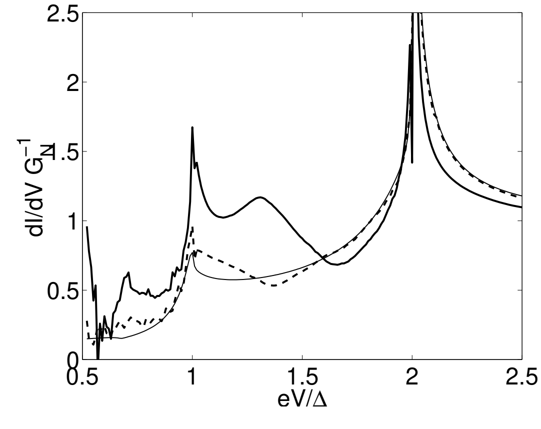

Figure 9.5: The differential conductance as a function of voltage for $\Gamma_L = 0.1, \Gamma_R = 0.3$ and $E_{Th} = 0.4\Delta$, for different magnetic fields $B = 0$ (solid), 0.8 and $B \quad B \quad _c$ (dashed). The OTBK-result is shown as a reference (thin solid). The number of transverse modes $N = 15$ and 1000 Hamiltonians of dimension $M = 300$ have been generated

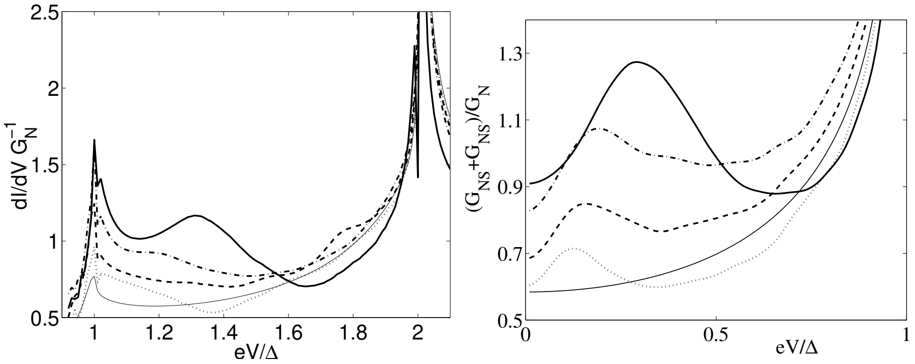

Figure 9.6: Left: The differential conductance as a function of voltage for $\Gamma_L = 0.1, \Gamma_R = 0.3$ and $E_{Th} = 0.4\Delta$, for different magnetic fields $B/B_c = 0$ (solid), 0.8 (dash-dotted), 1.6 (dashed) and $B \quad B_c$ (dotted). The OTBK-result is shown as a reference (thin solid). Right: The conductance $G^L_{NS} + G^R_{NS}$ of the corresponding N-dot-S system, as a function of voltage.

at $eV \approx \Delta + E_{Th}$ (The position of the peak is more exactly determined by the inverse escape time through the contact with largest transparency, i.e 0.3Δ in Fig. 9.6). By a comparison to the corresponding N-dot-S conductance, it is clear that this peak has the same origin as the peak in the N-dot-S case, i.e the enhanced amplitude for quasiparticles Andreev reflecting once, at energies E_{Th} away from Fermi energy. These are precisely the processes building up the two particle current, as discussed above. Since these processes have an onset at $eV = \Delta$ for the S-dot-S junction, the conductance features are shifted upwards Δ in energy compared to the N-dot-S case. The S-dot-S conductance peak is successively suppressed by applied magnetic field, and the conductance reaches a value independent on magnetic field at magnetic fields B_c strong enough to break TRS. The N-dot-S conductance shows exactly the same behavior.

There is however one important difference between the N-dot-S conductance and the S-dot-S conductance at $eV > \Delta$. The S-dot-S conductance peak is insensitive to temperatures $kT \ll \Delta$, because the distribution of the injected quasiparticles from the superconductors is unaffected by temperatures well below the superconducting gap, while already a temperature $kT \gg E_{Th}$ suppresses the N-dot-S peak. One should note that, just as for the N-dot-S conductance,[75] for similar barriers $\Gamma_L = \Gamma_R$, the peak is less pronounced and that for high transparency $\Gamma_L, \Gamma_R \approx 1$, the peak turns into dip.

With this comparison in mind, we return to the result for the conductance at voltages below Δ presented in Fig. 9.5 and note that for these voltages there is no possibility to make an analogue to the N-dot-S case, since the current is carried by quasiparticles that Andreev reflect two times or more in the junction. One can however expect that for a Thouless energy smaller than the distance between the sub-harmonic gap structures, the processes where quasiparticles Andreev reflect at energies E_{Th} away from Fermi energy have an enhanced amplitude. This is supported by the observation of the conductance peak at $eV \approx \Delta - E_{Th}$ in Fig. 9.5, which is found to result from the three particle current.

Along the same line, it is clear the coherent contribution to the differential conductance is manifested as additional subgap features at $eV \approx 2\Delta/(2m) \pm E_{Th}$, i.e at E_{Th} away from even SGS. The features above the SGS at $2m = 2, 4, 6, .$ are related to even particle currents I^p_{2m} while the features below are related are related to the odd particle currents I^p_{2m+1}. This can be understood from that even particle currents at the onset voltage $eV = 2\Delta/(2m)$, is carried by quasiparticles that Andreev reflect exactly at the Fermi energy, which gives that for voltages $\approx E_{Th}$ above onset, the particle current is carried by quasiparticles that all reflect within E_{Th} from

Fermi energy, giving a conductance anomaly at $eV \approx 2\Delta/(2m) + E_{Th}$. Odd particle currents, on the other hand, have a contribution from quasiparticles that are Andreev reflected within E_{Th} from the Fermi energy, first for voltages $eV \approx 2\Delta/(2m) - E_{Th}$.

There is no conductance feature around $eV = 2\Delta$, since the current at this voltage is carried by quasiparicles that Andreev reflect far away from Fermi energy or do not Andreev reflect at all. The reason for the slight modification of the conductance peak at $eV = 2\Delta$ in Fig. 9.6 is that amplitude of the conductance anomaly at $eV \approx \Delta + E_{Th}$ decays slowly with energy, and thus slightly affects the transport at $eV \sim 2\Delta$. It should be noted that it was recently predicted that the differential conductance of a long diffusive SNS junction[52] would show a qualitatively different behavior for odd and even SGS positions, however, no peaks at E_{Th} away from the even SGS were predicted.

Moreover, a similar differential conductance behavior was recently observed in planar diffusive junctions.[145] Although the system studied is different from a chaotic Josephson junction, the qualitative features are the same, i.e conductance peaks on top of the SGS at voltages $eV = \Delta \pm E_{Th}$, clearly demonstrated to be due to coherent effects, and no conductance peaks around the SGS at $eV = 2\Delta$.

For completely broken TRS, where the generalized OTBK-approach with $\mathcal{R} = \mathcal{T} = 1/2$ gives the current, it is interesting to calculate the current at asymptotically large voltage. For similar barrier transparencies $\Gamma_L = \Gamma_R = \Gamma$, one finds

$$\begin{aligned} \langle I_{exc} \rangle &= \frac{G_N \Delta}{e} \left[\frac{2-\Gamma}{\Gamma} \left(\frac{2+\Gamma}{\sqrt{2\Gamma}} \text{atan} \left(\sqrt{\frac{\Gamma}{2}} \right) - 1 \right) - 2 \right. \\ &+ \left. \frac{4\Gamma}{\sqrt{(1-\Gamma)(4-2\Gamma+\Gamma^2)}} \text{atanh} \left(2 \sqrt{\frac{1-\Gamma}{4-2\Gamma+\Gamma^2}} \right) \right]. \end{aligned} \tag{9.8}$$

The current changes from an excess current, $\langle I_{exc} \rangle = G_N \Delta/e(3/\sqrt{2}\text{atan}(1/\sqrt{2}) - 1/3$ for $\Gamma = 1$ to a deficit current $\langle I_{exc} \rangle = -4G_N\Delta/(3e)$ for $\Gamma \ll 1$, similar as found for the original OTBK-model.[92]

Finally, one can ask whether the results obtained are qualitatively valid for other junctions than chaotic. It is possible within our approach to calculate the current in a long diffusive wire junction with TRS broken in the wire, which gives, just as for the chaotic junction, a current equivalent to the OTBK-current in a SININIS junction, but now with a transmission probability l/L for the wire, with l the mean free path and L the length of the junction. It is however not clear how to treat the general problem with energy and magnetic field dependence of the scattering matrix within the outlined scattering approach.

9.2.3 Completely broken TRS, the OTBK-limit

As pointed out above, at completely broken TRS, the current reaches a universal limit, independent of Thouless energy and magnetic field, only dependent on the NIS-interface barrier transparency. It turns out that this universal limit corresponds exactly to the generalized OTBK-approach presented in the previous chapter, to leading order in $\Gamma_L N, \Gamma_R N$. This is shown below in, in the following way. First, to make contact to the OTBK-approach we introduce wavefunction coefficients $\hat{d}_m^{\uparrow,\downarrow,\pm}$ on the dot-side of the NIS-barrier. Then, a number of correlation functions between the ensemble averaged products of the wavefunction coefficients, e.g. $\langle \text{tr}[(\hat{d}_m^{\uparrow,+})^\dagger \hat{d}_{m'}^{\downarrow,-}] \rangle$ are calculated. Using these correlation functions, matching equations for distribution functions $\tilde{f}_m^{\uparrow\downarrow,\pm}$, in which the total average current can be expressed, are derived. Finally, it is shown that these distribution functions obey the same matching equations as the partial distribution functions of the generalized OTBK-approach and that the current expressions are just the same for the two approaches, i.e that the two approaches are equivalent.

The wavefunction amplitudes $\hat{d}_m^{\uparrow,\downarrow,\pm}$ on the dot-side of the NIS-barrier are related to the coefficients $\hat{c}_m^{\uparrow,\downarrow,\pm}$ on the superconducting side of the NIS-barrier, discussed in the previous chapter, via the scattering matrix of the NIS-interface barrier. This change of coefficients leads to new matching equations for the wavefunction coefficients on the dot-side of the NIS-barrier, corresponding to the matching Eqs. (8.19)-(8.21). The matching conditions for an injected electron like quasiparticle from left in mode q become at the left NIS-interface

$$\begin{pmatrix} \hat{d}_m^{\downarrow,-} \\ \hat{d}_m^{\uparrow,+} \end{pmatrix} = \begin{pmatrix} b_m^+ & a_m^+ \\ a_m^+ & b_m^- \end{pmatrix} \begin{pmatrix} \hat{d}_m^{\downarrow,+} \\ \hat{d}_m^{\uparrow,-} \end{pmatrix} + \delta_{m0}\delta_{nq}\sqrt{q_n^e}\sqrt{u^2-v^2} \begin{pmatrix} d_n^- \\ c_n^+ \end{pmatrix}. \tag{9.9}$$

and similarly at the right interface. We have introduced the scattering amplitudes at the NIS-interface $a_m^+ = \tilde{a}(E_m)$ and $a_m^+ = \tilde{a}(E_m)$ and similarily for the other Andreev scattering amplitudes, where $\tilde{a}, \tilde{b}, \tilde{c}$ and $\tilde{d}$ are given in Eq. (8.50). The electron and hole wavefunction coefficients are matched with the scattering matrix $\bar{S}$ of the dot without barriers as

$$\begin{pmatrix} \hat{d}_{2m}^{\downarrow,+} \\ \hat{d}_{2m+1}^{\uparrow,-} \end{pmatrix} = \bar{S}(E_{2m}+eV/2) \begin{pmatrix} \hat{d}_{2m}^{\uparrow,+} \\ \hat{d}_{2m+1}^{\downarrow,-} \end{pmatrix} \tag{9.10}$$

and

$$\begin{pmatrix} \hat{d}_{2m}^{\uparrow,-} \\ \hat{d}_{2m-1}^{\downarrow,+} \end{pmatrix} = \bar{S}^*(-[E_{2m}+eV/2]) \begin{pmatrix} \hat{d}_{2m}^{\downarrow,-} \\ \hat{d}_{2m-1}^{\uparrow,+} \end{pmatrix}. \tag{9.11}$$

The matching equations for left injected holes and right injected electrons and holes follow analogously.

The formal solutions for the wavefunction coefficients $\hat{d}_m^{\uparrow\downarrow,\pm}$ can be found in a way similar to the discussion in the previous chapter. It turns out that knowledge of the full solution is not necessary to prove the connection to the OTBK-approach, it suffices to know two identities for the ensemble averaged correlation functions between different wavefunction coefficients. The first is that i) coefficients with different energy indices m are uncorrelated, e.g.

$$\langle \mathrm{tr}[(\hat{d}_m^{\uparrow,+})^\dagger \hat{d}_{m'}^{\downarrow,-}] \rangle = 0 \text{ for } m \neq m' \tag{9.12}$$

and similarly for other correlators, where trace is taken over injection modes. The second is that ii) coefficients for quasiparticles incoming towards the NIS-interface with the same energy index m are uncorrelated, i.e.

$$\langle \mathrm{tr}[(\hat{d}_m^{\downarrow,+})^\dagger \hat{d}_m^{\uparrow,-}] \rangle = 0 \tag{9.13}$$

These two identities can be shown to hold to leading order in $\Gamma_L N, \Gamma_R N \gg 1$, i.e neglecting quantum corrections, using the diagrammatic technique for integrating over the unitary group, discussed in Chapter 6. To show this, we first note the following properties of the wavefunction coefficients $\hat{d}_m^{\downarrow,\uparrow,\pm}$. The wavefunction coefficients can be expanded into a sum of matrix amplitudes, describing the paths in energy position space, as $\hat{d}_m^{\downarrow,\uparrow,\pm} = \sum_l \hat{\alpha}_l$ where each $\hat{\alpha}_l$ is a product

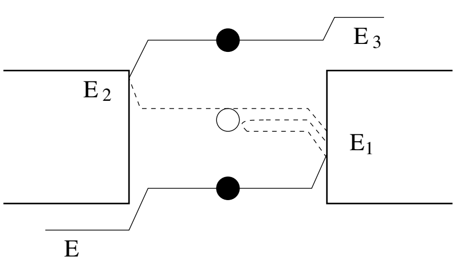

Figure 9.7: A schematic picture of a quasiparticle path in energy space, contribution to the three particle current I_3. Black (white) dots correspond to scattering of electrons (holes) at the dot.

of reflection and transmission amplitudes of the dot and Andreev reflection amplitudes at different energies. As an example, consider one path $\hat{\alpha}_{l'}$ contributing to the three particles current, shown in Fig. 9.7 The path shown in Fig. 9.7 has the ampltude $\hat{\alpha}_{l'} \propto t_2\tilde{a}(E_2)t_1'^*\tilde{b}(E_1)r_1'^*\tilde{a}(E_1)t_0$, where the reflection and transmission matrix amplitudes r, t', t and t' refer to scattering at the dot without barriers and we have introduced $r_m = r(E_m + eV/2)$ and $r_m^* = r_m^*(-[E_m + eV/2])$ and similarliy for the other scattering amplitudes. We now use the polar decomposition in Eq. (6.24) of the scattering matrix $\bar{S}$ at each energy, and write the scattering matrix amplitudes r, r', t and t' in terms of the unitary matrices U, V, U' and V' and the transmission eigenvalue matrices $\sqrt{D}$ and $\sqrt{1-D}$. It is important to note that due to the broken TRS, the unitary matrices U and U' and also V and V' are completely uncorrelated, as discussed in Chapter 5. Our example path is then given by $\hat{\alpha} \propto \tilde{a}(E_2)\tilde{b}(E_1)\tilde{a}(E_1)U_2\sqrt{D}V_2'V_1^*\sqrt{D}V_1'^*V_1^*\sqrt{1-D}U_1'^*U_0\sqrt{D}V_0'$ where the energy labels on the unitary matrices are the same as for the scattering amplitudes. We have neglected the energy dependence on the transmission eigenvalues, in line with the discussion in Chapter 5 on the N-dot-S conductance.

The diagrammatic representation of this amplitude (not taking the Andreev scattering amplitudes into account), is shown in Fig. 9.8. From Fig. 9.8 it is clear that the diagrammatic representation of the scattering matrix amplitudes has the property that the black and white dots must come alternating, an effect of that there are no transposed or Hermitian conjugated unitary matrices in the amplitude $\hat{\alpha}_{l'}$. Moreover, another important property is that each matrix amplitude $\hat{\alpha}_l$ is a unique product of transmission and reflection matrices, in the sense that there are not two amplitudes that contain exactly the same matrices in the same order (counting scattering amplitudes at different energies as well as scattering by electron and holes as "different")

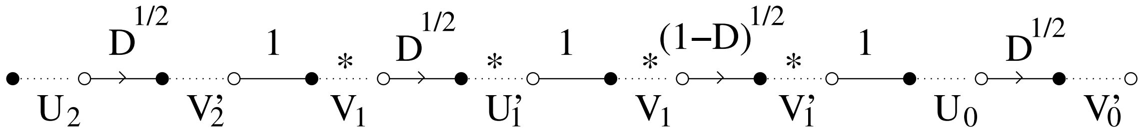

Figure 9.8: The diagrammatic representation of the scattering amplitude $U_2\sqrt{D}V_2'V_1^*\sqrt{1}\sqrt{D}V_1'^*V_1^*\sqrt{1}\sqrt{D}U_1'^*V_1^*\sqrt{D}U_1'^*U_0\sqrt{D}V_0'$, inserting unit matrices between neighboring unitary matrices for convenience.

Our aim is to show the relations (9.12) and (9.13) for the ensemble averaged correlation functions. To do this it is instructive to first consider the correlation function between a wavefunction coefficient and its Hermitian conjugate, e.g $\langle \mathrm{tr}[(\hat{d}_m^{\uparrow,+})^\dagger \hat{d}_m^{\uparrow,+}]\rangle$. To calculate this correlator we must in principle calculate all ensemble averaged products of scattering matrix amplitudes $\langle \mathrm{tr}(\hat{\alpha}_l^\dagger \hat{\alpha}_{l'})\rangle$, since we have $\langle \mathrm{tr}[(\hat{d}_m^{\uparrow,+})^\dagger \hat{d}_m^{\uparrow,+}]\rangle = \sum_{l,l'}\langle \mathrm{tr}(\hat{\alpha}_l^\dagger \hat{\alpha}_{l'})\rangle$. It turns out, however, that only the amplitudes multiplied their own Hermitian conjugates have a nonzero average, i.e $\langle \mathrm{tr}(\hat{\alpha}_l^\dagger \hat{\alpha}_{l'})\rangle \propto \delta_{l,l'}$. This is clear by studying the diagram in Fig. 9.9, drawn with the convention that all matrices belonging to $\hat{\alpha}_l$ are shown in the lower row and all matrices belonging to $\hat{\alpha}^\dagger_{l'}$ are shown in the upper row. For each given product $\mathrm{tr}(\hat{\alpha}^\dagger_l \hat{\alpha}_{l'}$, the ensemble average consists

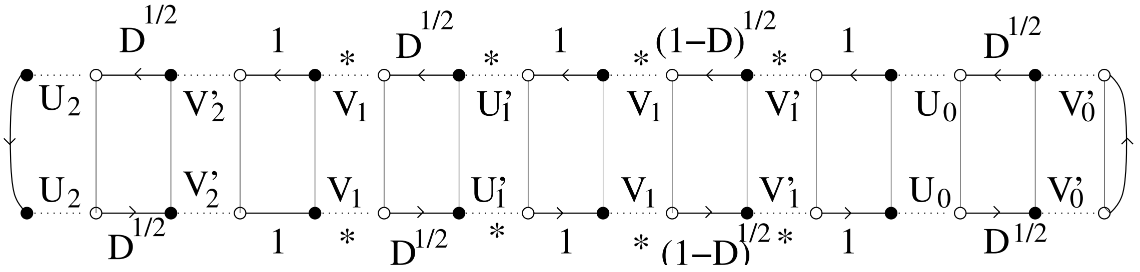

Figure 9.9: A diagram showing the matrix connections giving rise to a leading order contribution.

of summing up all possible diagrams where the different unitary matrices have been combined (shown with thin black lines in Fig. 9.9) according to the rules discussed in Chapter 2. We can start this combination by trying to connect the rightmost white dot in the lower line in Fig. 9.9. To obtain a highest order contribution (i.e neglecting quantum corrections) it must be combined with another white dot such that no further combinations give rise to thin lines crossing. It is then clear by inspection that it can only be combined with a white dot in the upper row. However, since all white dots in the upper row equivalently have to be combined with with dots in the lower row, the only possible connection that does not lead to that any remaining thin lines are crossed, is to connect it with the rightmost white dot in the upper line.

If the total diagram should be nonzero, the leftmost white dot in the upper and lower rows must correspond to the same unitary matrix, i.e a V'-matrix without complex conjugation. Since the rightmost scattering amplitude corresponds to the first scattering event after the quasiparticle has entered the junction, it means that the only reflection or transmission as electron at energy E_0 is possible (scattering as holes gives complex conjugated amplitudes). These scattering amplitudes are decomposed as $r_0 = V_0\sqrt{1-D}V'_0$ and $t_0 = U_0\sqrt{1-D}V'_0$, both with V'_0 as the last matrix, so the first vertical connection can be performed. However, when continuing with the neighboring black dot in the lower line, corresponding to U_0, it is clear that this can only be combined with $U^\dagger_0$ in the upper line, corresponding to transmission as the first scattering event. Continuing with the remaining dots in the lower line, it is clear along the same line, that only the scattering matrix amplitude $\hat{\alpha}_{l'}$ combined with its Hermitian conjugate, gives a leading order result.

This technical result simply means that all interference terms between different paths are cancelled on the average, and only the terms containg the same paths give a leading order contribution. From this we directly confirm the first rule in (9.12), since all the scattering matrix amplitudes belonging to the wavefunction amplitude with energy index m are different from the scattering matrix amplitudes belonging to the wavefunction amplitude with energy index m'. As an example, for $m' = m+1$ and m' odd, it is clear that all paths belonging to any amplitude at m' has to traverse the dot at energy m' an odd number of time, while all paths belonging to any amplitude at m has to traverse the dot at energy m' an even number, and thus giving zero correlation in line with the discussion.

The second rule in (9.13) follows from the observation that the two quasiparticles coming in towards the NIS-interface at E_m are always of different type, i.e one electron and one hole. This implies in the same way gives that these paths can not be equal and that the correlator is zero.

As was discussed in connection to the generalized OTBK-approach in the previous chapter, it is possible to decompose the OTBK-distribution functions into partial distribution functions

$f_m^{\uparrow,\downarrow,\pm}$, related via the matching Eqs. (8.48), (8.49) and (8.54)-(8.56), with the difference that the source term $T(E)f(E)$ is multiplied by a δ_{m0} since the injected quasiparticles are treated independently (and one also has to treat injection from the different sides independently).

To make contact with the OTBK-approach, we now introduce the ensemble averaged normalized correlation functions, on the form of distribution functions, e.g.

$$\tilde{f}_{m,e}^{\downarrow,+} = \langle \mathrm{tr}[(\hat{d}_m^{\downarrow,+})^\dagger \hat{d}_m^{\downarrow,+}] \rangle f/N, \tag{9.14}$$

where e denotes injected electron, and we start by considering left injected quasiparticles. Having established the correlation function rules in (9.12) and (9.13), we can perform the ensemble average directly on the matching equations in (9.10)- (9.9). At the left NIS-interface the matching equations become [matching distribution functions per unit energy, i.e multiplying each injected amplitude by dq/dE by changing from a summation over wavenumber to integration over energy]

$$\begin{aligned}
\tilde{f}_{m,e}^{\downarrow,-} &= \langle \mathrm{tr}\left[(b_n^+ \hat{d}_m^{\downarrow,+} + a_n^+ \hat{d}_m^{\uparrow,-} + c_n^+ \delta_{n0}) \times c.c.\right] \rangle \\
&= B_n \tilde{f}_{m,e}^{\uparrow,-} + A_n \tilde{f}_{m,e}^{\downarrow,+} + C_n f \delta_{n0}, \\
\tilde{f}_{m,e}^{\uparrow,+} &= A_n \tilde{f}_{m,e}^{\uparrow,-} + B_n \tilde{f}_{m,e}^{\downarrow,+} + D_n f \delta_{n0},
\end{aligned} \tag{9.15}$$

where the scattering probabilities $A_m = |a_m^\pm|^2$ and similarly B_m, C_m and D_m, and we have used that the average of any wavefunction coefficient itself is zero. Matching across the right interface follows analogously, and scattering across the dot gives

$$\begin{aligned}
\tilde{f}_{2m,e}^{\downarrow,+} &= \langle \mathrm{tr}\left[(r\hat{d}_{2me}^{\uparrow,+} + t'\hat{d}_{2m+1}^{\downarrow,-}) \times c.c.\right] \rangle = \frac{1}{2}\tilde{f}_{2m,e}^{\uparrow,-} + \frac{1}{2}\tilde{f}_{2m+1,e}^{\downarrow,-} \\
\tilde{f}_{m+1}^{\uparrow,-} &= \frac{1}{2}\tilde{f}_{2m,e}^{\uparrow,-} + \frac{1}{2}\tilde{f}_{2m+1,e}^{\downarrow,-}
\end{aligned} \tag{9.16}$$

where we have used that rules for the averaging gives

$$\langle \mathrm{tr}[(\hat{d}_{2m+1}^{\downarrow,-})^\dagger t'^\dagger t' \hat{d}_{2m+1}^{\downarrow,-}] \rangle = \langle \mathrm{tr}(t'^\dagger t') \rangle \langle \mathrm{tr}[(\hat{d}_{2m+1}^{\downarrow,-})^\dagger \hat{d}_{2m+1}^{\downarrow,-}] \rangle / N \tag{9.17}$$

and similarly for the other terms, and that $\langle \mathrm{tr}(t'^\dagger t') \rangle = \langle \mathrm{tr}(r^\dagger r) \rangle = N/2$.

Introducing the distribution functions, e.g. $\tilde{f}_{2m}^{\downarrow,+} = \tilde{f}_{2m,e}^{\downarrow,+} + \tilde{f}_{2m,h}^{\downarrow,+}$, summed over injected electrons and holes at the left side, we see that these distribution functions $\tilde{f}_m^{\downarrow\uparrow,\pm}$ obey exactly the same matching equations as the partial distribution functions of the generalized OTBK-approach [see (8.19)-(8.21)]. Moreover, the expression for the ensemble averaged particle currents weighted with the distribution functions f, i.e. $\langle I_m^p \rangle = Ne/h[(\tilde{f}_m^{\uparrow,-} - \tilde{f}_m^{\downarrow,-}) - (\tilde{f}_m^{\uparrow,+} - \tilde{f}_m^{\downarrow,+})$ is given on exactly the same form [see Eq. (8.59)]. This finally shows that the two approaches are equivalent.

Acknowledgements

It is my pleasant task here to thank those who in different ways have helped me along the way to this doctoral thesis.

First and foremost my thanks go to my supervisors Professor Göran Wendin and Assistant professor Vitaly Shumeiko. I am deeply indebted to them for support, encouragement, valuable comments and advice during my work. Both of them have combined their great experience and knowledge in physics with a never-ending positive attitude which has made my Ph.D.studies both inspiring and enjoyable.

I also wish to express special thanks to Professor C.W.J. Beenakker for giving me the opportunity to work for two months in the interesting and highly creative environment of the Lorentz Institute of the University of Leiden (Netherlands). During this time I had the privilege to work with Dr Henning Schomerus, who I appreciate not only for his strong mathematical skills but also for he beeing a very nice person. I really enjoyed the international and friendly atmosphere in Leiden in which Ph.D.students and Postdocs with various backgrounds interchanged ideas both inside and outside the university.

I also would like to express my gratitude to Professor Ulrich Merkt, who invited me to work with his experimental group at the University of Hamburg (Germany) for one month. In Hamburg I learnt more about experiments and the conditions under which experimental work is performed. I want to thank Andreas Richter for being a great host during my time at the university and I appreciate our ongoing physical discussions.

My thanks are also due to Professor Bart Van Wees and Dr Thomas Schäpers, with whom I have frequently discussed physics problems during the common conferences we attended over the years. I have also had fruitful collaborations and interesting discussions with Professor Per Delsing and Edgar Hürfeld at Chalmers. Their experimental work has been a help and an inspiration for my theoretical modeling and calculations.

I truly appreciate my fellow Ph.D.studens, who have strongly contributed to make my five years at Chalmers very pleasant. I am especially grateful to Göran Johanssson, Tomas Löfwander, Åke Ingerman and Jonn Lantz for interesting physical discussions, intellectual stimulation and great friendship. I also want to thank all colleagues who kept me company during lunches and coffee breaks over these years. The pauses between the working hours have been both interesting and relaxing thanks to you.

My research was financially supported by grants from TFR (Sweden) and NEDO (Japan), which is gratefully acknowledged. I also want to thank Erika Hult for facilitating the typographical layout of the thesis.

It is a great pleasure to thank my parents and grandmother for all support. Finally, most of all I would like to thank my beloved fiancée Helena, who has always been supporting and encouraging. Without your love and inspiration it would not have been possible.

Göteborg, February 2001 Peter Samuelsson

Bibliography

[1] Akazaki, T, H. Takayanagi, J. Nitta and T. Enoki, App. Phys. Lett **68**, 418 (1996).

[2] Akkermans E., A. Auerbach, J.E. Avron, and B. Shapiro, Phys. Rev. Lett **66**, 76 (1991).

[3] Allsopp, N.K. and C.J. Lambert, Phys. Rev. B **50**, 3972 (1994).

[4] Allsopp, N.K., J.S. Canizares, R.Raimondi, and C.J. Lambert, J. Phys. Condens. Matter. **8** L377. (1996).

[5] Alhassid, Y. Rev. Mod. Phys. **72**, 895, (2000).

[6] Altland, A., and M. Zirnbauer, Phys. Rev. Lett. **76**, 3420 (1996).

[7] Altshuler, B.L., D.E. Khmelnitskii, and B.Z. Spivak, Solid State Commun. **48** 841 (1983).

[8] Altshuler, B.L., Pis'ma Zh. Eksp. Teor. Fiz. **41**, 530, (1985) [JETP Lett. **41**, 648, (1985)].

[9] Altshuler, B.L., and B.I. Shklovskii, Zh. Eksp. Teor. Fiz. **91**, 220, (1986) [Sov. Phys. JETP **64**, 127, (1986)].

[10] Altshuler, B.L., and B.Z. Spivak, Zh. Eksp. Teor. Fiz. **92**, 609, (1987) [Sov. Phys. JETP **65**, 343, (1987)].

[11] Ambegaokar, V., and A. Baratoff, Phys. Rev. Lett. **10**, 486 (1963).

[12] Aminov, B.A., A.A. Golubov, and M. Yu. Kupriyanov, Phys. Rev. B. **53**, 365 (1996).

[13] Andersson, P.W. in *Ravello Lectures on the Many-Body problem*, edited by E.R. Gianello (Academic, New York, 1963).

[14] Andreev, A. F., Zh. Eksp. Teor. Fiz. **46**, 1823, (1964) [Sov. Phys. JETP **19**, 1228, (1964)].

[15] Andreev, A. F., Zh. Eksp. Teor. Fiz. **49**, 655, (1966) [Sov. Phys. JETP **22**, 455, (1966)].

[16] Andreev, A.V., O. agam, B.D. Simons, and B.L. Altshuler, Phys. Rev. Lett. **76**, 3947 (1996).

[17] Antonov, V.N., H. Takayanagi, F.K. Wilhelm, and A.D. Zaikin, Europhys. Lett. **50**, 250 (2000).

[18] Argaman, N., Y. Imry, and U. Smilansky, Phys. Rev. B **47**, 4440 (1993).

[19] Argaman, N., and A. Zee, Phys. Rev. B **54**, 7406 (1996).

[20] Argaman, N. Superlatt. and Microstr. **25** 861 (1999).

[21] Arnold, G.B., J. Low. Temp. Phys., **68** 1 (1987).

[22] Artmenko, S.N., A.F. Volkov, and A.V., Zaitsev, Solid. State. Commun. **30** 771 (1979).

[23] Arnold, G.B. J. Low. Temp. Phys. **59**, 143, (1985).

[24] Aslamasov, L.G., A.I. Larkin, and Yu. N. Ovchinnikov, Zh. Eksp. Teor. Fiz. **55**, 323, (1968) [Sov. Phys. JETP **28**, 171, (1969)].

[25] Aslamazov, L.G., and S.V. Lempitskii, Zh. Eksp. Teor. Fiz. **82**, 1671 (1982) [Sov. Phys. JETP **55**, 967 (1982)].

[26] Averin, D., and A. Bardas, Phys. Rev. Lett. **75**, 1831 (1995).

[27] P.F. Bagwell, Phys. Rev. B **46**, 12573 (1992).

[28] Baranger, H. U., and A. D. Stone, Phys. Rev. B **40**, 8169 (1989).

[29] Baranger, H. U., and P.A. Mello, Phys. Rev. Lett. **73**, 142 (1994).

[30] Baranger, H. U., and P.A. Mello, Phys. Rev. B **51**, 4703 (1995).

[31] Bardas, A., and D. Averin, Phys. Rev. B. **56**, R8518 (1997).

[32] Bardeen, J, L.N. Cooper, and J. Schrieffer, Phys. Rev. **108**, 1175 (1957).

[33] Bardeen, J., R. Kümmel, A.E. Jacobs and L. Tewordt, Phys. Rev. **187**, 187 (1969).

[34] Bardeen, J. and J.L. Johnsson, Phys. Rev. B **5**, 72 (1972).

[35] J.J.A. Baselmans, A.F. Morpurgo, B.J. van Wees, and T.M. Klapwijk, Nature **397**, 43 (1999).

[36] Bastian, G., E.O. Göbel, A.B. Zorin, H. Schulze, J. Niemeyer, T. Weimann, M.R. Bennett, and K.E. Singer, Phys. Rev. Lett. **81**, 1686 (1998).

[37] Baz, A.I., Ya. B. Zel'dovic and A.M. Perelomov, *Scattering, reactions and decay in nonrelativistic quantum mechanics*, (Jerusalem, 1969).

[38] Beenakker, C.W.J., and H. van Houten, Phys. Rev. Lett **66**, 3056 (1991).

[39] Beenakker, C.W.J., Phys. Rev. Lett **67**, 3836 (1991).

[40] Beenakker, C.W.J., and H. van Houten, Solid State Phys, **44**, 1, (1991).

[41] Beenakker, C.W.J., and H. van Houten, in *Single Electron Tunneling and Mesoscopic Devices*, Berlin, Springer (1991).

[42] Beenakker, C.W.J. in *Transport Phenomena in Mesoscopic Systems*, edited by H. Fukuyama and T. Ando, (Springer, Berlin, 1992)

[43] Beenakker, C.W.J. and H. van Houten, in*Nanostructures and Mesoscopic Systems*, edited by W.P. Kirk and M.A. Reed (Academic, New York, 1992)

[44] Beenakker, C.W.J., Phys. Rev. B **46**, 12841 (1992).

[45] Beenakker, C.W.J., Phys. Rev. Lett. **70**, 1155 (1993).

[46] Beenakker, C.W.J., Phys. Rev. B **47**, 15763 (1993).

[47] Beenakker, C.W.J. in *Mesoscopic Quantum Physics* edited by E. Akkermans, G. Montambaux, J.-L. Pichard, and J. Zinn-Justin (North-Holland, Amsterdam) (1995).

[48] Beenakker, C.W.J., Rev. Mod. Phys., **69**, 731 (1997).

[49] Belzig, W. C. Bruder, and G. Schön, Phys. Rev. B **54**, 9443 (1996).

[50] Belzig, W., F.K. Wilhelm, G. Schön, and A.D. Zaikin, Superlatt. and Microstr. **25**, 1251 (1999).

[51] Bezuglyi, E.V., E.N. Bratus, V.S. Shumeiko, and G. Wendin, Phys. Rev. Lett. **83**, 2050 (1999).

[52] Bezuglyi, E.V., E.N. Bratus, V.S. Shumeiko, G. Wendin, and H. Takayanagi, Phys. Rev. B **62**, 14439 (2000).

[53] Blom, H., A. Kadigrobov, A.M. Zagoskin, R.I. Shekter, and M. Jonson, Phys. Rev. B **57**, 9995 (1998).

[54] Blonder, G.E., M. Tinkham and T.M. Klapwijk, Phys. Rev. B **25**, 4515 (1983).

[55] Blonder, G.E. and M. Tinkham, Phys. Rev. B **27**, 112 (1983).

[56] Blümel, R., and U. Smilansky, Phys. Rev. Lett. **60**, 477 (1988).

[57] Bohigas, O., M.-J. Giannoni, and C. Schmit, Phys. Rev. Lett. **52**, 1 (1985).

[58] Bohigas, O., M.-J. Giannoni, A.M. Ozorio de Almeida, and C. Schmit, Nonlinearity **8**, 203 (1995);

[59] Bratus', E.N., V.S. Shumeiko, and G.Wendin, Phys. Rev. Lett. **74**, 2110 (1995).

[60] Brouwer, P. W., Phys. Rev. B **51**, 16878 (1995).

[61] Brouwer, P. W., and C.W.J. Beenakker, Phys. Rev. B **51**, 7739 (1995).

[62] Brouwer, P. W., and C.W.J. Beenakker, J. Math. Phys. (N.Y) **37**, 4904 (1996).

[63] Brouwer, P. W., and C.W.J. Beenakker, Phys. Rev. B **54**, 12705 (1996).

[64] Brouwer, P. W., PhD thesis, Leiden (1997).

[65] Brouwer, P.W., and C.W.J. Beenakker, Chaos, Solitons and Fractals, **7**, 1249 (1997).

[66] Brouwer, P. W., and C.W.J. Beenakker, Phys. Rev. B **55**, 4695 (1995).

[67] Büttiker, M., Y. Imry, and M.Y. Azbel, Phys. Rev. A. **30**, 1982 (1984).

[68] Büttiker, M., Phys. Rev. Lett **57**, 1761 (1986).

[69] Büttiker, M., and T. M. Klapwijk, Phys. Rev. B. **33**, 5114 (1986).

[70] Böttcher, K. and T. Kopp, Phys. Rev. B **55**, 11670 (1997).

[71] Chan, I.H., R.M. Clarke, C.M. Marcus, K. Campman, and A.C. Gossard, Phys. Rev. Lett **74**, 3876 (1995).

[72] Chang, L.F. and P.F. Bagwell, Phys. Rev. B **55**, 12678 (1997).

[73] Chrestin, A. T. Matsuyama and U. Merkt, Phys. Rev. B **94**, 498 (1994).

[74] Chrestin, A., R. Kürsten, K. Biedermann, T. Matsuyama, and U. Merkt, Superlatt. and Microstr. **25**, 711 (1999)

[75] Clerk, A.A., P.W. Brouwer, and V. Ambegaokar, Phys. Rev. B **62**, 10226 (2000).

[76] Cohen, M.H., L.M. Falicov, and J.C. Philips, Phys. Rev. Lett **8**, 316 (1962).

[77] Cook, P.M.A., V.C. Hui and C.J.Lambert, Europhys. Lett, **30**, 355 (1995).

[78] Cuevas, J.C., A. Martin-Rodero, and A. Levy Yeyati, Phys. Rev. B **54**, 7366 (1996).

[79] Cuevas, J.C., A. Martin-Rodero, and A. Levy Yeyati, Phys. Rev. Lett. **82**, 4086 (1999).

[80] Cuevas, J.C., and M. Fogelström, cond-mat/0101203.

[81] Cuevas, J.C., presentation at Chalmers University of Technology,

[82] Creutz, M. J. Math. Phys. (N.Y), **19**, 2043 (1978).

[83] Datta, S., *Electronic transport in mesoscopic systems* (Cambridge University Press, 1995).

[84] Dimoulas, A., J.P. Heida, B.J. van Wees, T.M. Klapwijk, W. van der Graaf, and G. Borghs, Phys, Rev. Lett. **74**, 602 (1995).

[85] Doron, E., and U. Smilansky, Phys. Rev. Lett **68**, 1255 (1992).

[86] Dyson, F.J., J. Math. Phys. (N.Y), **3**, 140 (1962).

[87] Efetov, K. B., Zh. Eksp. Teor. Fiz. **83**, 833 (1965) [Sov. Phys. JETP, **56**, 467 (1983)].

[88] Efetov, K. B., Adv. Phys. **32**, 53 (1983).

[89] Efetov, K.B., Phys. Rev. Lett. **74**, 2299 (1995).

[90] Fisher, D.S., and P.A. Lee, Phys. Rev. B **23**, 6851 (1981).

[91] Flensberg, K., J. Bindslev Hansen and M. Octavio, Phys. Rev.B, **38** 8707 (1988).

[92] Flensberg, K., and J. Bindslev Hansen, Phys. Rev.B, **40** 8693 (1989).

[93] Frahm, K.M., and J.-L Pichard, J. Phys. I France **5**, 847 (1995).

[94] Frahm, K.M., Europhys. Lett. **30**, 457 (1995).

[95] Frahm, K.M., P.W. Brouwer, J.A. Melsen, and C.W.J. Beenakker, Phys. Rev. Lett. **76**, 2981 (1996).

[96] Furusaki, A. and M. Tsukada, Physica B **165-166**, 967 (1990).

[97] Furusaki, A. and M. Tsukada, Phys. Rev. B **43**, 10164 (1981).

[98] Furusaki, A., H. Takayanagi, and M. Tsukada, Phys. Rev. B **45**, 10563 (1981).

[99] Fyodorov, Y.V. and H.J. Sommers, J. Math. Phys, **38**, 1918 (1997).

[100] de Gennes, P.G., *Superconductivity in Metals and Alloys* (Addison-Wesley Publishing, Reading, MA, 1989).

[101] Goffman, M.F., R. Cron, A. Levy Yeyati, P. Joyez, M.H. Devoret, D. Esteve, and M. Urbina, Phys. Rev. Lett. 85, 170 (2000)

[102] Gorelik, L.Y., V.S. Shumeiko, R.I. Shekhter, G. Wendin, and M. Jonson, Phys. Rev. Lett. **75**, 1162 (1995).

[103] Gor'kov, L.P. and G.M. Eliashberg, Zh. Eksp. Teor. Fiz. **48**, 1407 (1965) [Sov. Phys. JETP, **21**, 940 (1965)].

[104] Guhr, T., A. Müller-Groeling, and H.A. Weidenmüller, Phys. Rep. **299** 189 (1998).

[105] Gunsenheimer., U., U. Schüssler, and R. Kümmel, Phys. Rev. B **49**, 6111 (1994).

[106] Gunsenheimer, U., and A.D. Zaikin, Phys. Rev. B. **50**, 6317 (1994).

[107] Götz, M. M. Grajcar, E. Il'ichev, V.V. Khanin, A.B. Zorin, J. Niemeyer, and H.-G. Meyer, Phys. Rev. B **62**, R14645 (2000).

[108] Haberkorn,W., H. Knauer, and J. Richter, Phys. Stat. Sol. **47**, K161 (1978).

[109] Hamermesh, M., *Group Theory and its Applications to Physical Problems* (Addison-Wesley, Reading, M.A.).

[110] den Hartog, S.G., C.M.A. Kapteyn, B.J. van Wees, T.M. Klapwijk, W. van der Graaf and G. Borghs, Phys. Rev. Lett. **77**, 4954 (1996).

[111] Heida, J.P., B.J. van Wees, T.M. Klapwijk, G. Borghs, Phys. Rev. B 57, R5618 (1998).

[112] Heida, J.P., B.J. van Wees, T.M. Klapwijk, G. Borghs, Phys. Rev. B **60**, 13135 (1999).

[113] W.M. van Heuffelen, T.M. Klapwijk, D.R. Heslinga, M.J. de Boer, and N. van der Post, Phys. Rev. B **47**, 5170 (1993).

[114] Hoss, T., C.Strunk, T. Nussbaumer, R. Huber, U. Staufer, and C. Schönenberger, Phys. Rev. B. **62**, 4079 (2000).

[115] Hui, V.C., and C.J. Lambert, Europhys. Lett, **23**, 203 (1993).

[116] Huibers, A.G., S.R. Patel, C.M. Marcus, P.W. Brouwer, C.I. Duruös and J.S. Harris, Phys. Rev. Lett. 81, 1917 (1998).

[117] Hurd, M. and G. Wendin, Phys. Rev. B **49**, 15258 (1994).

[118] Ihra, W., M. Leadbeater, J.L. Vega, and K. Richter, cond-mat/9909100.

[119] Ilhan, H.T., H.V. Demir, and P.F. Bagwell, Phys. Rev. B **58**, 15120 (1998).

[120] Ilhan, H.T., and P.F. Bagwell, J. Appl. Phys. **84**, 6758 (1998).

[121] Imry, Y., in *Directions in Condensed Matter Physics,* edited by G. Grinstein and G. Mazenko, (World Scientific, Singapore), p. 101, (1986).

[122] Imry, Y. Europhys. Lett., **1**, 249 (1986).

[123] Ingerman, Å, G. Johansson, V.S. Shumeiko, and G. Wendin, cond-mat/0101283.

[124] C. Ishii, Prog. Theor. Phys. **44**, 1525 (1970).

[125] Jalabert, R.A., H.U. Baranger, and A.D. Stone, Phys. Rev. Lett **65**, 1442 (1990) .

[126] Jalabert, R.A., J.-L. Pichard, and C.W.J. Beenakker, Europhys. Lett. **27**, 255 (1994).

[127] Johansson, G., G. Wendin, K.N. Bratus', and V.S. Shumeiko, Phys. Rev. B **60**, 1382 (1999).

[128] Johansson, G., G. Wendin, K.N. Bratus', and V.S. Shumeiko, Superlatt. and Microstr. **25**, 906 (1999).

[129] Josephson, B.D., Phys. Lett. **1**, 251 (1962).

[130] Kadigrobov, A., A. Zagoskin, R.I. Schekter, and M. Johnson, Phys. Rev. B **52**, R8662 (1995).

[131] Keller, M.W., A. Mittal, J.W. Sleight, R.G. Wheeler, D.E. Prober, R.N. Sacks, and H. Shtrikmann, Phys. Rev. B **53**, R1693 (1996).

[132] Klapwijk, T.M., G.E.Blonder, and M. Tinkham, Physica B+C **109-110**, 1657 (1982).

[133] Kleinsasser, a.W., R.E. Miller, W.H. Mallison, and G.B. Arnold, Phys. Rev. Lett. **72**, 1738 (1994).

[134] Koops, M.C., G.V. van Duyneveldt, and R. de Bruyn Ouboter, Phys. Rev. Lett. **77**, 2542 (1996).

[135] Kosztin, I., D.M. Maslov, and P.M. Goldbart, Phys. Rev. Lett. **75**, 1735 (1995).

[136] Kresin, V.Z., Phys. Rev. B **34**, 7587 (1986).

[137] Kriman, A.M., N.C. Kluksdahl, and D.K. Ferry, Phys. Rev. B **36**, 5953 (1987).

[138] Kuhlmann, M., U. Zimmerman, D.Dikin, S. Abens, K.Keck, and V. Dimitriev, Z. Phys. B: Condens. matter, **96**, 13 (1994).

[139] Kuhn, D., N.M. Chtchelkatchev, G.B. Lesovik, and G. Blatter, Phys. Rev. B **63**, 054520 (2001).

[140] Kulik, I.O. Zh. Eksp. Teor. Fiz. **57**, 1745 (1969) [Sov. Phys. JETP **30**, 944 (1970)].

[141] Kulik, I.O. and R.I. Shekhter, Zh. Eksp. Teor. Fiz. **68**, 623 (1975) [Sov. Phys. JETP, **41**, 308 (1975)].

[142] Kulik, I.O. and A.N. Omelyanchuk, Pis'ma Zh. Eksp. Teor. Fiz. **21**, 216, (1975) [JETP Lett. **21**, 96, (1975)].

[143] Kulik, I.O. and A.N. Omelyanchuk, Fiz. Nizk. Temp. **3** 945 (1977) [Sov. J. Low. Temp. Phys. **3** 459 (1977)].

[144] Kuplevakhskii S.K, and I.I. Fal'ko, Fiz. Nizk. Temp. **17** 961 (1991) [Sov. J. Low. Temp. Phys. **17** 501 (1991)].

[145] Kutchinsky, J., R. Taboryski, C.B. Sörensen, A. Kristensen, P.E. Lindelöf, J. Bindslev-Hansen, C, Schelde Jacobsen, and J.L. Skov, Phys. Rev. Lett. **78**, 931 (1997).

[146] Kutchinsky, J., R. Taboryski, C.B. Sorensen, J. Bindslev-Hansen, and P.E. Lindelof, Phys. Rev. Lett **83**, 4856 (1999).

[147] Lambert, C.J., J. Phys. Condens. Matter. **3** 6579. (1991).

[148] Lambert, C.J., J. Phys. Condens. Matter. **5** 707 (1993).

[149] Lambert, C.J., and S.J. Robinson, Physica B. **194-196** 1641 (1994).

[150] Lambert, C.J. and R. Raimondi, J. Phys. Condens. Matter. **10** 901. (1998).

[151] Landauer, R., IBM J. Res. Dev. **1** 223, (1957).

[152] Landauer, R., Z. Phys. B. **68** 217, (1987).

[153] Leadbeater, M. and C.J. Lambert, Phys. Rev. B **56**, 826 (1997).

[154] Lee, P.A., and A.D. Stone, Phys. Rev. Lett. **55**, 1622 (1985).

[155] Ledermann, U., A. Fauchere, and G. Blatter, Phys. Rev. B **59**, R9027 (1999).

[156] Lempitskii, S.V., Zh. Eksp. Teor. Fiz. **85**, 1072 (1983), [Sov. Phys. JETP **58**, 624 (1983)].

[157] Lesovik, G.B., A. L. Fauchere, G. Blatter, Phys. Rev. B **55**, 3146 (1997).

[158] Likharev, K.K., Rev. Mod. Phys. **51**, 101 (1979).

[159] Lodder, A., and Yu. V. Nazarov, Phys. Rev. B **58**, 5783 (1998).

[160] Ludoph, B., N. van der Post, E. N. Bratus', E. V. Bezuglyi, V. S. Shumeiko, G. Wendin, and J. M. van Ruitenbeek

[161] Marcus, C.M., A.J. Rimberg, R.M. Westevelt, P.F. Hopkins, and A.C. Gossard, Phys. Rev. Lett. **69**, 506 (1992).

[162] Mahaux, C. and H.A. Weidenmüller, *Shell model approach to nuclear reactions* (North-Holland, Amsterdam 1969).

[163] Marmorkos, I.K., C.W.J. Beenakker, and R.A. Jalabert, Phys. Rev. B **48**, 2811 (1993).

[164] Martin, T.H., and R. Landauer, Phys. Rev. B. **45**, 1742 (1992).

[165] Mehta, M.L., and A. Pandey, J. Phys. A **16** L601 (1983).

[166] Mehta, M.L., *Random matrices* (Academic, New York 1991)).

[167] Mello, P.A., P. Pereyra, and N. Kumar , Ann. Phys. (N.Y.) **181**, 290 (1988).

[168] Mello, P.A., J. Phys. A **23**, 4061 (1990).

[169] Melsen, J. and C.W.J. Beenakker, Physica B **203**, 219 (1994).

[170] Melsen, J., P.W. Brouwer, K.M. Frahm, and C.W.J. Beenakker, Europhys. Lett. **35**, 7 (1996).

[171] J. Melsen, P.W. Brouwer, K.M. Frahm, and C.W.J. Beenakker, Physica Scripta, **T69**, 223 (1997).

[172] Morpurgo, A.F. and F. Beltram, Phys. Rev. B. **50**, 1325 (1994).

[173] Morpurgo, A.F., S. Holl, B.J. van Wees, and T.M. Klapwijk, Phys. Rev. Lett. **78**, 2636 (1997).

[174] Morpurgo, A.F B.J. van Wees, T.M. Klapwijk, and G. Borghs, Phys. Rev. Lett. **79**, 4010 (1997).

[175] Morpurgo, A.F., T.M Klapwijk, and B.J. van Wees, Appl. Phys. Lett. **72**, 966 (1998).

[176] Mur, L.C., C.J.P.M. Harmans, J.E. Mooij, J.F. Varlin, A. Rudra, and M. Ilegems, Phys. Rev. B **54**, R2327 (1996).

[177] Nakano, H., and H. Takayanagi, Solid State commun. **80**, 997 (1991).

[178] Nakano, H., and H. Takayanagi, Phys. Rev. B **47**, 7986 (1993).

[179] Naveh, Y., and D. V. Averin, Phys. Rev. Lett. **82**, 4090 (1999).

[180] Naveh, Y., V. Patel, D.V. Averin, K.K. Likharev, and J.E. Lukens Phys. Rev. Lett. **85**, 5404 (2000).

[181] Nazarov, Y. Phys. Rev. Lett **73**, 134 (1994).

[182] Nitta, J., T. Akazaki, H. Takayanagi, and K. Arai, Phys. Rev. B **46**, 14286 (1992).

[183] Neurohr, K., Th. Schäpers, J. Malindretos, S. Lachenmann, A.I. Braginski, H. Lüth, M. Behet, G. Borgs, and A.A. Golubov, Phys. Rev. B **59**, 11197 (1999).

[184] Oberholzer, S. E.V. Sukhorukhov, C. Strunk, C. Schönenberger, T. Heinzel, K. Ensslin, and M. Holland, cond-mat/0009087.

[185] Octavio, M., M. Tinkham, G.E. Blonder,and T. M Klapwijk, Phys. Rev. B. **27**, 6739 (1983).

[186] Pandey, A., and M.L. Mehta, Commun. Math. Phys. **87**, 449 (1983).

[187] Patel, S.R., S.M. Cronenwett, D.R. Stewart, A.G. Huibers, C.M. Marcus, C.I. Duruöz, J.S. Harris, Jr., K. Campman and A.C. Gossard, Phys. Rev. Lett **80**, 4522 (1998).

[188] Petrashov V.T., V.N. Antonov, P. Delsing, and T. Claeson, Phys. Rev. Lett **70**, 347 (1993).

[189] Petrashov V.T., V.N. Antonov, P. Delsing, and T. Claeson, Phys. Rev. Lett **74**, 5268 (1995).

[190] Petrashov. V.T., R. Sh. Shaikhaidarov, I.A. Sosnin, P. Delsing, T. Claeson, and A. Volkov, Phys. Rev. B. **58**, 15088 (1998).

[191] Porter, C.E., *Statistical theories of Spectra: Fluctuations* (Academic, New York 1965).

[192] van der Post, n., E.T. Peters, I.K. Yanson, and J.M. van Ruitenbeek, Phys. Rev. Lett. **73**, 2611 (1994).

[193] Richter, A. M. Koch, T. Matsuyama, and U. Merkt, Supercond. Sci. Technol.**12**, 874 (1999).

[194] Riedel, R.A. and P.F. Bagwell, Phys. Rev. B **48**, 15198 (1993).

[195] Rittenhouse, G.E. and J.M. Graybeal, Phys. Rev. B **49**, 1182 (1994).

[196] Samuel, S. J. Math. Phys. (N.Y.), **21**, 2695 (1980).

[197] Samuelsson, P., V.S. Shumeiko, and G. Wendin, Phys. Rev. B **56**, R5763 (1997).

[198] Samuelsson, P., J. Lantz, V.S. Shumeiko, and G. Wendin, Phys. Rev. B **62**, 1319 (2000).

[199] Samuelsson, P. and H. Schomerus, Phys. Rev. B **63**, 054512 (2001).

[200] Samuelsson, P., Å. Ingerman, V.S. Shumeiko, and G.Wendin, Physica C **63** (2001).

[201] Scheer, E., P. Joyez, D. Esteve, C. Urbina, and M.H. Devoret, Phys. Rev. Lett. **78**, 3535 (1997).

[202] Scheep, K.M., and G.E.W. Bauer, Phys. Rev. Lett. **78**, 3015 (1997).

[203] Schomerus, H., and C.W.J. Beenakker, Phys. Rev. Lett. **82**, 2951 (1999).

[204] Schrieffer, J.R., and J.W. Wilkins, Phys. Rev. Lett. **10**, 17 (1963).

[205] Schüssler, U. and R. Kümmel, Phys. Rev. B **47**, 2754 (1993).

[206] Schäpers, Th., A. Kaluza, K. Neurohr, J. Malindretos, G. Crecelius, A. van der Hart, H. Hardtdegen and H. Lüth., Appl. Phys. Lett. **71** 3575 (1997).

[207] Schäpers, Th., J. Malindretos, K. Neurohr, S. Lachenmann, A. van der Hart, G. Crecelius, H. Hardtdegen and H. Lüth., Appl. Phys. Lett. **73** 2348 (1998).

[208] Schäpers, Th., K. Neurohr, J. Malindretos, A. Kaluza, J.M. Pichard, and M. Lüth, Superlatt. and Microstr. **25**, 851 (1999).

[209] Shekhter, R.I., Zh. Eksp. Teor. Fiz. **63**, 1410 (1972) [Sov. Phys. JETP, **36**, 744 (1973)].

[210] Seviour, R. and A.F. Volkov, Phys. Rev. B **61**, R9273 (2000).

[211] Shaikhaidarov, R., A.F. Volkov, H. Takayanagi, V.T. Petrashov and P. Delsing, Phys. Rev. B **62**, R14649 (2000).

[212] Shekter, R.I., Zh. Eksp. Teor. Fiz. **63**, 1410 (1973) [Sov. Phys. JETP, **36**, 747 (1973)].

[213] Shumeiko, V.S., G. Wendin and E.N. Bratus, Phys. Rev. B **48**, 13129 (1993).

[214] Shumeiko V.S. and E.N. Bratus, Low. Temp. Phys. **23**, 181 (1997).

[215] Simmel, F, T. Heinzel, and D.A. Wharam, Europhys. Lett, **38**, 123 (1997).

[216] Sivan, U., F.P. Milliken, K. Milkove, S. Rishton, Y. Lee, J.M. Hong, V. Boegli, D. Kern, and M. deFranza, Europhys. Lett. **25**, 605 (1994).

[217] Sivan, U., R. Berkovits, Y. Aloni, O. Prus, A. Auerbach, and G. Gen-Yoseph, Phys. Rev. Lett. **77**, 1123 (1996).

[218] Smith, F.T., Phys. Rev. **118** 349 (1960).

[219] Spivak, B.Z. and D.E. Khmelnitskii, JETP Lett. **35** 412 (1982).

[220] Stone, A.D., and A. Szafer, IBM J. Res. Dev. **32** 384 (1988).

[221] Stone, A.D., P.A. Mello, K.A. Muttalib, and J.-L. Pichard, in *mesoscopic phenomena in solids*, edited by B. L. Altshuler, P.A. Lee and R.A. Webb (North-Holland, Amsterdam, 1991).

[222] Svidzinsky, A.V., T.N. Antsygina, and E.N. Bratus', Sov. Phys. JETP **34**, 860 (1972);

[223] Svidzinsky, A.V., T.N. Antsygina, and E.N. Bratus', J. Low Temp. Phys. **10**, 131 (1973).

[224] Szafer, A., and A.D. Stone, Phys. Rev. Lett **62**, 300 (1989).

[225] Taboryski, R., J. Kutchinsky, J. Bindslev-Hansen, M. Wildt, C.B. Sorensen, and P.E. Lindelof, Superlatt. and Microstr. **25**, 829, (1999).

[226] Takagi, S. Solid State Comm. **81**, 579 (1992).

[227] Takane, H., and H. Ebisawa, J. Phys. Soc. Jpn. **60**, 3130 (1991).

[228] Takayanagi, H., T. Akazaki, and J. Nitta, Phys. Rev. Lett **75**, 3533 (1995).

[229] Takayanagi, H., T. Akazaki, and J. Nitta, Phys. Rev. B **51**, 1374 (1995).

[230] Takayanagi, H., J. Bindslev Hansen, and J. Nitta, Phys. Rev. Lett **74**, 166 (1995).

[231] Taylor, B.N, and E. Burstein, Phys. Rev. Lett **10**, 14 (1963).

[232] Tinkham, M., *Introduction to Superconductivity*, (Mc Graw-Hill, 1996).

[233] van Wees., B.J., K.M.H. Lenssen, and C.J.P.M. Harmans, Phys. Rev. B **44**, 470 (1991).

[234] van Wees., B.J., P. de Vries, P. Magnée, and T.M. Klapwijk, Phys. Rev. Lett. **69**, 510 (1992).

[235] Verbaarschot, J.J.M., H.A. Weidenmüller, and M.R. Zirnbauer, Phys. Rep. **129**, 367 (1985).

[236] Volkov, A.F., and T.M. Klapwijk, Phys. Lett. A. **168**, 217 (1992).

[237] Volkov, A.F., Phys. Rev. Lett. **74**, 4730 (1995).

[238] Volkov, A.F. and V.V. Pavlovskii, JETP Lett. 64, 670 (1996).

[239] Volkov, A.F. and A.V. Zaitsev, Phys. Rev. B **53**, 9267 (1996).

[240] Volkov, A.F. and H. Takayanagi, Phys. Rev. B **56**, 11184 (1997).

[241] Warlamount, J.M., J.C. Brown, T. Foxe and R.A. Buhrman, Phys. Rev. Lett. **43**, 169 (1979).

[242] Wendin, G. and V.S. Shumeiko, J. Phys. Chem. Solids **56**, 1773 (1995).

[243] Wendin, G. and V.S. Shumeiko, Phys. Rev. B **53**, R6006 (1996).

[244] Wendin, G. and V.S. Shumeiko, Superlatt. and Microstr. **20**, 569 (1996).

[245] Wigner, E.P. Phys. Rev. **98** 145 (1955).

[246] Wilhelm, F., G. Schön and A. Zaikin, Phys. Rev. Lett. **81**, 1682 (1998).

[247] Yip, S.K., Phys. Rev. B **58**, 5803 (1998).

[248] Zaikin, A.D., and G.F. Zharkov, Zh. Eksp. Teor. Fiz. **78**, 721 (1980) [Sov. Phys. JETP, **51**, 364 (1980)].

[249] Zaikin, A.D., and G.F. Zharkov, Zh. Eksp. Teor. Fiz. **81**, 1781 (1981) [Sov. Phys. JETP, **54**, 944 (1981)].

[250] A.D. Zaikin, Zh. Eksp. Teor. Fiz. **84**, 1560 (1983) [Sov. Phys. JETP **57**, 910 (1983)].

[251] Zaitsev, A.V., Zh. Eksp. Teor. Fiz. **78**, 221 (1980) [Sov. Phys. JETP **51**, 111 (1980)].

[252] Zaitsev. A.V. Zh. Eksp. Teor. Fiz. **86**, 1742 (1984) [Sov. Phys. JETP, **59**, 1015 (1984)].

[253] Zaitsev, A.V., Pis'ma Zh. Eksp. Teor. Fiz. **51**, 35 (1990) [JETP Lett. **59**, 42 (1990)].

[254] Zaitsev, A.V., and D.V. Averin, Phys. Rev. Lett. **80**, 3602 (1998).

Paper I

Paper II

Paper III

Paper IV

Paper V